Universitat Autònoma de Barcelona

ANATOMIC AND PATHOLOGIC ASSESSMENT OF FELINE LYMPH NODES USING COMPUTED TOMOGRAPHY AND ULTRASONOGRAPHY

Mauricio Tobón Restrepo

ANATOMIC AND PATHOLOGIC ASSESSMENT OF FELINE LYMPH NODES USING COMPUTED TOMOGRAPHY AND ULTRASONOGRAPHY

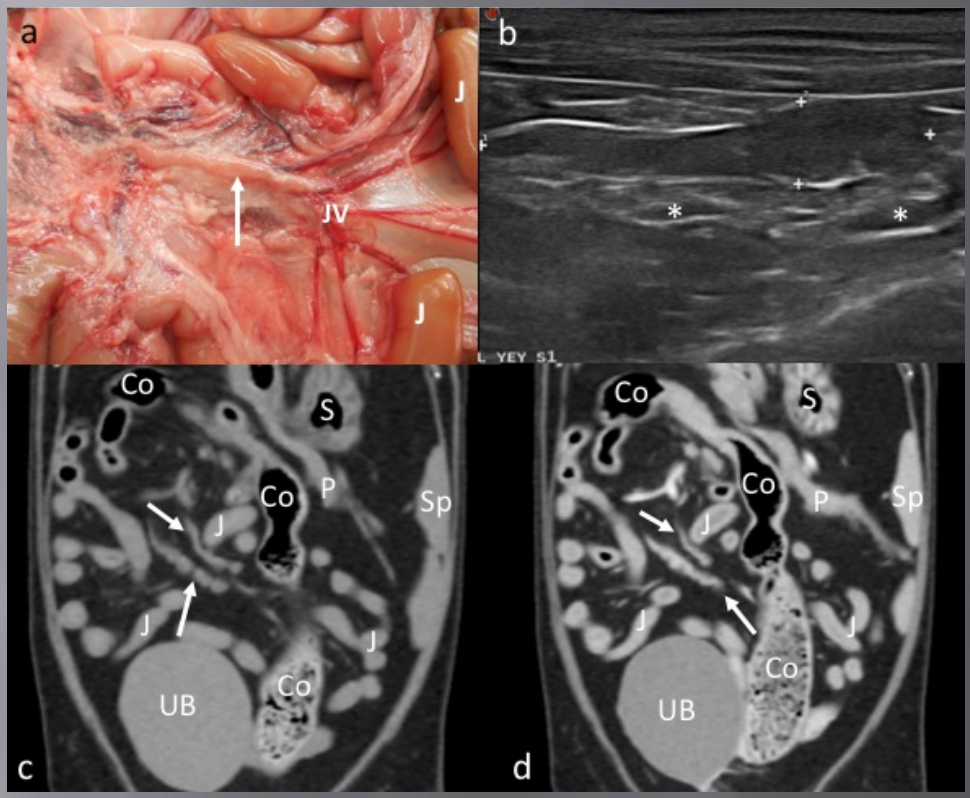

Doctorand: Mauricio Tobón Restrepo

Directores: Yvonne Espada Gerlach &
Rosa Novellas Torroja

Tesi Doctoral

Hospital Clínic Veterinari UAB

Barcelona, 29 de juliol de 2016

UAB Universitat Autònoma de Barcelona

This thesis has received financial support from the Colombian government through the "Francisco José de Caldas" scholarship program of COLCIENCIAS and from the Corporación Universitaria Lasallista.

Universitat Autònoma de Barcelona

Hospital Clínic Veterinari UAB

Departament de Medicina i Cirurgia Animals

Facultat de Veterinària

Universitat Autònoma de Barcelona

Anatomic and pathologic assessment of feline lymph nodes using computed tomography and ultrasonography

(Valoració anatòmica i patològica dels nòduls limfàtics felins mitjançant tomografia computada i ecografia)

Mauricio Tobón Restrepo

Directores

Dra. Yvonne Espada Gerlach

Dra. Rosa Novellas Torroja

Barcelona, 29 de juliol de 2016

UAB
Universitat Autònoma
de Barcelona

Departament de Medicina i Cirurgia Animals

Edifici V · Campus de la UAB · 08193 Bellaterra
(Cerdanyola del Vallès) · Barcelona · Spain
Tel. +34 93 581 10 91 · Fax +34 93 581 20 06
d.med.cirurgia.animal@uab.cat · www.uab.cat

Yvonne Espada Gerlach, Profesora Titular del Departamento de Medicina y Cirugía Animal de la Facultad de Veterinaria de la Universidad Autónoma de Barcelona y **Rosa Novellas Torroja,** Profesora Asociada del Departamento de Medicina y Cirugía Animal de la Facultad de Veterinaria de la Universidad Autónoma de Barcelona

HACEN CONSTAR

Que la tesis doctoral titulada: Anatomic and pathologic assessment of feline lymph nodes using computed tomography and ultrasonography, cuyo autor es el Médico Veterinario **Mauricio Tobón Restrepo**, ha sido realizada en el Departamento de Medicina y Cirugía Animal de la Universidad Autónoma de Barcelona bajo nuestra dirección.

Y para que así conste, a efectos de ser presentada como Tesis Doctoral para optar al título de Doctor en Veterinaria, firmamos este certificado.

Yvonne Espada Gerlach

Rosa Novellas Torroja

Cerdanyola del Vallés, 21 de Julio 2016

DEDICATED TO

A los que son la razón y la misión de esta tesis… LOS GATOS.

A mis padres y hermanos.

A Ismael.

Vor mijn poffertje.

ACKNOWLEDGMENTS

Tal vez es la parte que se pensaría más fácil de escribir, pero sin duda se juntan muchos sentimientos al momento de mirar atrás y ver todo lo que has aprendido y todas las personas que han estado a tu lado dándote una palabra de aliento… y es ahí cuando se asoma la lágrima…

Sin duda alguna, comienzo agradeciendo a los propietarios de todos los gatos incluidos en este estudio, sin ellos esto no habría sido posible.

A continuación agradezco a mis directoras de tesis, la Dra. Rosa Novellas y la Dra. Yvonne Espada. Muchas gracias por creer en mí, por apoyarme y por tenerme tanta paciencia. He aprendido mucho de vosotras y por siempre les estaré muy agradecido.

A mis patrocinadores en Colombia: Colciencias y La Corporación Universitaria Lasallista. Sin su apoyo económico, este sueño no se habría cumplido.

Al servei de diagnòstic per l'imatge del Hospital Clínic Veterinari de la Universitat Autònoma de Barcelona. Judith Saura, Raúl Altuzarra, Carlo Anselmi, Eli Domínguez. Muchas gracias por vuestra amistad, compañerismo, enseñanzas, apoyo y confianza. Toda vuestra ayuda en gran parte han hecho posible esta tesis. También os agradezco el que me hayáis contagiado del mundo del diagnóstico por imagen que se ha convertido en mi sueño y mi pasión. Os quiero montones.

To Maxim, your love and support, your patience helped me to keep this through and get the strength to finish it. Dank je wel schatje.

A todo el personal del Hospital Clínic Veterinari de la Universitat Autònoma de Barcelona por el apoyo logístico, las palabras de ánimo, la ayuda en conseguir los pacientes y el cuidado ofrecido a los mismos durante su recuperación de la anestesia.

Al servicio de anestesia del hospital, especialmente a Adrià Aguilar y Xavier Moll; siempre dispuestos para ayudarme de muy buena gana. Han sido muchas horas y muchos momentos de incertidumbre que hemos pasado juntos evaluando a todos los gatos, aprecio mucho todo lo que me apoyaron y aguantaron.

A los servicios de bioquímica y hematología de la facultad de veterinaria por vuestra diligencia al procesar las muestras y en la lectura de las citologías. Montse, Toni y la Dra. Cuenca.

A todos mis amigos en Colombia, Henry Daniel Espinosa, Juan Fernando Suárez, Héctor Buitrago, Luis Andrés Vergas, mis colegas veterinarios y mis compañeros de trabajo, por todo el apoyo y la compañía en la distancia.

A mis amigos en España, Miquel Ciurana, Miquel Falla, Juan Luis Castillo, Robert Kempton, José Rodríguez, Ignasi Oliver, Fernando y Joan Franch vuestro apoyo y amistad es una de las mejores cosas que me ha pasado en mi estancia en Barcelona. Gracias por enseñarme vuestra cultura, por abrirme vuestros hogares y ayudarme a reconocer que en este mundo hay personas como vosotros que desinteresadamente se ayudan las unas a las otras. Os quiero montones.

A Alejandro Durá, la amistad verdadera y el cariño sincero nacen de un corazón tan puro como el tuyo. Me has apoyado mucho más de lo que te puedas imaginar, siempre con tus palabras de ánimo, con tus consejos y tus soluciones a lo imprevisto. Estoy seguro que puedo seguir contando contigo para siempre. Te quiero un montón.

Y por último, y no porque sea menos importante, sino por el contrario porque son mi vida entera, a mis padres y hermanos, a mi precioso sobrino Ismael. Esta tesis es por ustedes y el estar lejos durante tantos años ha sido un alto precio a pagar. Los amo demasiado y los extraño cada segundo que paso lejos de casa.

Index

ABBREVIATIONS

ALT	*Alanine-aminotransferase*
AAxLN	*Accessory axillary lymph node*
AxLN	*Axillary lymph node*
CDCLN	*Caudal deep cervical lymph node*
CELN	*Caudal epigastric lymph node*
CoLN	*Colic lymph node*
CrMLN	*Cranial mediastinal lymph node*
CMLN	*Caudal mesenteric lymph node*
CT	*Computed tomography*
DDi-UU	*Imaging Division of the veterinary faculty of Utrecht University*
DFOV	*Display field of view*
DSCLN	*Dorsal superficial cervical lymph node*
FeLV	*Feline leukemia virus*
FHCV	*Fundació Hospital Clínic Veterinari*
FIP	*Feline infectious peritonitis*
FIV	*Feline immunodeficiency virus*
FNA	*Fine needle aspiration*
GGT	*Gamma-glutamyl-transferase*
GLN	*Gastric lymph node*
HLN	*Hepatic lymph node*
HU	*Hounsfield units*
ICLN	*Ileocecal lymph node*
InILN	*Internal iliac lymph node*
IsLN	*Ischiatic lymph node*
JLN	*Jejunal lymph node*
LALN	*Lumbar aortic lymph node*
LC	*Lymph center*
LL	*Left lateral*
LM	*Left medial*
LMR	*Left medial retropharyngeal*
LMRLN	*Left medial retropharyngeal lymph node*
LN	*Lymph node*
LTBLN	*Left tracheobronchial lymph node*

MHz	*Megahertz*
MILN	*Medial iliac lymph node*
MnLN	*Mandibular lymph node*
MPR	*Multiplanar reconstruction*
MRLN	*Medial retropharyngeal lymph node*
MRI	*Magnetic resonance imaging*
MTBLN	*Middle tracheobronchial lymph node*
NAV	*Nomina Anatomica Veterinaria*
PCR	*Polymerase chain reaction*
PET	*Positron emission tomography*
PLN	*Parotid lymph node*
PdLN	*Pancreaticoduodenal lymph node*
PoLN	*Popliteal lymph node*
RL	*Right lateral*
RM	*Right medial*
RMR	*Right medial retropharyngeal*
RMRLN	*Right medial retropharyngeal lymph node*
ROI	*Region of interest*
RTBLN	*Right tracheobronchial lymph node*
SaLN	*Sacral lymph node*
SCLN	*Superficial cervical lymph node*
SD	*Standard deviation*
SFOV	*Scan field of view*
SILN	*Superficial inguinal lymph node*
SLN	*Sternal lymph node*
SpLN	*Splenic lymph node*
UAB	*Universitat Autònoma de Barcelona*
US	*Ultrasonography*
VSCLN	*Ventral superficial cervical lymph node*

1. INTRODUCTION

1. INTRODUCTION

As part of the lymphatic and circulatory system, the lymph nodes play an important role in the diagnosis of neoplastic and infectious diseases.

In human medicine, lymph nodes are important structures that play a major role in tumor staging, choice of the therapy and predicting outcome of malignant diseases. In the last decades, invasive methods like surgical dissection of lymph nodes, serial histologic examination (fine needle aspirates) and even adjuvant chemotherapy have been considered the gold standard and efficient diagnostic tools. However, these techniques are expensive, time consuming and carry a significant risk of complications such as seromas, lymphedema, inflammation, and cosmetic alterations. Due to these facts, researchers have been focused (especially for neoplastic disease) in the improvement and understanding of non-invasive imaging techniques. So far, computed tomography (CT), magnetic resonance imaging (MRI) using lymphotropic contrast agents (USPIOs), and contrast enhanced ultrasonography (US) allowed a fair noninvasive assessment of lymph nodes in humans (Wunderbaldinger, 2006).

Previous studies in veterinary medicine have shown that US and CT are useful techniques to assess the lymph nodes, especially in dogs.
In 2004, Llabres-Diaz characterized the medial iliac lymph nodes in dogs and provided ultrasonographic features to be used as normal reference. The lack of available information regarding these lymph nodes in cats has caused the canine features to be applied to this species. Some information regarding imaging features of the feline lymph nodes are available. However, even though literature characterizing some of these feline lymph nodes is available, normal values for size and ability to depict many of them, especially with advance imaging techniques, such as CT, are lacking. This makes interpretation of studies in clinical patients difficult. Normal feline abdominal lymph nodes have been assessed with US (Schreurs et al., 2008). Normal retropharyngeal lymph nodes have been assessed using US and CT

(Nemanic & Nelson, 2012). Sentinel lymph nodes of normal mammary glands have been assessed using radiography and CT indirect lymphography (Patsikas et al., 2010). Nevertheless, there are some limitations in these studies, including small sample size (abdominal study made by Schreurs et al., 2008), not using contrast medium (retropharyngeal study (Nemanic & Nelson, 2012)), and assessment of only some of the body lymph centers (mammary lymph nodes study) (Patsikas et al., 2010). Therefore further studies involving the assessment of all the body lymph centers would be necessary to further characterize them.

To the authors knowledge there are no complete reports about normal features and assessment of all the feline lymph nodes using US and CT. On the other hand, only a limited number of studies comparing neoplastic and infectious diseases with normal lymph nodes are available, and there are no studies comparing the sensibility and specificity of US versus CT to differentiate normal from abnormal lymph nodes in cats.

2. LITERATURE REVIEW

2. LITERATURE REVIEW

2.1. Anatomy of the lymphatic system in the domestic cat

The study of the lymphatic system anatomy has leaded to improve our knowledge of its structure and function. According to Tompkins (1993), the lymphatic system is divided into primary and secondary lymphoid organs. The thymus and the bone marrow are the primary components. The spleen, lymph nodes, aggregated lymphoid tissue (tonsils), and lymphatic vessels are the secondary components. Another classification of the lymphatic system has been made by Bezuidenhout (2013) dividing it into a cellular and a vascular component. All the organs with lymphatic tissue and lymph nodes are the cellular component. The lymph capillaries, vessels, and ducts are the vascular component.

The lymphatic system‘s main functions are the immunological defense of the body and the draining and filtration of the lymph (Bezuidenhout, 2013; Dyce, Sack, & Wensing, 2002; Tompkins, 1993).

2.1.1. Lymph nodes *(lymphonodi)*

A lymph node (LN) is a small solid mass of lymphatic tissue (NAV, 2012). Normally, lymph nodes (LNs) are round or bean shaped structures located in the course of the lymphatic vessels (Tompkins, 1993). The LNs are considered to be the structural and functional unit of the lymphatic system (Bezuidenhout, 2013). They have a convex surface, which receives lymphatic afferent vessels, and a concave surface called the hilum. Bezuidenhout, (2013) described the hilum as the region of the lymph node that receives the blood supply and where the lymphatic efferent vessels leave the lymph node.

The LNs are named by regional location, and the number of nodes in a region varies among the species; in cats, the number, size, and presence of some LNs shows individual variations (Tompkins, 1993).

The LNs have two important functions. A lymph filter role that traps material received from the lymphatic afferent vessels, and a lymphocytes germinal center, providing a site for the immune response to develop (Bezuidenhout, 2013; Tompkins, 1993). The LNs have a special distribution in the body. Normally, they are located in places that provide maximum protection but without interfering in the functioning of the skeletal, muscular, and circulatory systems. It is common to find them in the adipose tissue, in the flexor angles of the joints, in the mediastinum, in the mesentery, and in the angles formed by the origin of many of the large blood vessels (Bezuidenhout, 2013).

The normal histology of a LN shows a capsule containing elastic and smooth muscle fibers, with an internal framework consisting of septa and trabeculae that sustain several lymph nodules. These lymph nodules are the structural unit of the lymph node, and contain the germinal center. They are mainly distributed in the cortex (Bezuidenhout, 2013).

2.1.2. Lymph centers (*lymphocentra)*

The Nomina Anatomica Veterinaria defines a lymph center as a lymph node or a group of lymph nodes that occurs in the same region of the body and receives afferent vessels from approximately the same region in most domestic mammals (NAV, 2012, p. 116).

a. Head and neck lymph centers

Three lymph centers have been reported in the head of domestic mammals (Figure 1): parotid, mandibular, and retropharyngeal; but only two have been

described for the neck: superficial cervical and deep cervical. These are also present in the cat.

- Parotid lymph center (*lymphocentrum parotideum*)

It is formed by 1 to 2 parotid LNs located at the cranial border of the parotid salivary gland, in contact with the superficial temporal vein. The afferent lymphatic vessels come from the dorsal aspect of the ear, the head, and neck; also lymph from the eyelids, the lips, and the parotid salivary gland drains to the parotid LN. The efferent drainage goes to the lateral retropharyngeal LN (NAV, 2012; Saar & Getty, 1982; Tompkins, 1993).

- Mandibular lymph center (*lymphocentrum mandibulare*)

Tompkins (1993) reported 2 mandibular LNs that form this lymph center; however, the NAV (2012) also report the presence of a mandibular accessory LN for this lymph center in the cat. The mandibular LNs lay medial and lateral to the facial vein at the angle of the mandibular bone, deep to the platysma muscle. They drain lymph from the lips, chin, lower jaw, eyes, part of the oral cavity, buccal salivary glands, and skin from the mandibular region. The efferent lymphatic vessels go to the medial retropharyngeal LN (Saar & Getty, 1982; Tompkins, 1993).

- Retropharyngeal lymph center (*lymphocentrum retropharyngeum*)

This consists of medial and lateral retropharyngeal LNs. Only one medial retropharyngeal lymph node has been reported and it is located adjacent to the carotid sheath at the level of the atlas and it is bounded medially by the pharyngeal musculature. It receives the lymph from the tongue, oral and nasal passages, thyroids, mandibular salivary glands, mandibular LNs, parotid LNs, and lateral retropharyngeal LNs. Its efferent vessels form the jugular trunk. A number of 3 to 4 lateral retropharyngeal LNs have been reported in most cats. They are located caudal to the parotid salivary gland

along the caudal auricular vein. They receive lymph that comes from the ear and parotid gland and drain to the medial retropharyngeal lymph node (NAV, 2012; Tompkins, 1993).

- Superficial cervical lymph center (*lymphocentrum cervicale superficiale*)

There are one ventral and two dorsal superficial cervical LNs in the cat. Tompkins (1993) described the location of the dorsal LNs deep to the *omotransversarius* muscle and cranioventrally to the *trapezius* muscle. They receive lymph from the dorsal part of the neck and from the forelimbs. Their efferent vessels go into the jugular trunk, tracheal trunk, and into the left side of the thoracic duct (Saar & Getty, 1982). The ventral superficial cervical LN lies on the external jugular vein, near the junction of the superficial cervical vein. It drains lymph from the ventral part of the neck and the thoracic inlet and its efferent vessels reach the jugular trunk, the tracheal trunk, or the thoracic duct (Saar & Getty, 1982; Tompkins, 1993).

- Deep cervical lymph center (*lymphocentrum cervicale profundum*)

It consists of the middle deep cervical (inconsistently present in cats) and the caudal deep cervical LNs located at the ventral surface of the trachea near the thoracic inlet. Their drainage areas are the thyroid glands, trachea, and cervical esophagus. Their efferent vessels go into the tracheal trunk (Saar & Getty, 1982; Tompkins, 1993). Bezuidenhout (2013) reported the presence of cranial deep cervical lymph nodes in 30% of dogs. However, this LN has been described only in 1% of the cats, located in the ventral aspect of the 20th to 23rd tracheal cartilages along the internal jugular vein (Sugimura, Kudo, & Takahata, 1955, 1959).

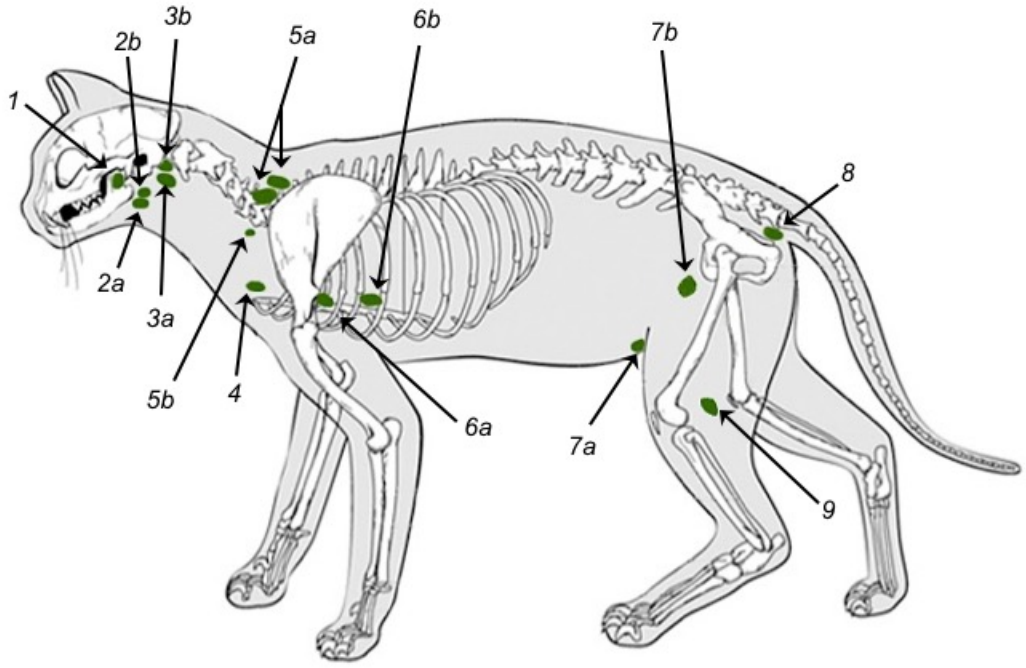

Figure 1. Superficial lymph centers in the cat. 1. Parotid. 2a & b. Mandibular (a. medial; b. lateral). 3 a & b. Retropharyngeal (a. medial; b. lateral). 4. Deep cervical. 5 a & b. Superficial cervical (a. dorsal; b. ventral). 6 a & b. Axillary (a. axillary LN; b. accessory axillary LN). 7a & b. Inguinofemoral (a. caudal epigastric LN; b. superficial inguinal LN). 8. Ischiatic. 9. Popliteal.
Adapted from a free picture in the website: https://nl.pinterest.com/pin/164240717636259107/

b. *Forelimb lymph center*

There is only one lymph center that drains all the lymph from the forelimb.

- Axillary lymph center (*lymphocentrum axillare*)

It consists of the axillary and accessory axillary LNs. In cats, Tompkins (1993) reports the presence of only one axillary LN on each side. It is located in the medial surface of the forelimb between the axillary and lateral thoracic veins. It drains the medial aspect of the forelimb and the lateral thoracic wall. Its efferent vessels end in the jugular venous angle. Three to 5 accessory axillary LNs are most commonly identified at the medial aspect of the *latissimus dorsi* muscle between the 3rd and 6th intercostal space along the lateral thoracic vein. The accessory axillary LNs drain the medial and cranial aspect of the forelimb, the skin of the lumbar region, the lateral chest walls, and the cranial half of the mammary glands. The efferent vessels end in the

axillary lymph node (Saar & Getty, 1982; Sugimura, Kudo, & Takahata, 1956).

c. Thoracic lymph centers

Four lymph centers have been described in the thorax (Figure 2). They can be divided into parietal and visceral lymph centers. The ventral and dorsal thoracic lymph centers are considered to be part of the parietal group. Mediastinal and bronchial lymph centers are considered to be part of the visceral group.

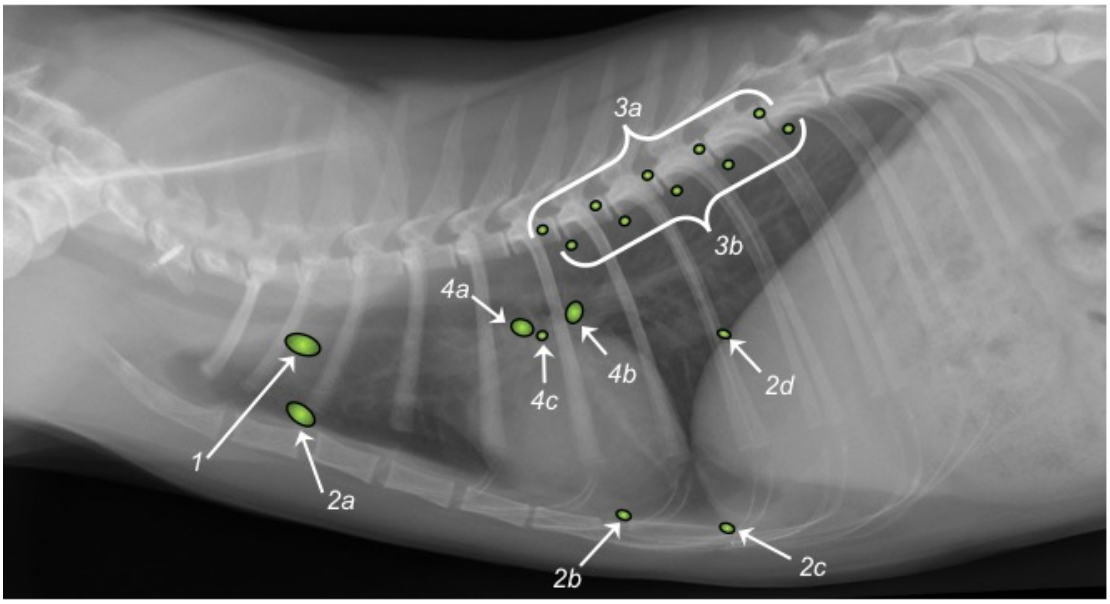

Figure 2. Thoracic lymph centers in the cat. 1. Cranial mediastinal. 2 a-d. Ventral thoracic (a. Cranial sternal LN; b. Caudal sternal LN; c. Superficial cranial epigastric LN; d. Phrenic LN). 3 a & b. Dorsal thoracic (a. Intercostal LNs; b. Aortic thoracic LNs). 4 a-c. Bronchial (a. Left/right tracheobronchial LNs; b. Middle tracheobronchial LN; c. Pulmonary LN).

- Dorsal thoracic lymph center (*lymphocentrum thoracicum dorsale*)

This lymph center is represented by two different groups of LNs:

~ The aortic thoracic LNs: round in shape and located along the azygos vein and the Aorta on the right side, at the ventral aspect of the body of the thoracic vertebras (Saar & Getty, 1982; Sugimura et al., 1959). This group of 1 – 5 LNs, drains the costal pleura and peritoneum, and

their efferent vessels end in the thoracic duct (Saar & Getty, 1982; Tompkins, 1993).

~ The intercostal LNs: this group of nodes can be found inconsistently at the level of the vertebral end of the intercostal spaces in contact with the intercostal vessels. Spheroidal in shape, they drain the lymph from the dorsal costal pleura. Some efferent vessels might go to the aortic thoracic LNs, or end directly in the thoracic duct (Saar & Getty, 1982; Sugimura et al., 1959).

- Ventral thoracic lymph center (*lymphocentrum thoracicum ventrale*)

This lymph center is represented by three groups of lymph nodes according to the NAV (2012):

~ Sternal LNs: the cranial sternal LN is the lymph node of this group that is most frequently found in cats. It lies along the internal thoracic vessels at the level of the second costal cartilage. Small nodes may be found caudally until the sixth costal cartilage covered by the *transversus thoracis* muscle (Saar & Getty, 1982; Sugimura et al., 1959). A second LN has been described between the pericardial branches of the thoracic internal vein in the pericardial vertex and is known as caudal sternal LN (NAV, 2012; Saar & Getty, 1982). These lymph nodes drain the ventral costal pleura, diaphragm, pericardium, heart, the cranioventral portion of the abdominal wall, and the cranial mediastinal LNs. The efferent vessels go to the thoracic duct and jugular trunk (Saar & Getty, 1982).

~ Superficial cranial epigastric LN (former xiphoid LN): In the cat, and also in the rabbit, this node has been described as being located deep to the *rectus abdominis* muscle, along the cranial epigastric vein and caudally to the xiphoid cartilage (NAV, 2012; Saar & Getty, 1982; Sugimura et al., 1956). It drains the cranial abdominal wall and the efferent vessels have not been described (Saar & Getty, 1982; Sugimura et al., 1956).

- ~ Phrenic LN: lies in the diaphragmatic pleura near the *foramen venae cavae*. Spherical in shape, this LN drains the diaphragm and its efferent vessels end at the sternal LN or mediastinal or bronchial lymph centers (Saar & Getty, 1982; Sugimura et al., 1959).

- Mediastinal lymph center (*lymphocentrum mediastinale)*

It is only represented by one group of 2 to 8 small and ellipsoid lymph nodes reported as cranial mediastinal LNs, which are located along the cranial vena cava and ventral aspect of the trachea and esophagus. These nodes drain the heart, trachea, thymus, and other LNs from the thoracic cavity. The efferent vessels end at the thoracic duct and the jugular trunk (Saar & Getty, 1982; Tompkins, 1993).

- Bronchial lymph center (*lymphocentrum bronchale)*

This lymph center is represented by two groups of LNs, as follows:

- ~ Tracheobronchial LNs: the position of this group is related to the tracheal bifurcation. In cats, at the cranial aspect of the main right bronchus lies the right tracheobronchial LN that drains lymph from the right lung, and in some cases from the pericardium, esophagus, and right pulmonary LN. Its efferent vessels end in the cranial mediastinal LNs. At the cranial aspect of the main left bronchus lies the left tracheobronchial LN that drains lymph from the left lung, and as in the right side, and less frequently, may receives lymphatic vessels from the pericardium, esophagus, and left pulmonary, middle tracheobronchial and phrenic LNs. Its efferent vessels end also in the cranial mediastinal LNs. At the caudal aspect of the carina lies the middle tracheobronchial LN. The afferent vessels come mainly from the lungs, diaphragm, and esophagus. Its efferent vessels end at the left tracheobronchial LN, cranial mediastinal LNs, lymphatic trunk, or directly at the cranial vena cava (Saar & Getty, 1982; Sugimura et al., 1959).

~ Pulmonary LNs: as in dogs, this group of nodes is often absent in cats. Small spherical nodes were described by Sugimura et al. (1959) on the dorsal surface of the main bronchi, between the pulmonary tissue and the tracheobronchial LNs. These nodes drain the lungs and their efferent vessels go to the tracheobronchial LNs (Bezuidenhout, 2013; Saar & Getty, 1982; Sugimura et al., 1959).

d. Abdominal and pelvic lymph centers

The lymph centers in these regions, as in the thorax, can be divided into visceral and parietal groups. Getty et al. (1982) reported three lymph centers for the visceral group: celiac, cranial mesenteric, and caudal mesenteric (Figure 3); and four lymph centers for the parietal group: lumbar, iliosacral, inguinofemoral, and ischiatic (Figures 1 & 4).

- Celiac lymph center (*lymphocentrum celiacum*)

This lymph center is represented by four groups of LNs:

~ Splenic LNs: Can be 1 – 3 in number and located along the splenic vein and its junction with the short gastric vein (Saar & Getty, 1982; Sugimura, Kudo, & Takahata, 1958). Spherical or ellipsoid in shape, these LNs drain the spleen, greater gastric curvature, including the cardia and fundus, and the pancreas (Getty et al., 1982; Sugimura et al., 1958; Tompkins, 1993). Afferent vessels may also come from gastric, pancreaticoduodenal, hepatic, and jejunal LNs (Saar & Getty, 1982; Sugimura et al., 1958). Efferent vessels drain into the celiac trunk.

~ Gastric LNs: one to 4 in number, these LNs are located at each side of the lesser curvature of the stomach. They drain the stomach and its efferent vessels go to the splenic and hepatic LNs (Saar & Getty, 1982; Sugimura et al., 1958; Tompkins, 1993).

~ Hepatic LNs: the existence of 1 to 6 hepatic LNs have been reported (Getty et al.,1982; Sugimura et al., 1958; Tompkins, 1993). They are

located around the junction of the gastroduodenal vein with the portal vein. Their drainage area is the liver, the stomach, the cranial duodenum, gastric LNs, and pancreaticoduodenal LNs. The efferent vessels drain into the celiac trunk (Saar & Getty, 1982; Tompkins, 1993).

~ Pancreaticoduodenal LN: just 1 in number, this node is located around the junction of the right gastroepiploic and cranial pancreaticoduodenal veins in the caudal part of the pylorus. The drainage area is the pancreas, cranial portion of the duodenum, and greater curvature of the stomach. The efferent vessels drain into the hepatic and, occasionally, into the splenic lymph nodes (Saar & Getty, 1982; Tompkins, 1993).

• Cranial mesenteric lymph center (*lymphocentrum mesentericum craniale*)

Three groups of LNs represent this lymph center as follows:

~ Jejunal LNs: these LNs are located in the mesojejunum along the jejunal branch of the cranial mesenteric artery. There are normally 5 – 6 nodes but the number may vary from 2 – 20 (Saar & Getty, 1982; Sugimura et al., 1958; Tompkins, 1993). They drain the jejunum, ileum, caudal portion of the duodenum, and pancreas. The efferent vessels contribute to form the intestinal trunk that joins the celiac trunk to form the visceral trunk that ends at the cisterna chyli (Saar & Getty, 1982).

~ Ileocecal LNs: situated along the cecal branches from the ileocolic vessels at both sides of the cecum. Normally there is one LN to each side but two have been also reported, and sometimes they can be absent. They drain the cecum and the last portion of the ileum. The efferent vessels drain into the right colic LNs (NAV, 2012; Saar & Getty, 1982; Sugimura et al., 1958; Tompkins, 1993).

~ Colic LNs: according to the NAV, the term *Lnn. colici* refers to all lymph nodes that are located along the various segments of the colon, except those that lie directly at the ileocolic junction (NAV, 2012, p.

117). Getty et al. (1982) reported that those located at the ileocolic junction in relation to the branches of the ileocolic artery, deep in the mesocolon, are the right colic LNs. The number of nodes in this group varies frequently (from 1 to 14), but in general 4 to 5 nodes are normally seen (Saar & Getty, 1982; Tompkins, 1993). The afferent vessels come from the ascending and transverse colon, ileum, cecum, and ileocecal lymph nodes. The efferent vessels end into the intestinal trunk (Saar & Getty, 1982; Sugimura et al., 1958; Tompkins, 1993).

- Caudal mesenteric lymph center (*lymphocentrum mesentericum caudale*)

It is only represented by the caudal mesenteric LNs. Normally 2 to 3 nodes can be found located at the bifurcation of the caudal mesenteric artery into cranial and caudal branches. The afferent vessels come from the descending colon and rectus. The efferent vessels drain into the medial iliac LNs, lumbar aortic LNs, or lumbar trunk (Saar & Getty, 1982).

- Lumbar lymph center (*lymphocentrum lumbale*)

As in canines, this lymph center consists of the lumbar aortic and renal lymph nodes in the cat.

~ Lumbar aortic LNs: they are located along the aorta and caudal vena cava, from the diaphragm to the deep circumflex iliac arteries. Sugimura et al. (1958) reported the existence of 4 – 11 nodes in 19/24 cats. According to Getty et al. (1982) and Tompkins (1993), afferent vessels drain the testes, ovaries (occasionally uterus and splenic, colic, and hepatic LNs), the dorsal wall of the abdomen, diaphragm, medial and internal iliac LNs, and the kidneys. The efferent vessels end into the lumbar trunk.

~ Renal LNs: located in relationship with the renal vessels, these LNs are difficult to differentiate from the lumbar aortic LNs. Getty et al. (1982) reported the existence of 3 to 4 nodes. The afferent vessels drain the kidneys, adrenal glands, peritoneum, abdominal wall, and

diaphragm, and occasionally the celiac lymph center, ovaries, and testes. The efferent vessels end into the cisterna chyli.

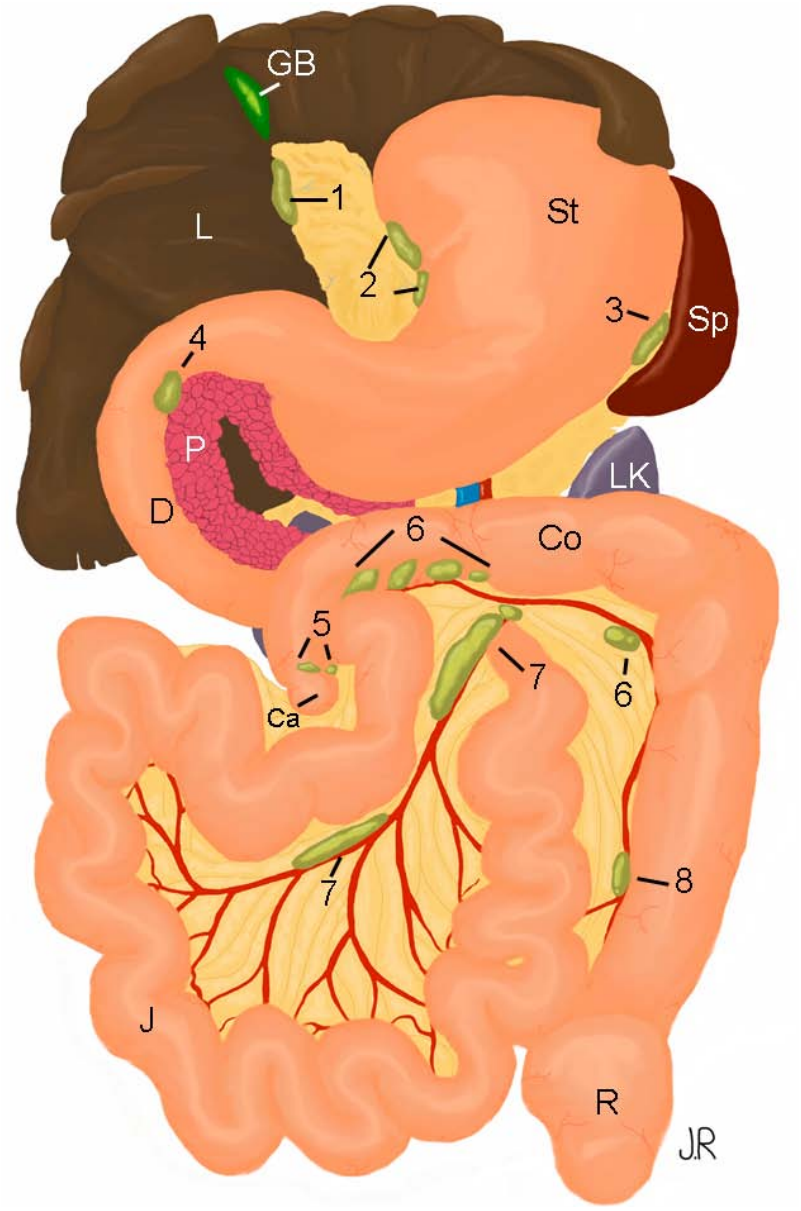

Figure 3. Diagram of the abdominal LNs and their relative anatomical positions. 1. Hepatic; 2. Gastric; 3. Splenic; 4. Pancreaticoduodenal; 5. Iliocaecal; 6. Colic; 7. Jejunal; 8. Caudal mesenteric; L: Liver; G: Gallbladder; St: Stomach; D: Duodenum; Sp: Spleen; P: Pancreas; J: Jejunum; Ca: Cecum; Co: Colon, R: Rectum; LK: Left kidney.

Adapted from the original drawing of José Rodriguez.

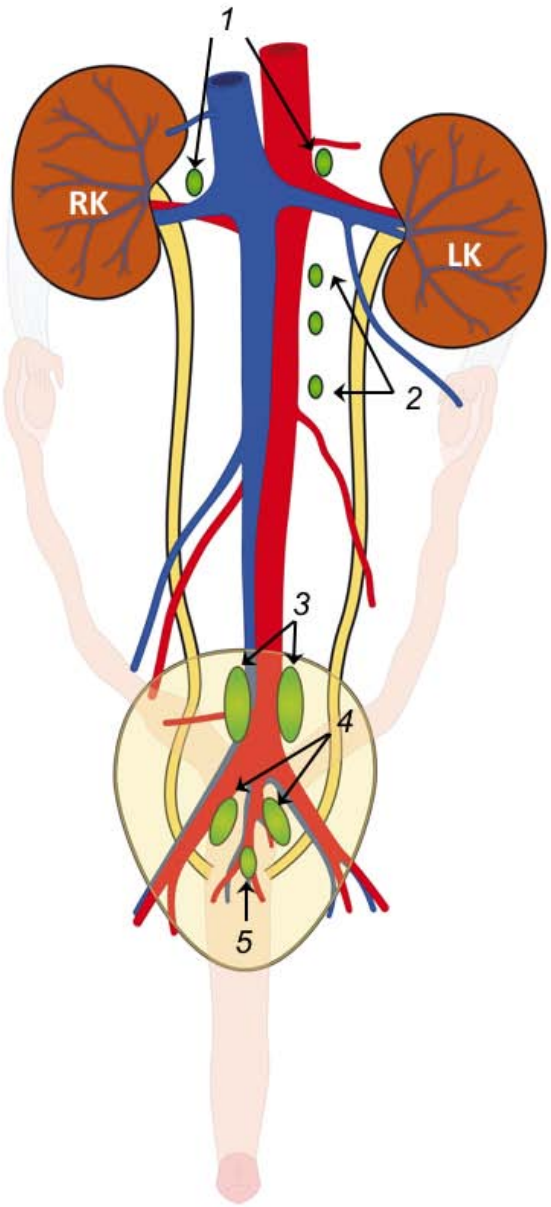

Figure 4. Lumbar & iliosacral lymph centers in the cat. 1. Renal. 2. Lumbar aortic. 2. Medial iliac. 3. Internal iliac 4. Sacral. RK: Right kidney. LK: Left kidney (Figure adapted from *Diagnóstico ecográfico en el gato*. Rosa Novellas et al. (Servet editorial, 2015))

- Iliosacral lymph center (*lymphocentrum iliosacrale*)

In cats, this lymph center consists of the medial iliac, internal iliac, and sacral LNs.

~ Medial iliac LNs: two to five in number, these nodes are located bilaterally along the aorta between the deep circumflex iliac and external iliac arteries. They receive afferent lymph from the uterus,

medial and caudal portions of the abdominal wall, hindlimbs, pelvis, tail and iliofemoral, inguinofemoral and ischiatic lymph centers. The efferent vessels form the lumbar trunks, and end into the cisterna chyli (NAV, 2012; Saar & Getty, 1982; Sugimura et al., 1958; Tompkins, 1993).

~ Internal iliac LNs: were formerly known as hypogastric LNs. They are located in relation to the internal iliac arteries and 2 – 3 nodes have been described. They drain lymph from the rectum, uterine body, bladder, the tail, and the skin surrounding the anus and the gluteal region. The efferent vessels end into the medial iliac LNs or lumbar trunks (Saar & Getty, 1982; Sugimura et al., 1958).

~ Sacral LNs: found in relation to the middle sacral vessels. These nodes are inconstantly found in cats. When they are present, they drain lymph from the rectum, pelvic wall, tail, and hindlimbs. The efferent vessels drain into the medial and internal iliac LNs (Bezuidenhout, 2013; Saar & Getty, 1982; Sugimura et al., 1958; Tompkins, 1993).

• Inguinofemoral lymph center (*lymphocentrum inguinofemorale*)

Formerly known as superficial inguinal lymph center, its designation was changed by the NAV because some structures are not exactly located in the inguinal area (NAV, 2012). This lymph center includes the superficial inguinal, subiliac, and caudal epigastric lymph nodes (NAV, 2012).

~ Superficial inguinal LNs: these nodes can be called mammary LNs in females and scrotal LNs in males. Their location is at the junction of the caudal superficial epigastric vessels with the external pudendal vessels in the inguinal region. One or two nodes can be found. The afferent vessels arise from the caudal abdominal wall, caudal epigastric LNs, skin from the gluteus and anal regions, and also the medial aspect of the hindlimb. In females, these LNs receive lymph from the caudal mammary glands and, in males, from the penis, prepuce, scrotum, and testis. The efferent vessels drain into the

medial iliac LNs (Bezuidenhout, 2013; NAV, 2012; Saar & Getty, 1982).

- ~ Subiliac LNs: according to Sugimura et al. (1956), they are rarely found. When present, they are located at the mid-cranial border of the *sartorius* muscle, along to one of the caudal branches of the deep circumflex iliac vessels. Their afferent vessels arise from the gluteal and lumbar regions and the skin of the hindlimb. Efferent vessels drain into the medial iliac LNs (Saar & Getty, 1982; Sugimura et al., 1956).
- ~ Caudal epigastric LNs: only present in the cat and the rabbit, these LNs are located along the caudal superficial epigastric vein more cranially than the superficial inguinal LNs. They are not always present. The afferent vessels arise from the abdominal wall and in females from the mammary glands of the middle abdomen. The lymph drain into the inguinal superficial LNs (Saar & Getty, 1982).

- Ischiatic lymph center (*lymphcentrum ischiadicum*)

It is only represented by the ischiatic LN. It is located along the caudal gluteal vessels, medially to the *gluteofemoralis* muscle in the ischiatic region. Afferent vessels arise from the tail, anal region, hindlimb, and popliteal LNs. Efferent vessels drain into the medial iliac LNs (Saar & Getty, 1982; Tompkins, 1993).

e. Hindlimb lymph centers

The lymph centers in this region drain lymph from the hindlimb as well as from the ventro-caudal portion of the abdominal wall. Getty et al. (1982) reported two lymph centers for the pelvic limb, the iliofemoral and the popliteal lymph centers.

- Iliofemoral lymph center (*lymphocentrum iliofemorale*)

It consists of the iliofemoral LN, but it is not always present. This node is located at the junction of the external iliac and deep femoral veins just dorsal to the inguinal canal. It drains lymph from the distal lateral surface of the hindlimb, the ventro-caudal portion of the abdominal wall and also from the popliteal and superficial inguinal LNs. The efferent vessels end into the medial iliac LNs (NAV, 2012; Saar & Getty, 1982).

- Popliteal lymph center (*lymphocentrum popliteum*)

In cats, as in dogs, this center is represented by the superficial popliteal LN. It is located subcutaneously in the popliteal fossa between the *semitendinosus* and *biceps femoris* muscles, at the caudo-proximal aspect of the *gastrocnemius* muscle. Normally there is only one node in each hindlimb. The afferent vessels arise from the distal part of the hindlimb. The efferent vessels drain into the iliofemoral and ischiatic LNs when they are present and/or the medial iliac LNs (NAV, 2012; Saar & Getty, 1982).

2.2. Ultrasonography of the lymphatic system

Ultrasound (US) is the term that describes sound waves of frequencies exceeding the range of human hearing and their propagation in a medium (Bushberg, Seibert, Leidholdt, & Boone, 2002b). In diagnostic US, a pulse of ultrasound waves is directed into the body (Kealy, McAllister, & Graham, 2011b). Interaction of the waves with the tissue's acoustic impedance produces an interpretable gray scale image of the organs.

2.2.1. Physical principles

Sound travels in waves that are able to carry information from one location to another (Drost, 2013). The way the waves interact with the tissues and transmit the information to the computer depends on the physic characteristics detailed below.

a. Propagation of sound

It refers to the way that the physical properties of a sound wave travel in the tissues. The sound wave is mechanical energy traveling through a continuous, elastic medium which causes the compression and rarefaction of the "particles" that compose it (Bushberg et al, 2002b). Compression is an increase of pressure that causes deformation in the tissue (Bushberg et al., 2002b; Mattoon & Nyland, 2015). Rarefaction follows compression, when the pressure is reduced the compressed particles transfer their energy to the adjacent one, this reduces the local pressure amplitude (Bushberg et al., 2002b). The velocity of propagation of the sound is affected by the tissue properties, mainly the tissue's resistance to compression, that includes the density and the elasticity (Mattoon & Nyland, 2015) and that increases in stiff tissues and decreases in high density tissues. Table 1 shows a list of the velocity of sound in different tissues according to their density.

Table 1. Velocity of sound and density from different materials and tissues

MATERIAL	Density (kg/m^2)	Velocity (m/s)
Air	1.2	331
Lung	300	600
Fat	924	1450
Water	1000	1480
Soft tissue	1050	1540
Kidney	1041	1561
Blood	1058	1570
Liver	1061	1549
Muscle	1068	1585
Skull bone	1912	4080
PZT[1]	7500	4000

[1]PZT: lead zirconate titanate (Modified from Bushberg et al., 2002)

b. Frequency

Defined as the number of times a wave oscillates through a cycle per second and it is expressed in hertz (Hz). It is inversely related to wavelength; the higher the frequency, the shorter is the wavelength and vice versa. This relation is very important for the image resolution. A short wavelength (high frequency) produces a better resolution. The formula:

$$\text{Velocity (m/sec)} = \text{frequency (cycles/sec)} \times \text{wavelength (m)}$$

shows the relationship between frequency, velocity, and wavelength (Bushberg et al., 2002b; Drost, 2013; Widmer, Mattoon, & Nyland, 2015).

c. Wavelength

The distance between compressions or rarefactions, or the distance traveled during one cycle. It is expressed in millimeters or micrometers (Bushberg et al., 2002b; Mattoon & Nyland, 2015).

d. Reflection

It is when a sound wave interacts with the tissue and is sent back toward the transducer and is the basis of ultrasound image. The reflection is affected by the angle in which the wave hits the tissue. A 90-degree angle is wanted for a better image quality (Drost, 2013; Mattoon & Nyland, 2015).

e. Refraction

It refers to the change in the direction of the US energy transmitted at the tissues boundary if the beam angle is not perpendicular to it, this might produce a change in the speed of the US wave; however, the frequency does not change. When a curved structure is being scanned, the combination of refraction and reflection contributes to the formation of an artifact called edge

shadowing laterally and distally to the structure (Bushberg et al., 2002b; Mattoon & Nyland, 2015).

f. Acoustic impedance

It is the product of the physical density of a tissue and the sound speed within the tissue. The amplitude of a returning echo is proportional to the difference in acoustic impedance between two tissues as the sound passes through their interface. Acoustic impedance can be calculated using the following formula:

$$Acoustic\ Impedance = Velocity \times Tissue\ density$$

Sound velocity in soft tissues is considered constant (1540m/s), therefore the acoustic impedance basically depends on the tissue density (Drost, 2013; Mattoon & Nyland, 2015).

2.2.2. Modes of image display

a. B-mode (Brightness mode, B-scan or gray scale)

It is the mode most frequently used for regular abdominal US as well as for the examination of other soft tissue regions. The image is made by a collection of dots that are presented in a black background (Drost, 2013). The returning echoes are digitalized and converted into various intensities of brightness in two dimensions on a gray-scale format and are displayed on a monitor (Kealy et al., 2011b). The brightness of the dot is proportional to the amplitude of the returned echo and the depth of the structure that returned the echo determines the position of the dots relative to the position of the transducer (Drost, 2013; Mattoon & Nyland, 2015).

2.2.3. Instruments

The machines used in diagnostic US have a pulser that applies timed high-voltage pulses to the piezoelectric crystals within the transducer to generate sound waves. The crystals are made of lead-zirconate-titanate (PZT), a ceramic material that produces a mechanic vibration when an electric pulse is applied (Bushberg et al., 2002b). The transducer or probe is the transmitter and receiver of sound waves to and from the body, respectively, and is key to the image formation. The electric pulse is transformed in a sound wave that is reflected by the tissues and sent back to the transducer that transforms it in an electric pulse. Images are formed on the computer screen. The US machines also have controls that allow the operator to change or adjust contrast, frequency, and focal points, among others (Drost, 2013; Kealy et al., 2011b; Mattoon & Nyland, 2015).

2.2.4. Ultrasonography of the normal lymph nodes

The appearance and ultrasonographic features of LNs have been studied in both human and veterinary medicine (Nyman & O'Brien, 2007; Wunderbaldinger, 2006). The evaluation of LNs size, shape, margins, echogenicity, echopattern (echotexture), acoustic transmission, vascular flow (presence and distribution), and measurement of vascular flow indices have been reported as important features in the determination of normality or abnormality of LNs in veterinary literature (Llabres-Diaz, 2004; Nyman, Kristensen, Skovgaard, & McEvoy, 2005; Nyman & O'Brien, 2007). In human medicine, LNs are described as low echogenic oval and round structures with a clear visible hilum containing the central vessels (Wunderbaldinger, 2006).

The LNs size can be assessed by a short-to-long-axis (S/L) ratio that helps to guide the diagnosis of lymphadenomegaly. A ratio ≤0.5 has been reported to be normal in medial iliac LNs in dogs (D'Anjou, 2008; Llabrés-Díaz, 2004).

Descriptions about the normal shape of LNs includes fusiform to oval (D'Anjou, 2008), slender (Nyman & O'Brien, 2007), round or oval to more elongate and fusiform (Mattoon, Berry, & Nyland, 2015). Normal margins have been described as smooth (D'Anjou, 2008), sharp (Nyman & O'Brien, 2007), or variable contour (Kealy, McAllister, & Graham, 2011a).

The normal echogenicity of the LNs have been reported to be nearly anechoic (Mattoon et al., 2015), hypoechoic (Kealy et al., 2011a), slightly hypoechoic, relatively isoechoic or even echogenic to adjacent fatty tissues (D'Anjou, 2008; Mattoon et al., 2015; Nyman & O'Brien, 2007). The normal echopattern has been described as homogeneous (Mattoon et al., 2015) or mildly heterogeneous (Nemanic & Nelson, 2012).

Superficial LNs are better assessed using a high frequency probe (7.5 – 13MHz or higher), considering that these structures are small in size and very often are loose in the surrounding fat. There are few reports about the technique to perform an ultrasonographic evaluation of the superficial LNs in the cat. Literature giving description of the features for superficial LNs is only available for the ultrasonographic evaluation of the retropharyngeal (Nemanic & Nelson, 2012) and popliteal LNs (Lee et al., 2012).

Abdominal LNs are not typically easy to assess. An important factor that should be taken into account is the body condition; as the body condition increases, the difficulty in identifying a normal LN also increases. The attenuation of the ultrasound beam caused by the fatty tissue that surrounds the LN could be an explanation for this (Mattoon et al., 2015).

Some other factors have to be considered when the thoracic and the abdominal LNs need to be assessed. The presence of air in the lungs and in the intestinal loops makes difficult the visualization of LNs due to the acoustic shadowing that it produces (Mattoon et al., 2015; Nyman & O'Brien, 2007).

An evaluation of the whole lymphatic system is never performed in a single patient because, in a clinical situation, a regional evaluation is usually required.

2.2.5. Ultrasonographic features of abnormal lymph nodes

Commonly, a malignant LN is rounded in shape with hypoechoic parenchyma (Nyman & O'Brien, 2007). However, if hemorrhage, coagulative necrosis or mineralization is present, the appearance of the LN is more heterogeneous (D'Anjou, 2008). Ultrasonographically, heterogeneity of LNs has been described as a significant finding associated with malignancy in dogs. However in cats, a statistical association of abdominal LNs heterogeneity with malignancy was not found (Kinns & Mai, 2007).

Lymphadenopathy is associated with reactive, inflammatory, and neoplastic processes. Ultrasonographic features between normal, reactive, and malignant (metastatic) lymphadenopathy overlap (Nyman & O'Brien, 2007). Massively enlarged LNs showing heterogenic areas may be related with benign or malignant infiltration and can be associated with a pyogranulomatous disease or neoplasia (D'Anjou, 2008).

In humans, contrast enhance ultrasound (CEUS) is preferred because allows an accurate noninvasive lymph node assessment and cancer staging (Wunderbaldinger, 2006). In veterinary medicine, descriptions of the applications and uses of this modality are limited. So far, the study of CEUS in dogs have lead to reports that advice its use for detection and characterization of focal lesions in the liver (Nakamura et al., 2010) and spleen (Rossi, Leone, Vignoli, Laddaga, & Terragni, 2008). A study has shown that contrast harmonic ultrasound accurately depicted angioarchitechture within lymphomatous nodes in dogs; this additional information can be used in determining the presence of malignant vascular

characteristics of LNs (Salwei, O'Brien, & Matheson, 2005). The use and applications of CEUS in cats are also limited. A recent study about normal vascular pattern and appearance of normal abdominal organ and mesenteric LNs concluded that CEUS can be used to estimate organ perfusion like in other species (Leinonen et al., 2010). Studies showing the utility of CEUS in differentiating vascular patterns in lymphadenopathies are lacking.

2.3. Computed tomography of the lymphatic system

Computed tomography (CT) was developed in the 70's as a computer system that allowed the acquisition and reconstruction of images from a specific region of the patient avoiding the superimposition among organs. CT technology was invented by Godfrey Hounsfield and Allan Cormack based on the mathematic principles of Radon that are also used in conventional radiography (Bushberg, Seibert, Leidholdt, & Boone, 2002a; D'Anjou, 2013). The first CT scans had long acquisition times, but with the advance of technology a full body CT scan can be nowadays done in seconds. In veterinary medicine, the first CT scans were performed in the late 80's and patients had to be taken to a human hospital to be scanned. The first CT scan for veterinary use was installed at the École Nationale Vétérinaire d'Alfort in Paris in 1989, allowing the beginning of CT diagnostic imaging in veterinary medicine (Schwarz & Saunders, 2011).

2.3.1. CT principles

Radon's mathematic principles proved that an image of an unknown object could be reproduced if an infinite number of projections through the object had been acquired. This means that the CT image is a picture of a slab (or slice) of the patient's anatomy (Bushberg et al., 2002a).

2.3.2. CT scans components

Basically all CT machines are conformed by the same components, and their designs vary depending on the manufacturer.

a. Gantry

Is a doughnut-shape ring that contains the rotating X-ray tube, the detectors array, the collimator and the hardware necessary to generate radiation and to detect the attenuated X-rays that had passed through the patient and that later allow the reconstruction of the images. The gantry has a hole in the center that allows the patient table to slide in and out according to the scanning protocols (Bushberg et al., 2002a; Saunders & Ohlerth, 2011). The gantry is one of the components that has had more modifications along the time helping in reducing the acquisition times, artifacts, and image quality (Bushberg et al., 2002a).

b. X-ray tube

A vacuum cage enclosing an X-ray tube, designed to resist the demanding protocols of a CT scan. One of the major differences with a conventional radiography tube is the fan beam geometry that it uses, producing a X-ray beam in a fan shape (Bushberg et al., 2002a; Saunders & Ohlerth, 2011).

c. Collimator

It is located between the X-ray source and the patient (pre-patient collimators) and between the patient and the detectors (post-patient collimators). The collimators are useful to ensure good image quality and to reduce unnecessary radiation doses to the patient. Another important characteristic is that the adjusted opening allows the selection of a slice width and the size and position of the focal spot (Saunders & Ohlerth, 2011).

d. Detector system

Another important component that is located in the gantry in an opposite position to the X-ray tube. In the 3rd generation scanners, a detector array rotates with the X-ray tube inside the gantry. It is long enough to receive the radiation from the fan beam, including the entire width of the patient; this conformation is widely used in most scanners. In the 4th generation scanners a detector array is disposed around the gantry ring. Nowadays, the detectors are made from ceramic solid-state materials because they have a better X-ray absorption efficiency. The detector has two main functions: 1) the reception of the incident X-ray photons, which have passed through the patient and 2) the transformation of the photon into a electrical sign, that is then amplified and converted from analog to a digital form (Bushberg et al., 2002a; Saunders & Ohlerth, 2011).

e. Patient table

It is made of carbonate fiber that will not produce artifacts in the image when scanned. Usually it is fixed in the ground but the height can be adjusted. The table slides in and out of the gantry opening, allowing the irradiation of a specific region of the patient that is the objective of the examination (Bushberg et al., 2002a).

f. Work station

It is normally located in a separate room covered with lead shields that provide protection against the radiation to the operators. The main computer to program protocols, to reconstruct, and to display the images is also located in this room (Saunders & Ohlerth, 2011).

2.3.3. Image acquisition principles

They involve all the steps that have to be taken into account when scanning. Body part selection is the first part of the process because it will determine the algorithms in which the image will be reconstructed. Normally CT scans use protocols that include the tube rotation time, mA, mAs and kV for different regions. An explanation of other concepts that need to be considered is given below.

a. Scan field of view (SFOV)

The x-ray fan beam circles the gantry while emitting radiation. The image is reconstructed from the data of the area in the gantry where there is a complete overlap of the x-rays fan beam projections. The region of the body that is to be scanned should not be outside the SFOV (Bushberg et al., 2002a; Schwarz & O'Brien, 2011).

b. Display field of view (DFOV)

Area of the SFOV from which the image is reconstructed (Bushberg et al., 2002a; Schwarz & O'Brien, 2011).

c. Slice thickness

Refers to the tissue thickness that will be used to attenuate the x-ray beam and from which the slice is reconstructed. The collimator and detectors array play an important role in the determination of slice thickness. The different tissues contained in a slice influence the quality of the image. An increase in the slice thickness can produce a better visualization of some structures, but can also increase the possibility of acquiring a blurry image (Schwarz & O'Brien, 2011).

d. Slice interval

It refers to the interval in which the images are acquired in sequential mode (axial); it can be programmed to be the same distance of the slice thickness to ensure continuous image acquisition. In helical mode, data are obtained continuously and this interval is not used (Schwarz & O'Brien, 2011).

e. Helical pitch

It is the expression of the relationship between the table increment during one full gantry rotation and the slice thickness. It is directly proportional to image blur, meaning that a high CT pitched scan produce a highly blurry image. A pitch of zero will result in a complete ring of data (sequential scan). A pitch of 1 results in a stretching of the helix by one degree that after one rotation the table will have moved by one slice or collimator width. The image reconstruction will be done with mathematical interpolation of the data contained in other parts of the helix. A very high pitch makes the mathematical interpolation (guesses) incorrect which produces a blurry image (Schwarz & O'Brien, 2011).

2.3.4. Image reconstruction

Determined by the different type of tissue that is contained in a slice thickness. The slice is divided in a matrix that is conformed by pixels showing the average attenuation of each voxel. In veterinary, a matrix of 512x512 is commonly used.

a. Voxel (Volume element)

Volume area obtained multiplying the slice thickness by the pixel area (Bushberg et al., 2002a).

b. Pixel (Picture element)

It is a 2D square that shows a shade from a gray scale (Hounsfield gray scale) that is obtained by averaging the attenuation values of all the tissues that are contained in the voxel. The pixel is the face of the voxel (Bushberg et al., 2002a).

c. Hounsfield Units (HU)

Developed by Geoffrey Hounsfield, these units correspond to the numeric values that give to each pixel a shade from a gray scale. The scale has “0” as a central value given to the attenuation of the water and is expressed as a specific tone of gray. Structures with more attenuating characteristics are represented with brighter gray colors until white is reached. Structures with less attenuating characteristics are represented in darker gray colors until black is reached. The range of the HU is -1000 to +3095 producing a total of 4096 shades of gray. However, the human eye cannot differentiate more than 90 shades of gray. To solve this problem, the image gray scale must be adjusted using the window width and level (Bushberg et al., 2002a; D’Anjou, 2013; Saunders & Ohlerth, 2011). Table 2 shows the reported HU for different organic tissues.

d. Window width

Range of HU numbers (minimum to maximum) displayed in the image. This determines image contrast.

e. Window level

It is the central HU number of the chosen window width. This determines image brightness. The window level should match the density level of the organ of interest.

The combination of the window width and level is responsible for the image display for the different windows: bone, soft tissue, lung, brain (D'Anjou, 2013; Saunders & Ohlerth, 2011).

Table 2. Hounsfield Units (HU) values for organic tissues and fluids

Tissue	HU standard value
Compact bone	>250
Trabecular bone	50 – 300
Coagulated blood	70 – 90
Thyroid gland	60 – 80
Liver	50 – 70
Whole blood	50 – 60
Brain gray matter	37 – 41
Muscle	35 – 50
Pancreas	30 – 50
Kidney	20 – 40
Brain white matter	20 – 34
Plasma	27 ± 2
Exudates (>30 g protein/L)	>18 ± 2
Transudates (<30 g protein/L)	<18 ± 2
Cerebrospinal fluid	5 – 10
Fat	-80 to -100
Lung	-950 to -550

Modified from Ohlerth & Scharf (2007)

2.3.5. Multiplanar reconstruction of images

CT scans normally reproduce images in an anatomical transverse plane. However, any other anatomic plane can be reconstructed with the data recovered by the scanner. Another type of reconstruction is the volume rendering that reproduce a 3D image of the patient (Saunders & Ohlerth, 2011).

2.3.6. Contrast studies

Iodinated contrast media are commonly used and provide information about blood flow, perfusion of tissues, and integrity of natural barriers. These media

are administrated with a catheter into the blood stream, usually a peripheral vein; however, intra arterial, intrathecal, and intra articular administration can also be performed depending on the procedure. The contrast agent is used with the purpose of intensifying the visualization of structures (mainly soft tissues) and its vascular permeability (D'Anjou, 2013).

2.3.7. Computed tomography of normal lymph nodes

In human medicine, CT is widely available and the systematic visualization of all LNs location, and combined evaluation of other lesions and surrounding structures is possible and has been done for the detection and follow up of diseases (Wunderbaldinger, 2006).

In veterinary medicine, the assessment of LNs also has an important role in grading or establishing the severity of the pathologies that can affect the patient. Only a few studies regarding the normal appearance of the LNs in the cat are available in the literature. Some studies have assessed the retropharyngeal (Nemanic & Nelson, 2012), the cranial mediastinal, and the tracheobronchial LNs (Henninger, 2003) in order to describe their appearance. A mildly heterogeneous, 20.7mm length X 13.1mm rostral height X 4.7mm rostral width of a medial retropharyngeal LN was reported as normal (Nemanic & Nelson, 2012). In the study for the cranial mediastinal and the tracheobronchial LNs, these were not identified and the authors report that the reason was they were not enlarged (Henninger, 2003).

In dogs, abdominal LNs have been described as commonly elongated in shape, homogeneously attenuating structures before (37HU, range: 20 – 52) and following (109HU, range: 36 – 223) the intravenous administration of contrast medium. Some LNs were slightly irregular or relatively more hyperattenuating in the periphery than centrally before and after contrast administration (Beukers, Vilaplana Grosso, & Voorhout, 2013).

There are no studies about the normal appearance of cervical and abdominal LNs in the cat.

2.3.8. Computed tomography of abnormal lymph nodes in the cat

In human medicine, the LNs are considered malignant in CT images if they present a short diameter of more than 10mm, a S/L ratio >0.5 or a L/S (long-to-short-axis) ratio <2, detectable extra nodal tumor spread and/or necrotic or cystic changes and/or heterogeneous contrast enhancement, or are clearly increased in number (Mohseni et al., 2014; Steinkamp et al., 1995; Steinkamp, Hosten, Richter, Schedel, & Felix, 1994; Tohnosu, Onoda, & Isono, 1989; Vassallo, Wernecke, Roos, & Peters, 1992). However, the low sensitivity in detecting LNs with an histologic diagnosis compatible with metastatic infiltration has lead to the combination of CT with other techniques like PET (positron emission tomography), improving the accuracy in the assessment of LNs and cancer staging (Wunderbaldinger, 2006).

In cats, there are studies about the characteristics of different diseases and some of them include a brief description of one or more LNs that are involved. In a study about nasal polyps in cats, mandibular and medial retropharyngeal LNs presenting ellipsoidal shape, heterogeneous contrast enhancing, hyperattenuating foci centrally and peripherally, and a length of 29.4mm were considered suggestive of lymphadenopathy (Oliveira, O'Brien, Matheson, & Carrera, 2012). In a study about the CT findings in fungal rhinitis and sinusitis, 5/9 cats had images compatible with lymphadenopathy. In 1/5 cats, enlarged right mandibular and retropharyngeal LNs with heterogeneously contrast enhancing with central hypoattenuation were seen. A homogenously enhancing of both LNs was present in 1/5 cats. In 3/5 cats only retropharyngeal lymphadenopathy was identified. Heterogeneous contrast enhancement with central hypoattenuation was present in 2/3 cats. A homogeneous enhancement of the retropharyngeal LNs was seen in 1/3

cats. No indication of size and HU were reported in this study (Karnik, Reichle, Fischetti, & Goggin, 2009). In a study regarding the CT features of oral squamous cell carcinoma, the maximum width of the mandibular (4.1 +/- 1.9mm) and the medial retropharyngeal (5.3 +/- 1.5mm) LNs was measured on postcontrast images (Gendler, Lewis, Reetz, & Schwarz, 2008). Other studies about thoracic neoplastic disease (Henninger, 2003) did not describe CT features of the identified LNs (tracheobronchial).

There is no literature about the assessment of pathologic abdominal LNs in the cat.

3. OBJECTIVES

3. Objectives

- To assess the CT and US ability to identify the lymph nodes of healthy cats comparing the imaging features with measurements from normal anatomic values.

- To characterize the lymph nodes in diseased cats using CT and US.

- To assess the ability of each imaging technique (CT and US) to discriminate between neoplastic and inflammatory changes in the lymph nodes.

4. STUDIES

4.1. Anatomic, computed tomographic, and ultrasonographic assessment of the lymph nodes in healthy adult cats: Part I. The head, neck, thorax, and forelimb.

Abstract

The assessment of the lymph nodes (LNs) is key in staging cancer patient. Descriptions about the normal computed tomography (CT) and ultrasound (US) features of feline LNs are limited in the veterinary literature. The purposes of this study were (i) to compare the size of the head, neck, forelimb, and thorax LNs obtained with US and CT in a group of healthy adult cats with measurements obtained from an anatomic study and (ii) to describe the US and CT features of these LNs in healthy adult cats. An anatomic study in 6 cadavers and an imaging study (CT and US) in 30 healthy cats were performed. The frequency of identification of the lymph centers varied among techniques and also, individually. The mandibular LNs (MnLNs) were the only ones identified in 100% of the cats both in the anatomic and the imaging studies. The medial retropharyngeal LNs (MRLNs) were identified in 100% of the cats using CT and US. The deep cervical LNs were not visualized in the cadavers. The cranial mediastinal and tracheobronchial LNs were not visualized using US. Length, width, and height were measured and compared among techniques. The length of the LNs on CT was higher when compared with US and anatomic lengths. The highest differences were in the MRLNs; the length in CT was 6mm larger than the length in US and anatomy. Ultrasonographically, LNs were relatively wider than on CT and anatomy. The highest differences were presented for the MRLNs and superficial cervical LNs (SCLNs). The height was the most variable measurement among techniques showing the highest statistically significant differences among them. The LNs identified with CT were most frequently isoattenuating or slightly hypoattenuating to the surrounding musculature, with homogeneous contrast enhancement. In US, most LNs were isoechoic or hypoechoic to surrounding fat tissue. The majority of LNs were fusiform or rounded. Nevertheless, the MRLNs, the dorsal SCLNs, and the accessory axillary LNs (AAxLNs) had miscellaneous shape. Some conditions that improved the visualization of the LNs were identified; the fat tissue provided a good contrast to differentiate the LNs from the other soft tissues. In thin cats, the CT contrast studies helped in the differentiation of the LNs. The measurements and features reported are proposed as reference values.

Introduction

Lymph nodes (LNs) characterization is important in the diagnosis and prognosis of neoplastic and infectious diseases (Nemanic, Hollars, Nelson, & Bobe, 2015; Nyman, Kristensen, Skovgaard, & McEvoy, 2005; Nyman & O'Brien, 2007). There is limited information regarding the imaging features of the lymph centers in the cat. Normal values for size, appearance, and ability to depict many of them using computed tomography (CT) and ultrasonography (US) are needed.

The lymph centers (LCs) for the head, neck, thorax, and forelimb are reported in the Nomina Anatomica Veterinaria (NAV). The parotid, mandibular, and retropharyngeal LCs are described in the head; the superficial and deep cervical LCs in the neck; and the axillary LCs in the forelimb. In the thorax, four LCs exist, divided into parietal and visceral LCs. The parietal LCs include those located on the inner side of the thoracic wall: the dorsal and ventral thoracic LCs. The visceral LCs include those located within the pleural and mediastinal spaces: the mediastinal and bronchial LCs (Bezuidenhout, 2013; NAV, 2012; Tompkins, 1993).

The normal length of the LNs in the cat has been reported in the anatomy literature mainly based on the studies made in Japan in the 50's (Saar & Getty, 1982; Sugimura, Kudo, & Takahata, 1955; Sugimura, Kudo, & Takahata, 1959). However, the normal width and height were not reported in those anatomic references.

Description of normal US and CT features of the lymph nodes in the head, neck, forelimb, and thorax of the cat is lacking in the current literature.

The aims of this study were: (i) to compare the size of the head, neck, forelimb, and thorax lymph nodes obtained with US and CT in a group of healthy adult cats with measurements obtained from an anatomic study; and (ii) to describe the US and CT features of these lymph nodes in healthy adult cats.

Materials and methods

The ethical committee of the Universitat Autònoma de Barcelona approved this study; reference number CEAAH 2255 of September 2013. The owner consent for all the patients and cadavers included in the study was also obtained.

Anatomical study

Animals

Feline cadavers referred for necropsy to the pathology department of the Universitat Autònoma de Barcelona, within 24 hours of dead, were prospectively included from January 2013 to June 2015.

Using a 24 scalpel blade, the skin was removed making an incision from the mandibular symphysis to the xiphoid process of the sternum. Then, the incision continued laterally and dorsally in the direction of the armpit and caudal to the scapula. A second incision was made around the elbow joint and in the medial aspect of the brachium to connect it with the first incision. The skin was then separated from the platysma and removed. Lymph nodes were searched at their anatomical location, mainly following the veins. The axillary lymph center was searched following the axillary and lateral thoracic vessels. Then, the costochondral joints were carefully cut in order to expose the thoracic cavity. The diaphragm was separated from the thoracic wall and blunt dissection was used to identify the lymph nodes inside the thorax. Postmortem coloring procedures for the lymphatic system were not performed because the cats were evaluated after several hours of dead.

The length, height, and width of each LN were measured using a manual dial caliper (Vernier 0 – 150mm/ 0.02 high precision). The length was defined as the largest dimension in the rostro/craniocaudal plane. Height was measured at the thickest point in the dorsoventral plane. Width was measured at the thickest point in the mediolateral plane. The number of lymph nodes per lymph center, as well as the anatomical landmarks, shape, and size was recorded.

Imaging study

Animals

Healthy cats older than 1 year of age were recruited at the Fundació Hospital Clinic Veterinari of the Universitat Autònoma de Barcelona (FHCV-UAB) from staff, students, and hospital clients. The animals were considered healthy based on physical exam, biochemical profile [calcium, glucose, potassium, total proteins, alanine-amino-transferase (ALT), gamma-glutamyl-transferase (GGT), cholesterol, urea, creatinine] and complete blood count. A SNAP® test to rule out the presence of feline immunodeficiency virus (FIV) antibodies and feline leukemia virus (FeLV) antigens, and a PCR test to rule out the presence of *Bartonella* sp were also performed.

Computed Tomography

The animals were sedated with an intramuscular administration of midazolam[1] (0.2mg/kg), butorphanol[2] (0.4mg/kg), and ketamine[3] (5mg/kg). Anesthesia was induced with Isoflurane[4] 5% dosage 100% O_2 at 4L/min and maintained with Isoflurane 1.5 – 2% in 100% of O_2 at 2L/min. The patients were positioned on the CT table in dorsal recumbency with the forelimbs and hindlimbs outstretched at the sides. A whole body scan was performed. Acquisitions were done in soft tissue algorithm, before and after the intravenous administration of 600mg/kg of Iopromide[5] (300mgI/ml) or Iopamidol[6] (300mgI/ml) in the cephalic vein. Scans were performed in a 16 slices helical CT-scanner[7] with a slice thickness of 0.625mm, interval thickness of 0.625mm, collimation pitch of 1.25mm, 120kV, 50 - 90mA, and a matrix of 512 x 512.

[1] Midazolam 15mg/3ml, Normon, Spain
[2] Torbugesic 10 mg/ml, Zoetis, Alcobendas (Madrid), Spain
[3] Imalgene 100 mg/ml, Merial, Barcelona, Spain
[4] Isoflurane, Abbott Laboratories, Berkshire, UK
[5] Ultravist® 300mg/ml, Bayer pharma AG, Berlin, Germany.
[6] Scanlux® 300mg/ml, Sanochemia pharmazeutika, Neufled/Leitha, Austria.
[7] General Electric® Brivo CT 385.

Image analysis: For each lymph node identified, CT characteristics and measurements were performed following previously described methods for the measurement and comparison of CT images (Nemanic & Nelson, 2012). All data were recorded for further analysis using an image archiving and communication system software.[8] Measurements were performed following previous descriptions for dogs (Beukers, Vilaplana Grosso, & Voorhout, 2013; Nemanic & Nelson, 2012). The length was determined using two previously reported methods; (1) Calculated CT LN length: multiplying the slice thickness by the number of transverse images that contained the lymph node; and (2) Measured CT LN length: in a multiplanar reconstruction (MPR) to generate a sagittal image of the LN at its maximal dimension from rostral/cranial to caudal; an electronic caliper was placed from the rostral/cranial to the caudal border to measure the length of the lymph nodes. Height and width were measured in transverse images at the rostral/cranial, middle, and caudal aspects of each lymph node. Height was defined as the distance from the ventral to the dorsal border in each position and width was defined as the distance from the medial to the lateral border in each position. The highest values were used for the statistical analysis. The short / long (S/L) axis ratio was calculated using the higher value of height divided by the value of length obtained in the multiplanar reconstruction and this was calculated for each LN. The shape of the lymph nodes was classified as rounded, elongated, or miscellaneous as previously reported by Beukers et al. (2013) and Nyman, Kristensen, Skovgaard, & McEvoy (2005). A lymph node was defined as rounded when the short axis/long axis ratio was >0.5. A short axis/long axis ratio ≤0.5 was used to classify a lymph node as elongated. Lymph nodes with a multilobular structure that did not fit the ratio were classified as miscellaneous. The attenuation (Hounsfield units) was determined by placing a circular/oval region of interest (ROI) of 2-4mm^2 over the same rostral/cranial, middle and caudal transverse slice where width and height measurements were performed. In small LN, ROIs were made as large as possible inside the lymph node margins. Attenuation measurements were performed before and following the administration of contrast medium. Mean

[8] Centricity PACS-IW, GE healthcare.

values for attenuation pre- and postcontrast were calculated using the three previously obtained measures. As in previously reported studies, lymph nodes attenuation was compared with the surrounding muscles and was classified as isoattenuating (same attenuation), slightly hypoattenuating (minimal homogeneous decrease in attenuation), hypoattenuating (marked homogeneous decrease in attenuation), hyperattenuating (homogeneous increase in attenuation) and heterogeneous (single or multiple areas of different attenuation within the LN). Following the administration of contrast medium the attenuation was classified as homogeneous, mildly heterogeneous (small, multiple areas of different contrast enhancement), heterogeneous (large, multiple areas of different contrast enhancement), and peripheral enhancement (contrast enhancement in a ring-like distribution with a hypoattenuating center). These features were used to establish CT reference values for feline lymph nodes.

Ultrasonography

Immediately after the CT scan and with maintained anesthesia, an ultrasound scan was performed to each animal. The hair of the ventral aspect of the neck was clipped from the intermandibular region to the mid-cervical region and extended laterally to include the parotid region (at the level of the mandibular angle). The axillary region extending ventrally to the sternum and the cranial aspect of the shoulders extending dorsally following the scapula at both sides were also clipped. The animals were positioned in dorsal recumbency with the neck extended and the forelimbs slightly extended to the sides. Right and left lateral recumbency was also used when the dorsal cervical LNs were assessed. Examinations were performed using an Esaote Mylab70 Xvision® machine with a 4 – 13MHz frequency linear transducer. Technical settings were adjusted to improve and obtain the optimal images of the LN in all the animals. Acoustic coupling gel[9] was generously applied to ensure an adequate skin-transducer contact. Sagittal and transverse images of each lymph node were recorded.

[9] Transonic gel®, Telic, Barcelona, Spain

Image analysis: for the sagittal plane, the transducer was placed with the guide pointing rostral/cranial, parallel (or slightly oblique) to the spine, and an image including the largest measurement of the LN was recorded. Measurements in this image were performed using an electronic caliper from the rostral/cranial to the caudal border (long axis) and was defined as the length of the LN. A second measurement was performed in the same image perpendicularly to the first measure at the point of maximum thickness (ventral to dorsal) and was defined as the height (short axis) of the LN. With these two measurements, the ratio short axis/long axis was calculated. For the transverse plane, the transducer was rotated 90º with the guide towards the right side of the patient selecting an image that contained the largest portion of the lymph node. A measurement was performed from medial to lateral and was considered as the LN width.

For each lymph node, echogenicity was recorded as hypoechoic, isoechoic, hyperechoic, or heterogeneous when compared to surrounding fat tissue. The presence of a hyperechoic central line that corresponds with the hilus was also recorded. The shape of each lymph node was evaluated following the same criteria as in CT. Margins were defined as smooth or irregular.

Statistics

Data were digitalized using Excel (2010)[10]. Statistical analyses were performed using the free available statistics software R (2015)[11]. The frequency of LNs identification, mean and SD of attenuation values pre and postcontrast administration, echogenicity, and the mean and SD of LNs measurements was calculated. Wilcoxon Signed Rank Test was used to compare the pair distribution between the calculated length and the length obtained with the multiplanar reconstruction (length MPR) of the LNs on CT images. After this, the length MPR was used in the pair comparison with the US. The rest of the LNs measurements (width and height) between TC and US were also compared with Wilcoxon Signed Rank Test. Mann-Whitney U test was used to compare the pair distribution of the LN measurements

[10] Microsoft office Excel, 2010

[11] R versión 3.2.3 (2015-12-10). Copyright © 2015, the R foundation for statistical computing.

(length MPR, width, and height) between TC and anatomy, and between US and anatomy. Each measurement was compared individually for each lymph center and not for the whole sample of identified LNs (No Post-Hoc corrections were used). A P value <0.05 was considered statistically significant.

Results

Animal description

Anatomic study: six feline cadavers were included. Causes of death were not related to neoplastic or inflammatory diseases according to the necropsy [heart failure (n=2), kidney failure (n=2), poisoning (n=1) and unknown (n=1)]. The average age was 6.8 years (range 1 – 16). Five cats were domestic shorthairs and one cat was a British longhair.

Imaging study: thirty cats were recruited. Age and weight averages were 3.7 years (range 1.5 – 17) and 4.4kg (SD 1.1), respectively. Twenty-nine cats were domestic shorthairs and 1 cat was a Persian. The group included 16.7% entire males (n=5), 20.0% neutered males (n=6), 30.0% entire females (n=9), and 33.3% neutered females (n=10). Biochemical determinations and complete blood count were within normal limits. All cats were negative for FIV/FeLV and *Bartonella sp.* tests. Table 1 shows the mean and SD for the length, width, and height, as well as the results of the statistical comparisons among techniques; table 2 shows the attenuation values (Hounsfield Units), and table 3 the ultrasonographic features.

Parotid lymph center (lymphocentrum parotideum)

In the anatomic study, the right and the left parotid lymph nodes (PLNs) were identified in 3 cadavers with a total of 6 PLNs (3 right and 3 left). All were round or ovoid, located rostral to the parotid salivary gland, and in 1 cat both PLNs were covered by the salivary gland. The parotid salivary gland duct runs

ventrally to the LN and the temporal superficial vessels run dorsally. Fat tissue could be found around the LNs.

On CT images, the right and left PLNs were identified in 8 cats, only the right PLN in 1 cat, and only the left PLN in 4 cats with a total of twenty-one LNs identified (9 right and 12 left) in 13/30 cats. The close contact with the parotid salivary gland made the differentiation between the LN and the glandular tissue challenging. However, the administration of contrast medium improved the visualization of these lymph nodes in some animals. When visible, they were ovoid in shape, homogeneously isoattenuating to the surrounding soft tissue in precontrast and showed homogeneous enhancement after contrast administration.

On US images, only 1 parotid LN was identified in 1/30 cats. It appeared elongated, slightly hypoechoic compared to fat tissue, surrounded by a thin hyperechoic halo, and located rostral to the parotid salivary gland (Figure. 1).

Mandibular lymph center (lymphocentrum mandibulare)

Four LNs were identified in the 6 cadavers for this lymph center. They correspond to the right lateral (RL), right medial (RM), left lateral (LL) and left medial (LM) mandibular LNs (MnLNs). Each pair of LNs (medial and lateral) were located on each side of the mandibular angle; the linguofacial vein ran between the medial and lateral MnLNs, being the most important anatomic landmark. All the MnLNs showed an elongated shape.

On the CT images, the four MnLNs were identified in the 30 cats with a total of 120 LNs. They were most frequently isoattenuating to the surrounding muscles, which made them challenging to identify in thin cats. After contrast administration, a homogeneous contrast enhancement was commonly observed. In the thin cats with isoattenuating LNs, the postcontrast images helped in the localization of these in the pre-contrast images.

On the US images, the four MnLNs were also identified in the 30 cats with a total of 120 LNs. They appeared elongated in sagittal and ovoid in transverse planes. As for the parotid LNs, their appearance was most frequently slightly hypoechoic in comparison to the fat tissue, surrounded by a thin hyperechoic halo. A hyperechoic central line was present in a 7.7% of the MnLNs. When

Doppler was used, on transverse images, a blood vessel was easily identified between the MnLNs compatible with the linguofacial vein (Figure. 2).

Retropharyngeal lymph center (lymphocentrum retropharyngeum)

The right and the left medial retropharyngeal LNs (MRLNs) were identified in 3 cadavers, and only the left MRLN in 2 cats for a total of 8 MRLNs (3 right and 5 left) in 5 cats. The RMRLNs and LMRLNs were located medially to the respective mandibular salivary gland and the *sternocephalicus* muscle, ventrally to the caudal aspect of the tympanic bullae, *longus colli* muscle at the level of the first 2 cervical vertebrae, and laterally to each carotid sheath. These MRLNs were commonly oval in shape. The lateral retropharyngeal LNs were not found in the anatomic study.

On the CT scans, both MRLNs were identified in the 30 cats for a total of 60 LNs. The MRLNs were frequently slightly hypoattenuating, followed by isoattenuating appearance and less frequently hypoattenuating. After contrast administration, the right and left MRLN frequently showed slightly heterogeneous contrast enhancement or homogeneous contrast enhancement, and less frequently heterogeneous contrast enhancement.

Ultrasonographically, both MRLNs were also identified in the 30 cats for a total of 60 LNs. The RMRLNs were frequently hypoechoic, and less frequently isoechoic or heterogeneous to the surrounding tissues. Meanwhile, the LMRLN was seen mainly hypoechoic. A small proportion of isoechoic or heterogeneous LMRLN was also seen.

Both MRLNs were commonly elongated (Figure. 3). In some of them a miscellaneous shape was observed. Also, in 13.3% of both right and left MRLN, a hyperechoic central line was identified.

The lateral retropharyngeal LNs were not found in this study.

Superficial cervical lymph center (lymphocentrum cervicale superficiale)

In four cadavers, one dorsal and one ventral superficial cervical lymph nodes (DSCLNs & VSCLNs) were found on both sides. Additionally, only 1 left DSCLN was seen in 2 cadavers, for a total of 18 SCLNs in 6 cadavers. The

DSCLNs were located deep to the *trapezium* and *omotransversarius* muscles, related with the superficial cervical vessels and surrounded by fat tissue. The VSCLNs were located dorsally to the junction of the superficial cervical vein with the external jugular vein. The DSCLNs were commonly miscellaneous and the VSCLNs were frequently seen with an elongated shape.

The DSCLNs and VSCLNs were commonly visualized on CT images. The most dorsally located DSCLN was found in all cats on the right side and in 29/30 cats on the left side. The most ventrally located DSCLN was found in 25/30 cats on the right side and in 24/30 cats on the left side. The VSCLNs were identified in 29/30 cats on the right side and in 25/30 cats on the left side. Both groups were more commonly observed with an isoattenuating or slightly hypoattenuating appearance. After contrast administration, they frequently showed a homogeneous contrast enhancement.

On US examination, 2 DSCLNs and 1 VSCLNs were commonly identified on each side. The most dorsally located DSCLN was found in 9/30 (30%) cats on the right side and in 6/30 (20%) cats on the left side at the level of the cranial angle of the scapula. The most ventrally located DSCLN was found in 29/30 (96.7%) cats on the right side and in 25/30 (83.3%) cats on the left side at the level of the mid-cranial border of the scapula. The identification of all the SCLNs in both sides was not possible in all the cats. One dorsal and one ventral SCLNs on each side were found in 2 cats. The identification of one right and one left DSCLNs was possible in 18 cats. The shape of the most dorsally located DSCLNs was most frequently fusiform. The most ventrally located DSCLNs were miscellaneous (from ovoid to elongated) and were the biggest of the DSCLN. These LNs were slightly hypoechoic to the surrounding fat. The VSCLNs were seen in 2/30 (6.7%) cats on each side. They were elongated and showed iso to hypoechoic appearance with smooth margins. A hyperechoic central line was visible in 1.8% of the SCLNs (Figure. 4).

Deep cervical lymph center (lymphocentrum cervicale profundum)

The middle or caudal deep cervical LNs were not visualized in either the anatomic study or in the US examination. However, in CT images one caudal deep cervical LN (CDCLN) was found in 11 cats. This CDCLN lied in the fat

tissue that is slightly cranial to the thoracic inlet, between the trachea and the *sternocephalicus* muscle. The CDCLNs were identified as elongated, isoattenuating (72.7%) or heterogeneous (18.2%) structures, and commonly enhanced homogeneously after contrast administration.

Axillary lymph center (lymphocentrum axillare)

In the anatomic study, both right and left axillary lymph nodes (AxLNs) were found in 3/6, and only the right AxLN was found in 1/6 cats, with a total of 7 AxLNs. The AxLNs were elongated or rounded (Fig. 5). The localization was immediately caudal to the axillary vessels at the level of the first intercostal space on each side of the thorax.

In CT images, both AxLNs were identified in 28/30 cats, and only the right AxLN was seen in 1/30 cats, for a total of 57 AxLNs. The presence of a central hypoattenuating area with negative attenuation values (-29.7 HU) as the attenuation of fat tissue was identified. This hypoattenuating tissue within the AxLN was surrounded by an oval ring shaped tissue that corresponded to the normal attenuation of lymphatic tissue in the periphery. The regions of interests (ROIs) for the measurement of the Hounsfield units were placed, as possible, in this peripheral tissue. However, inclusion of part of the center in smaller LN made this challenging. This explains the negative HU in the average of attenuation for these LNs. The AxLNs were seen slightly hypoattenuating (R: 48.3%; L: 50%), heterogeneous (R: 27.6%; L: 25%) or isoattenuating (R: 17.2%; L: 17.9%) in pre-contrast images. After contrast administration, the right and the left AxLN presented homogeneous contrast enhancement in 41.4% and 46.4% of the cases respectively. Peripheral enhancement was present in 41.4% of the right and 35.7% of the left AxLNs.

In US images, both AxLNs were identified in 29 cats, and only a right AxLN in 1 cat. The echogenicity of the AxLNs was the most variable among LNs. These LNs were more frequently isoechoic compared with the surrounding fat tissue. Additionally, a similar distribution of hyperechoic, hypoechoic, and heterogeneous echogenicity was also present in this group. The heterogeneous AxLNs presented a large hyperechoic center with a more

hypoechoic periphery (Figure. 5). A hyperechoic central line was identified in 13.6% of the AxLNs.

Another component of this lymph center are the accessory axillary LNs (AAxLNs). Both right and left AAxLNs were found in 1/6 cats in the anatomic study, along the lateral thoracic vessels.

On CT, the AAxLNs were easily identified. The number of these AAxLNs varied between sides (right and left) and among cats. At each side of the thorax 1 to 3 LNs were identified. A single LN located at the level of the third costocondral joint in the dorsal border of the *pectoralis profundus* muscle was seen in both sides in 21 cats. This LN appeared elongated or miscellaneous. Then one or two additional LNs were seen more caudally in 3 (2 right and 1 left), 4 (2 right and 2 left), 1 (3 right and 2 left), and 1 (2 right and 3 left) cats. The most caudal LN was seen almost reaching the costal arch and also in contact with the dorsal border of the *pectoralis profundus* muscle. The AAxLNs were more frequently isoattenuating, and less commonly slightly hypoattenuating to the surrounding muscles. After contrast, 100% of the AAxLN presented homogeneous contrast enhancement.

The frequency of visualization of these LNs using US was low. A single LN was seen in both sides in 3 cats. One and two right AAxLNs were seen in 2 cats. The AAxLN appeared most frequently hypoechoic, followed by isoechoic or heterogeneous with less frequency. They were elongated or rounded with smooth borders. No hyperechoic central line was identified in any of the LNs (Figure. 6).

Dorsal thoracic lymph center (lymphocentrum thoracicum dorsale)

The aortic thoracic and the intercostal LNs are described as components of this lymph center. However, they were not visible in either the anatomy or in the imaging study.

Ventral thoracic lymph center (lymphocentrum thoracicum ventrale)

The only member of this lymph center that was identified was the sternal lymph node (SLN). The superficial cranial epigastric LN (former xiphoid LN) and the phrenic LN were not visible in the anatomy nor in the imaging study.

The SLN was identified in 4/6 (66.7%) cadavers as an elongated or oval structure located at the dorsal aspect of the third sternebra and related with the internal thoracic vessels.

The appearance of the SLNs on CT transverse images, and on multiplanar reconstruction, was similar to the description for the AxLNs. They were frequently ovoid with soft tissue attenuation peripherally and a hypoattenuating center. Regarding their attenuation, 71.4% were classified as heterogeneous; 14.3%, 9.5%, and 4.8% were hypoattenuating, slightly hypoattenuating, and isoattenuating, respectively. On postcontrast images, the LNs showed most frequently a peripheral enhancement, and less frequently heterogeneous contrast enhancement. The rest of the SLNs showed a slightly heterogeneous (27.3%) or homogeneous (4.5%) contrast enhancement.

On the US images, the SLNs were identifed in 17/30 (56.7%) cats as isoechoic (47.0%), hypoechoic (35.3%), heterogeneous (11.8%) or hyperechoic (5.9%) with smooth borders. The SLN presented a hyperechoic central line with hypoechoic periphery in 17.6% of the LNs (Figure. 7).

Mediastinal lymph center (lymphocentrum mediastinale)

One cranial mediastinal LN (CrMLN) was identified in 5 cadavers in the anatomic study. A normal CrMLN was seen as a rounded or oval structure located in the mediastinum, between the trachea and the blood vessels.

In CT images, one CrMLN was identified in 15 cats, and 2 CrMLNs were seen in 1 cat. These LNs were slightly hypoattenuating (66.7%) or isoattenuating (33.3%). After contrast administration, the CrMLNs presented a homogenous contrast enhancement (75%) or less frequently a slightly heterogeneous contrast enhancement (25%).

Assessment of the CrMLN using US in healthy cats was not possible due to the impossibility to find an acoustic window through the normal pulmonary tissue.

Bronchial lymph center (lymphocentrum bronchale)

In the anatomic study, three tracheobronchial lymph nodes (TBLNs) were found corresponding to the right, left, and middle TBLNs, in each of the 6 cadavers. The right tracheobronchial LN (RTBLN) was visible between the main right bronchus and the azygos vein. The left tracheobronchial LN (LTBLN) was visible between the main left bronchus and the left pulmonary artery. The middle tracheobronchial LN (MTBLN) was found caudally to the carina.

In CT images, the right, left, and middle TBLNs were observed in 6, 13, and 24 cats respectively. Combinations of the frequency of identification were as follows: the three TBLNs in 5 cats, the right and left TBLNs in 1 cat, the left and the middle in 5 cats, only the middle TBLN in 14 cats, and only the left TBLN in 2 cats. The TBLNs were not visible in 3 cats. The use of postcontrast images in the localization of these LNs was fundamental. Also, the MTBLN was assessed first in sagittal images obtained with multiplanar reconstruction. On these images, the identification of the LN between the carina and the pulmonary blood vessels was easier improving its identification in other planes; the same was true for the right and left TBLNs. In precontrast images, they were commonly isoattenuating and less commonly slightly hypoattenuating. Postcontrast images commonly showed homogeneous or less commonly slightly heterogeneous contrast enhancement (Figure. 8).

Ultrasonographically it was impossible to obtain an acoustic window that allows the assessment of these lymph nodes in a healthy cat.

Statistical analysis

The means and SD for the length, height, and width measurements obtained in the anatomic and imaging studies of each lymph node are summarized in Table 1.

Measurements data from TC, US, and anatomy showed differences when compared by the Wilcoxon signed rank test (TC vs. US) and by the Mann-Whitney U test (TC & US vs. Anatomy). Those differences are shown in Table 1.

The comparison of the calculated length vs. the measured length in MPR on CT images showed statistically significant differences for the RLMnLN, MTBLN and RTBLN; and for the right and left RLNs, the most dorsally located left DSCLN and the most cranial left AAxLN. The MPR length was chosen for further comparison with US and anatomic lengths because it was considered to produce a more understandable dimension of the LN and its relative position in the body than the calculated length (the length of LNs with relative oblique position could have been underestimated with the calculated length). The length of the LNs on CT was higher than US and anatomic lengths. The highest differences were found in the MRLNs, the length in CT was 6mm larger than the length in US and anatomy.

A statistically significant difference was shown for the MnLN, MRLN, AxLN and SLNs between CT and US, and for the left MnLNs, MRLN, right and left VSCLN between CT and anatomy. In all the lymph nodes the lengths were higher on CT than on US or anatomy. The difference in lengths between US and anatomy were scarce (1 – 2mm) in most of the LN, but a statistically significant difference was observed only for the right MRLN. The length for this LN was higher in US than in anatomy (5mm).

Ultrasonographically, the LNs were relatively wider than on CT and anatomy. The highest differences were presented for the MRLNs and SCLNs. A statistically significant difference was seen in most groups of LNs, except for PLNs, VSCLNs, and AAxLNs, when comparing CT with US. When CT widths were compared with anatomy, a statistically significant difference was found only for MnLN (apart from the right lateral MnLN), left MRLN, and right TBLN. The comparison of widths between US and anatomy showed statistically significant differences for the right MnLNs, MRLNs, the most ventral right and left DSCLN, and the AxLNs.

The height was the most variable measurement among techniques showing the highest statistically significant differences among them. In the anatomic study, most of the LNs presented a height between 1.2 to 1.9mm, except the LMRLN (3.9mm) and SLN (2.3mm). These values were smaller compared with the height obtained with CT and US.

The mean and SD of the Hounsfield units, and the description of the attenuation for each group of lymph nodes is reported in Table 2. Most of the

lymph nodes were isoattenuating or slightly hypoattenuating to the surrounding musculature, and showed homogeneous contrast enhancement. Only the SLN (71.4%) and the AxLNs (R: 27.6%; L: 25%) presented heterogeneous attenuation in pre-contrast and postcontrast images.

The echogenicity and shapes percentages of the LNs are presented in Table 3. Most LNs were isoechoic or hypoechoic to surrounding tissue. The AxLN showed a high frequency of heterogeneous echogenicity compared with the rest of the lymph nodes. The majority of LNs were fusiform or rounded. Nevertheless, the MRLNs, DSCLNs, and AAxLNs had miscellaneous shape.

Discussion

In the anatomic study, the identification of most LNs was possible but not all of them could be properly dissected. A possible explanation for this is that some LNs can be very small and surrounded by a large amount of adipose tissue, making difficult to differentiate them from the fat (especially the superficial cervical, the deep cervical, and the dorsal thoracic lymph centers). The identification of the LNs from the head, neck, forelimb, and thoracic lymph centers in the cat was possible with diagnostic imaging techniques.

In this study, CT showed a higher frequency of LNs identification in comparison to US and even to the anatomic study, and that frequency was improved in postcontrast studies. The advantage of the CT over the other techniques could be due to the fact that the LNs are well-vascularized structures. Organs with good blood supply have an optimal enhancement after the administration of contrast medium which makes them easier to depict, as previously reported for the TBLN (Dennler et al., 2013). However, when the LNs were located close to another well-vascularized structure (e.g. salivary gland), to differentiate it from the glandular tissue was challenging (e.g. PLN and LRLN). Another important fact is the body condition; adipose tissue provides a good contrast in CT images. When LNs are surrounded by a fair amount of fatty tissue, their visualization improves as previously reported in dogs (Beukers et al., 2013; Rossi, Patsikas, & Wisner, 2011). However, a large amount of fat around the LNs could reduce the differentiation during the US evaluation.

The PLNs were difficult to identify in all the techniques. Their close anatomic relationship with the parotid salivary gland most likely impaired the visualization and correct measurement of this LN in CT images; a similar situation has been reported in dogs (Kneissl & Probst, 2007). The identified PLNs were surrounded by an optimal amount of fatty tissue that clearly separated them from the parotid salivary gland.

A facial hair trimming to assess the PLNs on US images was not performed for esthetical reasons. Therefore, the low resolution of the images did not allow an accurate assessment of these LNs.

The mandibular LN could be easily visualized in CT and US in cats. Similar results have been reported in dogs (Kneissl & Probst, 2007; Nyman et al., 2005). The CT and US mean length of the right and left MnLNs in this study were shorter (10.86-11.35mm on CT and 9.01-9.87mm on US) than those reported by Sugimura et al. (1955) for the same LNs in cadavers (19mm-24mm). However, the study of Sugimura et al. included very young animals (from 1 month to 6 year-old) and this could have an influence on their results. A previous report showed that young animals usually present bigger LNs in comparison with adults (Burns, Scrivani, Thompson, & Erb, 2008).

Ultrasonographic features for the MnLNs in healthy cats have not been previously reported. In this study, an elongated, hypoechoic to isoechoic structure with smooth margins and a thin hyperechoic peripheral rim was identified. This description is similar to previous reports for dogs (Nyman et al., 2005).

On CT images, the MnLNs were frequently seen with an isoattenuating appearance. The mean HU before and after contrast administration were similar to those reported in dogs (Kneissl & Probst, 2007).

The features like attenuation, echogenicity, and size of the MRLNs in healthy cats using CT and US found in this study are similar to what have been previously described (Nemanic & Nelson, 2012; Oliveira, O'Brien, Matheson, & Carrera, 2012).

The MRLNs measurements on CT showed the highest differences when compared with US and anatomy. The natural position of the MRLN makes that the transverse images obtained on CT do not correspond to an exact transverse slice of the lymph node but rather an oblique slice of it (Nemanic &

Nelson, 2012). Besides, in US the positioning of the probe to obtain appropriate images with a maximum long axis and short axis of the MRLN can be also slightly oblique. Nemanic & Nelson (2012) reported mild to moderate heterogeneous attenuation for the MRLN in healthy cats. In our study, slightly hypoattenuating to isoattenuating MRLN were more frequently found.

To the authors' knowledge, this is the first report with the description of normal US and CT features of the superficial and deep cervical lymph nodes. We found, two dorsal SCLN and one ventral SCLN related to the superficial cervical vessels with both imaging techniques (Saar & Getty, 1982). A differentiation was made between the two dorsal SCLNs that were found. The most dorsally located were smaller than the most ventrally located. On US assessment, the cranial border of the scapula and the fat tissue cranial to the *supraspinatus* muscle were used as an anatomic landmark to identify the DSCLN. This fat tissue is also visible on transverse CT images and helped in the identification of these LNs. However, the position of the forelimbs has an influence on the relative parallel or perpendicular disposition of the DSCLN with the spine. As described for the MRLN, this natural oblique position in transverse CT images could also explain the mean differences for length, width, and height among techniques for these LNs.

The VSCLNs were identified more frequently with CT compared with the other techniques. The localization of these LNs on US images was challenging.

The identification of the AxLNs and the AAxLNs was possible using CT and US following the anatomic landmarks obtained in the anatomic study, which was compatible with previous anatomic reports (Saar & Getty, 1982; Sugimura, Kudo, & Takahata, 1956; Tompkins, 1993). Sugimura et al. (1956) reported that the AxLNs were embedded in fatty tissue and were depressed, taking an ellipsoid shape. We assumed that the depression mentioned in that report might correspond in our study to the description of fatty hilus. This could explain the iso- to hyperechoic image in US and the hypoattenuating image in CT that made their visualization challenging (Nyman & O'Brien, 2007).

There were a few differences in the size measurements of the AxLNs between anatomic and imaging studies. The height of the AxLNs was the measurement in which higher statistically significant differences were found

among techniques. The height in cadavers was significantly smaller than the height in US and CT images. Even though the cadavers were fresh and dissection was made within 24h of death, we consider that the amount of blood and lymph within the LNs were different and could influence these measurements. More studies are needed to establish this correlation in cats. The mean length of the right and left AxLNs and AAxLNs in this study is smaller than described by Sugimura (1956). Probably the difference could be explained again by the young age of the cats used in Sugimura's study, where 16/24 cats were under 8 month-old.

The ventral thoracic lymph center is formed by the sternal, phrenic, and cranial epigastric LNs (NAV, 2012; Saar & Getty, 1982; Sugimura, Kudo, & Takahata, 1959). Sugimura et al. (1959) reported a frequency of presence of 100% for the SLN, and only 4.5% and 27% for the phrenic and cranial epigastric LN, respectively. In our study, only the SLN was commonly identified. It is probable that the location of the phrenic LN, which is located close to the *foramen venae cavae* (Saar & Getty, 1982), makes it difficult to assess with US and could be very hard to delineate from the liver or the vein in CT images in healthy cats. However, its presence should be considered in cases of soft tissue nodules or masses around the foramen.

The appearance of the normal SLN was similar to the descriptions for the AxLN (a hypoattenuating central area with peripheral soft tissue attenuation on CT image; a hyperechoic center on US images). In this study a normal SLN was 12.2 X 3.8 X 5.2mm (length X width X height) in CT and 7.3 X 4.9 X 3.7mm in US. These measurements were statistically different suggesting that CT measurements were larger compared with US. This result could be possibly influenced by the US scanning plane, displaying a relative oblique angle that was not a true sagittal plane of the LN; this effect has been previously described for the jejunal LNs in dogs (Agthe, Caine, Posch, & Herrtage, 2009). In a previous study of CT measurements of the SLN in 6 cats of 8 to 12 months-old, the results were surprisinly similar to those in our study 11.9 X 3.2 X 5.1 mm (Dennler et al., 2013). Factors that could contribute to these results are unclear. However, the cats included in Dennler's study presented a relative adult weight, ranged 2.4 - 3.6 kg. In our study, the mean weight was 4.4 kg (SD 1.1).

During the assessment of the cranial mediastinum in the CT images, an ill-defined soft tissue attenuating structure was identified commonly surrounding the great vessels, trachea, and lymph nodes mixed with fatty tissue. The nature of this structure is unclear and histopathology of this region was not performed in any of the cats. We hypothesized that could be fibrous tissue, thymus gland residual tissue or mixture of lymphatic vessels, nerves, and mediastinal membranes. As a result, this soft tissue made difficult the delineation of the CrMLN. However, a slightly hypoattenuating, elongated node was identified in 53% of the normal cats. Normal CrMLNs were not visible in US due to the impossibility to find an acoustic window avoiding the pulmonary tissue. Besides, the small size of the LNs, and the amount of fat in the mediastinal space might also influence.

The TBLNs showed a 100% frequency of identification in the anatomic study, however, identification in the imaging study was challenging. Endoscopic ultrasonography has been reported as a suitable procedure to assess the TBLNs in dogs (Gaschen, Kircher, & Lang, 2003; St-Vincent & Pharr, 1998). Unfortunately, in this study, endoscopic probes were not available to evaluate the TBLNs, therefore, no information about the US features was available. The CT images before and after the administration of contrast medium allowed the assessment of the TBLNs, being the middle TBLNs the one most frequently observed (80%). Sagittal multiplanar reconstruction of CT images was a very helpful tool to localize this LN and then it was easier to assess it in other planes.

There are several limitations in this study. First, the number of cats in the anatomic study was low (n=6), this was due to the low number of cats that die of causes not related to either neoplastic or inflammatory processes. Second, an important variability in the identification of each group of lymph nodes per lymph center was present. It was not possible to ensure the same number of LNs in each cat and for both imaging techniques, which has a direct influence on the type of statistical test that can be applied. Third, all the healthy cats included in the imaging study were carefully evaluated in an attempt to avoid the inclusion of cats with lymphadenopathy. However, fine needle aspirates for histologic examination were not performed in order to avoid complications in these cats and for ethical reasons. Fourth, the assessment of the lymph

nodes features and size was made only one time by one of the authors (MT); therefore, the interobserver or intraobserver analysis could not be performed.

In conclusion, the identification of lymph nodes in the head, neck, forelimb and thorax using US and CT is possible. Cats with a high body condition provide a good contrast in CT images to identify lymph nodes due to the amount of fat tissue around them. In very thin cats, the administration of contrast medium makes a lymph node recognizable because increases its delineation and differentiation from the surrounding muscles.

The AxLN and the SLN present a relatively large and fatty hilus; this creates a different appearance on CT and US images compared to other lymph nodes.

On CT images, a multiplanar reconstruction is a very useful tool that improves the accuracy of the assessment of the lymph nodes size avoiding the relatively oblique image in transverse slices of some lymph nodes (MRLNs, SCLNs) due to their natural position in the body.

To the authors' knowledge, this is the first report of the lymph nodes dimensions for the head, neck, forelimb, and thorax lymph centers using US and CT and comparing with an anatomic study in healthy cats

References

Agthe, P., Caine, A. R., Posch, B., & Herrtage, M. E. (2009). Ultrasonographic Appearance of Jejunal Lymph Nodes in Dogs Without Clinical Signs of Gastrointestinal Disease. *Veterinary Radiology & Ultrasound*, *50*(2), 195–200.

Beukers, M., Vilaplana Grosso, F., & Voorhout, G. (2013). Computed Tomographic Characteristics of Presumed Normal Canine Abdominal Lymph Nodes. *Veterinary Radiology & Ultrasound, 54(6), 610-617*.

Burns, G. O., Scrivani, P. V, Thompson, M. S., & Erb, H. N. (2008). Relation Between Age, Body Weight, and Medial Retropharyngeal Lymph Node Size in Apparently Healthy Dogs. *Veterinary Radiology & Ultrasound Ultrasound*, *49*(3), 277–281.

Dennler, M., Bass, D. a., Gutierrez-Crespo, B., Schnyder, M., Guscetti, F., Di Cesare, A., Glaus, T. M. (2013). Thoracic computed tomography, angiographic computed tomography, and pathology findings in six cats experimentally infected with *aelurostrongylus abstrusus*. *Veterinary Radiology and Ultrasound*, *54*(5), 459–469.

Gaschen, L., Kircher, P., & Lang, J. (2003). Endoscopic ultrasound instrumentation, applications in humans, and potential veterinary applications. *Veterinary Radiology and Ultrasound*, *44*(6), 665–680.

Kneissl, S., & Probst, a. (2007). Comparison of computed tomographic images of normal cranial and upper cervical lymph nodes with corresponding E12 plastinated-embedded sections in the dog. *Veterinary Journal*, *174*(2), 435–438.

NAV. (2012). *Nomina anatomica veterinaria*. (veterinary gross anatomical nomenclature International committee, Ed.) (Fifth Edit.). Oslo: ICVGAN.

Nemanic, S., Hollars, K., Nelson, N. C., & Bobe, G. (2015). Combination of Computed Tomographic Imaging Characteristics of Medial Retropharyngeal Lymph Nodes and Nasal Passages Aids Discrimination Between Rhinitis and Neoplasia in Cats. *Veterinary*

Radiology & Ultrasound, *56*(6), 617–627.

Nemanic, S., & Nelson, N. C. (2012). Ultrasonography and noncontrast computed tomography of medial retropharyngeal lymph nodes in healthy cats. *American Journal of Veterinary Research*, *73*(9), 1377–1385.

Nemanic, S., & Nelson, N. C. (2012). Ultrasonography and noncontrast computed tomography of medial retropharyngeal lymph nodes in healthy cats. *American Journal of Veterinary Research*, *73*(9), 1377–1385.

Nyman, H. T., Kristensen, A. T., Skovgaard, I. M., & McEvoy, F. J. (2005). Characterization of normal and abnormal canine superficial lymph nodes using gray-scale B-mode, color flow mapping, power, and spectral doppler ultrasonography: A multivariate study. *Veterinary Radiology and Ultrasound*, *46*(5), 404–410.

Nyman, H. T., & O'Brien, R. T. (2007). The Sonographic Evaluation of Lymph Nodes. *Clin Tech Small Anim Pract*, *22*(3), 128–137.

Oliveira, C. R., O'Brien, R. T., Matheson, J. S., & Carrera, I. (2012). Computed tomographic features of feline nasopharyngeal polyps. *Veterinary Radiology & Ultrasound. 53*(4), 406–11.

Rossi, F., Patsikas, M. N., & Wisner, E. R. (2011). Abdominal lymph nodes and lymphatic collecting system. In T. Schwarz & J. H. Saunders (Eds.),*Veterinary computed tomography* (pp. 371 – 379). Ames : Iowa: Wiley-Blackwell.

Saar, L. I., & Getty, R. (1982). Sistema linfático de los carnívoros. In R. Getty (Ed.), *S.Sisson - J.D.Grossman. Anatomía de los animales domésticos* (Fifth edit., pp. 1811–1831). Barcelona, Spain : Masson.

St-Vincent, R. S., & Pharr, J. W. (1998). Transesophageal ultrasonography of the normal canine mediastinum. *Veterinary Radiology & Ultrasound*, *39*(3), 197–205.

Sugimura, M., Kudo, N., & Takahata, K. (1955). Studies on the lymphonodi of cats: I. Macroscopical observations on the lymphonodi of heads and necks. *Japanese Journal of Veterinary Research*, *3*(2), 90 – 104.

Sugimura, M., Kudo, N., & Takahata, K. (1956). Studies of lymphonodi of cats: II. Macroscopical observations on the lymphonodi of the body surfaces, thoracic and pelvic limbs. *Japanese Journal of Veterinary Research*, *4*(3), 101 – 112.

Sugimura, M., Kudo, N., & Takahata, K. (1959). Studies on the lymphonodi of cats: IV. Macroscopical observations on the lymphonodi in the thoracic cavity and supplemental observations on those in the head and neck. *Japanese Journal of Veterinary Research*, *7*(1-4), 27 – 51.

Tompkins, M. B. (1993). Lymphoid system. In *Atlas of feline anatomy for veterinarians* (pp. 113 – 126). Philadelphia [etc.] : W.B. Saunders Company.

Table 1. Mean and SD for length (MPR, Calculated), width, and height of the LNs of the head, neck, forelimb, and thorax. Comparison among techniques.

	Length (mm)							
Lymph node	CT-MPR m (SD)	CT-Calc. m (SD)	US m (SD)	Anatomy m (SD)	MPR vs. Calc. (A)	CT-MPR vs. US (A)	CT-MPR vs. Anatomy (B)	US vs. Anatomy (B)
RP	5.56 (1.26)	6.57 (1.85)	-	5.00 (0.85)				
LP	5.62 (2.05)	6.37 (2.17)	10.00 (NC)	4.90 (0.26)				
RMMn	11.04 (3.03)	11.41 (3.47)	9.83 (2.84)	8.28 (4.82)	*	**		
RLMn	10.86 (3.23)	11.63 (3.92)	9.71 (2.28)	9.87 (2.24)		*		
LMMn	11.35 (2.77)	11.42 (3.65)	9.01 (2.67)	10.33 (3.28)		**	**	
LLMn	11.32 (2.45)	11.38 (3.35)	9.87 (2.08)	9.67 (2.75)		**	**	
RMR	21.25 (4.27)	18.63 (6.19)	13.38 (3.84)	7.63 (4.65)	**	**	**	*
LMR	20.42 (3.38)	17.77 (5.85)	14.26 (3.82)	13.90 (4.95)	**	**	*	
RDSC[1]	8.18 (3.65)	8.35 (3.57)	7.37 (4.39)	-				
RDSC[2]	6.73 (3.19)	8.30 (4.22)	8.38 (3.60)	9.35 (4.11)				
RVSC	7.92 (2.21)	8.18 (2.70)	10.15 (1.20)	11.25 (2.88)			*	
LDSC[1]	8.44 (4.02)	8.04 (3.98)	6.34 (2.39)	-				
LDSC[2]	6.03 (3.00)	7.54 (3.15)	7.48 (3.55)	7.55 (3.18)	**			
LVSC	8.28 (2.07)	8.72 (2.40)	9.70 (1.27)	12.07 (1.54)			**	
CDC	7.49 (3.81)	8.13 (3.64)	-	-				
RAx	8.82 (1.98)	9.62 (4.01)	7.80 (1.96)	8.28 (3.80)		**		
LAx	9.24 (2.01)	9.73 (2.47)	7.23 (1.73)	8.80 (2.79)		**		
RAAx[1]	14.18 (4.65)	14.48 (4.62)	9.30 (5.63)	17.00 (NC)				
RAAx[2]	6.69 (2.47)	7.80 (3.92)	6.30 (NC)	-				
LAAx[1]	13.43 (6.07)	13.71 (5.57)	9.77 (2.65)	5.9 (NC)	**			
LAAx[2]	9.54 (5.28)	9.80 (5.14)	-	-				
LAAx[3]	4.60 (NC)	5.00 (NC)	-	-				
S	12.24 (3.25)	13.59 (5.43)	7.35 (2.42)	8.62 (3.83)		**		
CrM	8.14 (4.03)	8.02 (4.09)	-	5.66 (2.44)				
MTB	4.82 (1.26)	5.59 (1.88)	-	6.32 (3.07)	*			
RTB	4.03 (0.77)	4.40 (1.13)	-	5.20 (2.41)	*			
LTB	5.62 (2.12)	5.86 (2.43)	-	6.45 (3.15)				

Continuation table 1. Mean and SD for length (MPR, Calculated), width, and height of the LNs of the head, neck, forelimb, and thorax. Comparison among techniques.

	Width (mm)						**Height (mm)**					
Lymph node	CT m (SD)	US m (SD)	Anatomy m (SD)	CT vs US (A)	CT vs Anatomy (B)	US vs Anatomy (B)	CT m (SD)	US m (SD)	Anatomy m (SD)	CT vs US (A)	CT vs Anatomy (B)	US vs Anatomy (B)
RP	3.52 (0.63)	-	3.17 (1.36)				4.43 (1.24)	-	1.43 (0.51)		*	
LP	3.19 (0.68)	9.30 (NC)	2.23 (0.55)				4.74 (1.15)	3.80 (NC)	1.30 (0.61)		*	
RMMn	5.71 (1.78)	6.83 (2.07)	4.38 (1.46)	**		**	2.87 (1.13)	2.66 (0.95)	1.60 (0.30)		**	**
RLMn	6.53 (1.65)	7.85 (1.95)	4.63 (0.82)	**	**	**	3.22 (0.95)	2.84 (0.81)	1.72 (0.41)	*	**	**
LMMn	5.40 (1.67)	6.23 (1.53)	4.42 (1.26)	**	**		2.84 (0.99)	2.51 (0.55)	1.70 (0.24)	*	**	
LLMn	6.88 (1.82)	7.60 (1.93)	4.23 (0.90)	**	**		3.43 (0.98)	3.05 (0.76)	1.52 (0.38)	**	**	
RMR	6.10 (8.54)	13.33 (3.22)	4.67 (3.76)	**		*	11.92 (2.41)	4.49 (1.14)	1.80 (0.82)	**	**	**
LMR	4.79 (2.03)	11.62 (2.46)	7.38 (2.73)	**	*	**	11.95 (2.47)	4.40 (1.37)	3.94 (3.16)	**	**	
RDSC[1]	4.56 (1.94)	8.21 (3.12)	-	**			4.85 (2.96)	2.51 (0.70)	-	**		
RDSC[2]	4.55 (1.05)	10.38 (5.21)	2.75 (2.09)	**		**	11.53 (4.80)	2.88 (0.79)	1.32 (0.85)	**	**	*
RVSC	3.72 (0.83)	6.60 (2.12)	3.12 (1.00)				4.00 (1.96)	3.40 (0.57)	1.20 (0.44)		**	
LDSC[1]	4.73 (1.96)	7.50 (3.97)	-	**			5.40 (2.26)	2.34 (0.66)	-	**		
LDSC[2]	4.36 (1.06)	7.98 (4.47)	2.85 (1.70)	*		**	10.36 (4.24)	2.40 (0.64)	1.25 (0.76)	*	**	*
LVSC	3.86 (1.21)	8.60 (3.11)	3.6 (1.79)				4.04 (1.70)	4.60 (0.28)	1.45 (0.98)		**	
CDC	3.19 (1.11)	-	-				3.38 (2.43)	-	-			
RAx	3.18 (1.02)	4.93 (1.08)	3.25 (1.21)	**		*	4.03 (1.48)	3.30 (0.97)	1.20 (0.36)	*	**	**
LAx	3.91 (1.45)	4.73 (1.20)	2.40 (0.66)	*		**	4.51 (1.65)	3.52 (1.12)	1.20 (0.17)	*	**	**
RAAx[1]	3.03 (1.04)	5.88 (2.14)	1.40 (NC)				4.38 (1.98)	2.48 (1.31)	0.70 (NC)			
RAAx[2]	2.81 (1.28)	6.50 (NC)	-				3.50 (1.24)	1.30 (NC)	-			
LAAx[1]	3.09 (1.13)	6.50 (1.59)	3.20 (NC)				3.98 (1.73)	2.87 (0.85)	2.00 (NC)			
LAAx[2]	2.85 (1.00)	-	-				3.65 (0.59)	-	-			
LAAx[3]	2.70 (NC)	-	-				4.10 (NC)	-	-			
S	3.88 (1.27)	4.96 (1.21)	4.28 (2.13)				5.20 (1.46)	3.72 (1.18)	2.25 (0.42)	*	**	*
CrM	3.26 (1.24)	-	3.84 (2.13)				3.42 (1.67)	-	1.88 (1.25)		*	
MTB	3.23 (0.99)	-	2.55 (1.13)				2.42 (0.59)	-	1.23 (0.50)		**	
RTB	3.87 (1.19)	-	2.03 (0.61)		**		3.25 (0.57)	-	1.20 (0.51)		**	
LTB	3.19 (1.12)	-	2.60 (1.26)				3.01 (1.00)	-	1.15 (0.33)		**	

RP: right parotid, LP: left parotid, RMMn: right medial mandibular, RLMn: right lateral mandibular, LMMn: left medial mandibular, LLMn: left lateral mandibular, RMR: right medial retropharyngeal, LMR: left medial retropharyngeal, RDSC1 and RDSC2: right dorsal superficial cervical, RVSC: right ventral superficial cervical, LDSC1 and LDSC2: left dorsal superficial cervical, LVSC: left ventral superficial cervical, CDC: caudal deep cervical, RAx: right axillary, LAx: left axillary, RAAx1 and RAAx2: right accessory axillary, LAAx1, LAAx2 and LAAx3: left accessory axillary, S: sternal, CrM: cranial mediastinal, MTB: medial tracheobronchial, RTB: right tracheobronchial, LTB: left tracheobronchial. NC: not calculated.

* p-value < 0.05

** p-value < 0.01

(A) Wilcoxon Signed Rank Test

(B) Mann-Whitney U Test

Table 2. Computed tomographic characteristics of the lymph nodes of the head, neck, forelimb, and thorax of healthy cats.

Lymph node	HU Precontrast				HU Postcontrast				Attenuation Precontrast (%)					Attenuation Postcontrast (%			
	Mean	SD	Min	Max	Mean	SD	Min	Max	Iso	S Hypo	Hypo	Hyper	Heter	Hom	S Het	Het	Peri
RP	36.52	9.53	18.67	50.67	131.67	55.46	65.00	257.67	88.89	11.11	0.00	0.00	0.00	100.00	0.00	0.00	0.00
LP	33.94	7.16	20.33	44.00	100.03	30.99	45.33	154.33	83.33	16.67	0.00	0.00	0.00	83.33	0.00	16.67	0.00
RMMn	38.74	11.98	12.33	60.67	137.07	33.46	60.00	209.67	63.33	20.00	16.67	0.00	0.00	90.00	6.67	3.33	0.00
RLMn	36.38	12.48	12.67	63.33	130.84	34.81	52.00	203.67	63.33	20.00	16.67	0.00	0.00	86.67	10.00	3.33	0.00
LMMn	38.54	14.52	6.00	57.67	134.43	33.64	68.33	195.67	63.33	20.00	16.67	0.00	0.00	86.67	6.67	6.67	0.00
LLMn	37.08	10.86	12.00	54.33	130.15	31.64	65.67	182.67	60.00	23.33	16.67	0.00	0.00	80.00	13.33	6.67	0.00
RMR	44.50	6.63	25.67	61.67	133.14	25.42	88.33	183.00	26.67	60.00	13.33	0.00	0.00	40.00	53.33	6.67	0.00
LMR	43.32	7.46	24.67	55.67	131.99	27.61	90.00	184.33	26.67	60.00	13.33	0.00	0.00	37.93	55.17	6.90	0.00
RDSC[1]	22.77	20.46	-39.67	50.00	92.71	30.12	30.33	159.67	52.00	28.00	8.00	0.00	12.00	88.00	0.00	0.00	12.00
RDSC[2]	31.71	15.52	-11.67	60.67	115.79	20.31	71.67	154.67	56.67	36.67	3.33	0.00	3.33	90.00	3.33	6.67	0.00
RVSC	32.76	13.84	1.00	59.00	122.14	28.99	60.00	177.67	44.83	37.93	10.34	0.00	6.90	79.31	10.34	6.90	3.45
LDSC[1]	25.67	23.48	-25.33	62.33	95.01	35.81	5.33	161.67	54.17	29.17	4.17	0.00	12.50	87.50	0.00	0.00	12.50
LDSC[2]	31.90	14.06	-9.00	58.33	116.09	24.08	67.00	154.67	64.29	32.14	3.57	0.00	0.00	96.43	0.00	3.57	0.00
LVSC	35.09	15.25	-19.67	51.33	119.36	31.78	52.00	176.00	56.00	28.00	4.00	0.00	12.00	80.00	8.00	8.00	4.00
CDC	33.03	19.80	-13.33	54.00	94.64	23.99	42.67	128.33	72.73	9.09	0.00	0.00	18.18	63.64	18.18	9.09	9.09
RAx	15.14	20.37	-29.67	54.33	77.62	36.51	17.33	147.67	17.24	48.28	3.45	3.45	27.59	41.38	17.24	0.00	41.38
LAx	20.08	19.43	-19.33	53.67	80.88	33.38	32.00	137.00	17.86	50.00	3.57	3.57	25.00	46.43	17.86	0.00	35.71
RAAx[1]	31.43	17.03	-16.67	56.67	97.66	25.92	29.67	143.00	70.00	30.00	0.00	0.00	0.00	100.00	0.00	0.00	0.00
RAAx[2]	20.67	23.36	-19.33	51.00	91.00	31.96	38.33	134.33	77.78	22.22	0.00	0.00	0.00	100.00	0.00	0.00	0.00
LAAx[1]	30.09	19.75	-35.67	57.00	96.44	26.00	26.67	150.67	70.00	30.00	0.00	0.00	0.00	100.00	0.00	0.00	0.00
LAAx[2]	31.29	15.78	-4.00	48.67	99.75	34.99	50.00	154.33	87.50	12.50	0.00	0.00	0.00	100.00	0.00	0.00	0.00
LAAx[3]	40.33	NC	40.33	40.33	86.33	NC	86.33	86.33	100.00	0.00	0.00	0.00	0.00	100.00	0.00	0.00	0.00
S	-9.43	27.75	-55.67	33.33	82.23	45.28	-12.33	181.67	4.76	14.29	9.52	0.00	71.43	4.55	27.27	0.00	68.18
CrM	30.21	11.92	10.67	52.00	96.08	37.40	33.00	174.67	75.00	25.00	0.00	0.00	0.00	75.00	25.00	0.00	0.00
MTB	20.10	18.93	-26.00	50.67	85.76	26.59	43.33	134.67	62.50	33.33	4.17	0.00	0.00	87.50	12.50	0.00	0.00
RTB	28.95	15.92	12.33	56.67	105.66	13.04	84.33	120.00	66.67	33.33	0.00	0.00	0.00	83.33	16.67	0.00	0.00
LTB	18.53	22.35	-39.67	39.67	90.25	47.31	4.67	178.67	58.33	33.33	8.33	0.00	0.00	91.67	8.33	0.00	0.00

RP: right parotid, LP: left parotid, RMMn: right medial mandibular, RLMn: right lateral mandibular, LMMn: left medial mandibular, LLMn: left lateral mandibular, RMR: right medial retropharyngeal, LMR: left medial retropharyngeal, RDSC[1] and RDSC[2]: right dorsal superficial cervical, RVSC: right ventral superficial cervical, LDSC[1] and LDSC[2]: left dorsal superficial cervical, LVSC: left ventral superficial cervical, CDC: caudal deep cervical, RAx: right axillary, LAx: left axillary, RAAx[1] and RAAx[2]: right accessory axillary, LAAx[1], LAAx[2] and LAAx[3]: left accessory axillary, S: sternal, CrM: cranial mediastinal, MTB: medial tracheobronchial, RTB: right tracheobronchial, LTB: left tracheobronchial. Iso: isoattenuating, S Hypo: slightly hypoattenuating, Hypo: hypoattenuating, Hyper: hyperattenuating. Hom: homogeneous, S Het: slightly heterogeneous, Het: heterogeneous, Peri: peripheral enhancement. NC: not calculated.

Table 3. Ultrasonographic features of the lymph nodes of the head, neck, forelimb, and thorax in healthy cats.

Lymph node	Echogenicity (%)				Shape (%)		
	Isoechoic	Hypoechoic	Hyperechoic	Heterogeneous	Rounded	Elongated	Miscellaneous
RP*	-	-	-	-	-	-	-
LP	0.00	100.00	0.00	0.00	0.00	100.00	0.00
RMMn	10.00	83.33	0.00	6.67	3.33	96.67	0.00
RLMn	10.00	90.00	0.00	0.00	0.00	100.00	0.00
LMMn	10.00	86.67	0.00	3.33	0.00	100.00	0.00
LLMn	6.67	93.33	0.00	0.00	0.00	100.00	0.00
RMR	23.33	66.67	0.00	10.00	0.00	83.33	16.67
LMR	13.33	73.33	0.00	13.33	0.00	86.67	13.33
RDSC[1]	3.45	82.76	0.00	13.79	6.90	89.66	3.45
RDSC[2]	11.11	88.89	0.00	0.00	0.00	88.89	11.11
RVSC	0.00	50.00	0.00	50.00	50.00	50.00	0.00
LDSC[1]	3.85	76.92	3.85	15.38	11.54	80.77	7.69
LDSC[2]	16.67	66.67	0.00	16.67	0.00	83.33	16.67
LVSC	5000	0.00	0.00	50.00	100.00	0.00	0.00
CDC*	-	-	-	-	-	-	-
RAx	46.67	16.67	16.67	20.00	63.33	36.67	0.00
LAx	37.93	17.24	17.24	27.59	65.52	34.48	0.00
RAAx[1]	20.00	60.00	0.00	20.00	0.00	80.00	20.00
RAAx[2]	0.00	100.00	0.00	0.00	0.00	100.00	0.00
LAAx[1]	33.33	66.67	0.00	0.00	0.00	100.00	0.00
LAAx[2]*	-	-	-	-	-	-	-
LAAx[3]*	-	-	-	-	-	-	-
S	47.06	35.29	5.88	11.76	52.94	47.06	0.00
CrM*	-	-	-	-	-	-	-
MTB*	-	-	-	-	-	-	-
RTB*	-	-	-	-	-	-	-
LTB*	-	-	-	-	-	-	-

* LNs that were not identified in US.

RP: right parotid, LP: left parotid, RMMn: right medial mandibular, RLMn: right lateral mandibular, LMMn: left medial mandibular, LLMn: left lateral mandibular, RMR: right medial retropharyngeal, LMR: left medial retropharyngeal, RDSC[1] and RDSC[2]: right dorsal superficial cervical, RVSC: right ventral superficial cervical, LDSC[1] and LDSC[2]: left dorsal superficial cervical, LVSC: left ventral superficial cervical, CDC: caudal deep cervical, RAx: right axillary, LAx: left axillary, RAAx[1] and RAAx[2]: right accessory axillary, LAAx[1], LAAx[2] and LAAx[3]: left accessory axillary, S: sternal, CrM: cranial mediastinal MTB: medial tracheobronchial, RTB: right tracheobronchial, LTB: left tracheobronchial.

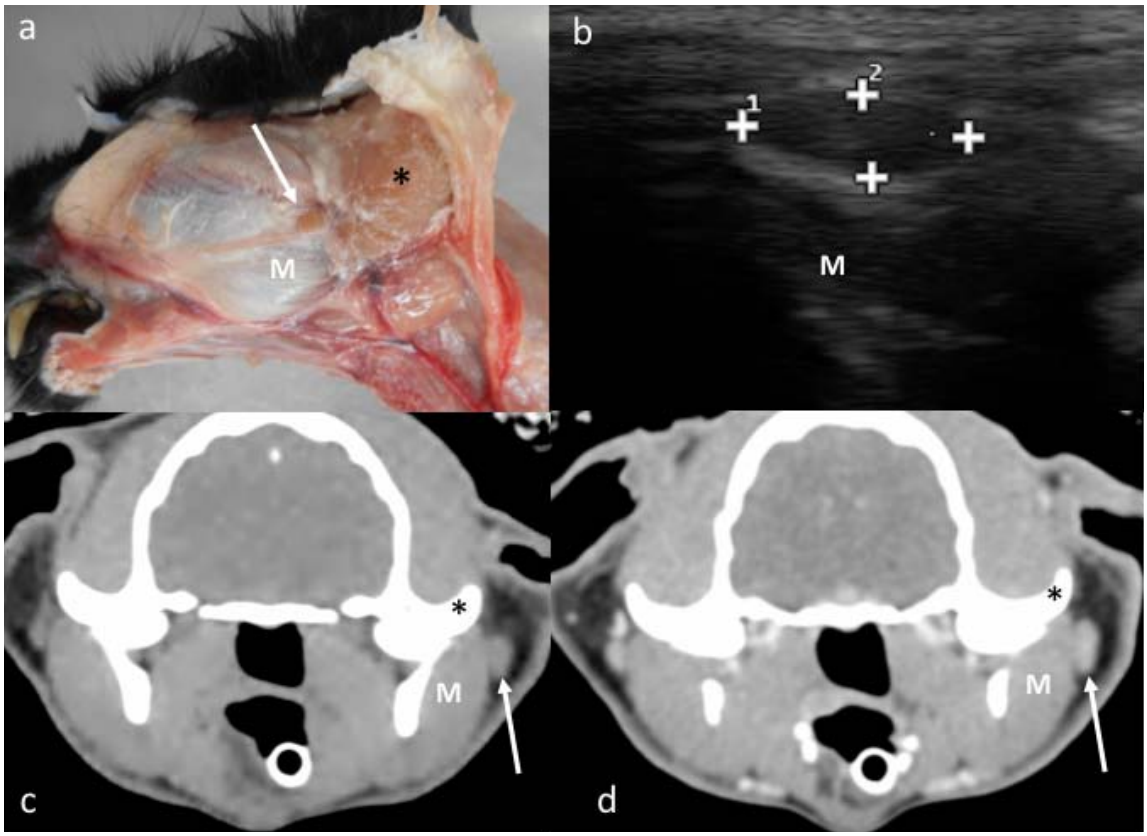

Figure1. Parotid lymph node. a. Image of the dissection showing the localization of the parotid LN (arrow) rostral to the parotid salivary gland (asterisk) and superficial to the *masseter* muscle (M). b. Ultrasonographic image showing an elongated, hypoechoic parotid LN between cursors, the *masseter* muscle (M) is seen in the far field. c – d. CT images indicating the localization of an isoattenuating parotid lymph node (arrow) in the precontrast image (c) with homogeneous contrast enhancement pattern (d). The *masseter* muscle (M) and the zygomatic arch (asterisk) are indicated.

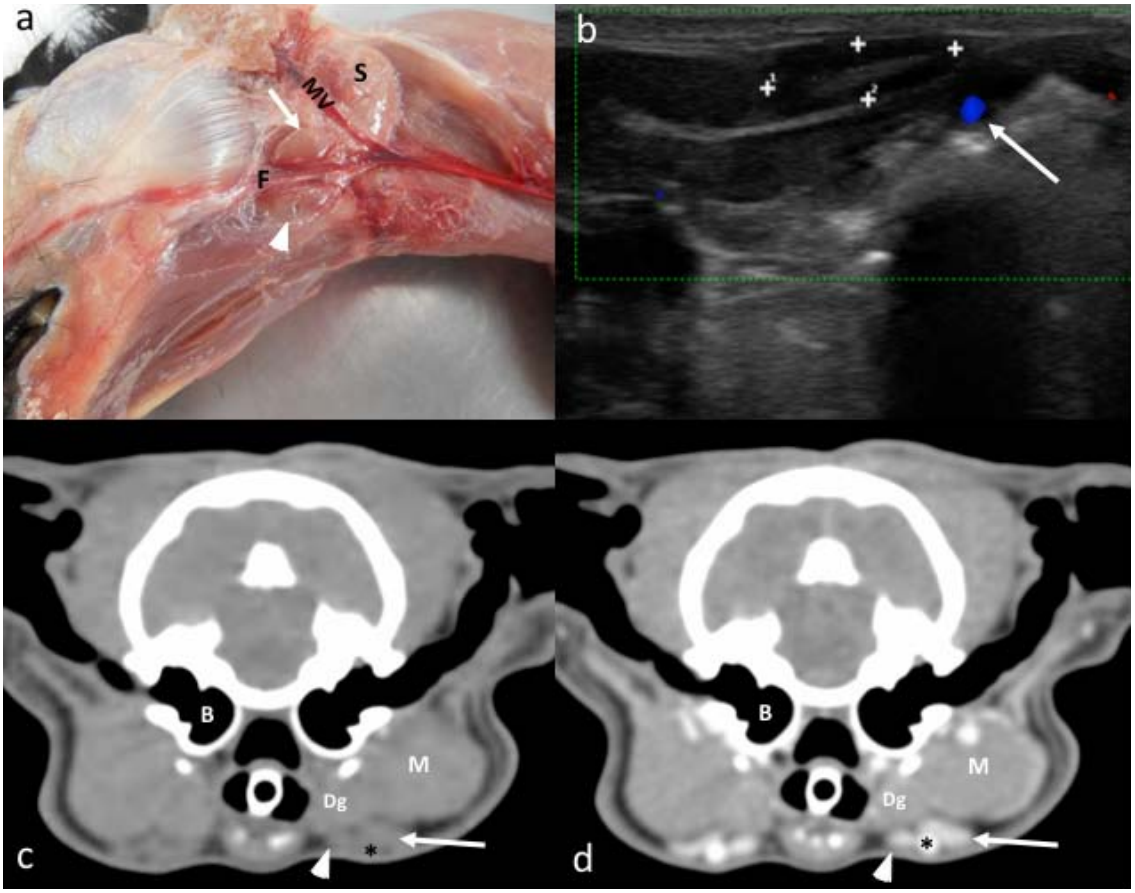

Figure 2. Mandibular lymph nodes. a. Image of the dissection showing the localization of the mandibular LNs (long arrow = lateral; arrow head = medial) rostral to the mandibular salivary gland (S). The linguofacial (F) and maxillary (MV) veins are indicated. b. Ultrasonographic image showing a transverse plane of a right lateral mandibular LN between cursors. Color Doppler shows the linguofacial vein (blue) medial to the LN. c – d. CT images indicating the localization of an isoattenuating mandibular LNs (long arrow= left lateral; arrow head= left medial) in the precontrast image (c) and homogeneous enhancement in the postcontrast image (d). The linguofacial vein is indicated (asterisk). The masseter muscle (M), digastric muscle (Dg), and tympanic bulla (B) are indicated.

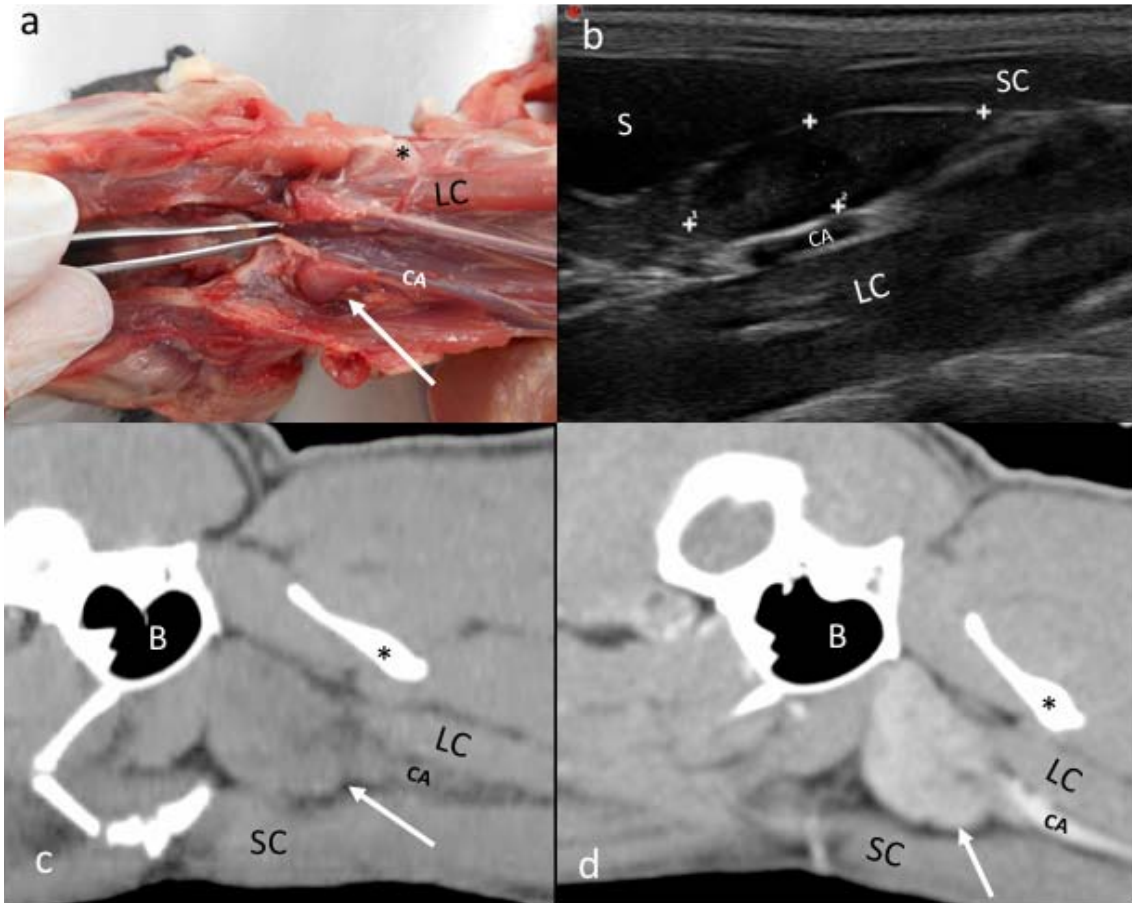

Figure 3. Retropharyngeal lymph nodes. a. Image of the dissection showing the localization of the medial retropharyngeal LNs (arrow) ventral to C1 (asterisk). The carotid artery (CA), and the *longus colli* muscle (LC) are indicated. b. Ultrasonographic image showing an elongated and hypoechoic medial retropharyngeal LN (between cursors) located caudal to the mandibular salivary gland (S), ventro-medial to the partially seen carotid artery (CA) and the *longus colli* muscle (LC). The *sternocephalicus* muscle (SC) is indicated. c – d. CT images indicating the localization of the medial retropharyngeal LN (arrow); in the precontrast image (c) the elongated isoattenuating node is visible caudo-ventral to the tympanic bulla (B), ventral to the *longus colli* muscle (LC) at the level of C1 (asterisk). The postcontrast image (d) shows a slightly heterogeneous contrast enhancement pattern. The *sternocephalicus* muscle (SC) is indicated.

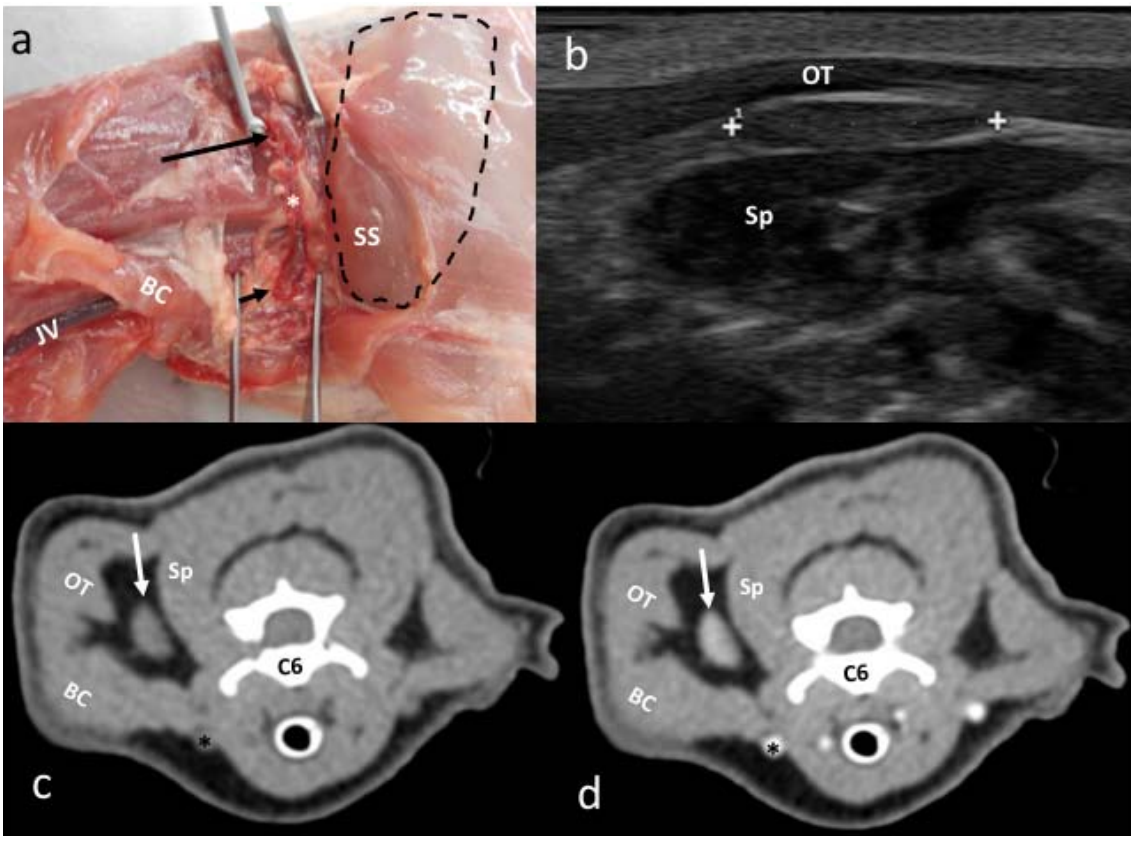

Figure 4. Superficial cervical lymph node. a. Image of the dissection showing the localization of the superficial cervical LNs (long arrow = dorsal; short arrow = ventral), cranial to the scapula (delineated area). The superficial cervical vessels (asterisk) are seen between the two nodes. The *brachiocephalic* (BC) and *supraspinatus* (SS) muscles and the jugular vein (JV) are indicated. b. Ultrasonographic image showing a fusiform, hypoechoic dorsal superficial cervical LN between cursors deep to the *omotransversarius* muscle (OT). Medial to the LN, the *splenius* muscle (Sp) is indicated. c – d. CT images indicating the localization of a slightly hypoattenuating dorsal superficial cervical LN (arrow) in the precontrast image (c), with a homogeneous contrast enhancement pattern in the postcontrast image (d). The sixth cervical vertebra (C6), the jugular vein (asterisk), the *brachiocephalic* (BC), *omotransversarius* (OT) and *splenius* (Sp) muscles are indicated.

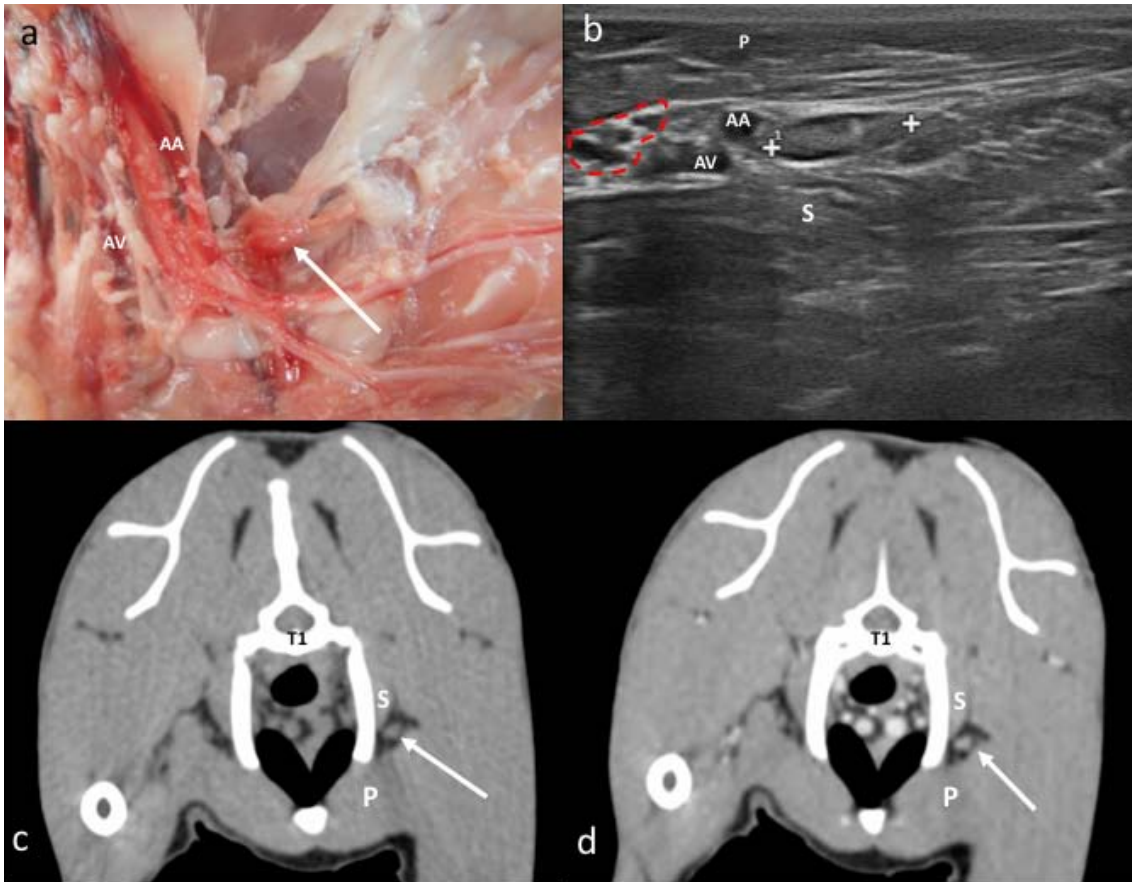

Figure 5. Axillary lymph nodes. a. Image of the dissection showing the localization of the axillary LN (arrow) embedded in the fat caudally to the axillary vessels (axillary vein= AV; axillary artery= AA). b. Ultrasonographic image showing a heterogeneous axillary LN (between cursors). A large central hyperechoic center with a hypoechoic periphery is seen. The LN is located caudal to the axillary vessels (axillary vein= AV; axillary artery= AA), the *pectoralis* muscle (P) is ventral to the LN (top part of the image is ventral. Part of the brachial plexus (delineated area) and the *scalenus* muscle (S) are indicated. c – d. CT images indicating the localization of a slightly hypoattenuating axillary LN (arrow) in the precontrast image (c) with a homogeneous contrast enhancement pattern in the postcontrast image (d). The first thoracic vertebra (T1), the *pectoralis* (P) and *scalenus* (S) muscles are indicated.

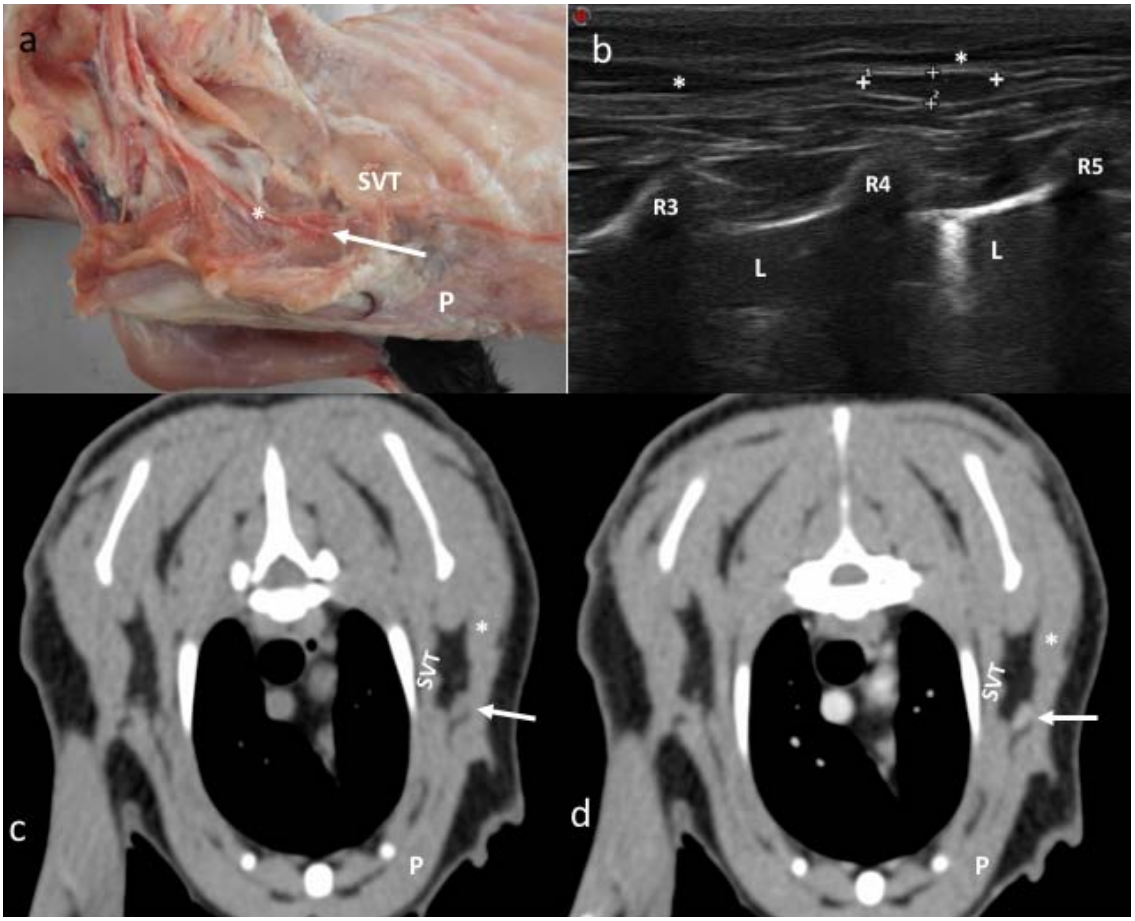

Figure 6. Accessory axillary lymph node. a. Image of the dissection showing the localization of the accessory axillary LN (arrow) around the 4th intercostal space, along the lateral thoracic vessels (asterisk), between the *pectoralis* (P) and *serratus ventralis thoracicus* (SVT) muscles. b. Ultrasonographic image showing an elongated, hypoechoic left accessory axillary LN between cursors, deep to the *cutaneous* muscles (asterisks). The third, fourth, and fifth ribs (R3, R4, R5) and the lung field (L) are indicated. c – d. CT images indicating the localization of a slightly hypoattenuating accessory axillary LN (arrow) in precontrast (c) with a homogeneous contrast enhancement pattern in the postcontrast image (d), dorsal to the *pectoralis* (P) muscle and between the *serratus ventralis thoracicus* (SVT) and the *latissimus dorsi* (asterisk).

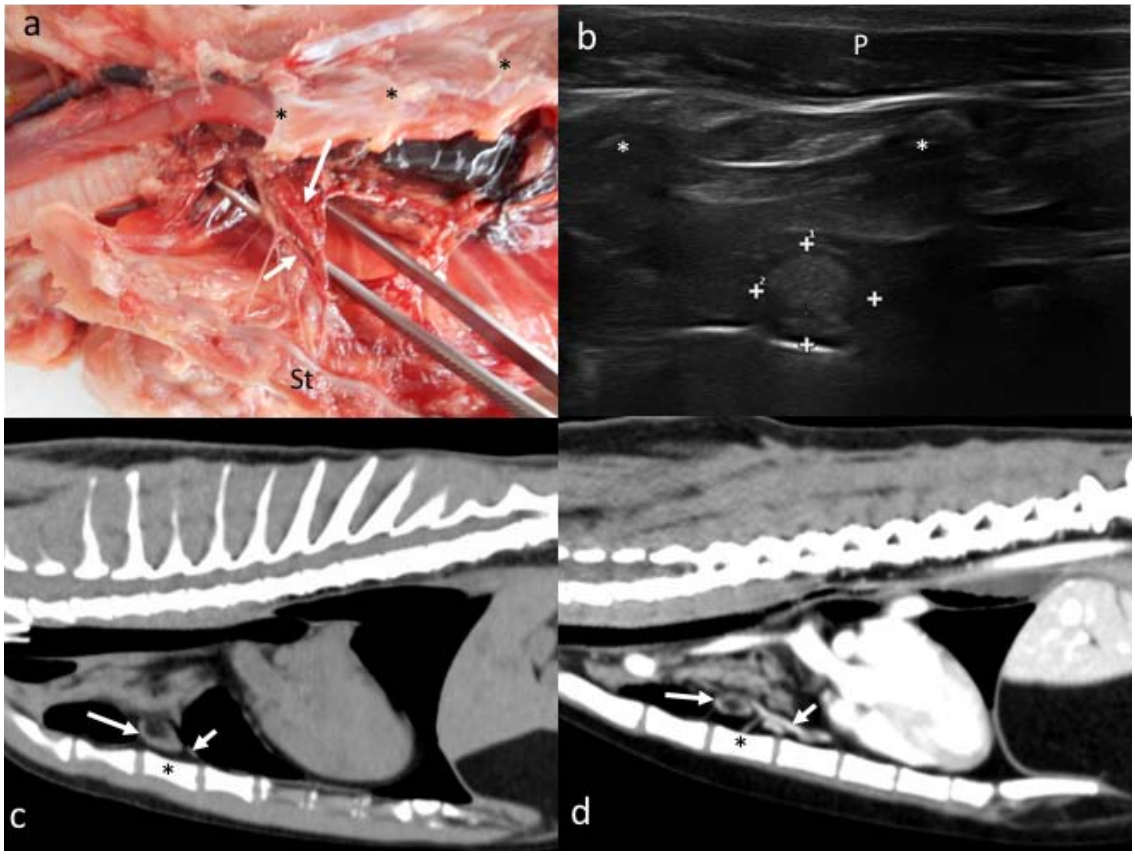

Figure 7. Sternal lymph node. a. Image of the dissection after parasternal thoracotomy showing the localization of the sternal LN (long arrow) along the internal thoracic vessels (short arrow) at the cranioventral aspect of the thorax. The sternum (St) has been ventrally pulled to allow the visualization of the SLN. b. Ultrasonographic image showing a rounded LN with a hyperechoic center and hypoechoic periphery between cursors. The second and third ribs (asterisks) and the *pectoralis* muscle (P) are indicated. c – d. CT sagittal images indicating the localization of the sternal LN in pre (c) and postcontrast (d) images (long arrows). The hypoattenuating center compatible with a fatty hilus is clearly visible. The third sternebra (asterisk) and internal thoracic vessels (short arrow) are indicated.

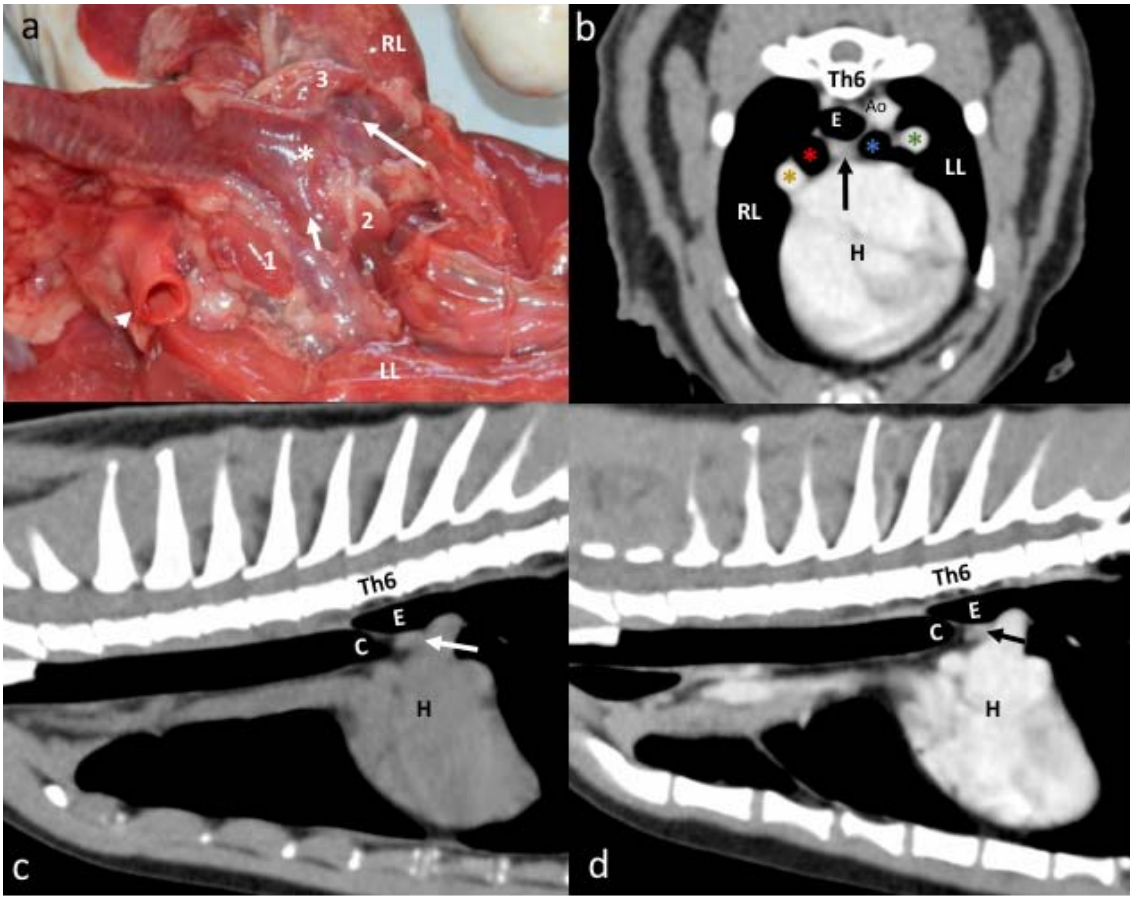

Figure 8. Tracheobronchial lymph nodes. a. Image of the dissection showing the localization of the left (1), middle (2), and right (3) tracheobronchial LNs in relation to the carina (asterisk) and the main *bronchi* (short arrow= left; long arrow= right). The aorta (arrow head), and the left (LL) and right (RL) lungs are indicated. b – d. CT images (b, transverse; c – d, sagittal) indicating the localization of an isoattenuating middle tracheobronchial LN (arrow) in the precontrast image (c) with a homogeneous contrast enhancement pattern in the postcontrast images (b & d), caudal to the carina (C) and ventral to the esophagus (E, with moderate amount of gas in the lumen). The heart (H) and sixth thoracic vertebra (Th6) are indicated. In b, the main *bronchi* (red asterisk= right; blue asterisk= left), the main pulmonary arteries (yellow asterisk= right; green asterisk= left), the aorta (Ao), and the right (RL) and left LL) lungs are indicated.

4.2. Anatomic, computed tomographic, and ultrasonographic assessment of the lymph nodes in healthy adult cats: Part II. The abdomen and hindlimb.

Abstract

The purposes of the study were to compare the dimensions of the abdomen and hindlimb lymph nodes measured with ultrasonography (US) and computed tomography (CT) with measurements obtained from an anatomic study, and to describe the features of these LNs using US and CT. In the anatomic study, 6 cadavers were dissected and in the imaging study 30 healthy cats were prospectively enrolled. In the dissection of the cadavers, at least one lymph node per lymph center was identified. Only the caudal epigastric LN (from the inguinofemoral lymph center) and the sacral LN (from the iliosacral lymph center) were not identified in any of the cadavers. All the lymph centers were visualized using CT with a variable frequency of identification. Factors like the amount of adipose tissue and the use of contrast medium subjectively improved the visualization of the lymph nodes. However, these factors were not included in the statistical analysis. Ultrasonographically, it was possible to identify almost all the LNs from each abdominal and hindlimb lymph center. The lumbar aortic, the internal iliac, the caudal epigastric, and the ischiatic LNs were not identified using US. Measurements of the length, width, and height were performed in each technique. Commonly, the measurements with CT were larger when compared with US and anatomy, although the main statistical differences were present in the comparison of height among techniques. The shape of the LNs was similar among techniques. Most of the identified LNs were elongated and a rounded shape was most common in hepatic, splenic, pancreaticoduodenal, colic, and popliteal LNs. A miscellaneous shape was commonly present in the jejunal LNs. The appearance of the LNs was mainly homogeneous in CT (before and after contrast administration) and in US. However, some LNs presented a more hyperattenuating periphery with a hypoattenuating center (before and after contrast administration). Something similar was detected with US, were some LNs presented a more hypoechoic / isoechoic periphery with a hyperechoic center (when compared with the surrounding tissue). Findings in this study indicated that the assessment of the LNs of the abdomen and hindlimb in the cat is possible with CT and US. The measurements and features reported are proposed as reference values.

Introduction

The abdominal lymph centers in the cat are divided into parietal and visceral groups as in dogs (Beukers, Vilaplana Grosso, & Voorhout, 2013; Bezuidenhout, 2013). The parietal group has four lymph centers (lumbar, iliosacral, inguinofemoral, and ischiatic), and the visceral group has three lymph centers (celiac, cranial and caudal mesenteric) (Saar & Getty, 1982). Previous studies regarding the ultrasonographic assessment of the abdominal cavity in the cat reported that the most frequently identified lymph nodes from the visceral group are the gastric, hepatic, pancreaticoduodenal, jejunal, ileocecal, and colic lymph nodes; and from the parietal group are the medial iliac and the superficial inguinal lymph nodes. The lymph nodes less frequently identified in the visceral group are the splenic and caudal mesenteric lymph nodes; and in the parietal group are the lumbar aortic, renal, internal iliac (formally called hypogastric Nomina Anatomica Veterinaria (NAV), (2012)), sacral, and caudal epigastric lymph nodes (D'Anjou, 2008; Schreurs et al., 2008). The peripheral lymph nodes of the abdomen are described as fusiform and slender in shape with ultrasonography (US). When compared with surrounding fat tissue, they appeared slightly round in shape, with regular margins and hypoechoic. Deep abdominal lymph nodes are more rounded and elongated in shape, slightly hypoechoic to surrounding peritoneum and fat and also with regular margins (D'Anjou, 2008; Mattoon, Berry, & Nyland, 2015; Nyman & O'Brien, 2007; Schreurs et al., 2008; Widmer, Mattoon, & Nyland, 2015). Getty et al. (1982) reported two lymph centers for the hindlimb in the cat, the iliofemoral and the popliteal lymph centers. The popliteal lymph node is described as an oval or rounded shaped node of variable size (short axis range of 2.8 – 6.5mm; long axis range of 4.3 – 12.0mm) in ultrasound (Lee et al., 2012).

There is scarce literature available on normal computed tomographic appearance of the abdominal lymph nodes in the cat. In dogs, abdominal lymph nodes have been described as homogeneously attenuating structures commonly elongated in shape. Some lymph nodes were slightly irregular or

relatively more hyperattenuating in the periphery than centrally before and after contrast administration (Beukers et al., 2013).

To the author's knowledge, studies comparing the dimensions and features of abdominal and hindlimb LNs between the US and CT techniques are lacking.

The aims of this study were: (i) to compare the size of the abdomen and hindlimb LNs obtained with US and CT in a group of healthy adult cats with measurements obtained from an anatomic study; (ii) to describe the features of the LNs in the abdomen and hindlimb using US and CT in a group of healthy adult cats.

Materials and methods

The ethical committee of the Universitat Autònoma de Barcelona approved this study; reference number CEAAH 2255 of September 2013. The owner consent from all the patients and cadavers included were also obtained.

Anatomical study

Animals

The same six feline cadavers included in the part I of the study (Tobón Restrepo et al., 2016) were used to perform the dissection of the abdominal and hindlimb lymph centers. The cats were prospectively included during January 2013 to June 2015 from the cadavers referred to the pathology department of the Universitat Autònoma de Barcelona within 24 hours of death.

Continuing the dissection, the skin was removed for the evaluation of the abdominal cavity as described in part I (Tobón Restrepo et al., 2016). A small incision was made immediately caudal to the xiphoid process in the *linea alba* with a 24 scalpel blade. The incision was continued caudally with Mayo

scissors until the pubic bone. Afterwards, the abdominal muscles were cut following the costal arch until the spine. Then, blunt dissection of the abdominal lymph nodes was performed with special care in avoiding great vessels rupture. Then, the skin was removed from the hindlimbs with an incision in the cranial aspect of the thigh until the talus. After that, the incision surrounded the talus and the skin was pulled off. The lymph nodes were searched following the previous anatomic descriptions (Saar & Getty, 1982; Schreurs et al., 2008; Tompkins, 1993). Measurements were recorded with the same methods as described in part I (Tobón Restrepo et al., 2016).

Imaging study

Animals

In this study, the same group of healthy cats described in the part I was used. Healthy cats older than 1 year of age were recruited at the Fundació Hospital Clinic Veterinari of the Universitat Autònoma de Barcelona (FHCV-UAB) from staff, students and owners. The healthy state of the cats was determined following the same test and protocols described in part I (Tobón Restrepo et al., 2016).

Computed tomography and ultrasonography

Preparation, anesthetic protocol, CT and US settings were the same used and described in part I (Tobón Restrepo et al., 2016).

In this study, the assessment of the abdominal cavity to identify the lymph nodes was performed following the anatomic references and literature. Using multiplanar reconstruction (MPR) on CT images, the lymph nodes along the intestinal tract (e.g. colic LNs), or along the great vessels of the abdomen (e.g. medial iliac LNs), were numbered from orad to aborad, and from cranial to caudal, respectively. In the case of the ileocecal LNs, the most ventral was

numbered as 1 and the dorsal as 2. In the case of the jejunal LNs, the LN at the medial or dorsal aspect of the jejunal vessels was numbered as 1 and the one lateral or ventral as 2. All these indications were done also during the US examination and in the anatomic study in order to get an accurate comparison of the different lymph centers.

Image analysis of the CT and the US characteristics and measurements from each lymph node identified were recorded following the same criteria reported in part I (Tobón Restrepo et al., 2016).

Statistical analysis

Microsoft Excel (2010)[12] was used to digitalize the data. Statistical analyses were performed using the free available statistics software R (2015)[13]. The frequency of LNs identification, mean and SD of attenuation values pre- and postcontrast administration, echogenicity, and the mean and SD of LNs measurements was calculated. Wilcoxon Signed Rank Test was used to compare the pair distribution between the calculated length and the length obtained in the multiplanar reconstruction (length MPR) of the LNs on CT images. After this, the length MPR was used in the pair comparison with the US. The rest of the LNs measurements (width and height) between TC and US were also compared with Wilcoxon Signed Rank Test. Mann-Whitney U test was used to compare the pair distribution of the LN measurements (length MPR, width, and height) between TC and anatomy, and between US and anatomy. Each measurement was compared individually for each lymph center and not for the whole sample of identified LNs (No Post-Hoc corrections were used). A P value <0.05 was considered statistically significant.

[12] Microsoft office Excel, 2010

[13] R versión 3.2.3 (2015-12-10). Copyright © 2015, the R foundation for statistical computing.

Results

Animal description

Anatomic study: six feline cadavers were included. Causes of death were not related to neoplastic or inflammatory diseases according to the necropsy (heart failure (n=2), kidney failure (n=2), poisoning (n=1) and unknown (n=1)). Average age was 6.8 years (range 1 – 16). Five cats were domestic shorthairs and one cat was a British longhair.
Imaging study: thirty cats were recruited. Age and weight averages were 3.7 years (range 1.5 – 17) and 4.4kg (SD1.1) respectively. Twenty-nine cats were domestic shorthairs and 1 cat was a Persian. The group included 16.7% entire males (n=5), 20.0% neutered males (n=6), 30.0% entire females (n=9), and 33.3% neutered females (n=10). Biochemical determinations and complete blood count were within normal limits. All cats were negative for FIV/FeLV and *Bartonella sp.* tests.

Table 1 shows the mean and SD for the length, width, and height, as well as the results of the statistical comparisons among techniques; table 2 shows the attenuation values (Hounsfield units), and table 3 the ultrasonographic features.

Celiac lymph center (lymphocentrum celiacum)

Gastric lymph nodes (GLNs): in the anatomic study, one round or ovoid GLN was found in 5 cadavers located always in the omentum of the gastric lesser curvature. A fair amount of fat tissue was covering the GLNs in most of the cases.

The frequency of identification of the GLNs on the CT images was higher than US. One GLN was identified in 22 cats, and two GLNs were identified in 6 cats. The GLN was not identified in 2 cats. The appearance of these LNs in

precontrast images was more frequently isoattenuating or slight hypoattenuating, and less frequently hypoattenuating or heterogeneous. A homogeneous contrast enhancement was most frequently seen, but in 14.29% of the LNs a peripheral enhancement was observed.

On the US assessment, the presence of one GLN was found in 26 cats. In 2 cats, two GLNs were seen. The GLN was not identified in 2 cats. All the identified GLNs were located in the omentum of the lesser curvature of the stomach. The probe was placed parallel to the spine immediately caudal to the xiphoid process, and then moved slightly to the left until an image with the liver to the left of the screen and the stomach to the right was obtained. The GLNs were identified in the fat tissue between the liver and the stomach. The nodes presented an ovoid shape and were heterogeneous, hypoechoic, or isoechoic in comparison to the surrounding fat tissue and with a thin hyperechoic halo. A hyperechoic central line was visible in the 33.33% of the cases (Figure 1).

Hepatic lymph nodes (HLNs): the presence of one HLN was found in 5 cadavers. They were located at the *porta hepatis*, ventral and slightly to the left of the portal vein.

On the CT images, the HLNs were seen in 22 cats. On precontrast images, the HLNs were isoattenuating (50.00%) or slight hypoattenuating (40.91%); after contrast administration they mainly showed a homogeneous contrast enhancement (86.36%), and less frequently a slightly heterogeneous (9.09%) or peripheral enhancement (4.55%). On the CT transverse images, these LNs were frequently identified dorsally and slightly to the right of the portal vein.

The frequency of identification of the HLNs on US images was similar to CT. The HLNs were visualized in 21 cats. These LNs showed more frequently a rounded shape (61.90%) and less frequently were elongated (33.33%) or miscellaneous (4.76%). Additionally, these LNs were most frequently isoechoic (42.86%) or hypoechoic (47.62%), and less frequently heterogeneous (9.52%). The HLNs were identified placing the probe parallel to the spine and caudally to the xiphoid process, and moving the probe

slightly to the right of the patient. The HLNs were seen adjacent to the portal vein while fanning slightly the probe right to left. A hyperechoic central line was visible in the 6.60% of the lymph nodes (Figure 2).

Splenic lymph node (SpLN): A single LN was identified in 2 cadavers. The SpLN was round in shape, and found embedded in the fat tissue of the splenic hilus.

On CT images, also a single SpLN was identified in 23 cats. The attenuation of the identified LNs showed the same frequency of isoattenuating (39.13%) and slightly hypoattenuating (39.13%) appearance. The remainder 21.74% of the LNs was classified as heterogeneous due to the presence of a hypoattenuating central area with soft tissue attenuation in the periphery. After contrast administration, 43.48% of the LNs presented homogenous contrast enhancement, 52.17% presented a peripheral contrast enhancement with a more hypoattenuating central area, and 4.35% were heterogeneous (Figure 3).

Ultrasonographically, this LN was identified also in 23 cats. The appearance of the SpLN was commonly hypoechoic (47.83%). However, a center isoechoic to the mesenteric fat within a hypoechoic periphery was identified in 34.78% of the SpLNs and these were classified as heterogeneous. An isoechoic and a hyperechoic appearance were seen in 8.70% of the LNs, respectively. A round shape was seen in 77.27% of SpLNs and, the remainder 22.73% was elongated. A hyperechoic central line was identified in 26.70% of the lymph nodes. The splenic vein was the main landmark to localize this LN, when present; the SpLN was adjacent to the vein in the fat tissue of the splenic hilus, close to the head of the spleen.

Pancreaticoduodenal lymph node (PdLN): was identified in all the cadavers, and was more often seen adjacent to the cranial pancreaticoduodenal vessels.

On the CT images, the PdLN was identified in 28 cats. This LN was most commonly slightly hypoattenuating (44.83%) or isoattenuating (27.59%) and less frequently heterogeneous (17.24%) or hypoattenuating (10.34%). After contrast administration, the contrast enhancement of the PdLN was variable, being homogeneous (31.03%), slightly heterogeneous (20.69%), heterogeneous (10.34%), or with a peripheral enhancement (37.93%).

On the US images, the PdLN was identified in 29 cats. A similar appearance in echogenicity to the described for the SpLN was observed for this LN. The PdLN was homogenously hypoechoic with a thin hyperechoic rim at the periphery in 37.93% of the cases. In 37.93% of the cases it presented a central area isoechoic to the mesenteric fat, surrounded by a hypoechoic ring and a thin hyperechoic rim at the periphery. This LN was found always on the right side, slightly caudal and ventral to the pylorus (figure 4).

Cranial mesenteric lymph center (lymphocentrum mesentericum craniale)

Jejunal lymph nodes (JLNs): in the anatomic study, 1 to 4 JLNs were identified. Three cadavers presented 4 JLNs. The presence of 3, 2, and 1 JLN was found in one cadaver each. These LNs were located along the jejunal vessels just proximal to the origin of the ileocolic artery. At least two large JLNs with a miscellaneous shape were identified in each animal. Smaller JLNs, rounded or elongated (Figure 5) were also present in some animals.

In the CT images, 1 to 3 JLNs were frequently identified. Three JLN were found in 15 cats. Two JLNs were present in 13 cats and only 1 JLN was seen in 2 cats. Their appearance was isoattenuating or slight hypoattenuating. More than one half of the JLNs presented a homogeneous contrast enhancement, the remainder presented slightly heterogeneous or heterogeneous contrast enhancement.

On the US assessment, 4 JLNs were present in 1 cat. The visualization of 3, 2, and 1 LNs was possible in 16, 11, and 1 cats, respectively. These LNs were mainly hypoechoic or isoechoic when compared with the surrounding fat

tissue. A hyperechoic central line was visible in only 5.20% of the LNs. The majority of the JLNs were classified as miscellaneous in shape. An elongated shape was less frequently observed.

Ileocecal lymph nodes (ICLNs): the presence of two ICLNs was observed in 4 cadavers, and only 1 ICLN was seen in 2 cadavers. They were located in the ileocecal ligament along the ileocecal vessels, one to each side of the cecum. These LNs were commonly rounded.

On the CT images, two ICLNs were identified in 26 cats, and only one in 2 cats. These LNs were located slightly caudal to the ileocolic junction always on the right side of the patient. On transverse slices, these LNs were identified in a dorsal and ventral position related to the ileocolic junction. The ICLNs were commonly isoattenuating or slight hypoattenuating, and less frequently heterogeneous. After contrast administration, the ICLNs frequently presented a homogeneous contrast enhancement, and with less frequency, these LNs showed slightly heterogeneous or heterogeneous contrast enhancement.

In the US assessment, two ICLNs were identified in 24 cats, and only one in 6 cats. These nodes were more frequently hypoechoic to isoechoic and less frequently heterogeneous in echogenicity. A hyperechoic central line was visible in 5.50% of the LNs. The ICLNs presented almost a similar distribution of shape, being rounded, elongated, or miscellaneous. The main landmark to find the ICLN was the ileocolic junction. An image of this with a sagittal plane of the ileum was obtained, and then a slight movement to the right of the patient allowed the visualization of these LNs (Figure 6).

Colic lymph nodes (CoLNs): 5 and 3 CoLNs were found in each of 2 cadavers. Additionally, the identification of 4 and 2 CoLNs was possible in one cadaver each. The CoLNs were located in the mesocolon, near the ascending and transverse colon. At least 2 LNs were bigger and more elongated than the rest, normally one near the ascending colon and one in a group of nodes located near the transverse colon.

On the CT images, the identification of 1, 2, 3, 4, and 5 CoLNs was possible in 12, 6, 4, 1, and 4 cats, respectively, for a total of 60 LNs in 27 cats. These LNs were commonly slight hypoattenuating or isottenuating. A homogeneous contrast enhancement was most frequently seen after contrast administration.

On US, only 1 CoLN could be successfully identified in 21 cats. This LN was close to the ileocolic junction. To differentiate it from the ICLNs the probe was displaced medially from the ileocolic junction instead of laterally as for the ICLNs. Frequently, the CoLNs were hypoechoic to the surrounding mesenteric fat, and less frequently isoechoic or heterogeneous. A hyperechoic central line was visible in 6.70% of these LNs. Almost half of these LNs were rounded, the rest were elongated or miscellaneous (figure 7).

Caudal mesenteric lymph center (lymphocentrum mesentericum caudale)

One to 4 caudal mesenteric lymph nodes (CMLNs) were identified in the cadavers. Two CMLNs were present in 1 cadaver. One, 3, and 4 CMLNs were found in 1 cadaver each. These LNs were located along the caudal mesenteric vessels and had an ovoid or rounded shape.

On CT images, one LN was seen in 14 cats; two, 3, and 4 CMLNs were found in 9, 3, and 2 cats, respectively. These LNs were commonly slightly hypoattenuating or isoattenuating. A homogeneous contrast enhancement was frequently seen after contrast administration. These LNs were seen on transverse images located slightly ventral to the descending colon and dorsolateral to the left aspect of the urinary bladder (figure 8).

On the US assessment, only one CMLN was identified in 10 cats. The CMLN was located between the bladder and the descending colon. This LN was commonly hypoechoic, with a thin hyperechoic rim and a fusiform elongated shape. A hyperechoic central line was visible in 3.30% of these LNs.

Lumbar lymph center (lymphocentrum lumbale)

Lumbar aortic lymph nodes (LALNs): the presence of 1, 2, and 3 small rounded LNs were seen in one cadaver each. These LNs were located along and between the aorta and caudal vena cava.

On CT images, one LALN was found in 3 cats, and 2 LALN were found in 2 cats. The presence of fat tissue around the aorta and caudal vena cava in these 5 cats gave enough contrast to differentiate these LNs from the surrounding tissue. However, the localization of the LALN on CT images was dorsal to the aorta rather then between this and the caudal vena cava. In the other 25 cats that was not the case. The LALNs were very small, rounded and slightly hypoattenuating. A homogeneous contrast enhancement was present (Figure 9).

The LALNs were not identified in the US assessment.

Renal lymph nodes (RLNs): the left and right RLNs could be identified only in 2 cadavers. These small and rounded LNs were seen in close contact with the renal vessels.

On CT images, both RLNs were identified in 5 cats, and only the right RLN was seen in 2 cats. These LNs presented a thin soft tissue attenuating periphery surrounding a hypoattenuating center. After contrast administration, a peripheral contrast enhancement was observed. These LNs were located dorsal and slightly cranially to each renal vessel.

On the US images, only the right RLN was seen in 2 cats. These LNs were hypoechoic and ovoid in shape.

Iliosacral lymph center (lymphocentrum iliosacrale)

Medial iliac lymph nodes (MILNs): One right and one left MILNs were identified in 5 cadavers. These LNs were located slightly dorsal and lateral to the external iliac arteries and extended cranially until the deep circumflex iliac vessels. These LNs were commonly elongated but some were bilobed.

On the CT images, both right and left MILNs were identified in 28 cats. The location of these LNs was as described in the anatomic study, and more specifically extending from the cranial end-plate of the seventh lumbar vertebra (L7) until the cranial end-plate of the first sacral vertebra (S1). Some MILNs were very thin in their mid-portion presenting a bilobed shape. More than a half of these LNs were isoattenuating, the rest of them were slightly hypoattenuating compared with the surrounding muscles. The MILNs presented most frequently a homogeneous contrast enhancement.

Ultrasonographically, both right and left MILNs were identified in all the cats. In 50% of the cases, the right and left MILNs were isoechoic to the surrounding tissue, the other half were hypoechoic (R: 26.67%; L: 30.00%) or heterogeneous (R: 23.33%; L: 20.00%). A hyperechoic central line was identified in 18.30% of the LNs. The MILNs were fusiform in 83.33% of the cases and miscellaneous in 16.67% (Figure 10).

Internal iliac lymph nodes (InILN): a right and left InILNs were found only in 1 cadaver, along the internal iliac vessels, and commonly presented an elongated shape.

On the CT images, both right and left InILNs were visualized in 17 cats, additionally, one right and one left InILN were identified in each of 2 cats. These LNs were located at the ventrolateral aspect of S1 (ventral to the sacral wings) along the iliac internal vessels in contact with the body of the ilium. Most of these LNs were isoattenuating, and less frequently, slightly hypoattenuating or hypoattenuating. After contrast administration, these LNs showed homogeneous contrast enhancement (Figure 11).

On US assessment, these LNs were not identified.

Sacral lymph nodes (SaLNs): these LNs were not identified in the anatomic study. On CT images, the right and the left SaLNs were identified in 2 cats. Only the right was identified in 6 cats, and only the left was identified in 2 cats. These LNs were located in the midline at the ventral aspect of S1. Most frequently, the SaLNs were isoattenuating, and a slightly hypoattenuating appearence was less common. After contrast administration, the SaLNs presented homogeneous contrast enhancement.

On US assessment, in 1/30 (3.33%) cats, a right SaLN was visualized only in sagittal plane, making possible to obtained length and height measurement. A transverse image was not possible to obtain, therefore, the width of this LN is not reported. The LN was hypoechoic, with fusiform shape and was located caudally to the aorta trifurcation.

Inguinofemoral lymph center (lymphocentrum inguinofemorale)

Superficial inguinal lymph nodes (SILNs): in the anatomic study, the right and the left SILNs were identified in 4 cadavers. The location of these LNs was cranial to the inguinal canal in contact with the external pudendal vessels, always embedded in fat tissue. Commonly, the SILNs presented fusiform shape.

On CT images, the right and left SILNs were identified in 24 cats. Other frequencies of detection are as follows: one right SILN, one left SILN, and one right and two left SILN were seen in one cat each. These LNs were identified slightly caudal and dorsal to the junction between the external pudendal and caudal epigastric vessels, ventral to the pubic bone. Commonly they were slightly hypoattenuating and, less frequently, isoattenuating. After contrast administration, most of them showed homogeneous enhancement, and they

were less frequently slightly heterogeneous or showed peripheral enhancement.

On the US assessment, the right and left SILNs were identified in 28 cats, and only the left SILN in 1 cat. Approximately half of these LNs were hypoechoic, the rest were heterogeneous (with more echogenic areas in the center of the LNs), isoechoic, and, less frequently hyperechoic. A hyperechoic central line was visible in 21.80% of these LNs (Figure 12).

Caudal epigastric lymph nodes (CELNs): this group of LNs was only identified in the assessment of the CT images. In 26 cats, one right and occasionally 3 (in 5/26) and one left and occasionally 2 (in 2/26) LNs were identified. Commonly these LNs were slightly hypoattenuating or isoattenuating in comparison with the muscle attenuation. After contrast administration, a homogeneous contrast enhancement was frequently seen; a peripheral or slightly heterogeneous contrast enhancement was less common. The location of these LNs was along the caudal epigastric vessels in the subcutaneous adipose tissue of the ventrolateral abdominal wall (at the level of L6-7) (Figure 13).

Ischiatic lymph center (lymphocentrum ischiadicum)

Ischiatic lymph nodes (IsLNs): the right and left IsLNs were found only in 1 cadaver. These rounded nodes were located at the base of the tail, partially covered by the *gluteofemoralis* muscle and embedded in adipose tissue.

On the CT images, both IsLNs were found in 1 cat. Additionally, five cats presented only the right IsLN, and 2 cats presented only the left IsLN. The location was as described in the anatomic study. These LNs were commonly rounded, isoattenuating, and less frequently slightly hypoattenuating and presented homogeneous contrast enhancement (Figure 14).

The IsLNs were not assessed with US.

Popliteal lymph center (lymphocentrum popliteum)

The right and left popliteal lymph nodes (PoLNs) were identified in all the cadavers. These nodes were commonly rounded, and were embedded in the adipose tissue located in the caudal aspect of the stifle joint and in contact with the medial aspect of the lateral saphenous vein.

On CT images, both PoLNs were identified in 29 cats. These LNs commonly presented a hypoattenuating center surrounded by soft tissue attenuation. Additionally, approximately half of them were slightly hypoattenuating compared with muscle attenuation. After contrast administration, the PoLNs showed frequently a homogeneous contrast enhancement, and less commonly, peripheral enhancement.

On the US assessment, the right and left PoLNs were identified in 29 cats, and only the left was seen in 1 cat. Commonly rounded, these nodes were the only ones in the study with varied echogenicity among patients showing similar distribution of isoechoic, hypoechoic, hyperechoic, and heterogeneous echogenicity (Figure 15).

Statistical analysis

The mean and SD of the length, width, and height measurements obtained in the anatomic and imaging studies of each LN are summarized in Table 1.

Measurements data from CT, US, and anatomy showed differences when compared with the Wilcoxon signed rank test (CT and US) and with the Mann-Whitney U test (CT, US and Anatomy). Those differences are also shown in Table 1.

In this study, the MPR length on CT images showed a better understanding of the dimensions of the abdominal LNs, as previously mentioned in the author's first report (Tobón Restrepo, et al. 2016), than the calculated length. Therefore, the MPR length was also chosen to compare between techniques

even though only a few significant differences were observed in the comparison of both CT measurements. The comparison of the MPR length of the LNs showed few differences with US and anatomy. The length of the HLN obtained with US was significantly lower when compared with CT and anatomy. Additionally, the length of the JLNs was almost 10mm higher in CT than in US, and this difference was statistically significant. The length of both ICLNs in anatomy was lower compared with CT and US showing statistical significance. Although the length of the MILNs in CT was higher than in anatomy and US, only the length of the right MILNs showed statistically significant differences between CT and anatomy.

The width of the lymph nodes in the anatomic study was often lower than the measures obtained by CT and US. Statistical significant differences were observed for the PdLN, the second and third JLNs, the ICLNs, the first CoLN, and the left ISLN. The width of the GLN in US was higher compared with CT and anatomy and the differences were statistically significant. The width of the right MILN in anatomy was slightly higher than in CT, being statistically significant.

The height was the measurement that showed more statistically significant differences among techniques. The height of the GLN, the SpLN, the PdLN, the JLNs, the left SILN, and the ICLNs was higher when obtained with CT and US than in cadavers, and showed statistically significant differences among techniques; besides, the height in CT was also statistically significantly higher than in US. Additionally, the height of the HLN, the CoLN (except the most caudal), the first CMLN, and the right MILN was higher when obtained with CT than with anatomy and the differences were statistically significant.

The mean and SD of the Hounsfield units and the description of the attenuation for each group of lymph nodes is reported in Table 2. Most of the lymph nodes were isoattenuating or slightly hypoattenuating to surrounding musculature. A negative mean HU was obtained in the left RLN and LALN. However, these LNs were very small and most of them had a hypoattenuatting center and were classified as heterogeneous.

After contrast administration, most of the LNs showed homogeneous contrast enhancement. However, the RLNs (right: 57.14%; left: 75.00%) were the group that frequently presented a heterogeneous attenuation, followed by the SpLN (21.74%), and PoLNs (17.24%). A peripheral contrast enhancement was present in 8 lymph nodes, being more frequent in the SpLN.

A description of the ultrasonographic features of the LNs in this study is summarized in Table 3. The majority of the lymph nodes were hypoechoic followed by isoechoic. A small percentage showed a center isoechoic to the mesenteric fat with a more hypoechoic periphery and a hyperechoic rim; therefore they were classified as heterogeneous. Mainly the GLNs, the SpLN, the MILNs, the SILNs, and the PoLNs presented a higher percentage of heterogeneity than the other lymph nodes.

An elongated shape was commonly found in the LNs of this study, however, rounded (HLN, SpLN, PdLN and PoLNs) and miscellaneous (JLNs, MILNs, and ICLNs) shapes were also present.

Discussion

The identification of almost all the lymph centers of the abdominal and hindlimb regions was possible in plain dissection. However, an accurate assessment of some lymph nodes (e.g. LALNs, SaLNs, and CELNs) was not achieved because their similar appearance with the surrounding fat tissue. A dyeing procedure was not performed previous to the dissection because the animals were presented to post mortem examination within 24 hours of death. In our study the mean length of the abdominal LNs in the anatomic study was smaller than the reports in the previous literature. Sugimura, Kudo, & Takahata, (1958) reported a mean length range for the abdominal LNs of 1 to 8cm. In that study, Sugimura included cats from 7 days to 10 years old, resulting in a 33.3% of cats under 1-year-old. Previous studies reported statistical significant differences in the size of LNs when comparing young vs adult animals (Burns, Scrivani, Thompson, & Erb, 2008; Krol & O ’brien, 2012).

The abdominal and hindlimb lymph nodes in dogs have been well documented in the anatomy books, and assessed using CT and US (Beukers et al., 2013; Bezuidenhout, 2013; NAV, 2012; Nyman, Kristensen, Skovgaard, & McEvoy, 2005; Rossi, Patsikas, & Wisner, 2011). In cats, the anatomic locations, landmarks, drainage areas and number of LN per lymph center have been well documented (NAV, 2012; Saar & Getty, 1982; Tompkins, 1993), however, in those anatomic references, not all the measurements of lymph nodes were reported. In our study we report not only the length of the abdominal and hindlimb LNs but their width and height as well.

To the authors' knowledge, this is the first report of the normal computed tomographic characteristics of the abdominal and hindlimb lymph nodes in the cat.

In one study from Schreurs et al. (2008), a description of the ultrasonographic characteristics of the LNs in the abdominal cavity was reported. In that study, Schreurs et al. reported the visualization of the MILNs, JLNs, HLNs, PdLN, SpLN, and LALNs with a frequency between 60 and 100% in the cat. In contrast, we found the ICLNs, CoLNs, and GLN also with a high frequency. Additionally, in our study the identification of the CMLNs was more frequent than in the Schreurs study. Differently from the Schreurs study, the LALNs, InILNs, left SaLN and left RLN were not found in our study. We hypothesize that the absence of identification of these LNs in our study, was due to the lack of contrast between these small structures and the tissues between the aorta and caudal vena cava. The use of real-time compound imaging US in Schreurs et al. study could be the reason for the differences with our study. This US modality produces a superior border definition and soft tissue contrast compared with B-Mode, and might have increased their ability to depict these LNs.

The popliteal LN was assessed in one study during ultrasound-guided intranodal injection of contrast medium, as part of a CT lymphography of the thoracic duct (Lee et al., 2012). The US characteristics were not provided but their measurements were similar to those in the present study.

Few statistical differences were found regarding the length of the LNs among techniques. The HLN and the JLNs showed lower lengths in US that in the other techniques. We hypothesized that the presence of gas in the stomach and intestinal loops, the location (HLN), and a miscellaneous shape (JLN) could have influenced the achievement of a correct acoustic window to obtain the whole length of these LNs. Similar limitation have been reported in dogs (Agthe, Caine, Posch, & Herrtage, 2009).

The mean length of the LNs on US in our study showed some differences with those reported by Schreur et al. (2008). The HLN and CMLN in our study were longer. Additionally, the PdLN and right SaLN in our study were shorter. The cause for these differences remains unclear, it is possible that the sample size, fasting period of the cats, the scanning planes, and the interobserver variability were contributing factors.

The width and height of the LNs obtained in the anatomic study were shorter than in the imaging techniques. Some of them showed statistical differences, mainly for the PdLN, JLN, ICLN, and CoLN. We hypothesized that the lack of blood perfusion and the loss of fluids after dead could contribute to these differences.

The height was the most variable measurement between CT and US. A possible explanation is that the relative orientation of LNs is likely to be influenced by patient position, scanning plane used for the assessment, and filled intestinal loops and peristalsis that could induce displacement in dorso-ventral or lateral direction of the LNs. All the cats in this study were positioned in dorsal recumbency for the acquisition of the CT images. However, avoiding an oblique orientation of the abdominal lymph nodes in CT transverse images was challenging. Similar limitations have been described in dogs (Beukers et al., 2013).

The attenuation and Hounsfield Units of the LNs in this study before contrast administration was consistent with the descriptions and values reported for dogs (Beukers et al., 2013) and for the medial retropharyngeal LN in healthy cats (Nemanic & Nelson, 2012). In our study, some of the LNs in the abdominal cavity (SpLN, RLN) and in the hindlimb (PoLN) showed a nodal

periphery isoattenuating or slightly hypoattenuating to the musculature, meanwhile the center of the node was hypoattenuating. This appearance has been reported for abdominal LNs in dogs (Beukers et al., 2013; Kneissl & Probst, 2007; Rossi et al., 2011), and for the sternal and axillary LNs in healthy cats (Tobón Restrepo et al. 2016), and it is produced by the presence of a fatty hilus. After contrast administration, a homogeneous contrast enhancement was more frequently visualized. In the LNs with a fatty hilus, a peripheral enhancement was observed. This phenomenon is due to the presence of vascularized nodal tissue in the periphery meanwhile the hilus had a less vascularized fat tissue.

The abdominal and hindlimb LNs were more frequently hypoechoic or isoechoic to the surrounding tissue. Similar descriptions have been reported for dogs (Agthe et al., 2009). The presence of a hyperechoic center, especially in the PoLNs, was most likely due to fat in the hilus (feature also visible in CT). This hyperechoic center was different than the described hyperechoic central line. This line was thin and well-defined, corresponding to the description of the hilus (D'Anjou, 2008; Nemanic & Nelson, 2012; Nyman & O'Brien, 2007; Tobón Restrepo, 2015).

The shape of the lymph nodes in this study is similar to that of the previous reports for dogs (Agthe et al., 2009; D'Anjou, 2008; Krol & O 'brien, 2012; Llabrés-Díaz, 2004; Nyman & O'Brien, 2007). The LNs that presented a rounded shape were small in size and had regular margins; the shape could be compared with the image in CT, being the same in all the cases. In previous reports, rounded lymph nodes in combination with increased size, loss of the hilus, and echotexture changes were suggestive of malignancy (De Swarte et al., 2011; Dennis, Kirberger, Barr, & Wrigley, 2010; Nyman et al., 2005). Such changes were not present in the rounded LNs in our study.

The present study included several limitations. The search of feline cadavers with cause of death other than neoplastic or inflammatory diseases was challenging resulting in a small sample size in the anatomic study. The use of ink solutions or other staining procedures in the cadavers were not performed, which could have assisted in the differentiation of the lymph nodes from the

surrounding fat tissue during dissection, especially in the sublumbar region and for the superficial lymph nodes. The animals used in the imaging study were assessed with US immediately after the CT scan. Therefore, the analysis of the CT images was not performed at the same time of the US examination, making an exact correlation in the number of LNs identified with both techniques challenging. In some of the patients, a period of apnea during the whole body CT scan was difficult to achieve, and movement artifact was present, especially in the cranial abdomen. This artifact reduced the identification of the LNs, mainly from the celiac lymph center. All the cats included in this study were fasted in order to avoid complications during anesthesia, however, some of them presented gas and feces in the colon that may have reduced the visualization of the LNs of the lumbar and iliosacral lymph centers.

In conclusion, the identification of the lymph nodes of the abdomen and hindlimb is possible with both imaging techniques. The length of the LNs is more challenging to assess with US than with CT when a multiplanar reconstruction is used. The LNs are more frequently isoattenuating to surrounding musculature in CT. However, some LNs can show a hypoattenuating center corresponding to a fatty hilus. Frequently, the abdominal and hindlimb LNs are hypoechoic or isoechoic. An elongated shape with regular margins was most frequently visible except for the JLNs, MILNs, and ICLNs that showed a miscellaneous shape and the HLN, SpLN, PdLN, and PoLNs that were rounded. To the authors' knowledge, this is the first report of the CT features of the abdominal and hindlimb LNs. Also, this is the first study comparing the size of this group of LNs with cadavers, US, and CT examinations.

References

Agthe, P., Caine, A. R., Posch, B., & Herrtage, M. E. (2009). Ultrasonographic Appearance of Jejunal Lymph Nodes in Dogs Without Clinical Signs of Gastrointestinal Disease. *Veterinary Radiology & Ultrasound*, *50*(2), 195–200.

Beukers, M., Vilaplana Grosso, F., & Voorhout, G. (2013). Computed Tomographic Characteristics of Presumed Normal Canine Abdominal Lymph Nodes. *Veterinary Radiology & Ultrasound. 54*(6), 610–617.

Bezuidenhout, A. J. (2013). The lymphatic system. In H. E. Evans & A. De Lahunta (Eds.), *Miller's anatomy of the dog* (Forth edit., pp. 535 – 562). St. Louis, Mo : Elsevier.

Burns, G. O., Scrivani, P. V, Thompson, M. S., & Erb, H. N. (2008). Relation Between Age, Body Weight, and Medial Retropharyngeal Lymph Node Size in Apparently Healthy Dogs. *Veterinary Radiology & Ultrasound Ultrasound*, *49*(3), 277–281.

D'Anjou, M.-A. (2008). Abdominal cavity, Lymph nodes, and Great Vessels. In D. Penninck & M.-A. D'Anjou (Eds.), *Atlas of small animal ultrasonography* (First edit., pp. 445 – 463). Ames : Iowa: Blackwell Publishing Ltd.

De Swarte, M., Alexander, K., Rannou, B., D'Anjou, M.-A. A., Blond, L., & Beauchamp, G. (2011). Comparison of sonographic features of benign and neoplastic deep lymph nodes in dogs. *Veterinary Radiology and Ultrasound*, *52*(4), 451–456.

Dennis, R., Kirberger, R. M., Barr, F., & Wrigley, R. H. (2010). *Handbook of small animal radiology and ultrasound : techniques and differential diagnoses* (Second edit.). Edinburgh [etc.] : Elsevier.

Kneissl, S., & Probst, a. (2007). Comparison of computed tomographic images of normal cranial and upper cervical lymph nodes with corresponding E12 plastinated-embedded sections in the dog. *Veterinary Journal*, *174*(2), 435–438.

Krol, L., & O 'brien, R. (2012). Ultrasonographic assessment of abdominal lymph nodes in puppies. *Vet Radiol Ultrasound*, *53*(4), 455 – 458.

Lee, N., Won, S., Choi, M. M., Kim, J., Yi, K., Chang, D., Yoon, J. (2012). CT thoracic duct lymphography in cats by popliteal lymph node iohexol injection. *Veterinary Radiology & Ultrasound*, *53*(2), 174–180.

Llabrés-Díaz, F. J. (2004). Ultrasonography of the medial iliac lymph nodes in the dog. *Veterinary Radiology & Ultrasound*, *45*(2), 156–165.

Mattoon, J. S., Berry, C. R., & Nyland, T. G. (2015). Abdominal Ultrasound Scanning Techniques. In J. S. Mattoon & T. G. Nyland (Eds.), *Small Animal Diagnostic Ultrasound* (Third., pp. 94 – 127). St. Louis, Missouri : Elsevier.

NAV. (2012). *Nomina anatomica veterinaria*. (Veterinary gross anatomical nomenclature International committee, Ed.) (Fifth Edit.). Oslo: ICVGAN.

Nemanic, S., & Nelson, N. C. (2012). Ultrasonography and noncontrast computed tomography of medial retropharyngeal lymph nodes in healthy cats. *American Journal of Veterinary Research*, *73*(9), 1377–1385.

Nyman, H. T., Kristensen, A. T., Skovgaard, I. M., & McEvoy, F. J. (2005). Characterization of normal and abnormal canine superficial lymph nodes using gray-scale B-mode, color flow mapping, power, and spectral doppler ultrasonography: A multivariate study. *Veterinary Radiology and Ultrasound*, *46*(5), 404–410.

Nyman, H. T., & O'Brien, R. T. (2007). The Sonographic Evaluation of Lymph Nodes. *Clin Tech Small Anim Pract*, *22*(3), 128–137.

Rossi, F., Patsikas, M. N., & Wisner, E. R. (2011). Abdominal lymph nodes and lymphatic collecting system. In T. Schwarz & J. H. Saunders (Eds.), *veterinary computed tomography* (pp. 371 – 379). Ames : Iowa: Wiley-Blackwell.

Saar, L. I., & Getty, R. (1982). Sistema linfático de los carnívoros. In R. Getty (Ed.), *S.Sisson - J.D.Grossman. Anatomía de los animales domesticos* (Fifth edit., pp. 1811–1831).

Barcelona, Spain : Masson

Schreurs, E., Vermote, K., Barberet, V., DAMINET, S., Rudorf, H., & Saunders, J. H. (2008). Ultrasonographic anatomy of abdominal lymph nodes in the normal cat. *Veterinary Radiology & Ultrasound*, *49*(1), 68–72.

Sugimura, M., Kudo, N., & Takahata, K. (1958). Studies on the lymphonodi of cats: III. Macroscopical observations on the lymphonodi in the abdominal and pelvic cavities. *Japanese Journal of Veterinary Research*, *6*(2), 69 – 88.

Tobón Restrepo, M. (2015). Ultrasound of the abdominal cavity, lymph nodes and large vessels. In R. Novellas Torroja, E. Dominguez Miño, Y. Espada Gerlach, Y. Martínez Pereira, & M. Tobón Restrepo (Eds.), *Diagnostic ultrasound in cats* (1st ed., pp. 211 – 229). Zaragoza: Spain: Servet editorial - Grupo Asís Biomedia S.L.

Tobón Restrepo, M., Espada, Y., Aguilar, A., Moll, X., & Novellas, R. (2016). Anatomic, computed tomographic, and ultrasonographic assessment of the lymph nodes in healthy adult cats: Part I. The head, neck, thorax, and forelimb. Pending of publication.

Tompkins, M. B. (1993). Lymphoid system. In *Atlas of feline anatomy for veterinarians* (pp. 113 – 126). Philadelphia [etc.] : W.B. Saunders Company.

Widmer, W. R., Mattoon, J. S., & Nyland, T. G. (2015). Peritoneal Fluid, Lymph Nodes, Masses, Peritoneal Cavity, Great Vessels Thrombosis and Focused Examinations. In J. S. Mattoon & T. G. Nyland (Eds.), *Small Animal Diagnostic Ultrasound* (Third edit., pp. 501 – 516). St. Louis, Missouri : Elsevier Saunders.

Table 1. Mean (m) and SD for length (MPR, Calculated), width and height of the LNs from the abdomen and hindlimb in healthy cats. Comparison among techniques.

				Length (mm)				
Lymph node	CT-MPR m (SD)	CT-Calc. m (SD)	US m (SD)	Anatomy m (SD)	MPR vs Calc. (A)	CT-MPR vs US (A)	CT-MPR vs Anatomy (B)	US vs Anatomy (B)
G[1]	6.58 (3.18)	6.34 (2.62)	5.99 (2.05)	8.56 (6.45)				
G[2]	6.12 (3.91)	4.48 (0.74)	4.00 (0.28)	-				
H	9.03 (2.77)	9.14 (3.26)	6.15 (2.32)	10.84 (2.17)		*		**
Sp	5.33 (2.01)	5.08 (1.63)	5.41 (2.03)	4.35 (2.62)				
Pd	6.38 (1.82)	7.20 (2.18)	5.76 (1.49)	5.60 (3.06)	**			
J[1]	36.97 (5.42)	34.50 (7.80)	25.05(6.19)	45.30 (10.83)	*	*		
J[2]	26.73 (4.75)	23.60 (7.20)	17.87 (7.74)	26.78 (12.45)	*	*		
J[3]	13.80 (2.50)	12.10 (3.40)	10.00 (2.34)	11.08 (1.50)		*		
J[4]	-	-	-	18.67 (18.58)				
IC[1]	7.38 (2.21)	7.82 (2.52)	7.13 (2.65)	5.78 (2.37)			*	
IC[2]	7.1 (1.96)	7.44 (2.76)	6.55 (1.92)	5.10 (0.88)				*
Co[1]	11.86 (3.71)	12.58 (4.00)	8.14 (2.39)	15.68 (10.59)		*		
Co[2]	7.57 (2.51)	8.63 (2.49)	-	8.75 (3.62)	*			
Co[3]	5.98 (1.92)	6.88 (3.25)	-	6.85 (1.45)				
Co[4]	4.06 (0.77)	4.76 (1.16)	-	6.70 (3.07)				
Co[5]	5.20 (3.52)	5.80 (2.42)	-	4.85 (2.89)				
CM[1]	10.34 (4.50)	11.37 (4.60)	10.00 (2.22)	7.34 (4.99)				
CM[2]	8.98 (4.44)	9.44 (4.27)	-	7.52 (2.23)				
CM[3]	10.88 (6.26)	10.24 (5.01)	-	6.80 (5.09)				
CM[4]	13.05 (0.49)	12.80 (0.42)	-	6.70 (-)				
LA[1]	3.93 (1.55)	4.25 (1.87)	-	3.57 (2.02)				
LA[2]	-		-	5.40 (3.25)				
LA[3]	-		-	4.50 (-)				
RR	9.30 (3.87)	9.20 (2.97)	8.10 (1.70)	11.40 (8.77)				
LR	8.80 (2.20)	9.25 (2.55)	-	8.65 (4.60)				

RMI	17.85 (4.85)	16.52 (4.78)	10.27 (3.56)	12.48 (6.58)	**
LMI	17.52 (4.11)	17.04 (7.03)	11.62 (3.46)	13.28 (4.74)	
RInI	8.17 (2.65)	7.96 (2.14)	-	12.00 (NC)	
LInI	8.66 (2.60)	8.08 (1.88)	-	6.70 (NC)	
RSa	5.09 (2.48)	5.58 (2.24)	5.20 (NC)	-	
LSa	4.65 (1.38)	5.65 (1.72)	-	-	
RSI	9.03 (3.17)	9.24 (3.03)	7.25 (1.75)	13.60 (5.62)	
LSI[1]	8.12 (3.23)	8.81 (4.14)	7.21 (2.28)	13.05 (5.33)	
LSI[2]	9.90 (NC)	6.90	-	-	
RCE[1]	12.55 (6.98)	12.25 (5.56)	-	-	
RCE[2]	7.53 (5.16)	7.83 (3.87)	-	-	
RCE[3]	12.70 (NC)	13.80 (NC)	-	-	
LCE[1]	13.37 (5.38)	13.71 (5.35)	-	-	
LCE[2]	16.25 (1.63)	15.00 (0.85)	-	-	
RIs	4.58 (1.28)	4.92 (1.65)	-	3.20 (-)	
LIs	4.63 (0.50)	5.63 (0.65)	-	3.30 (-)	
RPo	8.02 (1.78)	8.24 (1.93)	7.73 (2.36)	7.37 (2.28)	
LPo	8.49 (2.30)	8.14 (2.35)	7.88 (2.35)	6.63 (1.82)	

* p-value < 0.05 (A) Wilcoxon Signed Rank Test
** p-value < 0.01 (B) Mann-Whitney U Test

Continuation Table 1. Mean (m) and SD for length (MPR, Calculated), width and height of the LNs from the abdomen and hindlimb in healthy cats Comparison among techniques.

	Width (mm)						**Height (mm)**					
Lymph node	CT m (SD)	US m (SD)	Anatomy m (SD)	CT vs US (A)	CT vs Anatomy (B)	US vs Anatomy (B)	CT m (SD)	US m (SD)	Anatomy m (SD)	CT vs US (A)	CT vs Anatomy (B)	US vs Anatomy (B)
G[1]	3.30 (1.06)	4.87 (1.16)	3.14 (1.05)	**		*	3.04 (1.27)	2.50 (0.72)	1.1 (0.14)	*	**	**
G[2]	3.23 (1.11)	3.50 (2.40)	-				3.43 (0.86)	3.10 (0.28)	-			
H	3.89 (1.67)	5.33 (1.95)	4.20 (2.02)				4.48 (1.62)	2.92 (0.77)	2.44 (1.55)		*	
Sp	4.12 (1.32)	3.80 (1.31)	2.65 (1.20)				3.55 (1.38)	2.53 (0.94)	1.5 (0.71)	*	*	
Pd	6.05 (1.79)	5.77 (2.13)	2.55 (1.05)		**	**	4.31 (1.36)	3.17 (0.94)	1.1 (0.64)	**	**	**
J[1]	9.55 (4.44)	10.93 (5.23)	7.90 (3.50)				6.27 (2.58)	4.42 (1.55)	2.50 (1.87)		*	*
J[2]	9.58 (4.91)	15.27 (6.04)	5.40 (1.31)	*	*	*	5.78 (1.70)	4.23 (1.07)	1.55 (1.05)	*	*	*
J[3]	10.25 (3.06)	8.68 (4.69)	3.75 (0.71)		*	*	8.53 (4.11)	4.38 (1.75)	1.55 (0.24)	*	*	*
J[4]	-	-	3.67 (1.80)				-	-	-			
IC[1]	5.37 (1.54)	6.36 (2.84)	2.95 (0.91)		*	*	3.80 (1.20)	3.06 (1.01)	1.35 (0.39)	**	**	**
IC[2]	7.57 (9.06)	5.96 (2.32)	3.45 (1.05)		**	**	6.41 (9.8)	2.94 (0.59)	1.47 (0.57)	*	**	**
Co[1]	5.94 (3.02)	7.44 (3.38)	3.05 (0.63)		*	*	5.35 (2.98)	3.68 (1.29)	1.23 (0.46)		*	
Co[2]	5.09 (1.91)	-	4.08 (1.57)				3.70 (1.53)	-	1.35 (0.49)		*	
Co[3]	4.58 (1.50)	-	3.48 (1.12)				2.87 (0.92)	-	1.30 (0.47)		*	
Co[4]	5.40 (1.79)	-	3.40 (0.89)				3.36 (1.47)	-	1.20 (0.18)		*	
Co[5]	4.20 (1.68)	-	3.55 (1.77)				3.30 (1.00)	-	1.45 (0.21)			
CM[1]	5.14 (2.21)	7.77 (2.69)	3.12 (0.73)				3.51 (1.44)	3.50 (0.98)	1.66 (0.64)		*	
CM[2]	5.37 (2.36)	-	3.12 (0.75)				3.53 (1.55)	-	1.82 (1.20)			
CM[3]	6.38 (2.22)	-	4.00 (1.70)				3.62 (1.82)	-	1.90 (0.42)			
CM[4]	6.45 (2.05)	-	4.00 (NC)				4.30 (1.27)	-	1.90 (NC)			
LA[1]	2.17 (0.92)	-	1.70 (0.72)				1.82 (1.13)	-	0.87 (0.58)			
LA[2]	-	-	1.95 (0.35)				-	-	1.30 (NC)			
LA[3]	-	-	2.00 (NC)				-	-	0.90 (NC)			
RR	4.64 (1.61)	6.10 (2.69)	3.10 (0.42)				3.31 (1.07)	3.25 (0.64)	1.15 (0.21)			
LR	3.30 (1.29)	-	2.30 (NC)				2.95 (1.38)	-	1.30 (0.42)			

RMI	3.46 (1.25)	4.64 (1.72)	3.82 (1.08)	**		2.42 (0.65)	3.45 (1.34)	1.40 (0.87)	*	
LMI	3.31 (1.00)	4.12 (1.33)	2.88 (0.73)			2.60 (1.16)	3.28 (0.84)	1.56 (0.88)		
RInI	4.25 (1.91)	-	4.70 (NC)			3.10 (1.50)	-	2.50 (NC)		
LInI	4.07 (1.81)	-	4.40 (NC)			3.73 (1.71)	-	-		
RSa	4.76 (1.83)	-	-			2.09 (0.67)	2.00 (NC)	-		
LSa	4.72 (1.72)	-	-			2.17 (0.84)	-	-		
RSI	6.88 (2.53)	6.19 (3.11)	3.45 (1.69)			3.21 (1.14)	2.72 (0.90)	1.27 (0.72)		
LSI[1]	6.76 (2.95)	5.43 (1.82)	3.27 (1.49)	*	*	3.04 (1.28)	2.67 (0.62)	1.27 (0.70)	**	**
LSI[2]	6.90 (NC)	-	-			4.20 (NC)	-	-		
RCE[1]	5.80 (1.96)	-	-			3.88 (1.25)	-	-		
RCE[2]	4.30 (0.82)	-	-			3.83 (1.95)	-	-		
RCE[3]	6.90 (NC)	-	-			5.90 (NC)	-	-		
LCE[1]	5.72 (1.95)	-	-			3.83 (1.35)	-	-		
LCE[2]	5.60 (2.4)	-	-			5.00 (0.85)	-	-		
RIs	4.05 (0.76)	-	2.00 (NC)			2.42 (0.63)	-	1.00 (NC)		
LIs	3.73 (0.91)	-	6.00 (NC)			2.50 (0.1)	-	1.00 (NC)		
RPo	6.29 (1.65)	5.99 (1.26)	4.45 (2.52)			5.11 (1.83)	4.99 (1.24)	1.58 (0.93)		
LPo	5.97 (1.25)	6.05 (1.32)	4.10 (1.80)			5.42 (1.45)	5.11 (1.36)	1.67 (1.04)		

G: gastric LN; H: hepatic LN; Sp: splenic LN; Pd: pancreaticoduodenal LN; J: jejunal LNs; IC: iliocecal LNs; Co: colic LNs; CM: caudal mesenteric LNs; LA: lumbar aortic LNs; RR: right renal LN; LR: left renal LN; RMI: right medial iliac LN; LMI: left medial iliac; RInI: right internal iliac LN; LInI: left internal iliac; RSa: right sacral LN; LSa: left sacral LN; RSI: right superficial inguinal LNs; LSI: left superficial inguinal LNs; RCE: right caudal epigastric LNs; LCE: left caudal epigastric LNs; RIs: right ischiatic LN; LIs: left ischiatic LN; RPo: right popliteal LN; LPo: left popliteal LN; NC: not calculated.

Table 2. Computed tomography characteristics of the lymph nodes of the abdomen and hindlimb of healthy cats.

Lymph node	HU Precontrast				HU Postcontrast				Attenuation Precontrast (%)					Attenuation Postcontrast (%)			
	Mean	SD	Min	Max	Mean	SD	Min	Max	Iso	S Hypo	Hypo	Hyper	Heter	Hom	S Heter	Heter	Peri
G[1]	20.66	26.18	-55.33	63.33	94.65	30.96	20.33	151.33	50.00	42.86	3.57	0.00	3.57	82.14	3.57	0.00	14.29
G[2]	33.05	22.91	-12.00	46.33	102.95	9.62	90.67	114.67	66.67	33.33	0.00	0.00	0.00	100.00	0.00	0.00	0.00
H	35.36	10.73	13.67	50.33	122.30	25.31	66.33	170.00	50.00	40.91	4.55	0.00	4.55	86.36	9.09	0.00	4.55
Sp	5.81	32.72	-64.00	50.33	79.83	38.47	-0.67	125.33	39.13	39.13	0.00	0.00	21.74	43.48	0.00	4.35	52.17
Pd	27.56	21.91	-29.33	55.00	100.15	35.99	-6.67	148.33	27.59	44.83	10.34	0.00	17.24	31.03	20.69	10.34	37.93
J[1]	38.76	9.24	18.33	52.00	143.26	24.31	94.33	170.67	60.00	33.33	0.00	3.33	3.33	50.00	40.00	10.00	0.00
J[2]	41.17	7.93	30.67	57.67	145.95	23.12	98.00	171.00	64.33	25.00	0.00	3.66	7.10	53.60	35.71	10.71	0.00
J[3]	37.67	7.82	19.67	48.33	122.45	13.52	101.67	146.33	57.10	42.90	0.00	0.00	0.00	64.30	35.70	0.00	0.00
IC[1]	38.15	10.37	18.67	55.33	108.03	21.33	72.33	148.00	48.15	40.74	0.00	3.70	7.41	81.48	11.11	7.41	0.00
IC[2]	40.84	11.19	11.67	56.00	106.17	21.61	64.33	139.33	51.85	44.44	0.00	0.00	3.70	74.07	11.11	11.11	3.70
Co[1]	38.30	13.75	8.00	71.67	118.40	21.04	64.00	152.33	51.90	48.10	0.00	0.00	0.00	85.20	14.80	0.00	0.00
Co[2]	36.31	10.24	20.00	54.33	123.67	24.85	55.33	152.67	40.00	53.30	0.00	0.00	6.70	86.70	0.00	13.30	0.00
Co[3]	31.37	15.39	7.33	54.00	126.52	21.11	94.33	166.00	44.40	55.60	0.00	0.00	0.00	100.00	0.00	0.00	0.00
Co[4]	30.33	18.52	-2.00	44.33	129.67	20.90	108.33	161.00	20.00	80.00	0.00	0.00	0.00	100.00	0.00	0.00	0.00
Co[5]	34.33	11.41	22.33	45.67	127.00	27.83	91.33	157.33	25.00	75.00	0.00	0.00	0.00	100.00	0.00	0.00	0.00
CM[1]	41.07	9.63	19.00	58.67	116.44	23.65	68.67	163.00	41.38	48.28	0.00	0.00	10.34	82.76	13.79	3.45	0.00
CM[2]	43.00	9.79	23.33	59.33	118.10	24.00	82.67	163.67	35.71	57.14	0.00	0.00	7.14	78.57	14.29	7.14	0.00
CM[3]	36.80	12.26	15.67	47.67	115.80	13.15	98.67	128.33	20.00	80.00	0.00	0.00	0.00	100.00	0.00	0.00	0.00
CM[4]	51.66	10.37	44.33	59.00	130.66	30.17	109.33	152.00	100.00	0.00	0.00	0.00	0.00	100.00	0.00	0.00	0.00
LA[1]	-4.25	15.95	-23.33	10.67	61.00	21.34	37.33	89.00	25.00	75.00	0.00	0.00	0.00	100.00	0.00	0.00	0.00
RR	12.67	36.33	-33.67	60.00	76.71	30.75	33.00	115.33	42.86	0.00	0.00	0.00	57.14	0.00	0.00	14.29	85.71
LR	-4.50	18.91	-26.00	13.00	66.42	46.41	13.33	106.00	25.00	0.00	0.00	0.00	75.00	0.00	0.00	0.00	100.00
RMI	30.48	20.98	-18.33	56.67	109.80	33.54	46.33	166.33	57.14	42.86	0.00	0.00	0.00	92.86	3.57	3.57	0.00
LMI	37.62	17.11	-12.33	67.33	106.57	29.94	20.00	160.67	53.57	42.86	3.57	0.00	0.00	96.43	3.57	0.00	0.00
RInI	37.77	18.20	-3.33	58.00	120.25	24.10	80.33	165.00	68.42	26.32	5.26	0.00	0.00	73.68	21.05	0.00	5.26
LInI	38.25	20.71	-15.00	67.00	118.19	22.01	90.00	180.00	73.68	21.05	5.26	0.00	0.00	73.68	21.05	0.00	5.26
RSa	46.38	14.28	25.00	66.00	104.92	25.76	58.67	140.33	75.00	25.00	0.00	0.00	0.00	75.00	25.00	0.00	0.00
LSa	46.66	28.41	4.33	65.33	106.08	35.02	54.33	131.00	75.00	25.00	0.00	0.00	0.00	100.00	0.00	0.00	0.00
RSI	26.41	21.87	-37.00	60.00	99.48	35.05	11.00	169.67	35.71	64.29	0.00	0.00	0.00	92.86	3.57	0.00	3.57
LSI[1]	28.83	19.46	-34.67	61.00	95.57	32.81	-7.67	148.33	32.14	67.86	0.00	0.00	0.00	92.86	3.57	0.00	3.57

LSI[2]	54.00	NC	54.00	54.00	98.67	NC	98.67	98.67	0.00	100.00	0.00	0.00	0.00	100.00	0.00	0.00	0.00
RCE[1]	23.61	16.95	-22.67	50.00	106.91	38.95	35.00	206.67	34.62	57.69	0.00	0.00	7.69	76.92	11.54	0.00	11.54
RCE[2]	29.58	8.92	19.67	41.33	121.00	60.59	77.00	208.33	25.00	75.00	0.00	0.00	0.00	100.00	0.00	0.00	0.00
RCE[3]	24.67	NC	24.67	24.67	132.33	NC	132.33	132.33	0.00	100.00	0.00	0.00	0.00	100.00	0.00	0.00	0.00
LCE[1]	25.04	17.49	-32.00	49.00	112.68	37.10	26.33	178.67	30.77	61.54	0.00	0.00	7.69	80.77	7.69	0.00	11.54
LCE[2]	35.70	1.41	34.70	36.70	119.15	16.76	107.30	131.00	50.00	50.00	0.00	0.00	0.00	100.00	0.00	0.00	0.00
RIs	39.11	14.44	19.33	55.00	95.94	15.10	77.00	113.00	66.67	33.33	0.00	0.00	0.00	100.00	0.00	0.00	0.00
LIs	29.56	7.90	24.67	38.67	102.00	27.13	86.00	133.33	66.67	33.33	0.00	0.00	0.00	100.00	0.00	0.00	0.00
RPo	17.00	21.50	-32.67	45.00	91.12	36.12	-20.00	149.33	10.34	48.28	24.14	0.00	17.24	62.07	10.34	3.45	24.14
LPo	14.99	21.03	-34.33	47.67	92.30	32.39	14.33	171.67	6.90	51.72	24.14	0.00	17.24	55.17	10.34	3.45	31.03

G: gastric LN; H: hepatic LN; Sp: splenic LN; Pd: pancreaticoduodenal LN; J: jejunal LNs; IC: iliocecal LNs; Co: colic LNs; CM: caudal mesenteric LNs; LA: lumbar aortic LNs; RR: right renal LN; LR: left renal LN; RMI: right medial iliac LN; LMI: left medial iliac; RInI: right internal iliac LN; LInI: left internal iliac; RSa: right sacral LN; LSa: left sacral LN; RSI: right superficial inguinal LNs; LSI: left superficial inguinal LNs; RCE: right caudal epigastric LNs; LCE: left caudal epigastric LNs; RIs: right ischiatic LN; LIs: left ischiatic LN; RPo: right popliteal LN; LPo: left popliteal LN. Iso: isoattenuating; S Hypo: slightly hypoattenuating; Hypo: hypoattenuating; Hyper: hyperattenuating. Hom: homogeneous; S Het: slightly heterogeneous; Het: heterogeneous; Peri: peripheral enhancement. NC: not calculated.

Table 3. Ultrasonographic features of the lymph nodes of the abdomen and hindlimb in healthy cats.

Lymph node	Echogenicity (%)				Shape (%)		
	Isoechoic	Hypoechoic	Hyperechoic	Heterogeneous	Rounded	Elongated	Miscellaneous
G[1]	37.04	22.22	0.00	40.74	29.63	66.67	3.70
G[2]	0.00	50.00	0.00	50.00	50.00	50.00	0.00
H	42.86	47.62	0.00	9.52	61.90	33.33	4.76
Sp	8.70	47.83	8.70	34.78	77.27	22.73	0.00
Pd	24.14	37.93	0.00	37.93	51.72	48.28	0.00
J[1]	20.00	63.33	3.33	13.33	0.00	6.90	93.10
J[2]	28.60	57.10	3.60	10.70	0.00	14.29	85.71
J[3]	13.30	73.30	6.70	6.70	0.00	26.70	73.30
IC[1]	30.00	66.67	0.00	3.33	36.67	40.00	23.33
IC[2]	32.00	64.00	0.00	4.00	24.00	48.00	28.00
Co	19.05	71.43	0.00	9.52	42.86	28.57	28.57
CM	20.00	70.00	0.00	10.00	10.00	50.00	40.00
LA*	-	-	-	-	-	-	-
RR	0.00	100.00	0.00	0.00	0.00	100.00	0.00
LR*	-	-	-	-	-	-	-
RMI	50.00	26.67	0.00	23.33	0.00	83.33	16.67
LMI	50.00	30.00	0.00	20.00	0.00	83.33	16.67
RInI*	-	-	-	-	-	-	-
LInI*	-	-	-	-	-	-	-
RSa	0.00	100.00	0.00	0.00	0.00	100.00	0.00
LSa *	-	-	-	-	-	-	-
RSI	28.57	42.86	3.57	25.00	10.71	85.71	3.57
LSI	24.14	55.17	3.45	17.24	17.24	82.76	0.00
RCE*	-	-	-	-	-	-	-
LCE*	-	-	-	-	-	-	-
RIs*	-	-	-	-	-	-	-
LIs*	-	-	-	-	-	-	-
RPo	33.33	16.67	20.00	30.00	93.33	3.33	3.33
LPo	37.93	13.79	24.14	24.14	96.55	3.45	0.00

* LNs that were not identified in US.

G: gastric LN; H: hepatic LN; Sp: splenic LN; Pd: pancreaticoduodenal LN; J: jejunal LNs; IC: iliocecal LNs; Co: colic LNs; CM: caudal mesenteric LNs; LA: lumbar aortic LNs; RR: right renal LN; LR: left renal LN; RMI: right medial iliac LN; LMI: left medial iliac; RInI: right internal iliac LN; LInI: left internal iliac; RSa: right sacral LN; LSa: left sacral LN; RSI: right superficial inguinal LNs; LSI: left superficial inguinal LNs; RCE: right caudal epigastric LNs; LCE: left caudal epigastric LNs; RIs: right ischiatic LN; LIs: left ischiatic LN; RPo: right popliteal LN; LPo: left popliteal LN.

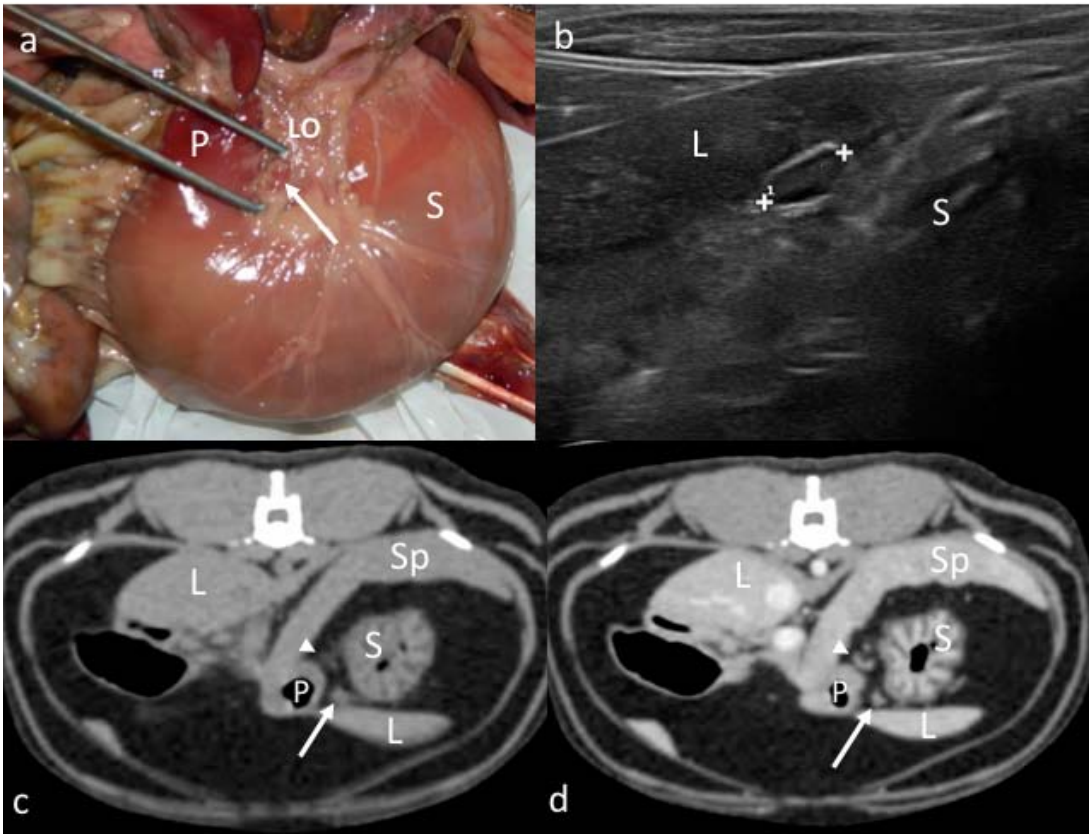

Figure 1. Gastric lymph node. a. Image of the dissection showing its localization (arrow) in the lesser omentum (LO) of the stomach (S), near the pylorus (P). b. Ultrasonographic image showing an elongated gastric LN (between cursors), with an isoechoic center and a hypoechoic periphery, located between the stomach (S) and the liver (L). c – d. CT images indicating the localization of an isoattenuating gastric LN (arrow) in the lesser omentum in the precontrast image (c) and with a homogeneous contrast enhancement pattern in the postcontrast image (d). A second LN (arrow head) is partially visible dorsally, between the stomach (S) and the spleen (Sp). The liver (L) and pylorus (P) are indicated.

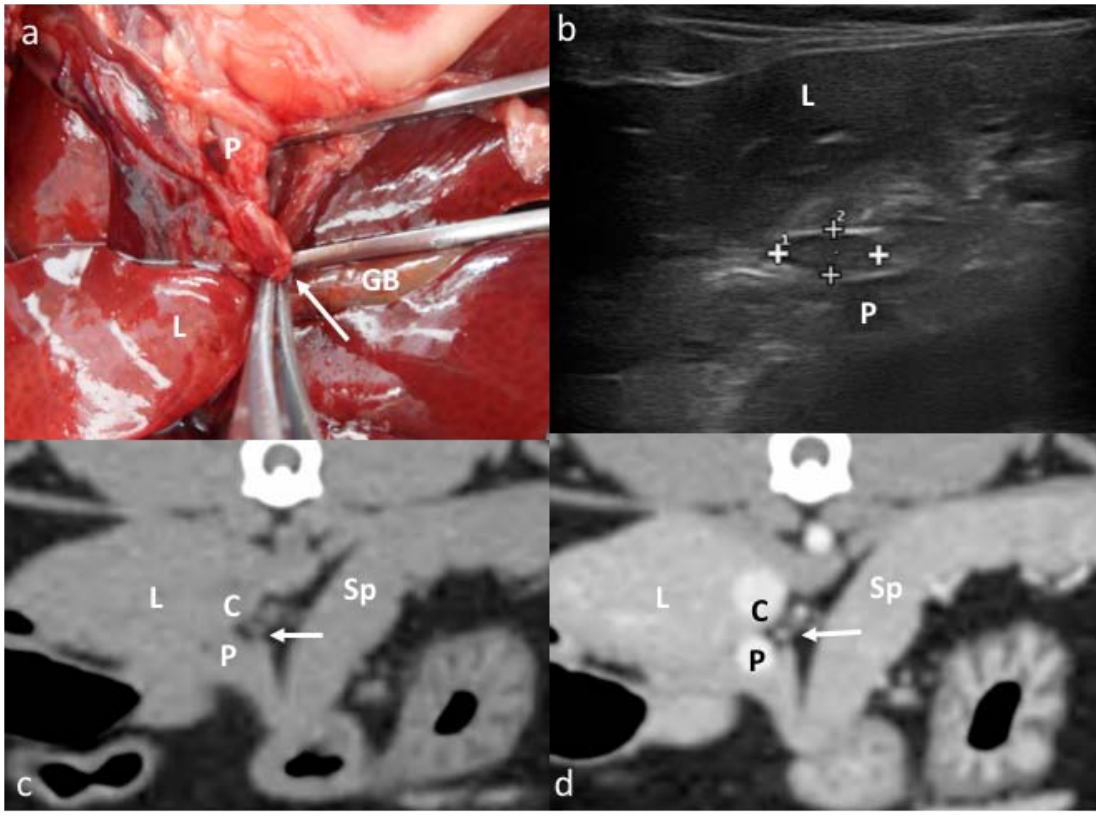

Figure 2. Hepatic lymph node. a. Image of the dissection showing the localization of the hepatic LN (arrow) in the *porta hepatis,* near to the portal vein (P). The liver (L) and gallbladder (GB) are indicated. b. Ultrasonographic image showing the hepatic LN (between cursors), in the *porta hepatis*. The liver (L) and a partially visible portal vein (P) are indicated. c – d. CT images indicating a slightly hypoattenuating hepatic LN (arrow) in the precontrast image (c) and with homogeneous contrast enhancement in the postcontrast image (d). It is located normally at the dorsomedial aspect of the portal vein (P), and ventromedial to the caudal vena cava (C). The liver (L) and the spleen (Sp) are indicated.

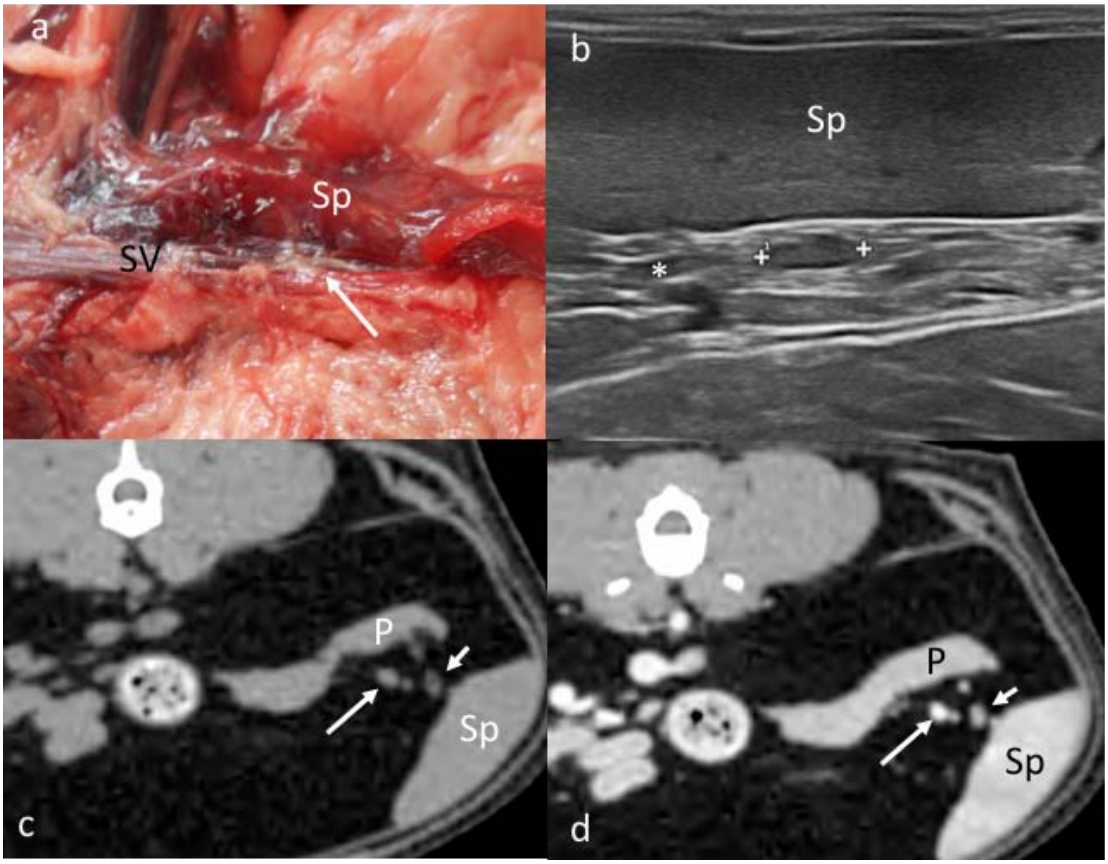

Figure 3. Splenic lymph node. a. Image of the dissection showing its localization (arrow) in the splenic hilus, along the splenic vein (SV). The spleen (Sp) is partially visible. b. US image showing the splenic LN (between cursors), at the splenic hilus. The spleen (Sp) and a partially visible splenic vein (asterisk) are indicated. c – d. CT images indicating the localization of the splenic LN (short arrow) seen slightly hypoattenuating with a hypoattenuating center in the precontrast image (c) and showing slightly heterogeneous contrast enhancement (d). The splenic vein (long arrow), the pancreas (P), and the spleen (Sp) are indicated.

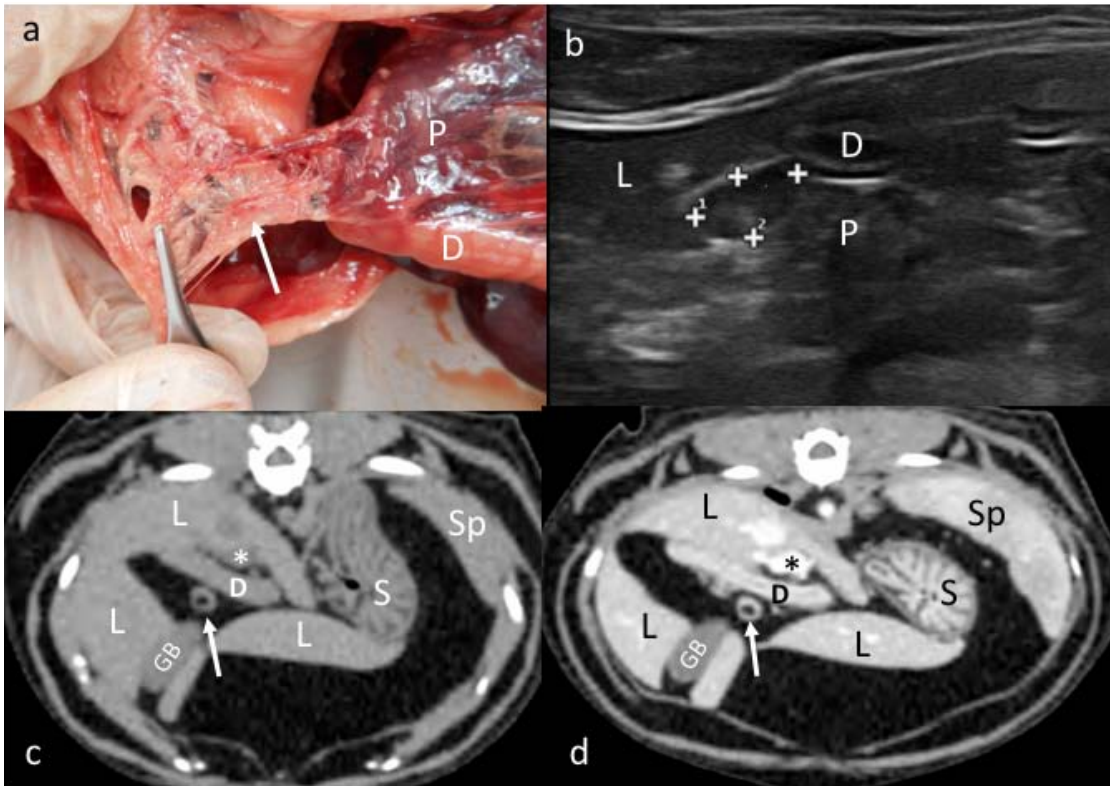

Figure 4. Pancreaticoduodenal lymph node. a. Image of the dissection showing the localization of the pancreaticoduodenal LN (arrow) in relation to the pancreas (P) and the duodenum (D). b. US image showing a heterogeneous, rounded pancreaticoduodenal LN (between cursors), between the duodenum (D), pancreas (P), and the liver (L). c – d. CT images indicating the localization of a rounded pancreaticoduodenal LN (arrow) seen isoattenuating with a hypoattenuating center in the precontrast image (c) and with peripheral homogeneous contrast enhancement in the postcontrast image (d). The liver (L), gall bladder (GB), duodenum (D), portal vein (asterisk), stomach (S), and spleen (Sp) are indicated.

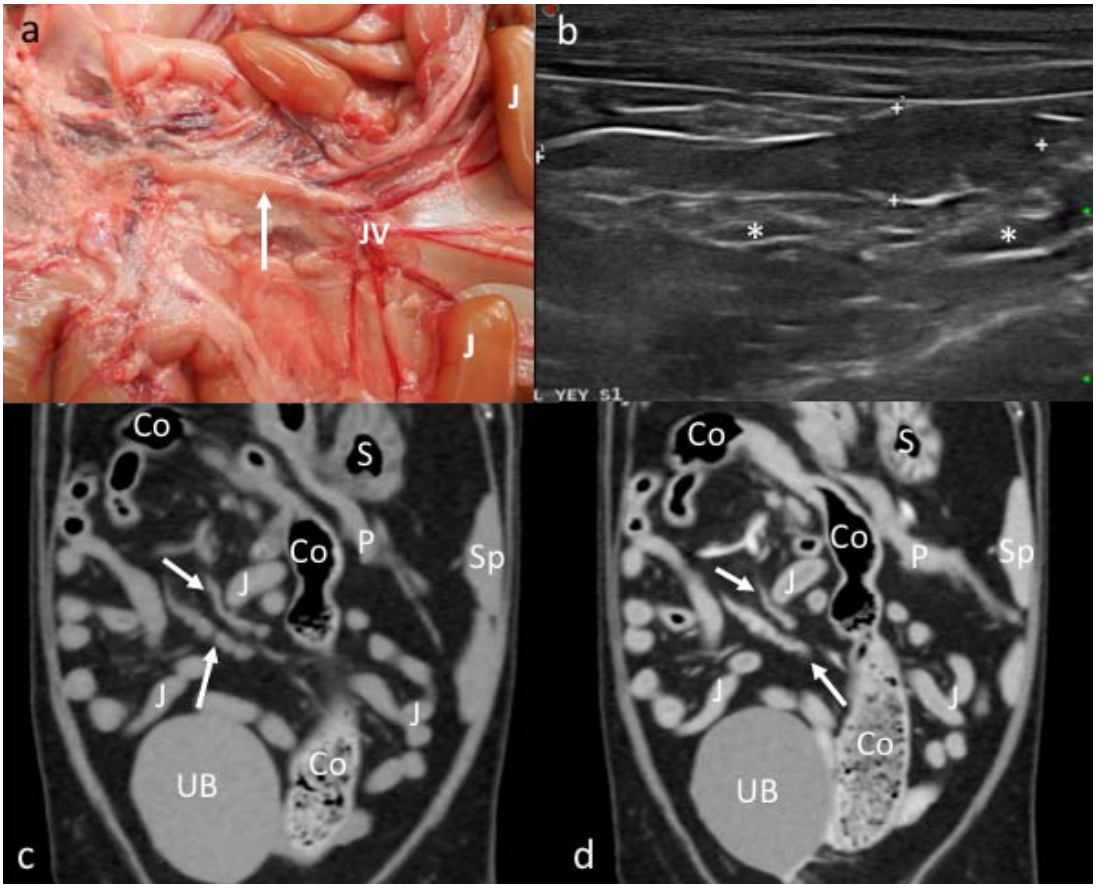

Figure 5. Jejunal lymph nodes. a. Image of the dissection showing the localization of the jejunal LN (arrow) in the mesentery along the jejunal vessels (JV). The jejunal loops (J) are indicated. b. US image showing a miscellaneous shaped, hypoechoic jejunal LN (between cursors). The jejunal vessels (asterisk) are partially seen. c – d. CT images in dorsal reconstruction indicating the localization of the jejunal LNs (arrows) seen isoattenuating in the precontrast image (c) and with homogeneous contrast enhancement in the postcontrast image (d). The jejunal loops (J), colon (Co), stomach (S), spleen (Sp), pancreas (P), and urinary bladder (UB) are indicated.

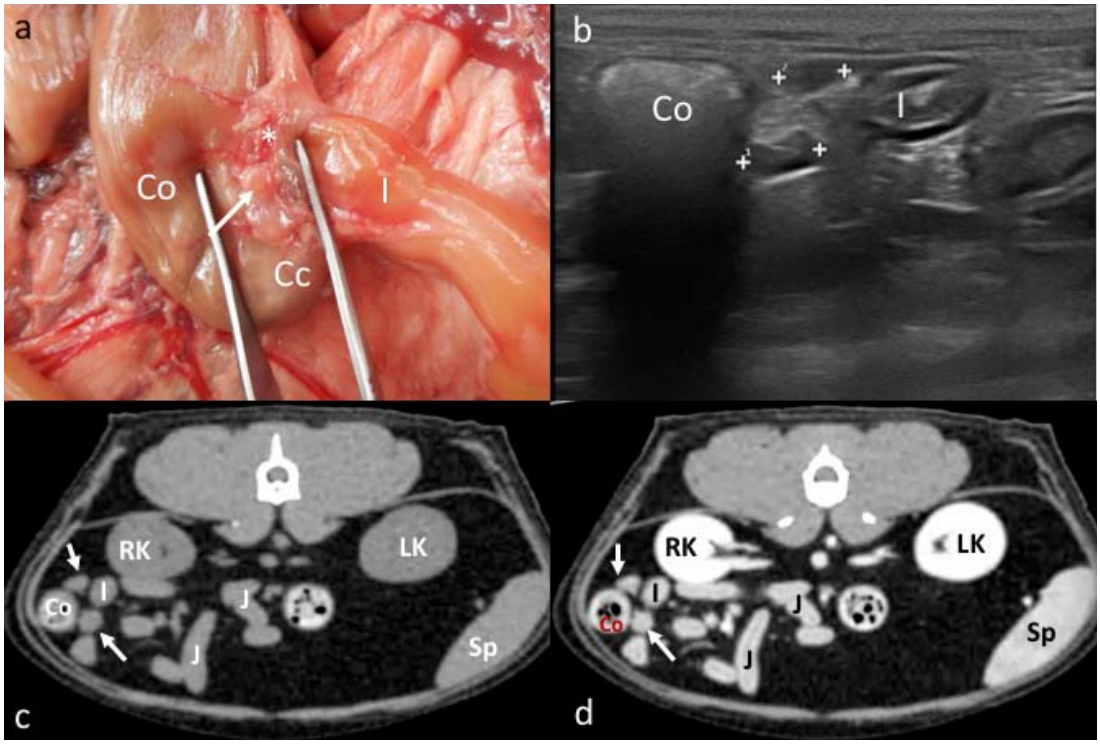

Figure 6. Ileocecal lymph nodes. a. Image of the dissection showing the localization of the ileocecal LNs (arrow) near the ileocolic junction, along the ileocolic vessels (asterisk). The ileum (I), cecum (Cc), and colon (Co) are indicated. b. US image showing 2 elongated and hypoechoic ileocecal LNs (between cursors) between the ascending colon (Co) and ileum (I). c – d. CT images indicating the localization of the ileocecal LN (arrows) seen isoattenuating in the precontrast image (c) and with homogeneous enhancement in the postcontrast image (d). The colon (Co), Ileum (I), jejunal loops (J), right (RK) and left (LK) kidneys, and spleen (Sp) are indicated.

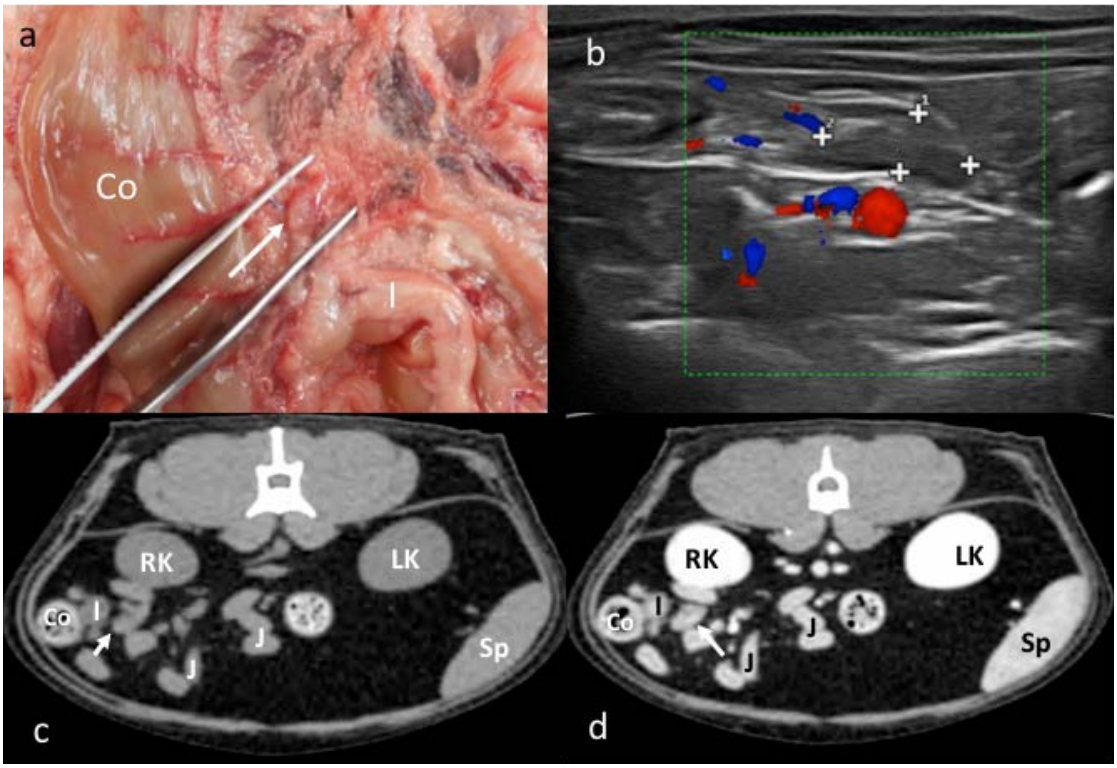

Figure 7. Colic lymph node. a. Image of the dissection showing the localization of the colic LN (arrow) near the ascending colon (Co) and ileum (I). b. Doppler US image showing the colic LN (among cursors), blood flow can be seen in the mesenteric vessels. c – d. CT images indicating the localization of the colic LN (arrow) seen isoattenuating in the precontrast image (c) and with homogeneous enhancement in the postcontrast image (d). The colon (Co), Ileum (I), jejunal loops (J), right (RK) and left (LK) kidneys, and spleen (Sp) are indicated.

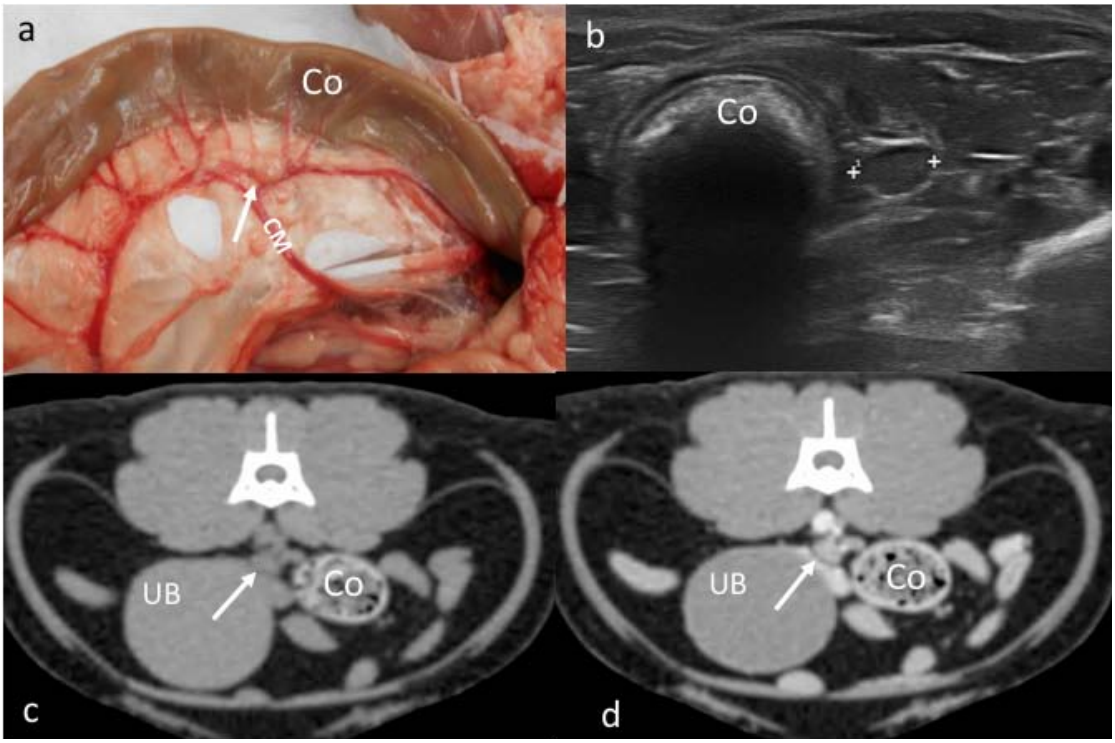

Figure 8. Caudal mesenteric lymph node. a. Image of the dissection showing the localization of the caudal mesenteric LN (arrow) near the descending colon (Co) along the caudal mesenteric vessels (CM). b. US image showing the caudal mesenteric LN (between cursors), near the descending colon (Co). c – d. CT images indicating the localization of the caudal mesenteric LN (arrow) seen isoattenuating in the precontrast image (c) and with homogeneous enhancement in the postcontrast image (d). The descending colon (Co) and the urinary bladder (UB) are indicated.

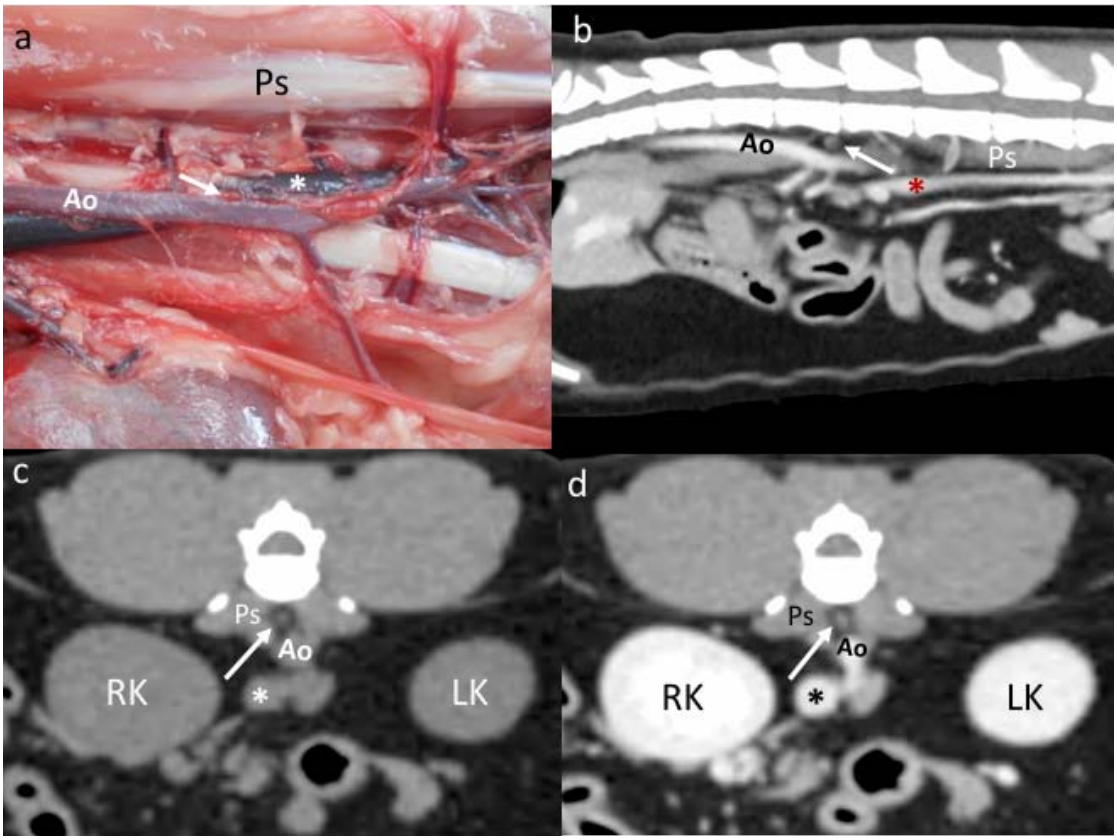

Figure 9. Lumbar aortic lymph nodes. a. Image of the dissection showing the localization of the lumbar aortic LN (arrow) between to the abdominal aorta (Ao) and the caudal vena cava (asterisk). The *psoas* (Ps) muscles are indicated. b - d. CT images indicating the localization of the lumbar aortic LN (arrow) in sagittal plane seen with heterogeneous contrast enhancement with a hypoattenuating central area postcontrast (b) and in transverse plane seen slightly hypoattenuating in the precontrast image (c) and with homogeneous enhancement in the postcontrast image (d). The *psoas* (Ps) muscles, aorta (Ao), caudal vena cava (asterisk), and right (RK) and left (LK) kidneys are indicated.

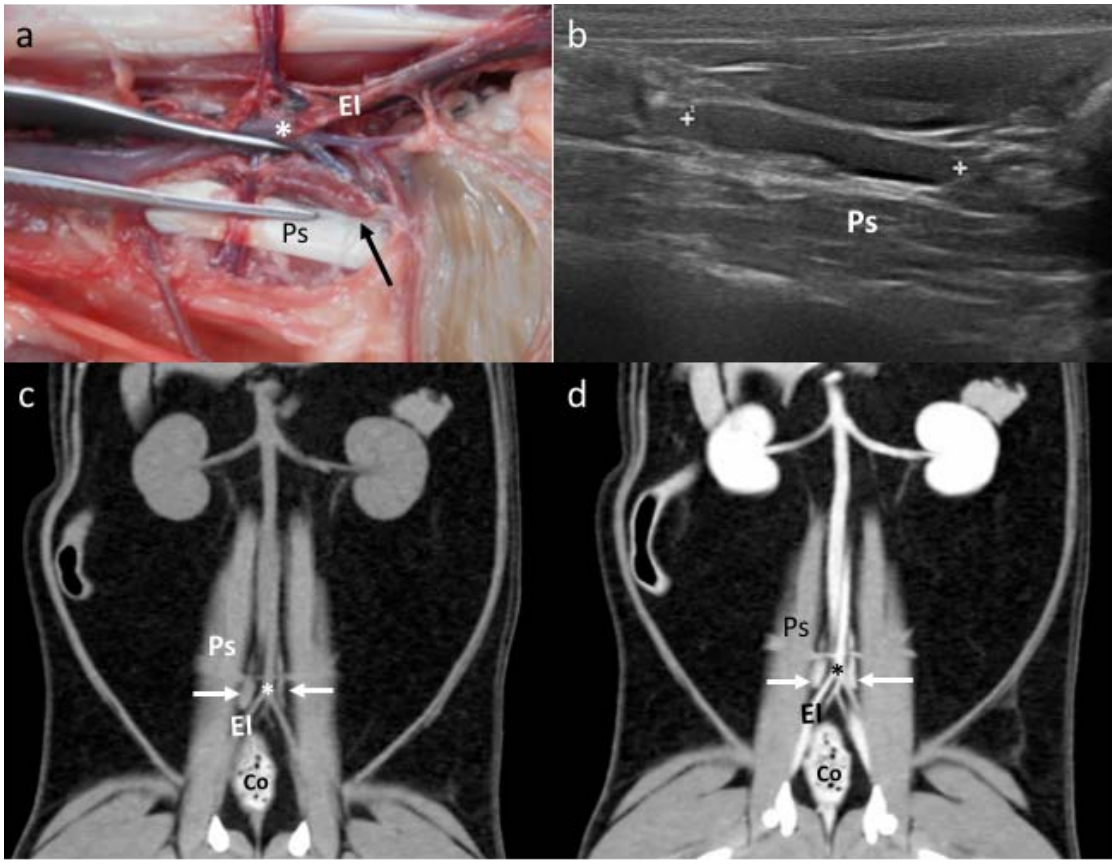

Figure 10. Medial iliac lymph nodes. a. Image of the dissection showing the localization of the medial iliac LNs (arrow) along the aortic trifurcation (asterisk) and the external iliac vessels (EI). The descending colon (Co) is indicated. b. US image showing an isoechoic medial iliac LN (between cursors) with fusiform shape located ventral to the *psoas* (Ps) muscles. c - d. CT images indicating the localization of the medial iliac LNs (arrows) in dorsal plane seen isoattenuating in the precontrast image (c) and with homogeneous enhancement in the postcontrast image (d), around the aortic trifurcation (asterisk) between the external iliac vessels (EI) and the *psoas* (Ps) muscles.

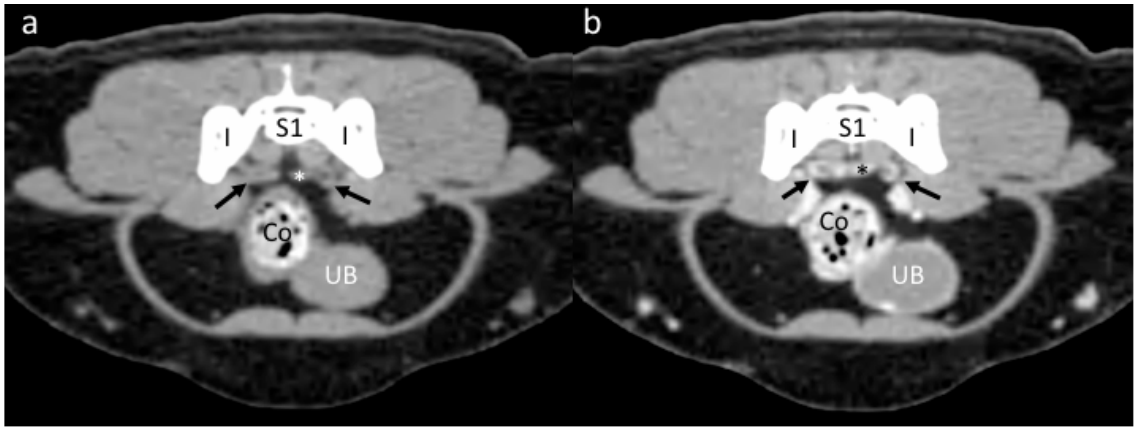

Figure 11. Internal iliac lymph nodes. a - b. CT transverse images indicating the localization of isoattenuating internal iliac LNs (arrows) in the precontrast image (a) that show homogeneous enhancement in the postcontrast image (b). The LNs are located near the medial aspect of the ilium (I), ventral to the sacrum (S1) and along the internal iliac vessels (asterisk). The colon (Co) and the urinary bladder (UB) are indicated.

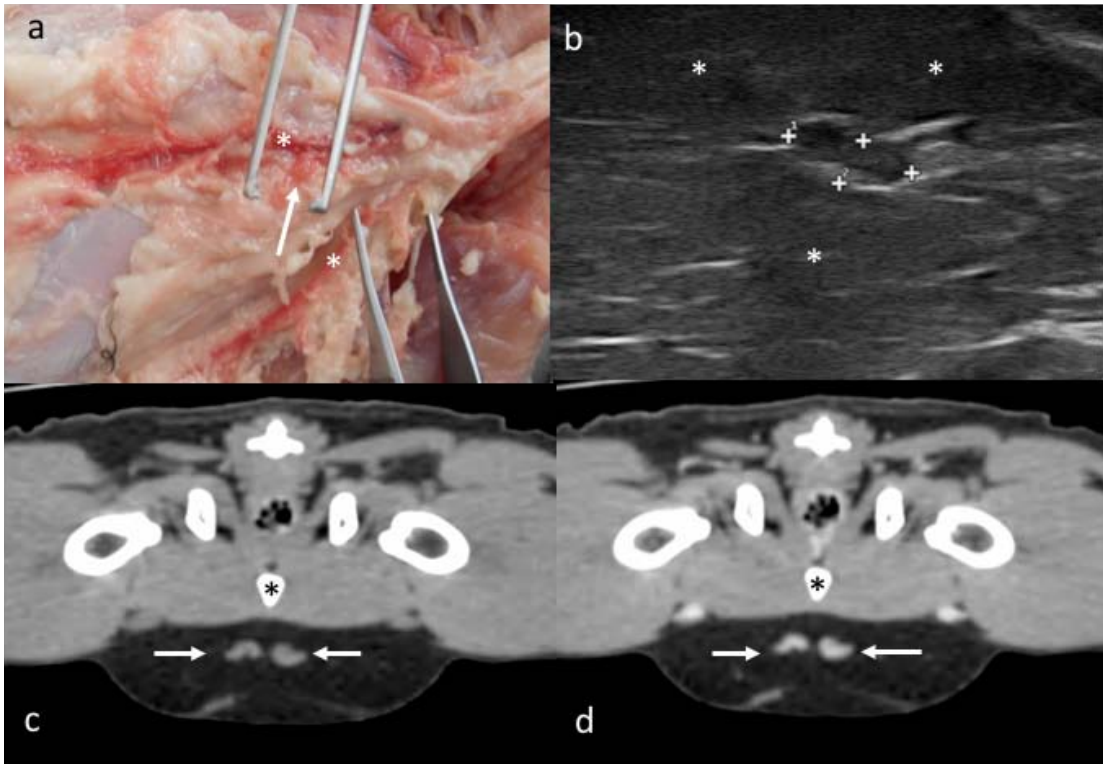

Figure 12. Superficial inguinal lymph nodes. a. Image of the dissection showing the localization of the superficial inguinal LNs (arrow) along the external pudendal vessels (asterisks). b. US image showing a heterogeneous superficial inguinal LN (between cursors) embedded in the inguinal adipose tissue (asterisks). c - d. CT transverse images indicating the localization of the superficial inguinal LNs (arrows) seen isoattenuating in the precontrast image (c) and with homogeneous enhancement in the postcontrast image (d). The pubis (asterisk) is indicated.

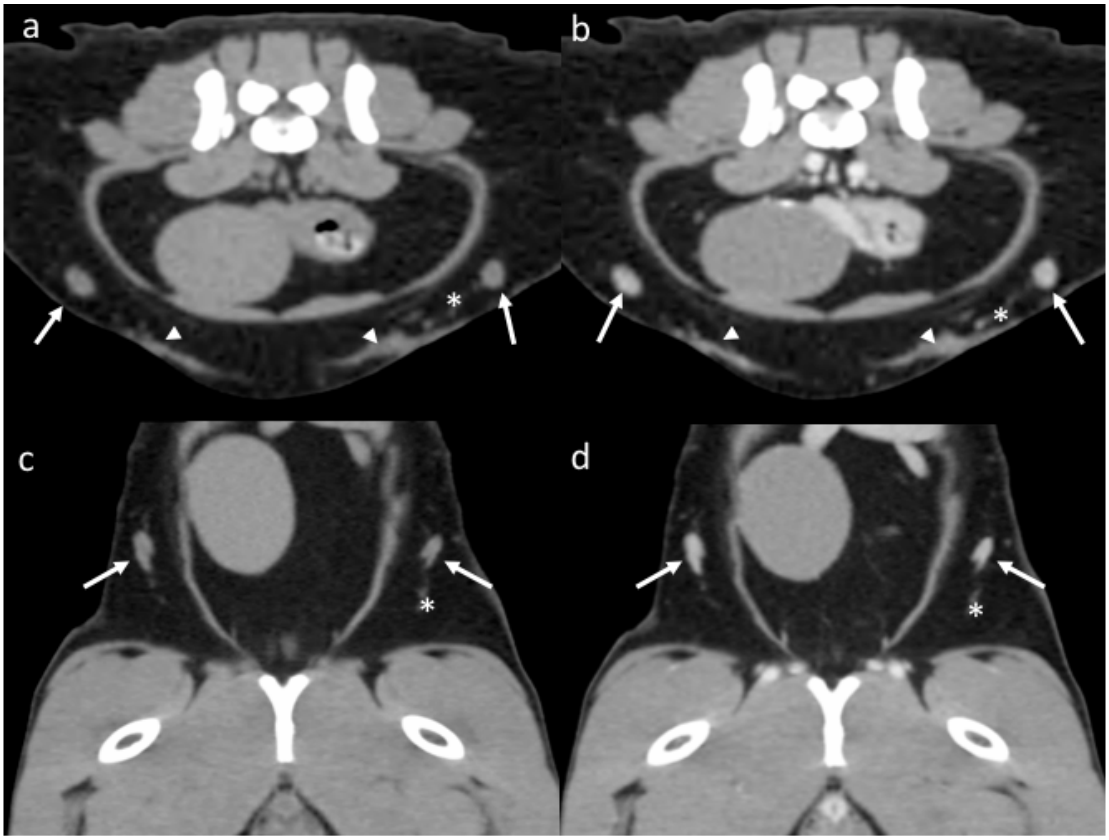

Figure 13. Caudal epigastric lymph nodes. a – d. CT transverse (a &b) and dorsal (c & d) images indicating the localization of the caudal epigastric LNs (arrows) in precontrast (a & c) and postcontrast (b & d) images, along the caudal epigastric vessels (asterisk). In a & b, mammary tissue is indicated (arrow heads).

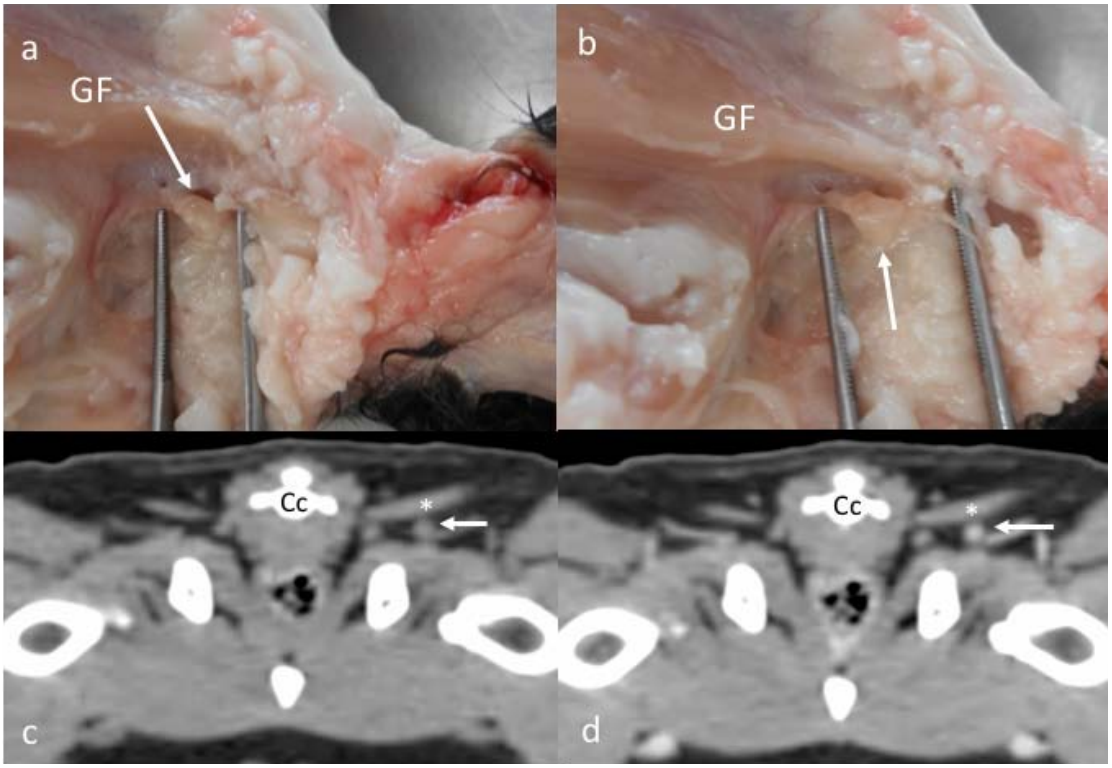

Figure 14. Ischiatic lymph node. a - b. Images of the dissection showing the localization of the ischiatic LN (arrow) deep to the *gluteofemoralis* muscle (GF). c - d. CT transverse images indicating the localization of the ischiatic LN (arrow) seen isoattenuating in the precontrast image (c) and with homogeneous enhancement in the postcontrast image (d), deep to the *gluteofemoralis* (asterisk) muscle. A coccygeal vertebra (Cc) is indicated.

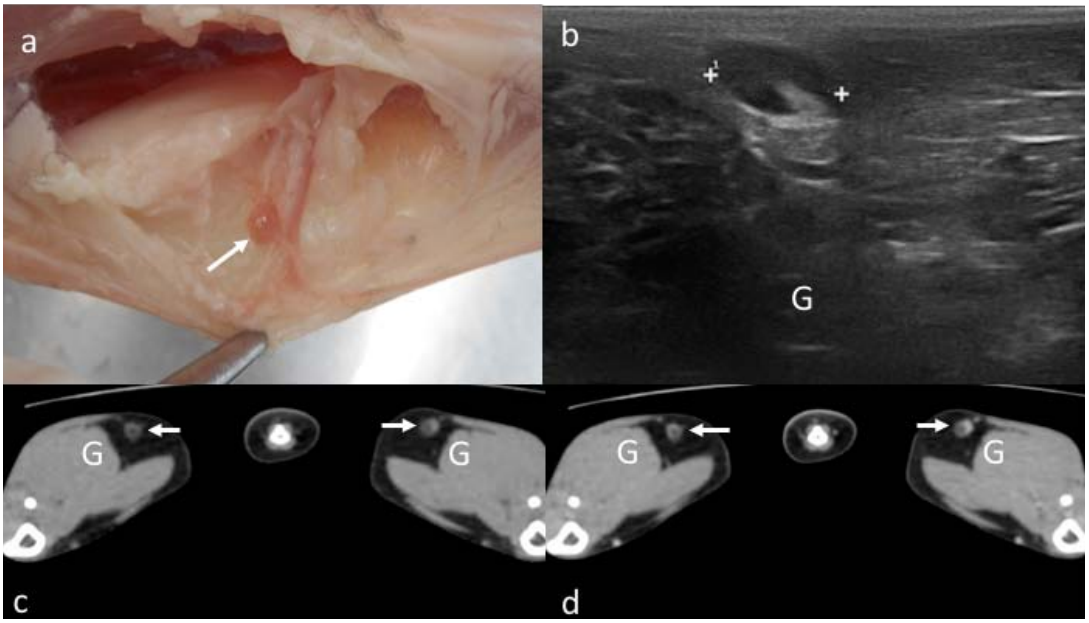

Figure 15. Popliteal lymph nodes. a. Image of the dissection showing the localization of the popliteal LN in the caudo-proximal aspect of the stifle joint (arrow). b. US image showing a heterogeneous (hyperechoic central area compatible with the hilus) popliteal LN (between cursors) caudally to the *gastrocnemius* muscle (G). c - d. CT images indicating the localization of the popliteal LN (arrows) seen heterogeneous with isoattenuating periphery and hypoattenuating center in the precontrast image (c) and with homogeneous peripheral enhancement in the postcontrast image (d). The *gastrocnemius* (G) muscles are indicated.

4.3. Assessment of normal and abnormal lymph nodes in cats using computed tomography and ultrasonography.

Abstract

The lymph nodes (LNs) of a group of diseased cats (case group) were prospectively assessed with computed tomography (CT) and ultrasound (US) and compared with the CT and US images of the LNs from a control group. The length, height, short / long axis ratio, Hounsfield units (HU), attenuation, echogenicity, shape, and margins of the LNs were compared to investigate differences between normal and abnormal LNs, and between CT and US diagnostic accuracy. Three regions of study were determined according to the localization of primary disease as follows: R1 (head and neck), R2 (thorax and forelimb), and R3 (abdomen and hindlimb). The LNs of the cats from the case group were divided into inflammatory or neoplastic category according to the results from the LNs' or primary lesion's cytology or biopsy. Thirty cats were recruited in the control group. For the analysis of each region, the lymph centers (LC) of the control group were matched with the affected lymph centers from the 29 cats included in the case group. In the R1, 62 (I= 14; N= 48) LNs on CT and 58 (I= 14; N= 44) LNs on US were included, representing at least one LN from the mandibular and retropharyngeal lymph centers. In the R2, 22 (I= 11; N= 11) LNs on CT and 18 (I= 8; N= 10) LNs on US were included, mainly from the axillary, cranial mediastinal, and ventral thoracic lymph centers. In the R3, 59 (I= 19; N= 40) LNs on CT and 69 (I= 19; N= 50) LNs on US were included, representing at least one LN from the celiac, cranial and caudal mesenteric lymph centers. The quantitative variables, length, height, and S/L ratio, obtained with both techniques, and the HU before contrast administration, were significantly different between the control and the case group for the R2 and R3. In the R1 the significant differences were found only for the length and height obtained with US, and the HU before and after contrast administration. The distribution of the qualitative variables (attenuation pre- and postcontrast, echogenicity, shape, and margins) among groups was significantly different in the case group compared with the control group. The heterogeneous and hypoattenuating appearance of the most neoplastic and some inflammatory LNs before and after contrast administration could suggest severe changes in the internal structure and vascularization but a certain degree of malignancy

was not possible to determine with CT. A better assessment and more precise measurements were obtained with CT than with US, especially in the R2 (thorax), due to the absence of the artifacts that were present in US. In conclusion, the results of this study allowed the identification of some features of the lymph nodes that are suggestive of abnormality. However, a differentiation between inflammatory and neoplastic processes is more challenging due to overlapping of the features in both techniques.

Introduction

With the new technologies, it is possible to acquire excellent quality images with ultrasonography (US) and with computed tomography (CT), not only in human medicine, but also in veterinary medicine (De Swarte et al., 2011; Nemanic, Hollars, Nelson, & Bobe, 2015; Nyman & O'Brien, 2007; Wunderbaldinger, 2006). This current situation has lead to increase research in order to understand the features of the normal lymph nodes and the changes observed in diseases (Henninger, 2003; Li et al., 2013; Nemanic et al., 2015; Nyman, Kristensen, Skovgaard, & McEvoy, 2005; Nyman & O'Brien, 2007; Salwei, O'Brien, & Matheson, 2005). One of the primary goals in the evaluation of the lymph nodes is to determine if the changes observed are correlated with histological changes, so this could lead to an early and less invasive diagnosis, staging, and prognosis of diseases (Nyman & O'Brien, 2007; Wunderbaldinger, 2006)

The lymph nodes react to endogenous and exogenous agents with a variety of specific morphological and functional responses. Histological changes observed in lymph nodes include necrosis, apoptosis, sinus ectasia, vascular lesions, amyloidosis, lymphadenitis, hyperplasia (e.g. immune, reactive, plasma cell), extramedullary hematopoiesis, lymphoma, and metastases (Elmore, 2006).

Morphologic changes of the lymph nodes (LNs) may be identified using US or CT images. Variations in size, shape, indistinct nodal margins, parenchymal heterogeneity, distinct distribution pattern of the vessels, variations in the

resistive and pulsatility indices, and loss of perinodal fat and hilus have been commonly reported in pathologic lymph nodes (Gendler, Lewis, Reetz, & Schwarz, 2008; Karnik, Reichle, Fischetti, & Goggin, 2009; Nemanic et al., 2015; Nyman & O'Brien, 2007; Tobón Restrepo et al., 2015). However, correlations with the findings in US and/or CT and a specific histologic change or disease in cats are needed.

The aims of the study were; (i) to investigate potential differences in the LNs features evaluated with CT and US between healthy cats and cats with disease, and (ii) to assess the ability of each imaging technique (CT and US) to discriminate between neoplastic and inflammatory changes in the lymph nodes.

Material and methods

This study was approved by the ethical committee of the Universitat Autònoma de Barcelona (reference number CEAAH 2255 of September 2013). Written owner consent was obtained prior inclusion of the cats in this study.

For the purpose of this study, the animals were divided into two groups, a control group and a case group.

Control group: the animals of this group were recruited prospectively from the owners and staff members of the Fundació Hospital Clinic Veterinari of the Universitat Autònoma de Barcelona (FHCV-UAB). The period of the study was September 2013 to July 2015. The group was conformed by healthy cats of more than 1 year of age. Health status was stated on bases of physical exam, biochemistry (calcium, glucose, potassium, total proteins, alanine-amino-transferase (ALT), gamma-glutamyl-transferase (GGT), cholesterol, urea, creatinine), and complete blood count. A SNAP® test to rule out the presence of FIV antibodies and FeLV antigens, and a PCR test to rule out the presence of *Bartonella* sp were performed.

Case group: patients with a neoplastic or infectious/inflammatory disease presented at the diagnostic imaging service of the FHCV-UAB, from November 2013 to April 2015, and presented at the diagnostic imaging division of the veterinary faculty of Utrecht University (DDI-UU), from April 2014 to July 2014 were included prospectively. In order to obtain a final diagnosis, the affected lymph nodes were evaluated with cytology (fine needle aspiration (FNA)), histopathology (US-guided biopsy or surgical excision), or at necropsy when possible. Animals in this group were divided in subgroups according to the affected regions as follows: Region 1: head and neck (R1); Region 2: thorax and forelimb (R2); Region 3: abdomen, pelvis, and hindlimb (R3). In each region, the LNs were classified into a neoplastic (N) or inflammatory (I) category according to the following criteria: 1. LNs with a final diagnosis of neoplasia, metastasis, or inflammatory process. 2. LNs with final diagnosis of reactive hyperplasia but with final diagnosis of neoplasia, metastasis, or inflammatory process from the primary lesion. 3. LNs from LCs in the same region with signs of lymphadenopathy (in CT and US) that were not sampled for cytology but with a final diagnosis of neoplasia, metastasis, or inflammatory process from the primary lesion.

Computed Tomography

Control group: Animals were sedated with an intramuscular administration of midazolam[14] (0.2mg/kg), burtorphanol[15] (0.4mg/kg) and ketamine[16] (5mg/kg). Anesthesia was induced with Isoflurane[17] 5% dosage 100% O_2 at 4L/min and maintained with Isoflurane 1.5 – 2% in 100% of O_2 at 2L/min. Then patients were positioned on the CT table in dorsal recumbency with the forelimbs and hindlimbs outstretched at the sides. A whole body scan was performed. Acquisitions were done in soft tissue algorithm, before and after the intravenous administration of 600mg/kg of Iopromide[18] (300mgI/ml) or Iopamidol[19]

[14] Midazolam 15mg/3ml, Normon, Spain
[15] Torbugesic 10 mg/ml, Zoetis, Alcobendas (Madrid), Spain
[16] Imalgene 100 mg/ml, Merial, Barcelona, Spain
[17] Isoflurane, Abbott Laboratories, Berkshire, UK
[18] Ultravist® 300mg/ml, Bayer pharma AG, Berlin, Germany.

(300mgI/ml). Scans were performed in a 16 slices helical CT-scanner[20]. Technical settings were a slice thickness of 0.625 mm, collimation pitch of 1.25mm, 120 kV, 50 - 90 mA, and a matrix of 512x512.

Case group: due to their clinical condition, each patient underwent anesthesia according to the indications of the anesthesia department of each Veterinary Teaching Hospitals. Then patients were positioned in dorsal recumbency. However, the sternal recumbency was used in patients with a critical clinical condition. A regional scan was performed in soft tissue algorithm before and after intravenous administration of 600mg/kg of Iopamidol (300mgI/ml) at the FHCV-UAB, and 600mg/kg of Iobitridol[21] (350mgI/ml) at DDI-UU. At the FHCV-UAB, scans were performed with the same CT-scanner and technical settings used for the control group. At DDI-UU, scans were performed in a single-slice helical CT scanner[22]. Scans were made in helical acquisition mode with slice thickness reconstructions of 0.6 - 1mm, collimation pitch of 1.25mm, 120 kV, 140 – 160 mA, and a matrix of 512x512.

Image analysis: All data were recorded for further analysis using an image archiving and communication system software[23]. For each lymph node identified, CT characteristics and measurements were performed. Height (short axis) and length (long axis) were obtained to perform a ratio (S/L ratio) in order to compare normal vs abnormal LNs. The height (short axis) was defined as the distance from the ventral to the dorsal border measured in a transverse image. The length (long axis) was determined using a multiplanar reconstruction to generate a sagittal image of the LN at its maximal dimension; an electronic caliper was placed from the rostral/cranial to the caudal border. The shape of the lymph nodes was classified as rounded, elongated, or miscellaneous as previously reported by Beukers et al. (2013) and Nyman, Kristensen, Skovgaard, & McEvoy (2005). Mean attenuation values (Hounsfield units) were determined by placing a circular/oval region of interest (ROI) of 2-4 mm^2 at 3 different places at rostral/cranial, middle, and caudal transverse images. In

[19] Scanlux® 300mg/ml, Sanochemia pharmazeutika, Neufled/Leitha, Austria.
[20] General Electric® Brivo CT 385.
[21] Xenetix 350® 350mg/ml, Guerbet, Paris, France.
[22] Philips Secura, Philips NV, Eindhoven, the Netherlands.
[23] Centricity PACS-IW, GE healthcare (Barcelona) & IMPAX 6, AFGA healthcare (Utrecht)

small LNs, ROIs were made as large as possible inside the lymph node margins. Measurements were performed on images before and following the administration of contrast medium. The lymph nodes attenuation was compared with the surrounding muscles and was classified as isoattenuating, slightly hypoattenuating, hypoattenuating, hyperattenuating, or heterogeneous. Following the administration of contrast medium the enhancement pattern was classified as homogenous, mildly heterogeneous, heterogeneous, and peripheral enhancement. These parameters were determined following the same criteria as in the author's previous reports (Tobón Restrepo et al. 2016a, Tobón Restrepo et al. 2016b).

Ultrasonography

Control group: An ultrasound scan was performed to each animal following the CT scans. Anesthesia was maintained with Isoflurane 1.5 – 2% in 100% of O_2 at 2L/min. The hair of some areas near to the localization of superficial lymph nodes was clipped (neck, shoulders, armpits, abdomen, caudal aspect of the stifle joint). The animals were positioned in dorsal recumbency with the neck extended and the forelimbs stretched caudally. Examinations were performed using an Esaote Mylab70 Xvision® machine with a 4 – 13 MHz high frequency linear transducer. Technical settings were adjusted to improve and obtain the optimal images of the LNs in all the animals. Coupling acoustic gel[24] was generously applied to ensure an adequate skin-transducer contact. Sagittal and transverse images of each lymph node were recorded.

Case group: Ultrasonography was also performed immediately after the CT. Anesthesia was also maintained according to the protocol chosen by the anesthesia service of either FHCV-UAB or DDI-UU. The hair of the region of interest was clipped as in the control group. Examinations at FHCV-UAB were performed using the same machine as in the control group, but at the DDI-UU were done using a Philips HD11 Ultrasound system® machine with a 7 – 15 MHz high frequency linear transducer.

[24] Transonic gel®, Telic, Barcelona, Spain

A fine needle aspiration was performed in abnormal lymph nodes of the case group when possible. Images of each lymph node in sagittal and transverse plane were recorded.

Image analysis: For each lymph node, the transducer was placed with the guide pointing rostral/cranial, parallel (or slightly oblique) to the spine, and an image including the largest measurement of the LN (sagittal plane) was recorded. The length was measured using an electronic caliper from the rostral/cranial to the caudal border (long axis). A second measurement was performed in the same image perpendicularly to the length at the thickest point (ventral to dorsal) and was defined as height. These two measurements were used to calculate the S/L ratio of each LN in US.

For each lymph node, echogenicity was recorded as hypoechoic, isoechoic, hyperechoic, or heterogeneous when compared to surrounding fat tissue. The shape of each lymph node in ultrasonography was evaluated following the same criteria as in CT. Margins were defined as smooth or irregular.

Statistical analysis

Data of this study were digitalized using Excel (2010)[25]. The statistical analyses were performed using SPSS software[26]. The continuous variables obtained in CT and US images in each sub-group were compared using nonparametric statistic as follows: inter-group general comparisons among control, inflammatory and neoplastic LNs were performed with the Kruskal-Wallis test. Inter-group pair comparisons (control and inflammatory; control and neoplastic; inflammatory and neoplastic) were performed with the Mann-Whitney U test. Intra-group pair comparisons (CT and US) were performed with the Wilcoxon test. Fisher exact test was used to evaluate the distributions of the frequencies for the categorical variables. The intra-group and inter-group comparisons were performed for the frequencies of CT and US features. The statistical significance was set to be $P<0.05$.

[25] Microsoft office Excel, 2010

[26] IBM SPSS statistic software version 21, 2012.

Results

Animal description

Control group: 30 cats were recruited in this group. Age and weight average were 3.7 years (range 1.5 – 17) and 4.4 kg (±1.10) respectively. Twenty-nine cats were domestic shorthairs and 1 cat was Persian. The group was conformed by 16.7% entire males (n=5), 20% neutered males (n=6), 30% entire females (n=9) and 33.3% neutered females (n=10). Biochemical determinations and complete blood count were within normal limits. All cats were negative for FIV/FeLV and *Bartonella sp.* tests.

Case group: 29 cats were recruited in this group. Age and weight averages were 9.1 years (range 0.7 – 16) and 3.6 kg (±1.13) respectively. Twenty-one cats were domestic shorthairs, 5 cats were Persian, and one each of the following breeds: Bombay, British shorthair, and Maine coon. The group was conformed by 17.2% entire males (n=5), 27.6% neutered males (n=8), 31.0% entire females (n=9), 24.1% neutered females (n=7). Eleven cats were presented with complains related to the head and neck and were included in the R1 group. Clinical complains were nasal discharge and stridor (n=4), and one each of the following: intraoral mass, mass in the right masseter region, exophthalmos, head tilt suggestive of vestibular syndrome, FIP suspicion, inspiratory and sometimes expiratory laryngeal/tracheal stridor, and intranasal mass. Eight cats presented with complains related to the thorax and forelimb, were included in the R2 group. Clinical complains comprised mediastinal mass (n=3), dyspnea (n=2), masses in the thoracic wall (n=2), and mass in the left forelimb (n=1). Twelve cats were presented with abdominal complains and were included in the R3 group. Clinical signs were vomiting (acute or chronic) (n=3), hepatic mass (n=2), FIP suspicion (n=2), and one each of the following: intestinal adenocarcinoma, mammary mass, lethargy, severe dermatitis, and weight loss. Of the 29 cats, 2 cats were presented with generalized lymphadenomegaly, therefore they were placed in more than one group.

Histopathology results from the FNA and biopsies.

The CT and US images of the control group were analyzed in order to identify all the lymph nodes per lymph center. After the assessment of the CT and US images of the case group, the lymph center from the control group included in the analysis was the one that matched with the affected lymph center in the case group. A total of 723 LNs (R1= 180; R2= 173; R3= 370) from the pre- and postcontrast CT images in the 30 cats of the control group were included. This corresponded to at least one LN per matched lymph center. Additionally, a total of 581 (R1= 180; R2= 85; R3= 316) LNs from the US images were included.

In the case group, a total of 143 and 145 LNs from CT and US respectively were included in the analysis.

In the animals of the R1, 62 (I= 14; N= 48) LNs on CT and 58 (I= 14; N= 44) LNs on US were included, representing at least one LN from the mandibular and retropharyngeal LCs. FNAs were obtained from the mandibular (n=7) and the medial retropharyngeal (n=8) LNs. A biopsy was taken from a mandibular (n=1) LN. Additionally, biopsies results from the nasal mucosa (n=4) and an intraoral mass (n=2) were available. A cytological diagnosis of reactive LN was obtained in 7/8 medial retropharyngeal LN and in 4/7 mandibular LN. A non-diagnostic cytology was obtained in 1/8 medial retropharyngeal LN and in 3/7 mandibular LNs. The biopsy of the mandibular LN concluded a pyogranulomatous lymphadenitis. Four cats with nasal biopsy presented a final diagnosis of chronic rhinitis (n=1), histiocytic sarcoma (n=1), B and T cell lymphoma (n=1), and nasal carcinoma (n=1). One cat with biopsy of an intraoral mass presented a diagnosis of squamous cell carcinoma.

For the R2, 22 (I= 11; N= 11) LNs on CT and 18 (I= 8; N= 10) LNs on US, mainly from the axillary, cranial mediastinal, and ventral thoracic lymph centers, were identified. FNAs were obtained from the sternal (n=3), the cranial mediastinal (n=2), the left axillary (n=1) and the right accessory axillary (n=1) LNs. Additionally, FNA from a mediastinal mass (n=1), a left forelimb mass (n=1), and a biopsy of a mediastinal mass (n=1) and cranial mediastinal LNs (n=2) were available. A cytological diagnosis of reactive LN was obtained in 1/3

sternal and 1/1 right axillary accessory LNs. A non-diagnostic sample was obtained in 1/3 sternal and 1/1 left axillary LNs. Mediastinal lymphoma was diagnosed in 1/2 cranial mediastinal and 1/3 sternal LNs, and epithelial dysplasia with inflammatory cells was diagnosed in 1/2 cranial mediastinal LNs. Additionally, the FNA of the mediastinal mass was compatible with lymphoma, and the mass in the forelimb was compatible with fibrosarcoma. The biopsies of the mediastinal mass and the cranial mediastinal LN (1/2) were compatible with ectopic thyroid C-cell tumor; mediastinal lymphoma was diagnosed in a cranial mediastinal LN (1/2).

In the R3, 59 (I= 19; N= 40) LNs on CT and 69 (I= 19; N= 50) LNs on US were identified, representing at least one LN from the celiac, cranial and caudal mesenteric LCs. FNAs were obtained from the jejunal (n=5), and the colic (n=2) LNs. Biopsies of the jejunal (n=3), and the caudal mesenteric (n=1) LNs were obtained. FNA of the liver (n=1) and biopsies from the jejunum (n=3), duodenum (n=1), omentum (n=1), and mammary gland (n=1) were available. The cytology was compatible with reactive LN in 3/5 jejunal LNs. A non-diagnostic test was obtained in 1/5 jejunal and 1/2 colic LNs. Lymphoma was diagnosed in 1/5 jejunal LNs, and in 1/2 colic LN. The biopsies of the jejunal LNs were compatible with grade 2 intestinal lymphoma (2/3) and FIP (1/3). Sinus ectasia was diagnosed in the caudal mesenteric LN. The FNA of the liver was suggestive of adenocarcinoma. The biopsies of the jejunum were compatible with grade 2 intestinal lymphoma in 1/3 jejunal samples, and 1/1 duodenum. Intestinal sarcoma was diagnosed in 1/3 jejunal samples. Biopsies of 1/3 jejunal samples and omentum were compatible with feline infectious peritonitis. Mammary carcinoma was diagnosed in 1/1 mammary gland.

CT and US features of LNs.

The mean and standard deviation (SD) of the length, height, S/L ratio of LNs obtained in both techniques for each region are summarized in tables 1 - 3. The qualitative features of the LNs were analyzed by the comparison of the frequencies distribution, and the results are summarized in the table 4.

In the R1, the comparisons among groups (Table 1) showed that the LNs were significantly longer in the inflammatory category in both techniques, when compared with the control group, and only significant for the CT, when compared with the neoplastic category. The height of the LNs in CT was higher in the inflammatory categories than in the others. However, there was no statistical difference among groups. On the other hand, the height in US was higher in the inflammatory category, followed by the neoplastic category and the smallest was in the control group. Being this distribution statistically significant in the inter-group comparisons, but not for the comparison between inflammatory and neoplastic. The S/L ratio was higher in the inflammatory category for the CT, but was slightly lower in the US when compared with the control group and the neoplastic categories (the height presented the same value for control and neoplastic). The inter-group comparisons (Table 1) did not show statistical differences for the S/L ratio. The intra-group comparison showed significant differences in height and S/L ratio in both categories of the case group. These were higher in CT when compared with US for both categories. The attenuation of the LNs before contrast administration presented a significantly different distribution between groups. A higher frequency of isoattenuating LNs was identified in all three compared groups, being significantly higher in the inflammatory category. However, the neoplastic category presented 12.5% of the LNs with heterogeneous attenuation, and the overall distribution of attenuation was significantly different when compared with the control group. After contrast administration, more than 50% of the LNs in the three groups showed homogeneous contrast enhancement, being higher in the control group (70.6%). However, both inflammatory and neoplastic LNs presented a significantly higher frequency of heterogeneous contrast enhancement when compared with the control group. The LNs of the inflammatory category presented the highest and the lowest HU before and after contrast administration, respectively. These differences were statistically significant for variables with the control group, but only after contrast with the neoplastic category. Ultrasonographicaly, the LNs of the control group and the inflammatory category where frequently hypoechoic, 82.2 % and 85.7% respectively, differing significantly from the neoplastic category in which heterogeneous echogenicity was found in the 52.3% of the LNs. A hyperechoic

hilus was only seen in the 6.1% of the LNs in the control group and it was not visualized in the case group. Fusiform LNs were frequently found in the three groups. However, 18.2% of the LNs in the neoplastic group were miscellaneous differing significantly from the 5% in the control group, but not from the 14.3% of the inflammatory category. The margins of the LNs were regular in 100% of the LNs in the control group. Even though regular margins were also frequently found in the case group, irregular margins were present in 14.3% and 6.8% of the inflammatory and neoplastic LNs, respectively. This margins distribution was significantly different between the two case categories and the control group.

In the R2, the assessment of the CT and US images showed that the mean length of the LNs in the inflammatory category was higher when compared with the mean values in the neoplastic category and in the control group, being statistically significant only for the comparison with the control group (Table 2) in both modalities. The neoplastic category presented LNs with higher height and S/L ratio than the other groups. On the US images, the length was significantly higher in the inflammatory category but the height and S/L ratio were significantly higher in the neoplastic category. In the intra-group comparisons (Table 2), the height and S/L ratio differed significantly between CT and US in the inflammatory category. In the neoplastic category, only the height differed significantly between CT and US. The attenuation of the LNs before contrast administration presented a significantly different distribution between the groups as seen in the R1. Isoattenuating LNs were identified frequently in the three groups. However, 20% of the LNs were hyperattenuating in the neoplastic group and this was statistically significant when compared with the control group. After contrast administration, the distribution of the frequencies differed statistically among the groups. The neoplastic and inflammatory categories showed 63.6% and 54.4% of the LNs with heterogeneous contrast enhancement compared with the 0.0% in the control group. The control group showed 67.1% of the LNS with homogeneous contrast enhancement. The mean HU before contrast administration was higher in the neoplastic category and this was significantly different when compared with the control group. The mean HU after the administration of contrast differed significantly between the

inflammatory and neoplastic categories, being higher in the inflammatory category, but there was no significant difference with the control group. In US, heterogeneous echogenicity was most frequently seen in inflammatory (62.5%) and neoplastic (60.0%) LNs and this was significantly different when compared with the LNs of the control group (41.2% were isoechoic). A hyperechoic hilus was only seen in 12.9% of the LNs in the control group, but was not identified in the case group. Eighty per cent of the neoplastic LNs presented rounded shape differing statistically from the control (55.3% rounded) and the inflammatory (62.5% fusiform) groups. The margins of the LNs were regular in 100% of the LNs in the control group as in the R1. However, the neoplastic and inflammatory LNs presented a 30.0% and 25.0% of LNs with irregular margins, respectively.

In the R3, the inter-group comparisons (Table 3) showed that the mean length and height, in CT and US, were significantly higher in both categories of the case group when compared with the control group. However, the inflammatory category showed larger LNs than the neoplastic category. When the comparison between the two categories of the case group was made, the length and height of the LNs in US were significantly higher in the inflammatory category. The S/L ratio in the case group was statistically higher when compared with the control group. No statistical differences were found between inflammatory and neoplastic S/L ratio of the LNs. In the intra-group comparison (Table 3), only the height in the neoplastic category was statistically higher in the CT compared with US. The attenuation of the LNs before contrast administration showed higher frequencies for the isoattenuating and the slightly hypoattenuating characteristics in all groups. Inflammatory LNs showed a higher frequency of isoattenuating (78.9%) when compared with neoplastic LNs and the control group. After contrast administration, 72.2% of the LNs in the control group showed homogeneous contrast enhancement. The inflammatory and neoplastic LNs showed a significantly higher proportion of heterogeneous contrast enhancement compared with the control group. The mean HU before contrast administration was significantly higher in the LNs of the inflammatory category when compared with the LNs of neoplastic category and the control group. The mean HU after the administration of contrast was significantly lower in the LNs of the neoplastic category when compared with the other groups.

The control group presented the highest HU after contrast. On US images, the LNs were hypoechoic in 53.5%, 73.7% and 50.0% for the control, inflammatory and neoplastic groups, respectively. Furthermore, the neoplastic LNs presented heterogeneous echogenicity in the 44.0% being only statistically different from the control group. The hyperechoic hilus was only seen in 16.1% of the LNs in the control group but was not identified in the case group. The shape was a very variable characteristic in the control group, with 43.7% of fusiform lymph nodes. On the other hand, the inflammatory category presented 63.2% of miscellaneous LNs, and the neoplastic category 50.0% of rounded LNs, showing significant differences with the control group but not between them. The margins of the LNs were irregular in 52.0% and 42.1% of the neoplastic and inflammatory categories, respectively, being significantly different from the control group that showed regular margins in 94.0% of the LNs.

Discussion

In this study, we show the comparison between the CT and US features of the lymph nodes in a group of healthy cats with the findings in a group of diseased cats. The enrollment of healthy cats (control group) in this study was based in the clinical tests and physical examination. The features of the LNs in the control group concurred with the previous descriptions of normal LNs in cats and dogs. On CT, the LNs were frequently iso- or slightly hypoattenuating in pre-contrast images with homogeneous contrast enhancement (Beukers et al., 2013; Nemanic & Nelson, 2012; Nyman et al., 2005). On US, the LNs were frequently isoechoic or hypoechoic. In some LNs a hyperechoic hilus was visible as previously reported (Nyman et al., 2005; Tobón Restrepo et al., 2015b). The majority of the LNs were elongated with smooth margins. However, rounded and miscellaneous LNs were found in the thorax and abdomen as previously reported (Beukers et al., 2013; D'Anjou, 2008; Hecht & Henry, 2007; Schreurs et al., 2008; Tobón Restrepo, 2015b).

Findings in our study suggest that inflammatory LNs are frequently longer and thicker than neoplastic or normal LNs. However, mean values were obtained with the combination of two or more lymph centers per region that could have an influence in this result. Additionally, in the patients with inflammatory diseases, severe pyogranulomatous lymphadenitis was observed, in the context of FIP. Marked LNs enlargement has been described in cats with FIP (Lewis & O'Brien, 2010).

In human medicine, the L/S ratio is used more frequently than the S/L ratio. It has been determined that a L/S ratio of <2 obtained with CT or US is statistically associated with malignancy in head and neck LNs (Mack, Rieger, Baghi, Bisdas, & Vogl, 2008; Mohseni et al., 2014; Steinkamp et al., 1995; Steinkamp, Hosten, Richter, Schedel, & Felix, 1994; Vassallo, Wernecke, Roos, & Peters, 1992). In veterinary medicine, the S/L ratio has been used instead in the differentiation of metastatic vs reactive or normal LNs. (Nyman, Kristensen, Flagstad, & Mcevoy, 2004; Nyman et al., 2005; Nyman & O'Brien, 2007; Tohnosu, Onoda, & Isono, 1989). Nyman et al. (2004) reported a S/L ratio obtained with US of >0.55 to be related with metastatic LNs, and a ratio of <0.55 to be related with a reactive or a normal LN. Likewise, a S/L ratio >0.5 of deep LNs in the dog was significantly associated with neoplasia (De Swarte et al., 2011). Similar results were obtained in our study. The control group showed S/L ratios <0.55 in the three regions, consistent with the previous descriptions. Interestingly, the S/L ratios of the inflammatory and neoplastic categories were <0.55 for both modalities in the R1. We observed that in this region, some mandibular and medial retropharyngeal LNs presented a homogeneous enlargement keeping their elongated shape. This could explain the small variation and the lack of significance in the S/L ratios when comparisons of ratios from normal LN with the ratios from the case group were performed. This situation is very different in the other 2 regions. The neoplastic category showed significantly higher S/L ratio (>0.55) in both modalities for the R2 and R3. This result is consistent with the previous reports that suggest that metastatic LNs presented somehow a rounded shape. However, in the R3, the S/L ratio of the LN in the inflammatory category was >0.55 for the CT images but <0.55 in US images. Previous studies have mentioned the impossibility to ensure an

accurate measurement of the full length specifically of the jejunal LNs with US (Agthe, Caine, Posch, & Herrtage, 2009). We also found difficult to assess accurately the LNs dimensions of the R3 with US in all the groups. In this region, the LNs of the neoplastic category were significantly bigger with CT when compared with US. An explanation for this is that with CT the assessment of the LN is more accurate due to the lack of superimposition of structures and the possibility to obtain multiplanar reconstructions. Another possible explanation is that the artifacts produced by the gas or feces in the intestines in US can significantly reduce the assessment of the abdominal structures including the LNs. The S/L ratios of the categories from the case group were not significantly different with CT for the R2 and R3 regions. This suggests that inflammatory LNs may increase considerably in size, especially, if the cat is presented with pyogranulomatous lymphadenitis.

In human medicine, LNs are considered malignant in CT images when there is necrotic or cystic changes and/or heterogeneous contrast enhancement, and/or detectable extra nodal tumor spread, and/or they are clearly enlarged in number (Steinkamp et al., 1994; Wunderbaldinger, 2006). In veterinary medicine, mandibular and medial retropharyngeal LNs presenting ellipsoidal shape, heterogeneous contrast enhancement, and hyperattenuating foci (centrally and peripherally) were considered suggestive of lymphadenopathy in cats with nasal polyps (Oliveira, O'Brien, Matheson, & Carrera, 2012). In previous studies, the medial retropharyngeal LNs of cats with nasal lymphoma demonstrated more contrast enhancement and were more homogeneous than those with nasal carcinoma; additionally, the medial retropharyngeal LNs of cats with eosinophilic rhinitis showed a more symmetric and homogeneous pattern of contrast enhancement than cats with suppurative rhinitis (Nemanic et al., 2015). The mandibular and the medial retropharyngeal LNs were most frequently enlarged and showed heterogeneous contrast enhancement with central hypoattenuation in cats with fungal rhinitis and sinusitis (Karnik et al., 2009). Gendler et al. (2008) reported that the mandibular and the medial retropharyngeal LNs were enlarged and showed a rim-enhancement pattern with decrease hilar attenuation in cats with oral squamous cell carcinoma. In our study, the distribution of frequencies for the attenuation before contrast was

significantly variable. However, a higher frequency of isoattenuating LNs was identified in the three groups for the three regions. There were significant differences in the distribution of attenuation between the control group and the neoplastic category in the three regions. The neoplastic category presented high frequencies of heterogeneous attenuating and hypoattenuating LNs. Meanwhile, the inflammatory category presented a similar frequency distribution of attenuation with the control group. Furthermore, in the R1 and R3, the inflammatory category presented the highest frequency of isoattenuating LNs. The cellular conformation/infiltration of the LN, the amount of cellular degradation, and the alteration in the vasculature could explain the different distribution among groups. We hypothesized that the loss of the perihilar fat could influence in the homogeneity of the attenuation in the case group compared with the normal group. Nevertheless, the exact cause remains unclear. In the postcontrast images, a high frequency of homogeneous enhancement was generally seen in the R1 and R3. In the R2, the case group presented heterogeneous contrast enhancement frequently meanwhile the control group was frequently homogeneous. Our results suggest that inflammatory and neoplastic LNs can exhibit heterogeneous contrast enhancement in similar proportions. A statistical significant difference was only determined in the R2, were all the inflammatory LNs were slightly heterogeneous or showed heterogeneous contrast enhancement, meanwhile neoplastic LNs presented 40% of homogeneous enhancement. Additionally, in the R3, the inflammatory LNs showed peripheral contrast enhancement more frequently than in the neoplastic category and in the control group. We hypothesized that the presence of pyogranulomatous lymphadenitis and sinus ectasia in some LNs of the inflammatory group could have an influence in this result. Elmore, (2006) described that the internal structure of the lymph nodes, with pyogranulomatous changes or sinus ectasia, is replace by intranodal abscesses or cavities filled with lymph. The neoplastic changes in the LNs (due to primary neoplasia or metastasis) normally produce loss of the normal architecture, capsular and perinodal fat invasion, presence of monomorphic population of lymphocytes and changes in nodal size and shape (Elmore, 2006). The LNs of the case group showed significantly higher HU than the control group. After contrast, the HU values were statistically higher in the case

group for the R1. In the R2 the HU values were similar among groups. In the R3, the HU values in the control group were significantly higher than in the case group. We consider that a higher frequency of heterogeneous contrast enhancement in the case group could influence these results due to the inclusion of areas of reduced contrast enhancement in the ROI.

The internal echogenicity of benign or neoplastic LNs is described in human medicine as isoechoic and hypoechoic in comparison with adjacent tissue, respectively (Khanna, Sharma, Khanna, Kumar, & Shukla, 2011; Mohseni et al., 2014; Steinkamp et al., 1995; Tohnosu et al., 1989). In veterinary medicine, previous reports in dogs referred to heterogeneous echogenicity in LNs in lymphoma and anal sac carcinoma (Llabrés-Díaz, 2004). In a study about abnormal superficial LNs in the dog, normal and reactive LNs were most frequently isoechoic, meanwhile LNs with lymphoma, and metastatic were hypoechoic (Nyman et al., 2005). The results of the present study suggest that neoplastic LNs are usually either hypoechoic or heterogeneous. Meanwhile inflammatory LNs are most frequently hypoechoic. In the R1, the comparison between the categories of the case group showed significant differences suggesting that neoplastic LNs are more heterogeneous with US and inflammatory LNs are most frequently hypoechoic. This result is different to previous reports in which inflammatory LNs were often isoechoic (Nyman et al., 2004; Nyman & O'Brien, 2007), but in agreement with another study that found that inflammatory and neoplastic LNs can have a similar proportion of heterogeneous echogenicity in cats (Kinns & Mai, 2007).

In our results, normal LNs had regular margins and frequently a fusiform shape in the R1 and R3 and were often rounded in the R2 as previously described (Tobón Restrepo, 2015a; Tobón Restrepo et al., 2015b). Other reports mentioned that the US features related with lymphadenopathy are a plump shape with rounded borders and irregular margins (Khanna et al., 2011; Mohseni et al., 2014; Nyman & O'Brien, 2007). In accordance with those, the neoplastic LNs in our study presented a significantly more frequent rounded shape compared with the inflammatory LNs and the control group, that were often fusiform. The LNs in the case group often presented regular margins in the inflammatory category. However, irregular margins were seen in markedly

enlarged lymph nodes, for example jejunal LNs with pyogranulomatous lymphadenopathy in the cases diagnosed with FIP. The neoplastic category presented the highest frequency of irregular margins in the LNs of the case group.

There are limitations in this study, the prospective nature makes the cases selection challenging. In some cases, it was impossible to repeat the FNA after a laboratory result of non-diagnostic smear due to owner consent or anesthetic risk for the patient. The FNA of LNs has been reported as a technique that is highly operator dependent. Other important factors include that immature or neoplastic lymphoid cells are fragile, and LNs aspirates can yield perinodal fat or other tissues. (Amores-Fuster, Cripps, Graham, Marrington, & Blackwood, 2015). Smears with non-diagnostic results limited the inclusion of more LNs in our study. The repeatability of the diseases was low; even though the study was performed in two university hospitals, the anesthetic risk, the owners' consent, and the viability of a LN sampling affected the inclusion of many patients. Another limitation in this study is the small number of LNs and the lack of definitive diagnoses from other LNs of the same patient that could be included in the statistical analysis to identify patterns of changes in the different groups of specific diseases.

The results of this study allowed the identification of some features of the lymph nodes that could be suggestive of abnormality. However, a differentiation between inflammatory and neoplastic processes is more challenging. A better assessment and more precise measurements are obtained with CT than with US, especially in the thorax, due to the absence of the artifacts that are present in US. In our study the attenuation of the inflammatory and neoplastic LNs before and after contrast administration could suggest severe changes in the internal structure and vascularization but is not possible to determine a certain degree of malignancy with CT. Ultrasound could have a slight advantage over the CT assessing the vascularization of the LNs with color or power Doppler. Unfortunately, this function was not performed in our study because it is time consuming leading to an undesirable extended anesthesia time. Biopsy and fine needle aspirates (with several repetitions) are still the gold standard to obtain a final diagnosis of lymph nodes pathology.

In conclusion, LNs of cats with inflammatory or neoplastic processes exhibit features that could be used to differentiate them from normal LNs using both CT and US. Overlapping in the features of both techniques in the categories of the case group prevent an accurate and significant distinction between inflammation and neoplasia. Further studies with a larger sample size could provide more information to complement this study.

References

Agthe, P., Caine, A. R., Posch, B., & Herrtage, M. E. (2009). Ultrasonographic Appearance of Jejunal Lymph Nodes in Dogs Without Clinical Signs of Gastrointestinal Disease. *Veterinary Radiology & Ultrasound*, *50*(2), 195–200.

Amores-Fuster, I., Cripps, P., Graham, P., Marrington, A. M., & Blackwood, L. (2015). The diagnostic utility of lymph node cytology samples in dogs and cats. *The Journal of Small Animal Practice*, *56*(2), 125–9.

Beukers, M., Vilaplana Grosso, F., & Voorhout, G. (2013). Computed Tomographic Characteristics of Presumed Normal Canine Abdominal Lymph Nodes. *Veterinary Radiology & Ultrasound, 54*(6), 610–617.

D'Anjou, M.-A. (2008). Abdominal cavity, Lymph nodes, and Great Vessels. In D. Penninck & M.-A. D'Anjou (Eds.), *Atlas of small animal ultrasonography* (First edit., pp. 445 – 463). Ames : Iowa: Blackwell Publishing Ltd.

De Swarte, M., Alexander, K., Rannou, B., D'Anjou, M.-A. A., Blond, L., & Beauchamp, G. (2011). Comparison of sonographic features of benign and neoplastic deep lymph nodes in dogs. *Veterinary Radiology and Ultrasound*, *52*(4), 451–456.

Elmore, S. A. (2006). Histopathology of the Lymph Nodes. *Toxicologic Pathology*, *34*, 425–454.

Gendler, A., Lewis, J. R., Reetz, J. A., & Schwarz, T. Computed tomographic features of oral squamous cell carcinoma in cats: 18 cases (2002–2008). , Journal of the American Veterinary Medical Association 319–325 (2008). - American Veterinary Medical Association.

Hecht, S., & Henry, G. (2007). Sonographic Evaluation of the Normal and Abnormal Pancreas. *Ultrasound*, *22*(3), 115–121.

Henninger, W. (2003). Use of computed tomography in the diseased feline thorax. *Journal of Small Animal Practice*, *44*(2), 56–64.

Karnik, K., Reichle, J. K., Fischetti, A. J., & Goggin, J. M. (2009). Computed Tomographic Findings of Fungal Rhinitis and Sinusitis in Cats. *Veterinary Radiology & Ultrasound*, *50*(1), 65–68.

Khanna, R., Sharma, A. D., Khanna, S., Kumar, M., & Shukla, R. C. (2011). Usefulness of ultrasonography for the evaluation of cervical lymphadenopathy. *World Journal of Surgical Oncology*, *9*(1), 29.

Kinns, J., & Mai, W. (2007). Association between malignancy and sonographic heterogeneity in canine and feline abdominal lymph nodes. *Veterinary Radiology & Ultrasound*, *48*(6), 565–569.

Lewis, K. M., & O'Brien, R. T. (2010). Abdominal ultrasonographic findings associated with feline infectious peritonitis: A retrospective review of 16 cases. *Journal of Animal Hospital Association*, *46*, 152–160.

Li, L., Mori, S., Kodama, M., Sakamoto, M., Takahashi, S., & Kodama, T. (2013). Enhanced sonographic imaging to diagnose lymph node metastasis: importance of blood vessel volume and density. *Cancer Research*, *73*(7), 2082–92.

Llabrés-Díaz, F. J. (2004). Ultrasonography of the medial iliac lymph nodes in the dog. *Veterinary Radiology & Ultrasound*, *45*(2), 156–165.

Mack, M. G., Rieger, J., Baghi, M., Bisdas, S., & Vogl, T. J. (2008). Cervical lymph nodes. *European Journal of Radiology*, *66*(3), 493–500.

Mohseni, S., Shojaiefard, A., Khorgami, Z., Alinejad, S., Ghorbani, A., & Ghafouri, A. (2014). Peripheral lymphadenopathy: Approach and diagnostic tools. *Iranian Journal of Medical Sciences*, *39*(2 SUPPL.), 158–170.

Nemanic, S., Hollars, K., Nelson, N. C., & Bobe, G. (2015). Combination of Computed Tomographic Imaging Characteristics of Medial Retropharyngeal Lymph Nodes and Nasal Passages Aids Discrimination Between Rhinitis and Neoplasia in Cats. *Veterinary Radiology & Ultrasound*, *56*(6), 617–627.

Nyman, H. T., Kristensen, A. T., Flagstad, A., & Mcevoy, F. J. (2004). A review of the sonographic assessment of tumor metastases in liver and superficial lymph nodes. *Veterinary Radiology & Ultrasound*, *45*(5), 438–448.

Nyman, H. T., Kristensen, A. T., Skovgaard, I. M., & McEvoy, F. J. (2005). Characterization of normal and abnormal canine superficial lymph nodes using gray-scale B-mode, color flow mapping, power, and spectral doppler ultrasonography: A multivariate study. *Veterinary Radiology and Ultrasound*, *46*(5), 404–410.

Nyman, H. T., & O'Brien, R. T. (2007). The Sonographic Evaluation of Lymph Nodes. *Clin Tech Small Anim Pract*, *22*(3), 128–137.

Oliveira, C. R., O'Brien, R. T., Matheson, J. S., & Carrera, I. (2012). Computed tomographic features of feline nasopharyngeal polyps. *Veterinary Radiology & Ultrasound*, *53*(4), 406–11.

Salwei, R. M., O'Brien, R. T., & Matheson, J. S. (2005). Characterization of lymphomatous lymph nodes in dogs using contrast harmonic and power doppler ultrasound. *Veterinary Radiology and Ultrasound*, *46*(5), 411–416.

Schreurs, E., Vermote, K., Barberet, V., Daminet, S., Rudorf, H., & Saunders, J. H. (2008). Ultrasonographic Anatomy of Abdominal Lymph Nodes in the Normal Cat. *Veterinary Radiology & Ultrasound*, *49*(1), 68–72.

Steinkamp, H. J., Cornehl, M., Hosten, N., Pegios, W., Vogl, T., & Felix, R. (1995). Cervical lymphadenopathy: Ratio of long- to short-axis diameter as a predictor of malignancy. *British Journal of Radiology*, *68*(807), 266–270.

Steinkamp, H. J., Hosten, N., Richter, C., Schedel, H., & Felix, R. (1994). Enlarged cervical lymph nodes at helical CT. *Radiology*, *191*, 795–798.

Tobón Restrepo, M. (2015a). Ultrasound of the abdominal cavity, lymph nodes and large vessels. In R. Novellas Torroja, E. Dominguez Miño, Y. Espada Gerlach, Y. Martínez Pereira, & M. Tobón Restrepo (Eds.), *Diagnostic ultrasound in cats* (1st ed., pp. 211 – 229). Zaragoza: Spain: Servet editorial - Grupo Asís Biomedia S.L.

Tobón Restrepo, M., Novellas, R., Espada, Y., Aguilar, A., Moll, X., & Boroffka, S. (2015b). Ultrasonography and computed tomography features of lymph nodes in healthy cats. In *Abstracts from the 2014 european veterinary diagnostic imaging annual conference.*

Veterinary Radiology & Ultrasound (Vol. 56, p. 700). Utrecht, The Netherlands.

Tobón Restrepo, M., Espada, Y., Aguilar, A., Moll, X., & Novellas, R. (2016a). Anatomic, computed tomographic, and ultrasonographic assessment of the lymph nodes in healthy adult cats: Part I. The head, neck, thorax, and forelimb. Pending of publication.

Tobón Restrepo, M., Novellas, R., Aguilar, A., Moll, X., & Espada, Y. (2016b). Anatomic, computed tomographic, and ultrasonographic assessment of the lymph nodes in healthy adult cats: Part II. The abdomen and hindlimb. Pending of publication.

Tohnosu, N., Onoda, S., & Isono, K. (1989). Ultrasonographic evaluation of cervical lymph node metastases in esophageal cancer with special reference to the relationship between the short to long axis ratio (S/L) and the cancer content. *JCU J Clin Ultrasound*, *17*(2), 101–106.

Vassallo, P., Wernecke, K., Roos, N., & Peters, P. (1992). Differentiation of benign from malignant superficial lymphadenopathy: the rol of high-resolution US. *Radiology*, (183), 215–220.

Wunderbaldinger, P. (2006). Problems and prospects of modern lymph node imaging. *Modern Lymphnode Imaging*, *58*(3), 325–337.

Table 1. Mean and SD for the quantitative variables obtained with CT and US of the LNs in the R1 (head and neck). Inter and intra group comparison among techniques.

Features	Control (C)			Inflammatory (I)			Neoplastic (N)		
Computed tomography	n	Mean	SD	n	Mean	SD	n	Mean	SD
Length (mm)	180	14.38	5.59	14	16.74	4.62	48	13.64	5.64
Height (mm)	180	6.04	4.49	14	8.36	6.24	48	5.77	4.21
S/L ratio	180	0.39	0.20	14	0.50	0.41	48	0.44	0.41
HU PC	180	39.76	11.28	14	49.50	8.27	48	43.67	16.17
HU AC	180	132.94	30.93	14	117.74	5.74	48	140.34	21.08
Ultrasonography									
Length (mm)	180	11.01	3.59	14	15.31	3.49	44	13.14	5.42
Height (mm)	180	3.32	1.25	14	4.35	2.02	44	4.06	2.01
S/L ratio	180	0.31	0.09	14	0.28	0.07	44	0.31	0.09

Features	Comparisons	*P*-Value			
		CT	**US**	**Inflammatory**	**Neoplastic**
Length	C x I x N*	0.068	**0.000**		
	C x I†	**0.044**	**0.000**		
	C x N†	0.356	**0.009**		
	I x N†	**0.025**	0.050		
	CT x US ¶			0.184	0.058
Height	C x I x N*	0.241	**0.018**		
	C x I†	0.099	**0.028**		
	C x N†	0.906	**0.037**		
	I x N†	0.113	0.636		
	CT x US ¶			**0.013**	**0.000**
S/L ratio	C x I x N*	0.964	0.398		
	C x I†	0.791	0.182		
	C x N†	0.975	0.902		
	I x N†	0.801	0.217		
	CT x US ¶			**0.041**	**0.003**
HU PC	C x I x N*	**0.014**			
	C x I†	**0.002**			
	C x N†	0.503			
	I x N†	0.080			
HU AC	C x I x N*	**0.009**			
	C x I†	**0.047**			
	C x N†	0.109			
	I x N†	**0.000**			

* Kruskal-Wallis test, † Mann-Whitney U test, ¶ Wilcoxon test. Statistic significant when P>0.05. S/L ratio: short / long axis ratio; HU PC: Hounsfield units precontrast; HU AC: Hounsfield units after contrast.

Table 2. Mean and SD for the quantitative variables obtained with CT and US of the LNs in the R2 (thorax and forelimb). Inter and intra group comparison among techniques.

Features	Control (C)			Inflammatory (I)			Neoplastic (N)		
Computed tomography	n	Mean	SD	n	Mean	SD	n	Mean	SD
Length (mm)	173	10.89	4.65	11	17.28	4.74	11	12.53	7.86
Height (mm)	173	4.21	1.67	11	8.86	2.77	11	9.09	6.51
S/L ratio	173	0.43	0.18	11	0.53	0.16	11	0.83	0.56
HU PC	173	20.81	23.56	11	35.00	12.94	10	44.40	15.56
HU AC	173	88.95	34.06	11	99.42	21.16	11	82.24	11.38
Ultrasonography									
Length (mm)	85	7.65	2.35	8	12.08	4.88	10	11.72	8.53
Height (mm)	85	3.37	1.12	8	3.99	0.91	10	6.92	4.59
S/L ratio	85	0.46	0.15	8	0.36	0.13	10	0.65	0.23

Features	Comparisons	*P*-Value			
		CT	**US**	**Inflammatory**	**Neoplastic**
Length	C x I x N*	**0.001**	**0.026**		
	C x I†	**0.000**	**0.008**		
	C x N†	0.891	0.267		
	I x N†	0.071	0.657		
	CT x US¶			0.069	0.594
Height	C x I x N*	**0.000**	**0.026**		
	C x I†	**0.000**	0.074		
	C x N†	**0.018**	**0.030**		
	I x N†	0.818	0.327		
	CT x US¶			**0.017**	**0.017**
S/L ratio	C x I x N*	**0.017**	**0.008**		
	C x I†	0.053	0.056		
	C x N†	**0.027**	**0.018**		
	I x N†	0.577	**0.008**		
	CT x US¶			**0.036**	0.374
HU PC	C x I x N*	**0.001**			
	C x I†	0.054			
	C x N†	**0.001**			
	I x N†	0.159			
HU AC	C x I x N*	0.201			
	C x I†	0.206			
	C x N†	0.252			
	I x N†	**0.045**			

* Kruskal-Wallis test, † Mann-Whitney U test, ¶ Wilcoxon test. Statistic significant when P>0.05. S/L ratio: short / long axis ratio; HU PC: Hounsfield units precontrast; HU AC: Hounsfield units after contrast.

Table 3. Mean and SD for the quantitative variables obtained with CT and US of the LNs in the R3 (abdomen, pelvis and hindlimb). Inter and intra group comparison among techniques.

Features	Control (C)			Inflammatory (I)			Neoplastic (N)		
Computed tomography	n	Mean	SD	n	Mean	SD	n	Mean	SD
Length (mm)	370	11.56	9.05	19	20.36	13.50	40	13.61	7.94
Height (mm)	370	4.18	2.02	19	8.74	3.69	40	7.62	3.95
S/L ratio	370	0.50	0.30	19	0.63	0.47	40	0.64	0.34
HU PC	370	32.72	19.37	19	42.33	8.80	40	35.18	14.40
HU AC	370	111.63	31.71	19	106.91	23.37	40	103.71	22.73
Ultrasonography									
Length (mm)	316	9.24	6.33	19	16.89	9.92	50	11.69	7.06
Height (mm)	316	3.20	1.18	19	7.68	4.01	50	5.55	2.95
S/L ratio	316	0.42	0.18	19	0.51	0.19	50	0.54	0.19

Features	Comparisons	*P*-Value			
		CT	**US**	**Inflammatory**	**Neoplastic**
Length	C x I x N*	**0.000**	**0.000**		
	C x I†	**0.001**	**0.000**		
	C x N†	**0.006**	**0.020**		
	I x N†	0.085	**0.039**		
	CT x US ¶			0.619	0.722
Height	C x I x N*	**0.000**	**0.000**		
	C x I†	**0.000**	**0.000**		
	C x N†	**0.000**	**0.000**		
	I x N†	0.311	**0.026**		
	CT x US ¶			0.381	**0.014**
S/L ratio	C x I x N*	**0.007**	**0.000**		
	C x I†	0.321	**0.037**		
	C x N†	**0.002**	**0.000**		
	I x N†	0.408	0.510		
	CT x US ¶			0.246	0.092
HU PC	C x I x N*	**0.032**			
	C x I†	**0.009**			
	C x N†	0.682			
	I x N†	**0.032**			
HU AC	C x I x N*	0.085			
	C x I†	0.461			
	C x N†	**0.033**			
	I x N†	0.372			

* Kruskal-Wallis test, † Mann-Whitney U test, ¶ Wilcoxon test. Statistic significant when P>0.05. S/L ratio: short / long axis ratio; HU PC: Hounsfield units precontrast; HU AC: Hounsfield units after contrast.

Table 4. Comparison of CT and US characteristics of LNs in the control and case groups per regions.

Features	R1								R2								R3							
	Control		Inflammatory		Neoplastic		Comparisons	P-Value	Control		Inflammatory		Neoplastic		Comparisons	P-Value	Control		Inflammatory		Neoplastic		Comparisons	P-Value
Computed tomography	n	%	n	%	n	%			n	%	n	%	n	%			n	%	n	%	n	%		
Precontrast																								
Isoattenuating	91	50.6	11	78.6	25	52.1	C x I x N	**0.001**	80	46.2	5	45.5	4	40.0	C x I x N	**0.013**	172	46.5	15	78.9	21	52.5	C x I x N	**0.000**
Slightly hypoattenuating	61	33.9	2	14.3	11	22.9	C x I	0.156	56	32.4	2	18.2	1	10.0	C x I	0.133	168	45.4	3	15.8	10	25.0	C x I	**0.025**
Hypoattenuating	28	15.6	1	7.1	6	12.5	C x N	**0.000**	4	2.3	2	18.2	1	10.0	C x N	**0.011**	5	1.4	1	5.3	7	17.5	C x N	**0.000**
Hyperattenuating	0	0.0	0	0.0	0	0.0	I x N	0.410	2	1.2	0	0.0	2	20.0	I x N	0.756	3	0.8	0	0.0	0	0.0	I x N	0.310
Heterogeneous	0	0.0	0	0.0	6	12.5			31	17.9	2	18.2	2	20.0			22	5.9	0	0.0	2	5.0		
After contrast																								
Homogeneous CH	127	70.6	7	50.0	26	54.2	C x I x N	**0.000**	116	67.1	0	0.0	4	36.4	C x I x N	**0.000**	269	72.7	7	36.8	13	32.5	C x I x N	**0.000**
Slightly heterogeneous CH	43	23.9	1	7.1	4	8.3	C x I	**0.000**	20	11.6	5	45.5	0	0.0	C x I	**0.000**	52	14.1	3	15.8	13	32.5	C x I	**0.001**
Heterogeneous CH	10	5.6	6	42.9	18	37.5	C x N	**0.000**	0	0.0	6	54.4	7	63.6	C x N	**0.000**	18	4.9	5	26.3	10	25.0	C x N	**0.000**
Peripheral enhancement	0	0.0	0	0.0	0	0.0	I x N	0.899	37	21.4	0	0.0	0	0.0	I x N	**0.012**	31	8.4	4	21.1	4	10.0	I x N	0.445
Ultrasonography																								
Isoechoic	22	12.2	2	14.3	5	11.4	C x I x N	**0.000**	35	41.2	0	0.0	0	0.0	C x I x N	**0.001**	82	25.9	2	10.5	2	4.0	C x I x N	**0.000**
Hypoechoic	148	82.2	12	85.7	16	36.4	C x I	1.000	22	25.9	3	37.5	4	40.0	C x I	**0.010**	169	53.5	14	73.7	25	50.0	C x I	0.352
Hyperechoic	0	0.0	0	0.0	0	0.0	C x N	**0.000**	11	12.9	0	0.0	0	0.0	C x N	**0.003**	7	2.2	0	0.0	1	2.0	C x N	**0.000**
Heterogeneous	10	5.6	0	0.0	23	52.3	I x N	**0.000**	17	20.0	5	62.5	6	60.0	I x N	1.000	58	18.4	3	15.8	22	44.0	I x N	0.074
Shape																								
Rounded	1	0.6	0	0.0	2	4.5	C x I x N	**0.005**	47	55.3	2	25.0	8	80.0	C x I x N	**0.014**	89	28.2	7	36.8	25	50.0	C x I x N	**0.000**
Elongated	170	94.4	12	85.7	34	77.3	C x I	0.243	37	43.5	5	62.5	1	10.0	C x I	0.064	138	43.7	0	0.0	3	6.0	C x I	**0.000**
Miscellaneous	9	5.0	2	14.3	8	18.2	C x N	**0.002**	1	1.2	1	12.5	1	10.0	C x N	**0.036**	89	28.2	12	63.2	22	44.0	C x N	**0.000**
							I x N	1.000							I x N	**0.027**							I x N	0.363
Margins							C x I x N	**0.000**							C x I x N	**0.000**							C x I x N	**0.000**
Regular	180	100.0	12	85.7	41	93.2	C x I	**0.005**	85	100.0	6	75.0	7	70.0	C x I	**0.007**	297	94.0	11	57.9	24	48.0	C x I	**0.000**
Irregular	0	0.0	2	14.3	3	6.8	C x N	**0.007**	0	0.0	2	25.0	3	30.0	C x N	**0.001**	19	6.0	8	42.1	26	52.0	C x N	**0.000**
							I x N	0.585							I x N	1.000							I x N	0.592

Statistic significant when P>0.05

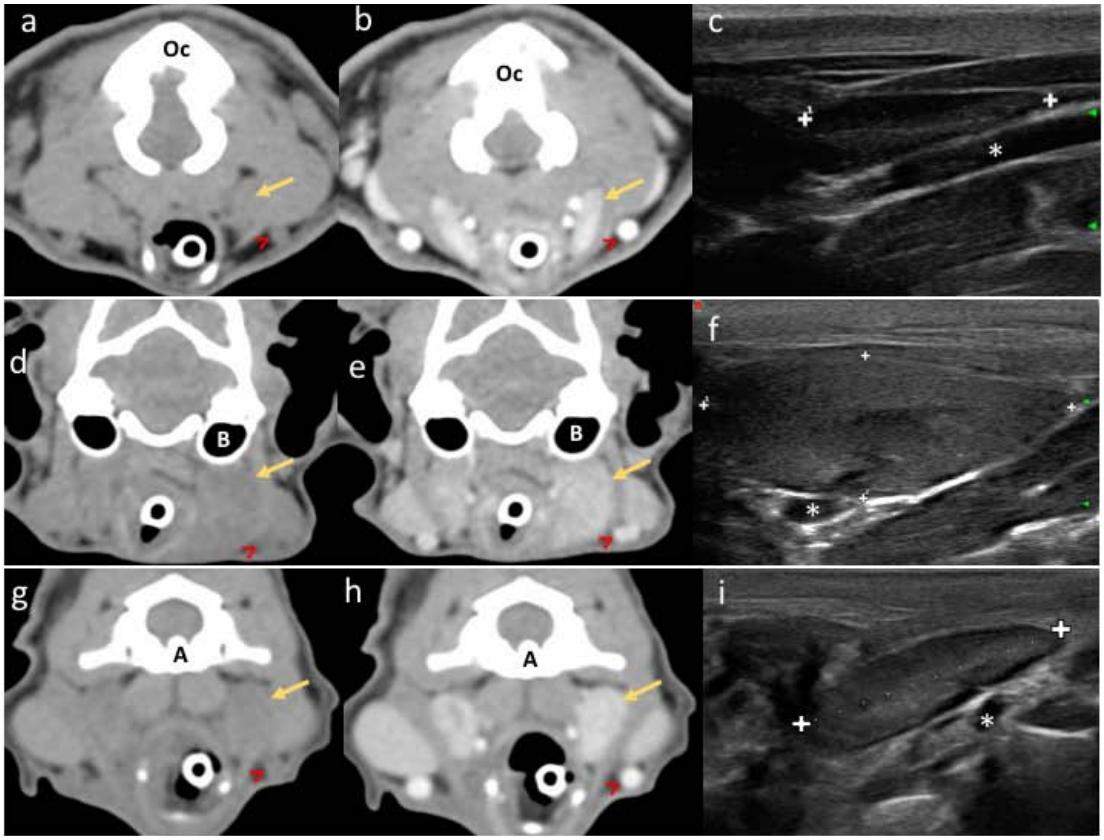

Figure 1. Lymph nodes in three patients of the R1: (a – c). Normal appearance of the retropharyngeal LN (RPLN). The LN (yellow arrow) is visible in CT transverse images with a fusiform shape, isoattenuating to the surrounding musculature in the precontrast image (a), and shows homogeneous contrast enhancement (b). The occipital bone (Oc) and the external jugular vein (open arrow head) are indicated. On the US image (c) from the same patient, a heterogeneous (hypoechoic) LN with fusiform shape is visible (between cursors). The carotid artery (asterisk) is indicated.

(d – f). Inflammatory RPLN in a patient with pyogranulomatous lymphadenitis. The LNs (yellow arrow) in CT transverse images are asymmetrically enlarged, with a miscellaneous shape, slightly hypoattenuating compared with the surrounding muscle in precontrast (d) and with slightly heterogeneous contrast enhancement (e). The tympanic bullae (B) and external jugular vein (open arrow head) are indicated. On US images (f) of the same patient, the LN is enlarged, mainly hypoechoic with mild irregular margins and fusiform shape (between cursors). The carotid artery (asterisk) is partially seen.

(g – i). Neoplastic RPLN in a patient with oral squamous cell carcinoma. The LNs (yellow arrow) in CT transverse images are asymmetrically enlarged with fusiform shape, slightly hypoattenuating (g) compared to the surrounding muscles and with homogeneous (left) and slightly heterogeneous (right) contrast enhancement (h). The atlas and dens of the axis (A) and the jugular vein (open arrow head) are indicated. On US images (i) of the same patient, a heterogeneous LN with fusiform shape and slightly irregular margins is visible (between cursors). The carotid artery (asterisk) is indicated.

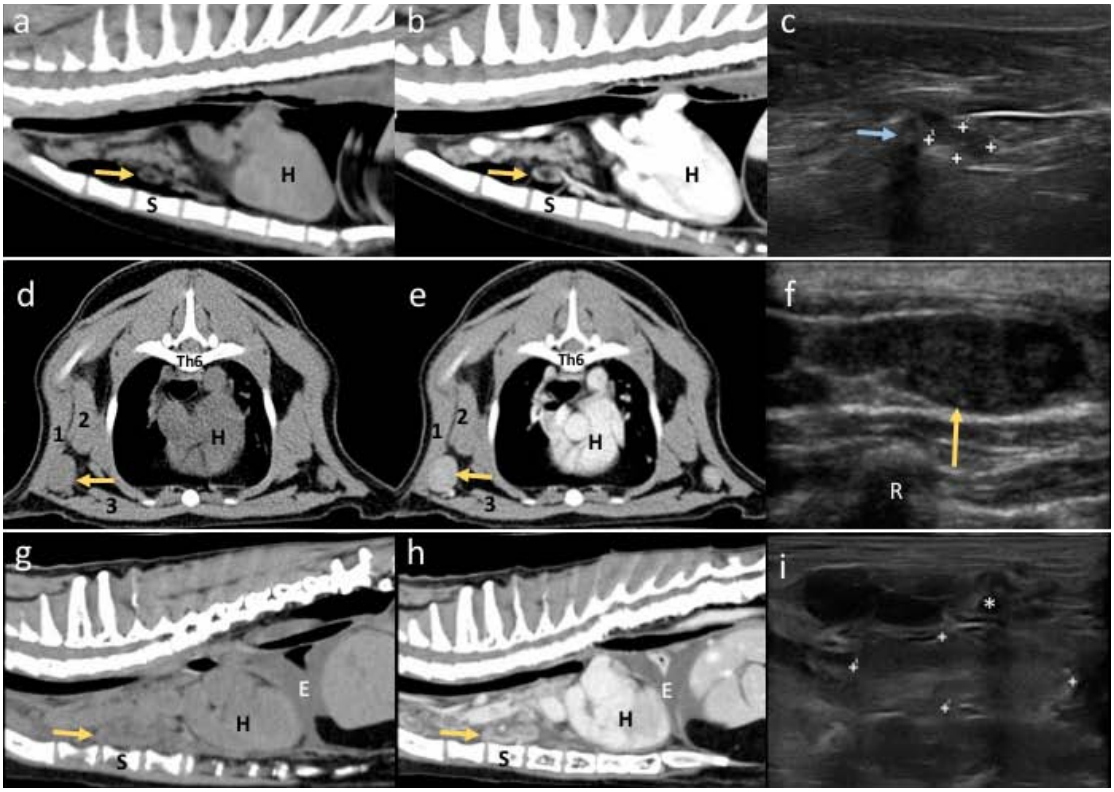

Figure 2. Lymph nodes in three patients of the R2: (a – c). Normal appearance of the sternal LN (SLN). The LN (yellow arrow) is visible in CT sagittal images with a fusiform shape, isoattenuating to the musculature with a hypoattenuating center in the precontrast image (a), and with heterogeneous contrast enhancement (b). The heart (H) and the 3rd sternebra (S) are indicated. US image (c) of the same patient, in which a hypoechoic LN with a hyperechoic central line (hilus) and fusiform shape is visible (between cursors). The 3rd rib (blue arrow) is indicated.

(d – f). Inflammatory accessory axillary LNs in a patient with multiple abscesses in the thoracolumbar region. The LNs (yellow arrow) in CT transverse images are asymmetrically enlarged, with a rounded shape, isoattenuating to the musculature in precontrast images (d) and show homogeneous contrast enhancement (e). The heart (H), 6th thoracic vertebra (Th6), and the muscles *latissimus dorsi* (1), *serratus ventralis* (2), and *pectoralis* (3) are indicated. On US images (f) of the same patient, the LN (yellow arrow) is enlarged, hypoechoic, with irregular margins and a miscellaneous shape. The 5th rib (R) is indicated.

(g – i). Neoplastic SLN in a patient with mediastinal lymphoma. The LN (yellow arrow) in CT sagittal images is enlarged, has a miscellaneous shape, and heterogeneous attenuation in pre- (g) and postcontrast (h) images. The 3rd sternebra (S), the heart (H) and pleural effusion (E) are indicated. On US images (i) of the same patient, a heterogeneous (mainly isoechoic) LN with miscellaneous shape and irregular margins is visible (between cursors). The cartilage of the 4th rib (asterisk) is indicated.

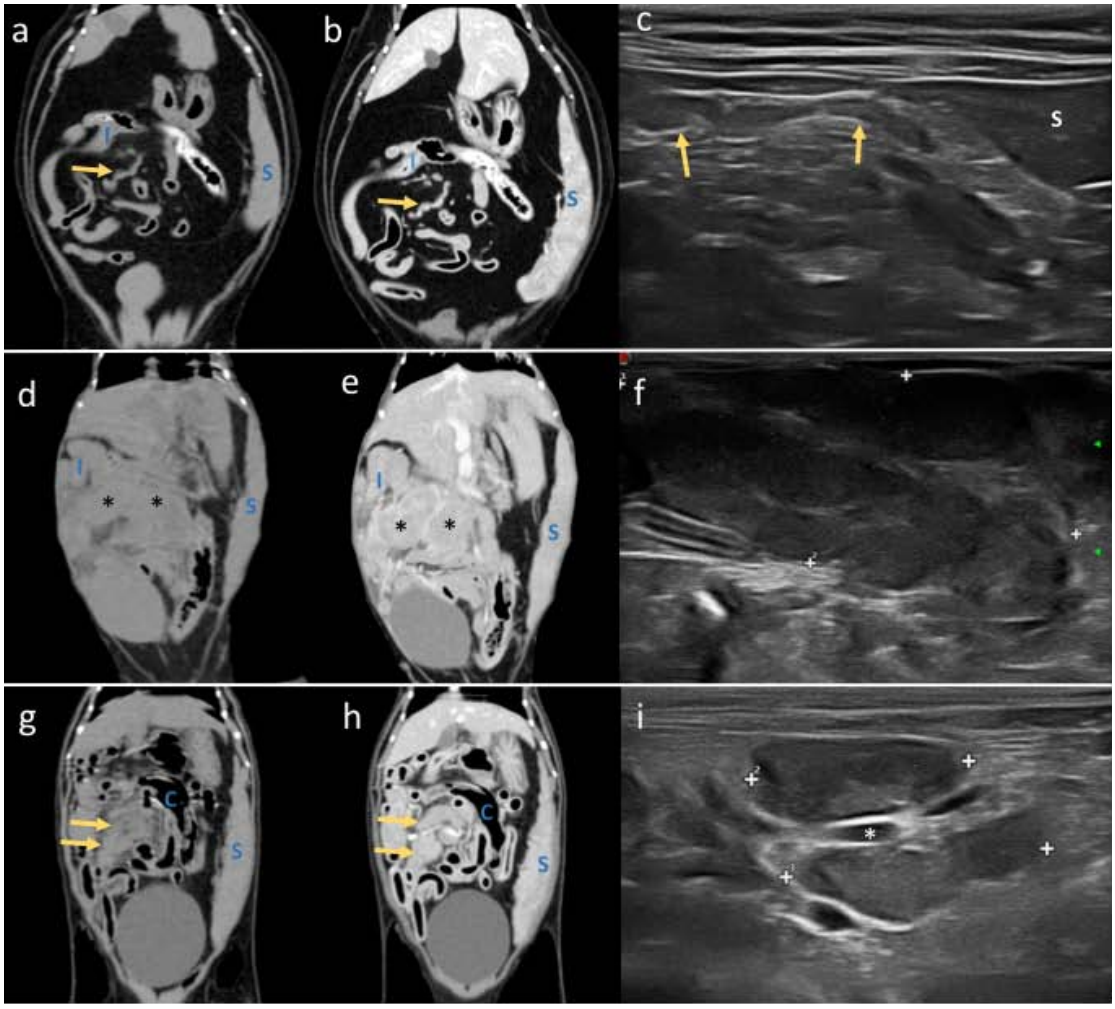

Figure 3. Lymph nodes in three patients of the R3: (a – c). Normal appearance of the jejunal LN (JLN). The LN (yellow arrow) is visible in CT dorsal images with a miscellaneous shape, isoattenuating to the muscles in precontrast image (a), and with homogeneous contrast enhancement (b). The spleen (S) and the ilecocolic junction (I) are indicated. US image (c) of the same patient in which a hypoechoic LN with miscellaneous shape is visible (yellow arrows). The spleen (S) is indicated.

(d – f). Inflammatory JLNs in a patient with pyogranulomatous lymphadenitis associated with feline infectious peritonitis (FIP). The LNs (asterisks) in CT dorsal images are symmetrically enlarged, with a miscellaneous shape, isoattenuating to the muscles in precontrast (d) and with heterogeneous contrast enhancement (e). The spleen (S), and ileocolic junction (I) are indicated. US images (f) of the same patient; the LN (between cursors) is enlarged, shows heterogeneous echogenicity with irregular margins and miscellaneous shape.

(g – i). Neoplastic JLNs in a patient with alimentary lymphoma. The LNs (yellow arrow) in CT dorsal images are enlarged, with a miscellaneous shape, isoattenuating in precontrast images (g) and with homogeneous contrast enhancement (h). The spleen (S) and the colon (C) are indicated. US images (i) of the same patient; heterogeneous LNs with miscellaneous shape and irregular margins are visible (between cursors). The jejunal vessels (asterisk) are partially seen between the 2 JLNs.

5. GENERAL DISCUSSION

A better understanding in the assessment of cat's lymph nodes with CT and US is presented in this thesis. There are 19 lymph centers in the cat according to previous reports (NAV, 2012; Saar & Getty, 1982; Tompkins, 1993). In this thesis, at least a representative lymph node from 17 lymph centers was successfully identified. The dorsal thoracic and iliofemoral lymph centers could not be identified in any cat and with any of the methods used in this study.

Anatomic, computed tomographic, and ultrasonographic assessment of the lymph nodes in healthy adult cats

The dissection of 6 cadavers allowed the identification of at least one lymph node per lymph center and provided the reference landmarks to search the same lymph nodes on CT and US images. As previously reported, the lymph nodes are embedded in fat tissue (Saar & Getty, 1982) and the amount of this is proportional to the body condition of the animal. The length, height, and width of each lymph node were obtained and compared among techniques (anatomy, CT, and US). The measurements obtained in the anatomic study were in general shorter than those obtained with CT and US. Additionally, these measurements were also shorter than those previously reported in anatomic studies in cats (Saar & Getty, 1982; Sugimura, Kudo, & Takahata, 1955, 1956, 1958, 1959). We hypothesized that the age of the included animals (very young animal were included in previous studies) and dissection process made after 24 hours of dead (unknown degree of dehydration or volume loss after the blood supply has stop) could have an influence in these results.

The number of LN identified with CT per lymph center was higher than with the other techniques. The higher number of identified LNs was influenced by the lack of superimposition of structures in CT, the body condition of the animals, and the use of contrast medium. The measurements obtained with CT were in general higher than those obtained in anatomy and with US. Additionally, the comparisons showed that there were statistically significant

differences in the measurements, specially the height, among techniques. These significant differences were also more frequently identified in the head and neck lymph centers. We found that the possibility of obtaining reconstructed images (multiplanar reconstruction) with the CT allowed a much better understanding and assessment of the lymph nodes. In our study, CT images were performed with a slice thickness of 0.6mm, which produces high resolution reconstructions with a very clear contour of the structures. We found that with reconstructed images, the overestimation of the length and height is prevented in comparison with the transverse slices. This is because a complete parallel position of the LN with the table cannot be ensured, as previously described (Sarah Nemanic & Nelson, 2012). Also, in thin animals in which the lymph nodes showed border effacement with the surrounding tissue, the use of contrast medium improved their identification. The LNs identified with CT were most frequently isoattenuating or slightly hypoattenuating to the surrounding musculature, with homogeneous contrast enhancement. Similar findings have been previously described in humans, dogs, and for some LNs in cats (Beukers, Vilaplana Grosso, & Voorhout, 2013; S Nemanic & Nelson, 2012; Wunderbaldinger, 2006). However, some LNs (e.g. axillary, sternal, and popliteal LNs) presented a isoattenuating periphery with a hypoattenuating center (before and after contrast administration) due to a fatty hilus (Beukers et al., 2013; Kneissl & Probst, 2007; Rossi, Patsikas, & Wisner, 2011).

The number of identified LNs with US was reduced compared with the other techniques. This result was directly influenced by the superimposition of the gastrointestinal tract with gas or feces that produced artifacts in the images; the impossibility to assess the thoracic cavity for the mediastinal, dorsal thoracic, and bronchial lymph centers; difficulty in identifying some LNs in animals with an elevated body condition; and, in a lesser degree, the poor skin-probe contact in some areas that were not completely clipped and the experience of the operator for the initial scans. The measurements obtained with US were significantly different from the CT, specially in those LNs were the position in transverse images on CT were somewhat oblique, and in

those were artifacts produced in US resulted in underestimation of their size. The LNs measurement with US in our study showed some differences with those reported by Schreur et al. (2008) for the abdomen. The cause for these differences remains unclear, it is possible that the sample size, fasting period of the cats, the scanning planes, and the interobserver variability were contributing factors.

In US, most LNs were isoechoic or hypoechoic to the surrounding fat tissue. The majority of LNs were fusiform or rounded. Nevertheless, the MRLNs, the dorsal SCLNs, and the accessory axillary LNs (AAxLNs) had miscellaneous shape. Some LNs presented a hypoechoic / isoechoic periphery with a hyperechoic center when compared with the musculature (e.g. axillary, sternal, and popliteal) due to the presence of a fatty hilus. This description is similar to previous studies (Agthe, Caine, Posch, & Herrtage, 2009; D'Anjou, 2008; S Nemanic & Nelson, 2012; Nyman, Kristensen, Skovgaard, & McEvoy, 2005; Nyman & O'Brien, 2007).

Assessment of normal and abnormal lymph nodes in cats using computed tomography and ultrasonography

Comparisons of the LNs features from the head, neck, forelimbs, thorax, abdomen, and hindlimbs between healthy cats and cats with inflammatory and neoplastic diseases were performed.

The quantitative variables, length, height and S/L ratio, obtained with both techniques, and the HU before contrast administration, were significantly different between the control and the case group for the region of the thorax and forelimb, and the region of the abdomen and hindlimb. In the region of the head and neck, statistical differences between the control and case groups were only observed for the HU before and after contrast administration and for the length and height obtained with US. The S/L ratios were no significant different between the inflammatory and neoplastic categories in both techniques for the region of the abdomen and hindlimb, and only for the CT in the region of the thorax and forelimb. It was observed

that inflammatory LNs may increase considerable in size, especially, if a pyogranulomatous process is taking place which could explain the similar ratios and the lack of statistical difference.

The LNs of the control group on CT images were frequently iso- or slightly hypoattenuating in precontrast images and showed homogeneous contrast enhancement (Beukers et al., 2013; Kneissl & Probst, 2007; Rossi et al., 2011). In the case group, the neoplastic category presented high frequencies of heterogeneous attenuating and hypoattenuating LNs. Meanwhile, the inflammatory category presented a similar frequency of attenuations to the control group. Furthermore, in the region of the thorax and forelimb and the region of the abdomen and hindlimb, the inflammatory category presented the highest frequency of isoattenuating LNs. The heterogeneous and hypoattenuating appearance of the most neoplastic and some inflammatory LNs before and after contrast administration could suggest severe changes in the internal structure and vascularization but a certain degree of malignancy was not possible to determine with CT.

On US, LNs in the control group were frequently isoechoic or hypoechoic and some of them presented a hyperechoic hilus, characteristics described in previous studies (Agthe et al., 2009; D'Anjou, 2008; S Nemanic & Nelson, 2012; Nyman et al., 2005; Nyman & O'Brien, 2007). In the case group, neoplastic LNs were either hypoechoic or heterogeneous, meanwhile inflammatory LNs were more frequently hypoechoic. In the region of the head and neck, results suggest that neoplastic LNs are more heterogeneous and inflammatory LNs are more frequently hypoechoic. This result is different to previous reports in which inflammatory LNs were often isoechoic (Nyman, Kristensen, Flagstad, & Mcevoy, 2004; Nyman & O'Brien, 2007), but in agreement with another study that found that inflammatory and neoplastic LNs can have a similar proportion of heterogeneous echogenicity in cats (Kinns & Mai, 2007).

The majority of the LNs in the control group were elongated (a small proportion presented rounded and miscellaneous shape specially in the thorax and abdomen) with smooth margins as already described (D'Anjou,

2008; Nyman et al., 2004; Nyman & O'Brien, 2007). As previously described, the neoplastic LNs in our study presented a rounded shape more frequently than the inflammatory LNs and the control group, that were often fusiform (Khanna, Sharma, Khanna, Kumar, & Shukla, 2011; Mohseni et al., 2014; Nyman & O'Brien, 2007). The LN in the inflammatory category often presented regular margins. However, irregular margins were seen in markedly enlarged lymph nodes (e.g. jejunal LNs with pyogranulomatous lymphadenitis). The neoplastic category presented the highest frequency of irregular margins in the LNs of the case group.

Further studies with a larger sample size and comparing specific neoplastic and inflammatory process are needed for a better understanding of the changes in the LNs in the disease cat. This thesis could be the beginning of future research lines involving other images techniques and description of different features of the feline LNs (that those described in this thesis) that are of common use in human medicine.

6. CONCLUSIONS

1. The LNs of healthy cats can be successfully identified with CT images, and the use of contrast medium and multiplanar reconstruction improves the assessment of their size.
2. The identification of LNs in healthy cats with US could be achieved for almost all corporal regions but the thoracic cavity (especially dorsal thoracic, mediastinal, and bronchial lymph centers). The presence of air in the lung and intestines, food in the stomach and fecal material in the colon, are factors that limit the assessment.
3. The LNs of healthy cats on CT images were frequently iso- or slightly hypoattenuating in precontrast images with homogeneous contrast enhancement, and on US were frequently isoechoic or hypoechoic and a low percentage presented a hyperechoic hilus.
4. The measurements on CT were significantly larger when compared with US and anatomy. The measurements in both techniques are proposed as reference values.
5. The short-to-long-axis (S/L) ratio of the LNs obtained with US and CT in diseased cats was frequently significantly different from the healthy cat.
6. The neoplastic category presented high frequencies of heterogeneous attenuating and hypoattenuating LNs on CT and were frequently hypoechoic or heterogeneous on US. Meanwhile, the inflammatory category presented higher frequencies of iso- to slightly hypoattenuating appearance on CT and were more frequently hypoechoic.
7. Overlapping in the features of both techniques in the categories of the case group prevents an accurate distinction between inflammation and neoplasia.

7. SUMMARY

The lymph nodes (LNs) are structures that play an important role in the diagnosis and prognosis of neoplastic and infectious diseases. Descriptions about the changes in size (increase of a short-to-long-axis ratio (S/L)>0.5), the shape (from elongated to rounded) and the internal structure of LNs assessed with ultrasound are associated with lymphadenopathy in humans and dogs. However, there are few studies assessing these parameters in cats. The aims of the studies described in this thesis were (i) to assess the ability to identify the LNs of healthy cats with computed tomography (CT) and ultrasonography (US) and to compare the imaging measurements with measurements from normal anatomic values; (ii) to characterize the LNs in diseased cats using CT and US; and (iii) to assess the ability of each imaging technique (CT and US) to discriminate between neoplastic and inflammatory changes in the LNs.

The number of LNs identified with CT was higher than with US and anatomy. The measurements obtained with CT were in general higher than those obtained in anatomy and with US. Additionally, the comparisons showed that there were statistically significant differences in the measurements, specially the height, among techniques. With CT-reconstructed images, the overestimation of the length and height is prevented in comparison with the transverse slices. The LNs identified with CT showed a similar appearance than previously described being most frequently isoattenuating or slightly hypoattenuating to the surrounding musculature, with homogeneous contrast enhancement.

Most LNs were isoechoic or hypoechoic to the surrounding fat tissue on US images. The majority of LNs were fusiform or rounded. Some LNs presented a hypoechoic/isoechoic periphery with a hyperechoic center when compared with the musculature, due to the presence of a fatty hilus.

The length, height, and S/L ratio, obtained with CT and US, and the HU before contrast administration were significantly different between the control and the case group for the thorax and forelimb, and the abdomen and hindlimb regions. In the region of the head and neck, statistical differences between the control and case groups were only observed for the HU before and after contrast administration and for the length and height obtained with

US. The S/L ratios were no significant different between the inflammatory and neoplastic categories in both techniques for the region of the abdomen and hindlimb, and only for the CT in the region of the thorax and forelimb. The neoplastic category presented high frequencies of heterogeneous attenuating and hypoattenuating LNs. Meanwhile, the inflammatory category presented a similar frequency of attenuations to the control group. The heterogeneous and hypoattenuating appearance of the most neoplastic and some inflammatory LNs before and after contrast administration could suggest severe changes in the internal structure and vascularization but a certain degree of malignancy was not possible to determine with CT.

On US, the neoplastic LNs were most frequently hypoechoic or heterogeneous, meanwhile inflammatory LNs were more frequently hypoechoic. In the region of the head and neck, results suggest that neoplastic LNs are more heterogeneous and inflammatory are more frequently hypoechoic.

The neoplastic LNs in our study presented a rounded shape more frequently than inflammatory LNs and the control group, in which they were often fusiform. The inflammatory LNs often presented regular margins. However, irregular margins were seen in markedly enlarged lymph nodes, especially in neoplastic LNs.

In conclusion, identification of the LNs of the cat is possible with both techniques. Computed tomography was more accurate in the detection and performance of measurements of the LNs than US. However, overlapping in the features of both techniques in the categories of the case group prevents an accurate distinction between inflammation and neoplasia.

8. RESUM

Els nòduls limfàtics (NLs) són estructures importants en el diagnòstic i pronòstic de malalties tant neoplàsiques com infeccioses. Estudis previs han associat els canvis observats per ecografia respecte a la grandària (augment del ratio eix-curt-eix llarg (S/L) a > 0,5), la forma (de allargada a arrodonida) i l'estructura interna dels NLs en éssers humans i gossos amb limfadenopatia. No obstant això, hi ha molt pocs estudis en gats en els quals es descriguin aquests paràmetres amb tomografia computada (TC) o ecografia (US). Els objectius d'aquesta tesi van ser: (i) avaluar la capacitat de la TC i US per identificar els NLs de gats sans i comparar les mesures obtingudes amb les tècniques d'imatge amb els valors anatòmics; (ii) caracteritzar els NLs en gats malalts utilitzant TC i US; i (iii) avaluar la capacitat de cada tècnica de d'imatge (TC i US) per discriminar entre canvis neoplàsics i inflamatoris en els NLs.

El nombre dels NLs identificats amb TC va ser més gran que amb US i que en l'estudi anatòmic. Les mesures obtingudes amb TC eren en general més altes que les obtingudes en l'anatomia i US. A més, les comparacions van mostrar diferències significatives entre les tècniques en les mesures, especialment l'altura. L'ús de reconstrucció multiplanar en TC va evitar la sobreestimació de la longitud i l'altura detectada en els talls transversals. Els NLs identificats amb TC van mostrar una aparença similar a la descrita en el gos, essent freqüentment isoatenuats o lleugerament hipoatenuats respecte a la musculatura que els envolta i amb realç homogeni de contrast.

En US, la majoria dels NLs van ser isoecoics o hipoecoics respecte al greix circumdant i amb forma allargada o arrodonida. Alguns NLs es van observar amb perifèria hipoecoica/isoecoica i centre hiperecoic en comparació amb la musculatura, a causa de la presència de greix a l'hili.

La longitud, l'alçada i la ratio S/L, obtinguts amb TC i US, a més de les unitats Hounsfield (HU) abans de l'administració de contrast, van mostrar diferències estadísticament significatives entre els grups control i de casos per a les regions del tòrax i extremitat anterior i abdomen extremitat posterior. A la regió del cap i el coll, les diferències estadístiques entre els grups de control i de casos es van observar només per a l'HU abans i

després de l'administració de contrast i de la longitud i l'altura obtinguda per US. La ratio S/L obtingut per ambdues tècniques no va mostrar diferències entre les categories inflamatòries i neoplàsiques per a la regió de l'abdomen i les extremitats posteriors, però si en la regió del tòrax i les extremitats anteriors únicament amb TC. Els NLs neoplàsics van ser freqüentment hipoatenuats i heterogenis. Mentre que els inflamatoris van presentar distribució d'atenuacions amb freqüències similars al grup control. L'aspecte heterogeni i hipoatenuat freqüent en els NLs neoplàsics i alguns inflamatoris abans i després de l'administració de contrast podria suggerir canvis severs en l'estructura interna i la vascularització del NL, tot i que no va ser possible determinar un grau determinat de malignitat amb TC.

En US, els NLs neoplàsics van ser freqüentment hipoecoics o heterogenis. Els NLs inflamatoris van ser freqüentment hipoecoics. A la regió del cap i el coll, els NLs neoplàsics van ser més heterogenis amb més freqüència i els NLs inflamatoris més freqüentment hipoecoics.

Els NLs neoplàsics van ser freqüentment arrodonits i amb marges irregulars a diferència dels nóduls inflamatoris i del grup control, els quals sovint eren fusiformes. Els NLs en la categoria d'inflamatoris sovint presentaven marges regulars. Tanmateix, es va observar marges irregulars en NLs molt augmentats de mida, especialment en la categoria de neoplàsia.

En conclusió, els NLs del gat és poden identificar amb les dues tècniques. La tomografia computada va ser més precisa en la detecció i realització de mesures dels LNs que l'US. No obstant això, la superposició de les característiques en ambdues tècniques en les categories del grup cas impedeix una distinció precisa entre inflamació i neoplàsia.

9. RESUMEN

Los nódulos linfáticos (NLs) son estructuras importantes en el diagnóstico y pronóstico de enfermedades tanto neoplásicas como infecciosas. Estudios previos han asociado los cambios observados por ecografía respecto al tamaño (aumento del ratio eje-corto-eje-largo(S/L) a >0,5), la forma (de alargada a redondeada) y la estructura interna de los NLs en humanos y perros con linfadenopatía. Sin embargo, existen muy pocos estudios en gatos en los que se describan estos parámetros con tomografía computarizada (TC) o ecografía (US). Los objetivos de esta tesis fueron: (i) evaluar la capacidad de la TC y la US para identificar NLs de gatos sanos y comparar las mediciones de imagen con valores anatómicos obtenidos; (ii) caracterizar los NLs de gatos enfermos utilizando TC y US; y (iii) evaluar la capacidad de cada técnica de imagen (TC y US) para discriminar entre cambios neoplásicos e inflamatorios de los NLs.

El número de NLs identificados fue mayor con TC que con US y anatomía. Las mediciones obtenidas con TC generalmente fueron más altas que las obtenidas en anatomía y US. Además, las comparaciones mostraron diferencias significativas entre las técnicas en las mediciones, especialmente la altura. El uso de la reconstrucción multiplanar en TC evitó la sobreestimación de la longitud y la altura detectada en los cortes transversales. Los LNs identificados con TC mostraron una apariencia similar a la descrita en el perro, siendo frecuentemente isoatenuantes o ligeramente hipoatenuantes respecto a la musculatura circundante y con captación homogénea de contraste.
En US, la mayoría de los NLs fueron isoecoicos o hipoecoicos respecto a la grasa y con forma alargada o redondeada. Algunos LNs se observaron con periferia hipo/isoecoica y centro hiperecoico en comparación con la musculatura, debido a la presencia de grasa en el hilio.

La longitud, la altura y la ratio S/L obtenidos con TC y US, además de las unidades Hounsfield (HU) antes de la administración de contraste, fueron estadísticamente significativas entre los grupos control y caso para las regiones del tórax y miembro anterior, y abdomen y miembro posterior. En la

región de la cabeza y el cuello, las diferencias estadísticas entre los grupos control y caso fueron observadas solamente para las HU antes y después de la administración de contraste y para la longitud y la altura obtenidas por US. La ratio S/L obtenido con ambas técnicas no mostró diferencias entre las categorías inflamatorias y neoplásicas para la región del abdomen y extremidades posteriores, pero si en la región del tórax y extremidades anteriores únicamente con TC. Los NLs neoplásicos fueron frecuentemente hipoatenuantes y heterogéneos. Mientras que, los inflamatorios presentaron distribución de atenuaciones con frecuencias similares al grupo control. La apariencia heterogénea e hipoatenuante en los NLs neoplásicos y algunos inflamatorios antes y después del contraste podría sugerir cambios importantes en la estructura interna y la vascularización del NL, aunque no se pudo identificar el grado determinado de malignidad con TC.

En US, los NLs neoplásicos fueron frecuentemente hipoecoicos o heterogéneos. Los NLs inflamatorios fueron frecuentemente hipoecoicos. Para la región de la cabeza y el cuello, los NLs neoplásicos fueron más frecuentemente heterogéneos y los NLs inflamatorios más frecuentemente hipoecoicos.
Los NLs neoplásicos fueron más frecuentemente redondeados que los inflamatorios y los del grupo control, los cuañes eran más frecuentemente fusiformes. Los NLs en la categoría de inflamatorios presentaban con frecuencia márgenes regulares. Sin embargo, se observaros márgenes irregulares en NLs muy aumentados de tamaño, especialmente en la catergoría de neoplasia.

En conclusión, los NLs del gato se pueden identificar con ambas técnicas. La tomografía computarizada fue más precisa en la detección y realización de mediciones de los NLs que la US. Sin embargo, la superposición de las características en ambas técnicas en las categorías del grupo caso no permitió una distinción precisa entre la gatos con inflamación o neoplasia.

10. OTHER STUDIES DERIVED FROM THIS THESIS

Abstract presented as an oral communication at the EVDI annual meeting, Utrecht (the Netherland), August 2014:

Tobón Restrepo, M., Novellas, R., Espada, Y., Aguilar, A., Moll, X., & Boroffka, S. (2015b). Ultrasonography and computed tomography features of lymph nodes in healthy cats. In Abstracts from the 2014 european veterinary diagnostic imaging annual conference. Veterinary Radiology & Ultrasound (Vol. 56, p. 700). Utrecht, The Netherlands.

Conclusion:
When imaging the joints of medium to large breed dogs, we recommend using CT exposure setting ≥140 kVp, a bone+ reconstructive kernel and a segmentation smoothing factor of 0.3 to generate the highest quality of images for rapid prototyping.

GET THEM EARLY . . . EXPERIENCE WITH A DIAGNOSTIC IMAGING BASED WIDENING PARTICIPATION PROGRAMME FOR PRIMARY SCHOOL CHILDREN

R. Weller, G. Kimble, S. B. Channon From the Diagnostic Imaging, The Royal Veterinary College, London, UK (Weller, Kimble, Channon).

Background:
Inspiring children from a wide range of background to consider studying science is part of the work done by RVC Access and Widening Participation (promoted and legislated by the government), with the aim of helping young people have a fair chance of applying to higher education. It is important that children and teenagers have the opportunity to encounter motivating examples of biomedical sciences not only at a stage when they may start to be thinking about future study options, but before then, particularly if they have few role models who have attended university in their own circles of family and friends.
Purpose:
It is important that children and teenagers have the opportunity to encounter motivating examples of biomedical sciences not only at a stage when they may start to be thinking about future study options, but before then, particularly if they have few role models who have attended university in their own circles of family and friends. With this in mind, we have created a 60-min session to engage primary school children in biomedical sciences, comprising five 10-min stations.
Methods:

1. The Tesco quiz: radiographs of everyday objects (fruit, cereals, pastries, chocolate bars, and electronic gadgets) were shown and the children matched these to the supplied objects.
2. "Heads, shoulders, knees and toes"—children matched the radiographs to their own body and displayed the skeletons of dogs and horses.
3. "Spot the fracture": children identified fractures on radiographs and skeletons.
4. "Spot the difference": computed tomographic images with obvious left-right asymmetry were displayed and the children asked to spot the difference.
5. "Watch your muscles move": an ultrasound machine was used to show children how their arm and leg muscle moved when they changed position. Each station was looked after by a veterinary undergraduate student as a facilitator. Each primary school student was given a mini radiograph on a string as a reward and a black piece of paper and a bit of chalk and was asked to draw a whole skeleton or bone as homework.

Findings:
"Smiley face" feedback was excellent and negative verbal feedback focused on the fact that they were not allowed to eat the chocolate bars (school policy).
Conclusion:
The developed session based on mini station caters to the short attention span of the targeted age group. By linking the familiar with the unfamiliar first, the students lost their original "fear of the unknown" and the playful nature of the session made it age appropriate but still encouraged students to think outside their usual "box."

ULTRASONOGRAPHY AND COMPUTED TOMOGRAPHY FEATURES OF LYMPH NODES IN HEALTHY CATS

M. Tobon Restrepo, R. Novellas, Y. Espada, A. Aguilar, X. Moll, S. A. E. B. Boroffka From the Departament de Medicina i Cirurgia Animals, Universitat Autonoma de Barcelona, Bellaterra, Barcelona, Spain (Tobon Restrepo, Novellas, Espada, Aguilar A, Moll), GIVET, Universitaria Lasallista, Medellin, Colombia (Tobon Restrepo), and Division of Diagnostic Imaging, Faculty of Veterinary Imaging, Utrecht University, Utrecht, the Netherlands (Boroffka).

Background:
Lymph node (LN) characterization is important for diagnosis and prognosis of neoplastic and infectious diseases. Information regarding imaging features of the normal anatomy of feline LNs is limited. Normal values for size, appearance, and ability to depict many of them using computed tomography (CT) and ultrasonography (US) are needed.
Purpose:
The aims of the study were (1) to assess the ability of US and CT to identify feline LNs in healthy cats and (2) to compare the imaging features with measurements from normal anatomic references.
Methods:
Anatomical study: five fresh feline cadavers were used to dissect all LNs using previously reported anatomic landmarks. Length, width, and thickness were measured using a manual caliper. Imaging studies: healthy cats were enrolled for the study. Complete body CT was performed using a 16-slice CT scanner. Images were acquired with soft tissue algorithms pre- and postcontrast administration. After CT, an ultrasonographic study was performed in order to identify all the peripheral, thoracic, and abdominal LNs using a 4–13 MHz linear array transducer. Sagittal and transverse images of identified LNs were stored. Long and short axis measurements were performed with an electronic caliper.
Findings:
Fifteen cats were included. A total of 54 different LNs were found and described in the anatomic study. Thirty-nine (72.2%) and 47 (87%) LNs were identified with CT in pre- and postcontrast images, and 35(64%) were identified with US. At least one LN per lymph center was identified with both CT and US. Ultrasonographically, peripheral LNs were fusiform and slender in shape, and slightly hypoechoic, with the exception of the axillary and popliteal LNs that were more frequently hyperechoic and with regular margins. Thoracic and abdominal LNs were more rounded and elongated in shape, isoechoic to surrounding fat and also with regular margins. In the CT studies, LNs most frequently had regular margins, rounded to elongated shape, and a homogeneous structure before and after the contrast administration. In obese cats, LNs were more difficult to identify by US and their identification was more time consuming. However, an increase in body fat made easier the visibility of LNs in CT images.
Conclusion:
Contrast-enhanced CT allowed the visualization of more LNs than noncontrast-enhanced CT and US. A possible explanation is the difficulty to evaluate the LNs of the thoracic cavity in US examinations. A previous study reported a higher visibility of abdominal LNs in CT images of dogs with more intra-abdominal fat; the same situation was seen in the cats of this study. US and CT features of peripheral, abdominal, and thoracic LNs in healthy cats are similar to those previously reported for healthy dogs.

COMPARISON OF COMPUTED TOMOGRAPHY AND RADIOGRAPHY FOR THE EVALUATION OF SMALL INTESTINAL OBSTRUCTION IN DOGS

W. T. Drost, E. M. Green, L. J. Zekas, G. G. Habing From the Veterinary Clinical Sciences, Diagnostic Imaging & Radiation Oncology Service (Drost, Green, Zekas) and Veterinary Preventive Medicine, The Ohio State University, Columbus, OH (Habing).

Background:
Vomiting, often caused by intestinal obstruction, is common in dogs. Initial screening for intestinal obstruction includes radiography; equivocal radiographic signs often necessitate reevaluation or additional imaging procedures. In people, CT for intestinal obstruction is highly sensitive, specific, and accurate.
Purpose:
To determine the sensitivity and specificity of abdominal CT for detection of canine intestinal obstruction. Compare the sensitivity and specificity of CT to abdominal radiographs for detection of canine intestinal obstruction.
Methods:
Twenty dogs were enrolled. Fifteen dogs with clinical signs of gastrointestinal disease and five dogs without clinical signs of gastrointestinal disease and normal intestinal radiographs. All dogs had digital three-view abdominal radiographs and abdominal CT (pre- and postcontrast). Seventeen dogs had abdominal surgery for intestinal evaluation including all five dogs without clinical signs. Three dogs had follow-up to determine that the clinical signs resolved. Three experienced radiologists reviewed the imaging studies and were asked their confidence level for intestinal obstruction on a five-point scale and if they would recommend surgery. Sensitivity and specificity was calculated.
Findings:
For the 20 dogs of various breeds, the average age was 6.1 years (range, 4 months and 12 years). Nine male (five castrated) and 11 female (10 spayed) dogs. Eight dogs had surgically confirmed intestinal obstruction and 12 dogs did not have obstruction. Seven dogs had intestinal foreign bodies and one dog had an intussusception. Of the dogs without intestinal obstruction, two had histopathologically confirmed enteritis, one had ischemic necrosis, one had pancreatitis, two had colonic foreign bodies, and four had nonintestinal neoplasia. All three radiologists agreed on 14/20 (70%) of the radiographic studies and 16/20 (80%) of the CT studies. Using a consensus opinion of the three radiologists, abdominal radiographs had sensitivity = 87.5% and specificity = 75%, while abdominal CT had sensitivity = 87.5% and specificity = 91.67%. Two radiologists were slightly more confident in their CT findings compared to radiographic findings.
Conclusion:
For experienced radiologists, abdominal radiographs and abdominal CT are sensitive and specific for the detection of intestinal obstruction in dogs. This reemphasizes the use of abdominal radiographs as an initial screening test for dogs with possible intestinal obstruction. Further investigation could focus on which cases would benefit from an abdominal CT study vs. follow-up radiographs and if results would be similar for less-experienced image interpreters.

TRIPLE PHASE COMPUTED TOMOGRAPHY PERFUSION CHARACTERISTICS OF NON-NEOPLASTIC AND NEOPLASTIC SPIROCERCOSIS-INDUCED OESOPHAGEAL NODULES

R. Kirberger, N. Cassel, N. Stander, E. Dvir From the Department of Companion Animal Clinical Studies, Faculty of Veterinary Science, University of Pretoria, Onderstepoort, Republic of South Africa (Kirberger, Cassel, Stander, Dvir).

Background:
Spirocercosis in dogs results in a caudal esophageal nodule that may undergo neoplastic transformation to a sarcoma over time.
Purpose:
The objective of this prospective study was to determine if computed tomography angiography (CTA), particularly nodule perfusion characteristics, could distinguish between non-neoplastic and neoplastic nodules in a cohort of dogs with spirocercosis-associated caudal esophageal nodules.
Methods:
Thirty-eight dogs with spirocercosis were prospectively recruited. Dogs were classified into neoplastic ($n = 15$) or non-neoplastic ($n = 23$) nodule groups based on tissue biopsy, postmortem histology, or response to treatment. Pre- and postcontrast (2 ml/kg of iohexol 300 mg I/ml at 3 ml/s using a pressure injector) early arterial, late arterial, and venous CTA images were evaluated at 6, 35, and 65 s postinjection trigger, respectively. Regions of interest (ROIs) were taken of the largest possible normal esophageal wall as well as of nodules (excluding the wall) at three different transverse slices and mean Hounsfield units (HU) as well as standard deviations recorded and averaged. The ROIs were placed in the same position on the same slice in each phase. Necropurulent areas with no perfusion and with HU < 25 as well as areas of mineralization were excluded from the ROI. Additionally, a

Abstract presented as poster at the SEVC-AVEPA 2014, Barcelona, Spain. October 2014: Computed tomography characteristics of the Os penis in the cat

COMPUTED TOMOGRAPHY CHARACTERIZATION OF THE *OS PENIS* IN THE CAT

Tobón Restrepo M, Espada Y, Altazurra R, Domínguez E, Novellas R.

Objectives: To assess the ability of computed tomography (CT) to visualize the *os penis* (OP) in the cat.

Materials and Methods: Computed tomography from cats that underwent an abdominal or pelvic CT before and following intravenous administration of contrast medium at the Fundació Hospital Clínic Veterinari from Universitat Autònoma de Barcelona, between October 2013 and April 2014 were reviewed retrospectively. Cats were included in the study if (1) they were no affected by any urinary disease and (2) the external genitals were completely included in the scan. Images were reviewed using a soft tissue and bone algorithms. Width and thickness were measured using an electronic calliper in transverse images. Length was determined using two previously reported methods[1], (i) with an electric calliper in sagittal images obtained in the multiplanar reconstructions in both algorithms, (ii) and multiplying slice thickness by the number of consecutive transverse slices that contained the OP. Attenuation values were also measured using a round or oval region of interest (ROI) including as much as possible of the OP, without including other tissues. Groups of ages and intact/castrated condition were used as independent variables to compare between cats with and without visible OP. *Chi*-square, T-test, Pearson correlation and one-way ANOVA with a 95% confidence interval were used in the statistical analysis.

Results: Twelve cats were included in the study. A cylindrical bone-tissue attenuating structure inside the *glans penis* compatible with the OP was visible in 11/12 (91.7%) cats. Mean age of the animals with visible OP was 6.2 years (range 0.25 – 11). The OP could not be identified in a 13-year-old castrated cat (8.3%). There was no statistical difference for the visualization of an OP between intact (4/12) vs. castrated (8/12) cats (P = 0.460) or between age groups (≤5y: 6/12; 6-10y: 3/12; ≥11y: 3/12) (P = 0.195). All identified OP had a cylindrical shape. Mean OP width and thickness values in soft tissue (1.45mm; 1.44mm) and bone (1.27mm; 1.08mm) algorithms showed no statistical difference and no correlation with groups of age and intact/castrate condition. Mean OP length showed similar values with both estimation methods (i. Soft 3.46mm Bone 2.9mm; ii.3.4mm) and no statistical difference was found. Mean attenuation before contrast was 230 Hounsfield Units (HU) (range 109 – 402 HU) for soft tissue and 292 HU (range 117 – 528 HU) for bone. Mean attenuation after contrast was 293 HU (range 138 – 427 HU) for soft tissue and 392 HU (range 239 – 682 HU) for bone. No correlation between attenuation values in both algorithms with groups of ages and intact/castrate condition was found.

Discussion and Conclusions: A 5 – 8 mm long *os penis* without a ventral groove has been reported in the normal cat[2]. In the present study, cats showed a shorter cylindrical bone with no presence of a ventral groove. In a previous study, a statistical difference in the identification of OP when comparing analog vs. digital X-rays, with 16% and 38% frequencies respectively was found[3]. In this study, CT showed a frequency of identification

of the OP of 91.7%, which is higher than both analog and digital X-rays reports. No statistical difference between groups of ages and intact/castrate condition with the attenuation values may suggest that the OP mineralization starts early and continues even if the animals have been castrated. On the other hand, slightly higher values in the attenuation values of OP in post contrast images might be due to the presence of contrast agent inside the vascularization of *corpus cavernosus* that contains the bone[1, 4]. Even though ROI measurements were placed carefully, Corpus *cavernosus* tissue might be included due to the OP small diameter. Cats in this study have no signs or evidence of urinary tract disease; this is an important clinical fact because OP might be misinterpreted as signs of urethroliths or dystrophic mineralization of the urethral wall[3]. Lack of confirmation by histopathology of the OP dimensions is a limitation due to the retrospective nature of the study. For authors knowledge this is the first report of the *os penis* characteristics by CT in the cat.

1. Nemanic S, Nelson NC. Ultrasonography and noncontrast computed tomography of medial retropharyngeal lymph nodes in healthy cats. American Journal or Veterinary Research 2012; 73(9): 1377 – 1385.

2. König E, Liebich HG: Male genital organs. In König-Liebich (ed): Veterinary anatomy of domestic mammals: textbook and colour atlas. 4th edition. Stuttgart, Editorial Schattauer, 2009, 407 - 422.

3. Piola V, Posch B, Aghte P, et al.: Radiographic characterization of the os penis in the cat. Veterinary Radiology & Ultrasound 2011; 52(3): 270 – 272.

4. Dyce KM, Sack WO, Wensing CJG. The pelvis and reproductive organs of the dog and cat. In Dyce KM, Sack WO, Wensing CJG (eds): Textbook of veterinary anatomy. 4th edition. Philadelphia, Saunders, 2010, 454 – 475.

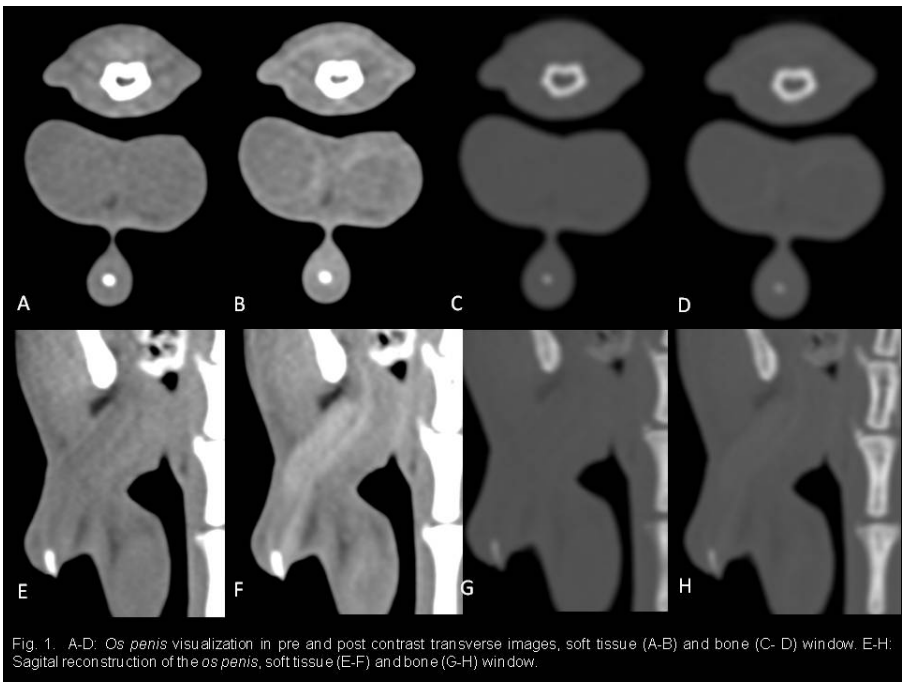

Fig. 1. A-D: *Os penis* visualization in pre and post contrast transverse images, soft tissue (A-B) and bone (C- D) window. E-H: Sagital reconstruction of the *os penis*, soft tissue (E-F) and bone (G-H) window.

Abstract accepted as poster at the SEVC-AVEPA 2015, Barcelona, Spain. October 2015: Diagnosis of gallbladder agenesis in a cat using ultrasonography, computed tomography and abdominal laparoscopy.

21st FECAVA EuroCongress
Federation of European Companion Animal Veterinary Associations
SEVC
IX SOUTHERN EUROPEAN VETERINARY CONFERENCE
50 CONGRESO NACIONAL AVEPA
XII Congreso FIAVAC
Federación Iberoamericana de Asociaciones Veterinarias
15-17 October 2015 · Barcelona, Spain

DIAGNOSIS OF GALLBLADDER AGENESIS IN A CAT USING ULTRASONOGRAPHY, COMPUTED TOMOGRAPHY AND ABDOMINAL LAPAROSCOPY

Mauricio Tobón Restrepo[1] , Yvonne Espada Gerlach[2] , Lluvia Castro[2] , Laura Santos Benito[2] , Adrián Aguilar Catalán[2] , Carlos Olmedo[2] , Carlo Anselmi[2] , Raul Altuzarra Fernández[2] , Rosa Novellas Torroja[2]
[1] Universitat Autònoma de Barcelona, Departament de Medicina i Cirurgia Animals, Cerdanyola del vallés, Spain. & Corporación Univrsitaria Lasallista, GIVET, Medellin, Colombia. [2] Universidad Autònoma de Barcelona,Departament de Medicina i Cirurgia Animals, Cerdanyola del vallés, Spain.

INTRODUCCIÓN Y CASO CLÍNICO / INTRODUCTION AND CASE REPORT

Agenesis of the gall bladder is a rare condition that has been reported in humans with an identified hereditary component[1]. This condition has been also previously described in dogs, two Maltese and one Chihuahua[2–4]. Clinical signs of liver disease such as bilious vomit and/or elevated liver enzymes have been described. In one case, the absence of the gall bladder was suspected by abdominal ultrasonography and confirmed with exploratory laparotomy and retrograde cholangiography[2]. In another case, radiographs and abdominal ultrasound were performed with inconclusive findings and the diagnosis was made by exploratory laparotomy[4]. In the last case, radiographic findings were consistent with microhepatia and ultrasonography showed signs of a portosystemic shunt and absence of the gallbladder; final diagnosis was made by exploratory laparotomy[3]. To the authors knowledge gallbladder agenesis has not been previously reported in cats.

DISCUSIÓN / DISCUSSION

An 18-months old female domestic shorthair cat was enrolled in a research study about the normal appearance of lymph nodes using computed tomography and ultrasonography previous to routine ovariohysterectomy. The patient was alert, bright and responsive. No history of vomiting, weight loss, dysphagia, previous surgeries, or other abnormalities were reported by the owner. Physical examination and preoperative laboratory tests were unremarkable. Liver enzymes were within normal limits (ALT 46 UI/L, reference range from 6 to 83 UI/L; gamma GT 1 U/L, reference range from 1.3 to 5.1 U/L; urea 42.9 mg/dL, reference range from 42.8 to 64.2 mg/dL). Anesthesia was induced with isoflurane 5% dosage 100% O2 at 4L/min. Maintenance of anesthesia was done with isoflurane 1.5 – 2% in 100% of O2 at 2L/min. A whole body computed tomography in dorsal recumbency with arms and legs outstretched at the sides was performed. Acquisitions were done in soft tissue algorithm, before and after the intravenous administration of 2ml/Kg iopamidol (Scanlux® 300mg/ml, non ionic contrast medium). Scans were performed in a 16 slices helical CT (General Electric®). Machine settings were 0.625 mm of slice thickness, 0.625 mm of interval thickness, 1.25 mm of collimator pitch, 120 kV, 50 - 90 mA, matrix of 512x512. The liver appeared as a homogenous soft tissue attenuating structure (60 HU) located within the margins of the costal arch. The hepatic margins were sharp and well defined. The vasculature was visible and within normal limits in pre-contrast images, and after contrast administration, the liver parenchyma enhanced homogeneously (160 HU). A homogenously enhanced portal vein and branches were visible in the post contrast images with normal distribution. A tubular soft tissue attenuating structure, of 2.6mm in diameter and with no contrast enhancement could be followed from the region of the *porta hepatis* to the cranial duodenal flexure, being compatible with the common bile duct. The gallbladder was not identified neither in pre- nor in post contrast images. Ultrasonography was performed using an Esaote Mylab70 Xvision® machine with a 4 – 13 MHz high frequency linear transducer. The liver was identified with a normal homogenously hypoechoic parenchyma compared to the spleen and isoechoic compared to the falciform fat. The portal vein and its branches were identified with a normal diameter and distribution. The gallbladder was not identified at the area between the quadrate and right medial lobes. The bile duct, with a diameter of 2.3 mm could be identified close to the portal vein using Doppler. No portosystemic shunt or signs of liver parenchyma lesions were identified. Abdominal laparoscopy was performed using a forward-oblique telescope 30º, 5mm diameter, 30cm length (ST endoscopia®) with a Tele pack vet X monitor (Karl Storz®). A completely exploration of the porta hepatis could be performed. The quadrate and right medial lobes were identified but no gallbladder was seen. A slightly distended bile duct was seen and followed to its junction at the duodenum and no abnormalities were visible. Ovariohysterectomy was performed and the patient was discharged with no complications after surgery. On follow up 2-months later, the owners reported a healthy cat. No vomits or changes in the normal behavior were seen at the moment. A blood test was performed to determine liver enzymes (using the same reference range ALT was 39 UI/L, gamma GT 1 U/L and urea 38.8 mg/dL) with values within normal limits.

CONCLUSIONES / CONCLUSIONS

Agenesis of the gallbladder is a rare anomaly in both humans and dogs[1,3]. The condition is more frequently noted during necropsy. In human medicine, no visualization of the gallbladder in ultrasound is not considered enough evidence of agenesis and surgery is recommended if the patient is showing clinical signs[1]. However, in the veterinarian literature, all the reported cases in dogs included animals with clinical signs or laboratory abnormalities compatible with liver disease. Radiographs and abdominal ultrasound images were inconclusive for the diagnosis of agenesis of the gallbladder but were compatible with liver disease[2–4]. The case presented here is a cat without any clinical signs of liver disease. Computed tomography and ultrasonography showed a normal liver parenchyma without the presence of the gallbladder compatible with agenesis. However, the sensitivity and specificity of those techniques have not been studied. Prognosis for cats with gallbladder agenesis is unknown; this case suggests that cats with gallbladder agenesis may live without developing clinical signs of liver disease if no other abnormalities are present (e.g. congenital biliary tree atresia)[5]. When the gallbladder is not visualized during ultrasonography or computed tomography, agenesis must be included in the differential diagnosis and further test are recommended in order to reach a final diagnosis.

BIBLIOGRAFÍA /BIBLIOGRAPHY

1. Tang L-M, Wang X-F, Ren P-T, Xu G-G, Wang C-S. The diagnosis of gallbladder agenesis: two cases report. Int J Clin Exp Med. 2015;8(2):3010-3016.
2. Kamishina H, Katayama M, Okamura Y, et al. Gallbladder agenesis in a Chihuahua. J Vet Med Sci. 2010;72(7):959-962.
3. Austin B, Tillson DM, Kuhnt LA. Gallbladder agenesis in a Maltese dog. J Am Anim Hosp Assoc. 2006;42(4):308-311.
4. Liptak JM, Swinney GR, Rothwell TL, Hunt GB. Aplasia of the gallbladder in a dog. J Small Anim Pract. 2000;41(4):175-177.
5. Hampson E, Filippich LJ, Kelly WR, Evans K. Congenital biliary atresia in a cat: a case report. J Small Anim Pract. 1987;28(1):39-48.

21st FECAVA EuroCongress
Federation of European Companion Animal Veterinary Associations
SEVC
IX SOUTHERN EUROPEAN VETERINARY CONFERENCE
50 CONGRESO NACIONAL AVEPA
XII Congreso FIAVAC
Federación Iberoamericana de Asociaciones Veterinarias
15-17 October 2015 · Barcelona, Spain

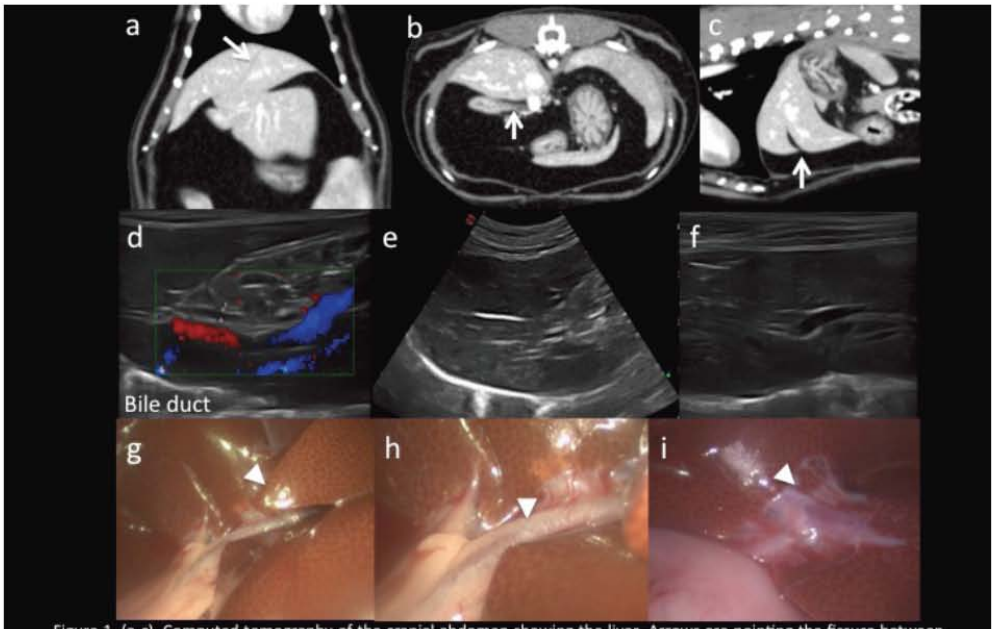

Figure 1. (a-c). Computed tomography of the cranial abdomen showing the liver. Arrows are pointing the fissure between the quadrate and right medial lobes with absence of the gallbladder (a, c). The bile duct is also visible in b (arrow). (d-f) Ultrasonography of the liver showing normal parenchyma, the bile duct with a 2.3mm diameter is showed in d (between cursors), the portal vein (in red-cranialy- and blue-caudaly) and caudal vena cave (in blue in the far field) are visualized with Doppler. (g-i) Images from laparoscopy showing the quadrate lobe (arrow head) in g, the bile duct (arrow head) in h and the absence of the gallbladder with only a connective tissue between the liver lobes (arrow head) in i.

Book Chapter

Tobón Restrepo, M. (2015). Ultrasound of the abdominal cavity, lymph nodes and large vessels. In R. Novellas Torroja, E. Dominguez Miño, Y. Espada Gerlach, Y. Martínez Pereira, & M. Tobón Restrepo (Eds.), *Diagnostic ultrasound in cats* (First edit., pp. 211 – 229). Zaragoza, S: Servet editorial - Grupo Asís Biomedia S.L.

12

Ultrasound of the abdominal cavity, lymph nodes and large vessels

Mauricio Tobón Restrepo

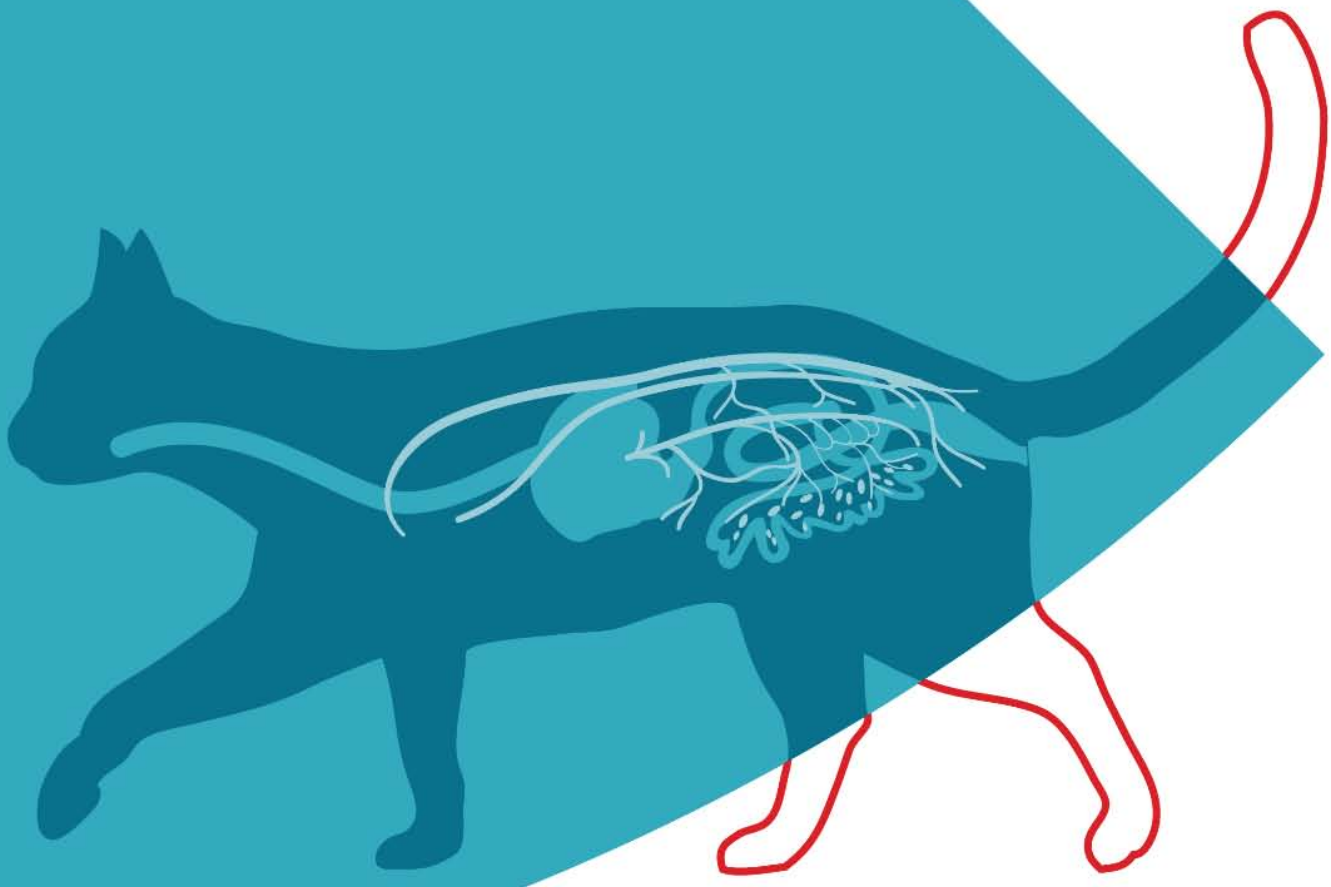

SCANNING TECHNIQUE

To obtain an appropriate acoustic window the patient should be positioned in left or right lateral or dorsal recumbency. The patient's hair should be clipped from the xiphoid process to the pubis, as well as on both sides of the abdomen following the costal arch nearly until it reaches the transverse process of the lumbar vertebrae (D'Anjou, 2008; Kinns and Mai, 2011; Mattoon et al., 2015).

High-frequency (7.5 MHz or higher) micro-convex or linear transducers are recommended for visualising the lymph nodes (LNs) and large vessels given that they are very small structures and can be embedded in fat. For larger cats, micro-convex transducers can be used to examine the deepest LNs, such as the hepatic or gastric lymph nodes, and vessels such as the portal vein (PV) or the caudal vena cava (CVC) in the cranial abdomen (D'Anjou, 2008; Mattoon et al., 2015).

ULTRASOUND OF THE NORMAL ABDOMINAL CAVITY, LYMPH NODES AND LARGE VESSELS

From an anatomical point of view, the peritoneum is defined as a serous membrane composed of the mesothelium, squamous cells and connective tissue (Evans and De Lahunta, 2013; Saar and Getty, 1982). The parietal peritoneum lines the internal surface of the abdominal and pelvic walls. The visceral peritoneum, either partially or completely, invests the organs in the abdominal and pelvic cavities. The connecting peritoneum consists of double folds, called the mesentery, omentum and ligaments, extending between the organs or connecting them to the parietal peritoneum (Evans and De Lahunta, 2013). The peritoneum produces small amounts of a viscous liquid to minimise friction between organs. This liquid is not usually visible with ultrasound; while it is located in the peritoneal cavity, which is defined as the space between the parietal and visceral peritonea (D'Anjou, 2008; Evans and De Lahunta, 2013).

The parietal peritoneum is observed as a fine hyperechoic line deeper than the abdominal wall in the near field of the image (Fig. 1). The visceral peritoneum also appears as a fine hyperechoic line covering the organs (known as the serous tunic) and can be distinguished around the intestinal loops, the stomach, the bladder and externally investing the capsule of the liver and spleen (Fig. 2). The connecting peritoneum is the tissue extending between the abdominal organs; the three peritoneal folds are the omentum, mesentery and ligaments (Fig. 3). In cats, the falciform ligament is surrounded by abundant fat and located ventral to the liver. It is either isoechoic or hypoechoic (it can occasionally be hyperechoic) with respect to the liver parenchyma, but it has a more granular echotexture (Fig. 4). The anatomical boundary between the two structures is the hyperechoic liver capsule. In the feline species this line is subtle and may not be recognised for what it is by inexperienced sonographers. This means that the fat of the falciform ligament may be confused with the liver parenchyma and can even lead to the collection of aspiration or biopsy samples which contain fat instead of liver (Widmer et al., 2015).

KEY POINTS

- Cats are easily stressed. It is therefore recommended that they are examined in a quiet room with a comfortable environment, which will make the patient more susceptible to cooperation. Otherwise they need to be sedated in order to obtain accurate ultrasound results.
- As the feline body condition increases so does the difficulty in identifying the normal lymph centres because the ultrasound beam is attenuated by the fat surrounding the nodes. In addition, gas in the intestinal loops causes acoustic shadowing which hinders the view of the intra-abdominal LNs (D'Anjou, 2008; Kinns and Mai, 2011; Mattoon et al., 2015).

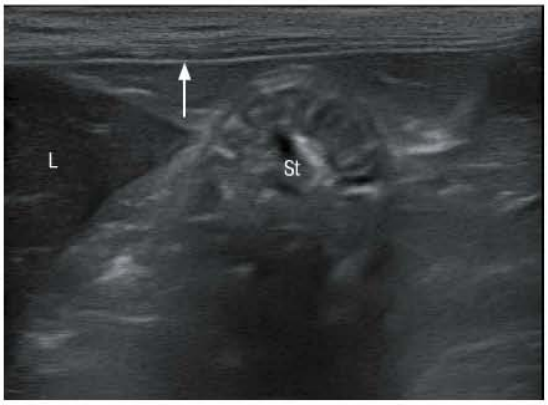

Figure 1. The parietal peritoneum (arrow) seen as a hyperechoic line in the deepest layer of the abdominal wall. The liver (L) and stomach (St) are also visible in the image.

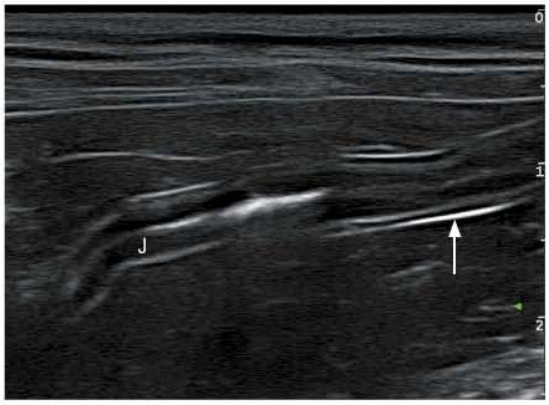

Figure 2. The visceral peritoneum (white arrow) appears as a hyperechoic line in the last sheet of layering of the wall of a jejunal loop (J).

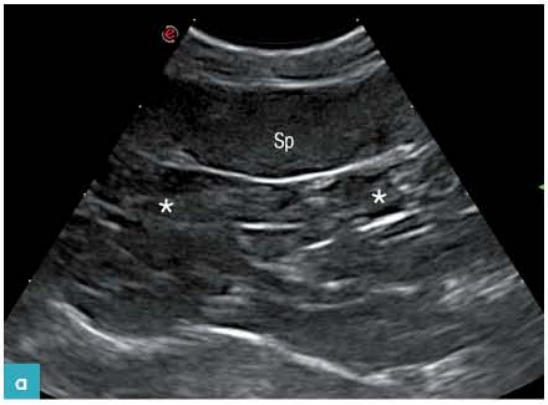

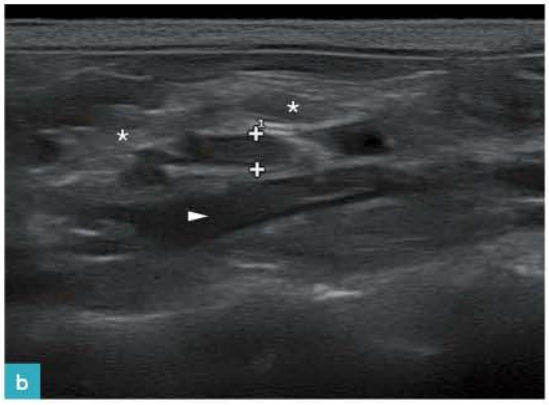

Figure 3. The connecting peritoneum (asterisks) is visible as a heterogeneous tissue; it is more hyperechoic than the spleen (Sp) in (a) and ventral to the left adrenal gland (between callipers) and the aorta (arrowhead) in (b).

Figure 5 illustrates the position of the abdominal LNs in cats. The abdominal lymph centres are categorised as either parietal or visceral. Four parietal (lumbar, iliosacral, inguinofemoral and ischiatic) and three visceral (coeliac, cranial mesenteric and caudal mesenteric) lymph centres have been identified (Saar and Getty, 1982). The most readily recognisable LNs in the visceral group are: gastric, hepatic, pancreaticoduodenal, jejunal, iliocaecal and colic (Fig. 6). From the parietal group, it is easy to identify the medial iliac and superficial inguinal lymph nodes (Fig. 7). The less commonly observed lymph centres within the visceral group are the splenic and caudal mesenteric LNs (Fig. 8) and from the parietal group the lumbar aortic, renal, internal iliac (previously known as the hypogastric) (NAV, 2012), sacral and caudal epigastric LNs. The superficial abdominal LNs (superficial inguinal and medial iliac) appear as slender fusiform structures. In comparison

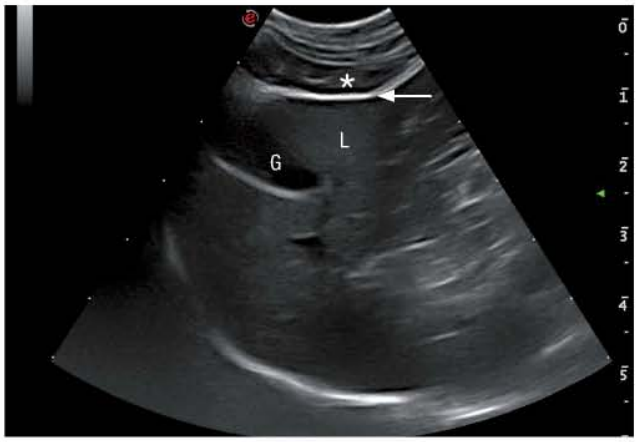

Figure 4. Falciform fat (asterisk) located ventral to the liver (L). Note the hyperechoic line corresponding to the liver capsule (white arrow) and which helps to distinguish the liver parenchyma from the adipose tissue. G: gallbladder.

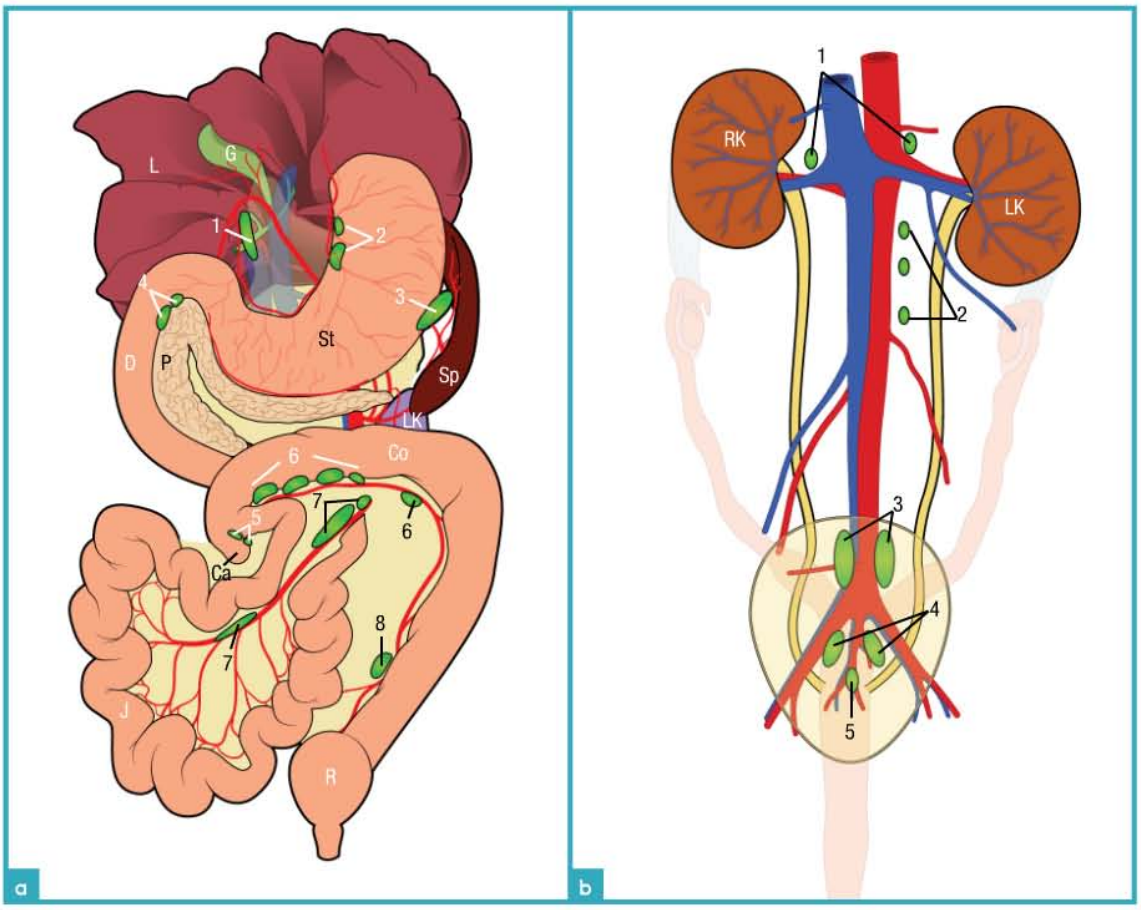

Figure 5. (a) Diagram of the abdominal lymph nodes and their relative anatomical positions. 1: hepatic; 2: gastric; 3: splenic; 4: pancreaticoduodenal; 5: iliocaecal; 6: colic; 7: jejunal; 8: caudal mesenteric; L: liver; G: gallbladder; St: stomach; D: duodenum; Sp: spleen; P: pancreas; J: jejunum; Ca: caecum; Co: colon, R: rectum; LK: left kidney. (b) Diagram demonstrating the most relevant parietal lymph nodes. 1: renal; 2: lumbar aortic; 3: medial iliac; 4: internal iliac; 5: sacral; RK: right kidney; LK: left kidney.

Figure 5a is based on an original drawing by José Rodríguez.

with the surrounding fat they have regular margins with an echogenic capsule, while the parenchyma is between iso- and hypoechoic relative to the fat. The deep abdominal LNs are elongated (jejunal, caudal mesenteric) or oval (all others), slightly hypoechoic in comparison with the peritoneum and surrounding fat, and they have regular margins. Table 1 lists the anatomical positions and sizes of the aforementioned lymph nodes.

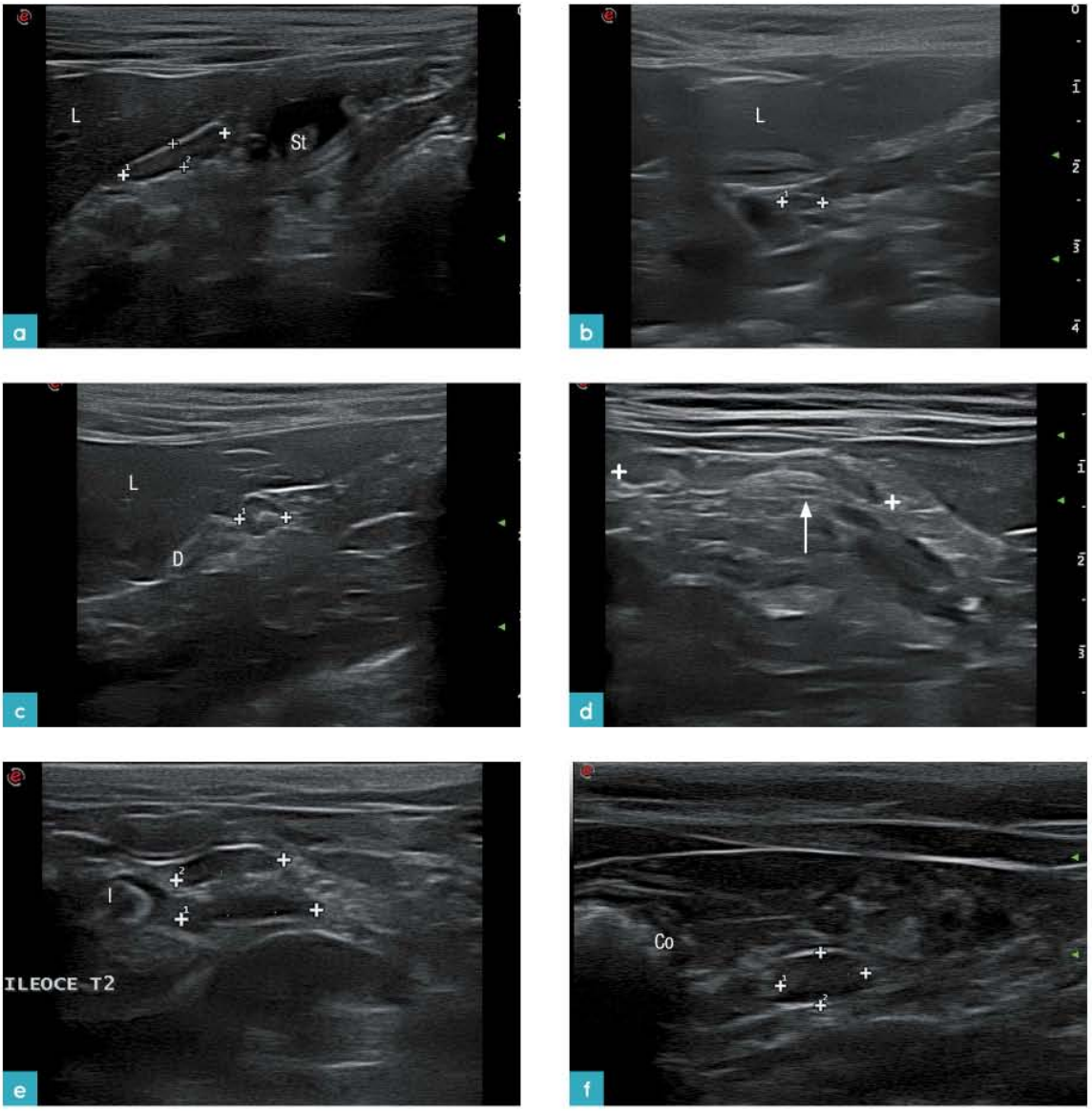

Figure 6. Images of the more readily identified LNs belonging to the visceral group. The majority are slightly hypoechoic and vary between round and oval in shape. (a) Gastric LN (between callipers) located on the lesser curvature of the stomach (St). L: liver. (b) Hepatic LN (between callipers) located on the hepatic hilum, close to the portal vein. L: liver. (c) Pancreaticoduodenal LN (between callipers) positioned ventrally between the duodenum (D) and pancreas. (d) Jejunal LN (between callipers) located on the mesojejunum following the course of the jejunal vessels (arrow). This example shows a typically elongated shape. (e) Ileocaecal LNs (between callipers) positioned on both sides of the ileocolic junction. I: ileum. (f) Colic LN (between callipers) observed close to the colon (Co). It has a slightly rounded shape.

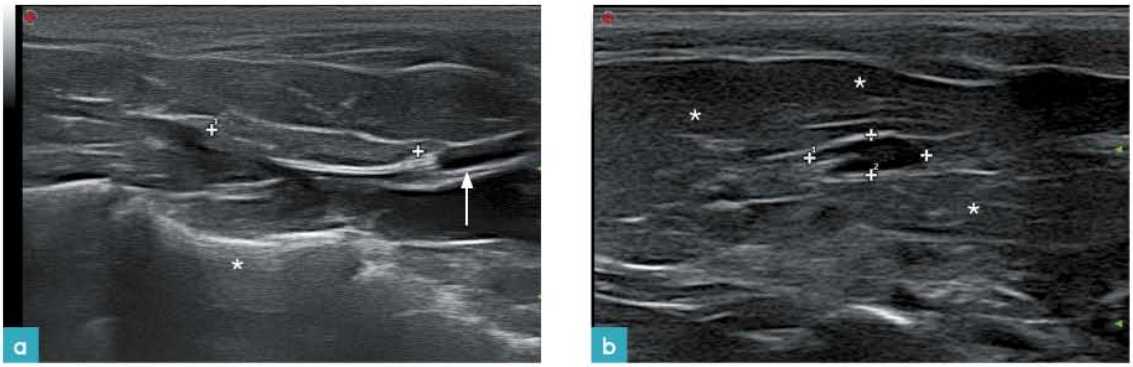

Figure 7. Views of the more readily identified LNs belonging to the parietal group. They are generally elongated and between iso- and hypoechoic. (a) Medial iliac LN (between callipers) position in relation to the aorta and its external iliac branches (arrow). A lumbar vertebral body is also visible (asterisk). (b) Superficial inguinal LN (between the callipers). Note the hypoechoic parenchyma with a slightly hyperechoic centre and its hyperechoic capsule which helps to differentiate it from the surrounding fat (asterisk).

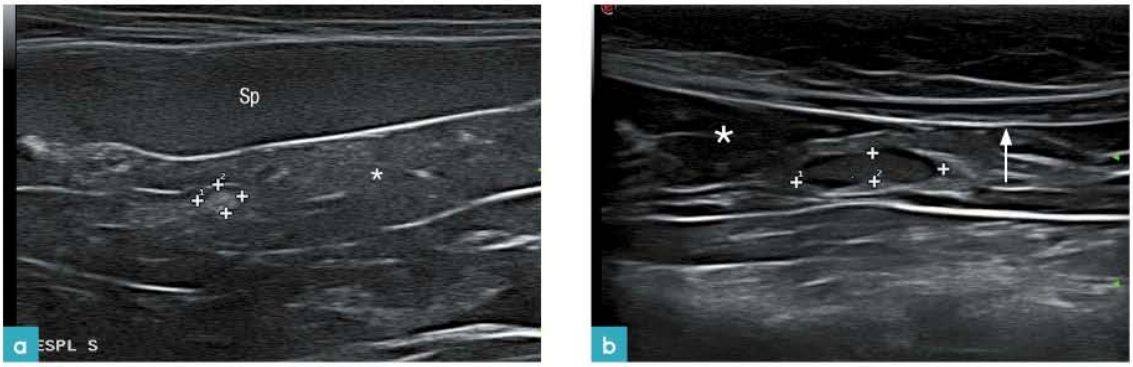

Figure 8. Images of the less readily identified visceral LNs. (a) Splenic LN (between callipers) located close to the splenic hilum following the splenic vein and embedded in the gastrosplenic ligament (asterisk). It is rounded and occasionally has a hyperechoic centre, particularly in obese patients, which makes it difficult to identify. Spleen (Sp). (b) Caudal mesenteric LN (between callipers). There is a slight hypoechoic halo and a more hyperechoic centre. This centre is normally located cranial to the bladder, between the bladder and the descending colon (not included in the image), marginally to the right of the midplane and relatively close to the surface. The abdominal wall (arrow) and part of the mesenteric fat surrounding the node (asterisk) are both visible.

The abdomen receives its blood supply from branches of the aorta (coeliac, cranial mesenteric, renal, deep circumflex iliac, external iliac, internal iliac and median sacral arteries). The abdomen's veins are divided into two groups: those which drain into the CVC and those which drain into the PV. In order to examine the aorta and CVC the transducer needs to be placed parallel to both sides of the lumbar vertebral bodies. The abdominal aorta runs from the diaphragm down to the level of L6, is positioned slightly to the left of the midline and can be identified as an anechoic tubular structure with a hyperechoic wall (Figs. 9a and 9b) and acoustic enhancement which is more evident in a transverse view. A routine ultrasound examination can also identify all the branches of the aorta. The CVC runs to the right of the aorta and has a similar ultrasound appearance. However, unlike the aorta, the CVC easily collapses when compressed with the transducer (Fig. 9c). On ultrasound the PV is found at the height of the porta hepatis and its tributary veins can be identified caudally (gastroduodenal, splenic, cranial and caudal mesenteric). The portal vein is located slightly to the right of the abdomen (Fig. 9d).

Table 1. Location and size of abdominal lymph nodes. Measurements by Saar and Getty (1982) † and Schreurs et al. (2008) ‡.

Lymph centre	Lymph node	Size		Anatomical location
		Anatomy†	Ultrasound‡	
Coeliac	Hepatic	1.5–30.5 mm	2.1–16.0 mm	Around the junction between the gastroduodenal and portal veins, and close to the porta hepatis.
	Gastric	1.0–20.0 mm	4.6–6.4 mm	Embedded in the lesser omentum, in the lesser curvature of the stomach and close to the cardia or the pylorus.
	Splenic	2.0–22.0 mm	5.0–11.2 mm	Along the splenic vein and its junction with the short gastric veins.
	Pancreaticoduodenal	2.0–22.0 mm	6.6–13.0 mm	Next to the junction between the pancreaticoduodenal and right gastroepiploic veins, on the caudal aspect of the pylorus.
Cranial mesenteric	Jejunal	5.0–79.0 mm	11.4–39.0 mm	Located in the mesojejunum, along the jejunal branch of the cranial mesenteric artery.
	Ileocaecal	3.0–14.0 mm	6.7–23.2 mm	On both sides of the ileocolic junction, in the ileocaecal fold, and along the caecal branches of the ileocolic vessels, on both sides of the caecum.
	Colic	1.0–34.0 mm	4.6–12.1 mm	Along various segments of the colon, except those situated directly in the ileocolic junction.
Caudal mesenteric	Caudal mesenteric	5.0–14.5 mm	6.0 mm	In deep areas of the mesentery, close to the descending colon, at the bifurcation of the mesenteric artery into its cranial and caudal branches.
Lumbar	Renal	0.5–14.5 mm	4.7–7.7 mm	Between the adrenal gland and renal vessels.
	Lumbar aortic	0.5–17.5 mm	2.1–16.7 mm	Along the aorta and caudal vena cava, between the diaphragm and deep circumflex iliac arteries.
Iliosacral	Medial iliac	1.0–27.5 mm	5.0–23.3 mm	On both sides of the aorta, between the deep circumflex iliac and external iliac arteries.
	Internal iliac	< 5.0 mm	ND	Close to the internal iliac arteries.
	Sacral	ND	9.2–10.0 mm	Caudal to the origin of the internal iliac and median sacral arteries.
Inguinofemoral	Superficial inguinal	19.5 mm	ND	In the inguinal region, near the junction between the caudal superficial epigastric vessels and the external pudendal vessels.

ND: No data.

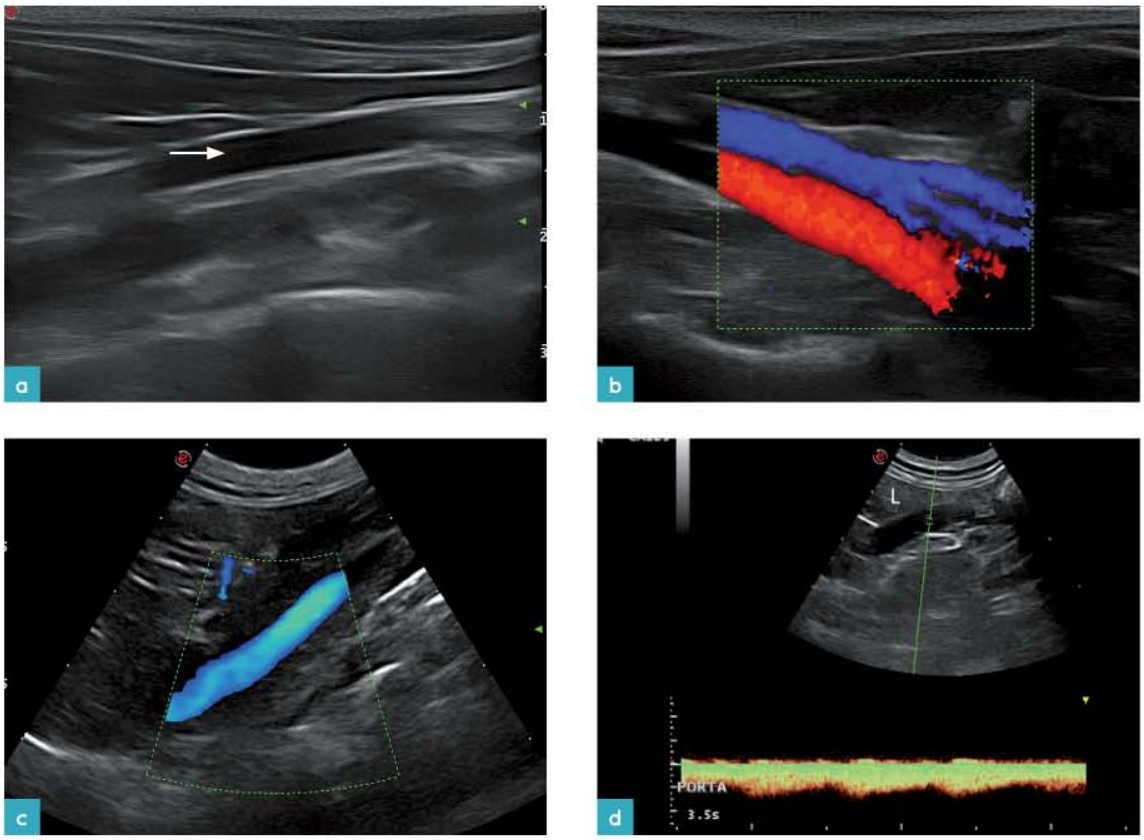

Figure 9. (a) Sagittal view of the aorta (arrow), visible as an anechoic tubular structure with an echogenic wall. (b) Colour Doppler ultrasound of the aortic bifurcation (in blue, with the flow going away from the transducer), some of its branches are also visible. The caudal vena cava is located (in red, with the flow coming towards the transducer). (c) Colour Doppler image of the caudal vena cava in the cranial abdomen, close to the liver. The blue colour shows that the flow is away from the transducer. (d) Pulsed-wave Doppler of the portal vein entering the liver (L). There is venous flow moving away from the transducer, with a velocity that is almost constant throughout the cardiac cycle and less than the baseline.

ULTRASOUND IN ABDOMINAL CAVITY, LYMPH NODE AND LARGE VESSEL LESIONS

A complete ultrasound examination not only evaluates the abdominal organs, but the peritoneal and retroperitoneal spaces must also be assessed, as should the lymphatic and vascular structures contained within the abdominal cavity.

There are many indications for performing an abdominal ultrasound and the technique is often used to complement radiography (Kinns and Mai, 2011). In general, conditions affecting the abdominal organs can also have an impact on the abdominal cavity, lymph nodes and large vessels. It is very important to pay attention to any changes in each of these structures in order to make a comprehensive and definitive diagnosis, as well as to understand certain changes in the organs, such as the observation of a hyperechoic peritoneum due to free fluid in the abdomen, i.e., peritoneal effusion (Mattoon et al., 2015).

PERITONEAL EFFUSION

Although we previously stated that the peritoneum produces a small volume of liquid to help reduce friction between the organs, an increase in the amount of free fluid seen in the peritoneal space is a sign of disease. It has been reported that more than 2 ml of free fluid per kilogram (D'Anjou, 2008) or per pound (Widmer et al., 2015) of live weight can be detected with ultrasound and is a specific sign of peritoneal effusion. Small amounts of free fluid are difficult to visualise and associate with specific conditions.

The position of the fluid in the peritoneal space depends on its nature and the severity of effusion; therefore, it is recommendable to examine the dependent portions of the abdomen in lateral recumbency. The presence of anechoic, or occasionally hypoechoic, triangular areas close to the base of the urinary bladder, between the abdominal wall and the spleen, between the liver and the stomach, between the diaphragm and the liver, or between the hepatic lobes, is compatible with free fluid (D'Anjou, 2008; Widmer et al., 2015) (Fig. 10).

The fluid can be sometimes be retained among the peritoneal folds or be located around an organ or lesion (e.g., peripancreatic oedema due to pancreatitis). Cats with severe hydronephrosis and/or hydroureter may present signs that can be confused with free fluid or fluid trapped between the peritoneum, so great care should be taken with the diagnosis (D'Anjou, 2008).

Another important factor to consider is that the appearance of free fluid can be modified by changing the machine settings. Although the nature of the fluid can roughly be determined by its echogenicity, the results should be interpreted carefully. It has been reported that the transudates are anechoic due to their low cellularity, modified transudates are hypoechoic to slightly echogenic and exudates can be isoechoic in comparison with the surrounding tissue due to their high cellularity (e.g., purulent or haemorrhagic). The fluid may contain cell debris or small gas bubbles (D'Anjou, 2008; Spaulding, 1993; Widmer et al., 2015).

Figure 10. Fourteen-year-old cat with chronic diarrhoea and weight loss. Ultrasound provides evidence of an intestinal mass and peritoneal effusion. There is anechoic free fluid (asterisk) between the liver lobes (L). The diaphragm (arrow) is visible in the far field.

A large amount of free fluid could be the result of ascites (secondary to right heart failure, liver disease, portal hypertension, hypoproteinaemia, obstruction of the CVC, a neoplasm or other causes).

A haemorrhagic effusion or haemoperitoneum can be observed secondary to non-neoplastic (coagulopathies, trauma, spontaneous liver rupture in amyloidosis, rupture of a vascular anomaly) or neoplastic causes (most frequently haemangiosarcoma and hepatocellular carcinoma, while hepatic cholangiocarcinoma, splenic lymphoma, splenic histiocytic sarcoma, nephroblastoma, splenic adenocarcinoma and lymphoma are less common); both non-neoplastic and neoplastic causes are observed with an equal frequency (Culp et al., 2010).

Other possible findings are uroabdomen (due to rupture of the urinary tract), protein-rich transudate (due to feline infectious peritonitis), bile peritonitis (due to rupture of the gallbladder or bile duct) and chyloperitoneum (due to a neoplasm or portal obstruction) (Dennis et al., 2010; Widmer et al,. 2015).

PNEUMOPERITONEUM

Hyperechoic lines with reverberation artefacts that reduce the visual clarity of the abdominal organs indicate the presence of free gas. Free gas can situate itself in contact with the non-dependent abdominal wall, between the hepatic lobes, intestinal loops, stomach and omentum (D'Anjou, 2008). Radiography is however a more sensitive technique than ultrasound for the detection of free gas (Dennis et al., 2010; Widmer et al., 2015).

KEY POINTS

Causes of free gas in the feline peritoneum are (D'Anjou, 2008; Dennis et al., 2010):

- iatrogenic causes (e.g., recent laparotomy or following a pneumocystograph) (Fig. 11),
- perforation of the gastrointestinal tract secondary to neoplasia, ulceration or trauma,
- entry of gas through the abdominal wall secondary to a penetrating wound, abdominal drainage tube or feeding tube,
- pneumothorax spreading to the abdominal cavity, and
- peritonitis due to *Clostridium* spp.

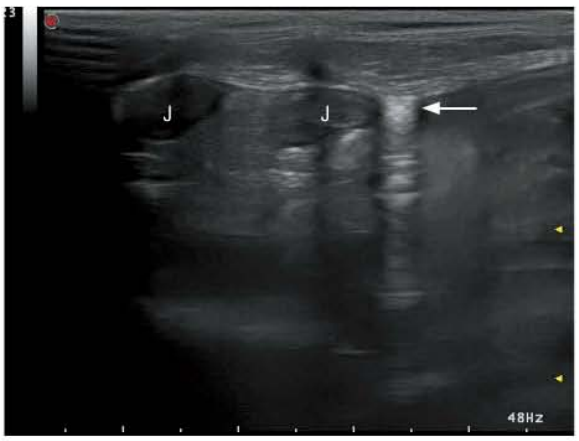

Figure 11. Abdomen of a female cat following an ovariohysterectomy. The image shows a hyperechoic line with reverberation (arrow) in contact with the abdominal wall, compatible with free gas inside the peritoneal cavity. J: jejunum.

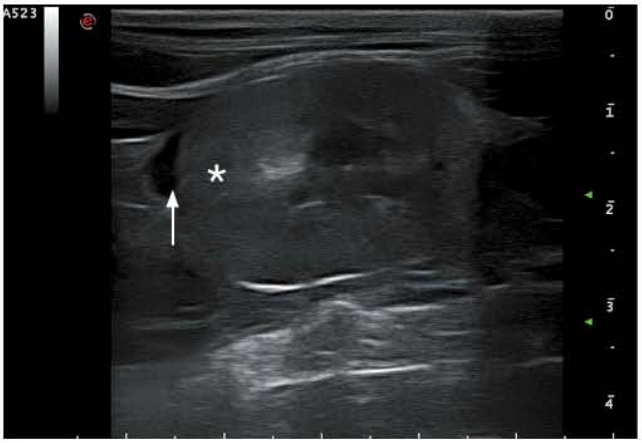

Figure 12. Male cat with IRIS Stage 2 kidney disease. Retroperitoneal free fluid (arrow) is visible around the cranial pole of the left kidney (asterisk).

RETROPERITONEAL EFFUSION

Several disorders can cause an accumulation of fluid in the retroperitoneal space, which takes on a striated appearance as the fluid forms anechoic or hypoechoic fusiform regions between the hyperechoic retroperitoneal fat (Dennis et al., 2010).

It is not always easy to discern whether the fluid is in the retroperitoneal or peritoneal space; nevertheless moving the patient will cause peritoneal fluid to be displaced, whereas retroperitoneal fluid will remain in the same position (Widmer et al., 2015).

Retroperitoneal free fluid may be the result of injuries to the adrenal glands, kidneys, ureters, large vessels and lymphatic trunks (Fig. 12). The retroperitoneal effusion fluid could be blood, urine, pure or modified transudate, although a definitive diagnosis to identify the type of fluid requires its aspiration and subsequent analysis (Dennis et al., 2010; Widmer et al., 2015).

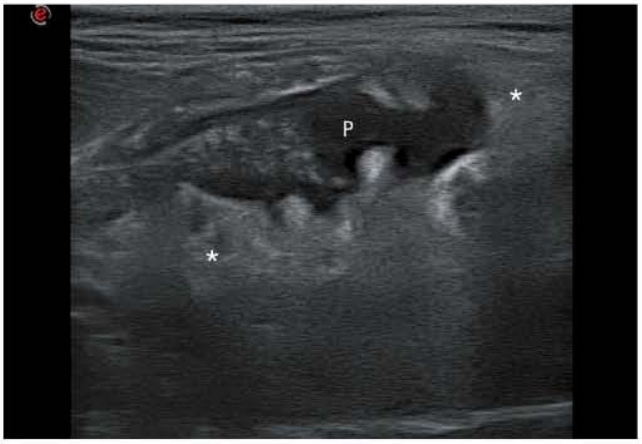

Figure 13. Male cat with polytrauma after falling from a significant height. The pancreas (P) is heterogeneous but with a more hypoechoic portion on the left lobe and irregular margins. The mesentery (asterisks) surrounding the pancreas reveals a hyperechoic and irregular appearance, compatible with steatitis and pancreatitis due to the trauma.

PERITONITIS AND STEATITIS

Peritonitis typically reveals a variable quantity of free fluid, which is often moderately echogenic or hyperechoic due to its high cellularity. The free fluid may be less echogenic in cases of feline infectious peritonitis (FIP) (Spaulding, 1993). The peritoneum, omentum and mesentery tend to be hyperechoic, thickened and hyperattenuating (D'Anjou, 2008), which blocks the penetration of the ultrasound.

Steatitis or inflammation of the mesenteric fat is observed as areas of hyperechoic mesenteric fat. This lesion is related to others nearby (such as pancreatitis or an intestinal lesion), recent surgery or trauma (Fig. 13).

Another pathological process reported is pansteatitis, which is caused by a dietary excess of polyunsaturated fatty acids and mainly observed in animals that consume fish-based diets (Cropper, 1980; Watson, 1980). A case of a male cat with pansteatitis revealed a hyperechoic omentum with diffusely distributed hypoechoic foci (Zini et al., 2007).

LYMPHADENOPATHY

Ultrasound changes in the abdominal lymph nodes with regards to shape, margins, size, echogenicity, echotexture and vascular flow distribution have been recognised as characteristics which help to differentiate between benign and malignant lymphadenopathies (D'Anjou, 2008; Nyman and O'Brien, 2007).

A malignant LN frequently has a rounded shape and hypoechoic parenchyma (Nyman and O'Brien, 2007) (Fig. 14). Nevertheless, if accompanied by haemorrhage, necrosis or calcification, then the LN acquires a more heterogeneous appearance (D'Anjou, 2008) (Fig. 15). On ultrasound, the heterogeneity of the LN is a significant finding in dogs that indicates malignancy. This association in cats has not however been confirmed (Kinns and Mai, 2007).

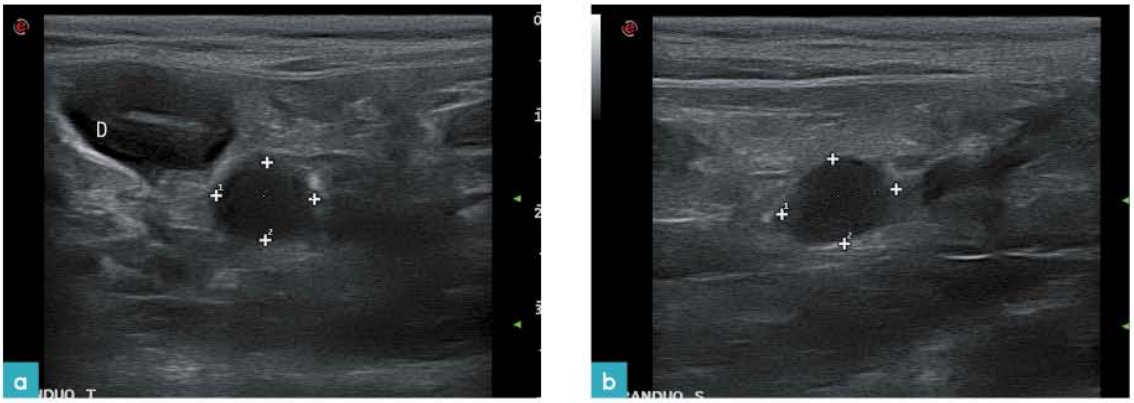

Figure 14. Patient with an intestinal lymphoma. (a) Transverse view. (b) Sagittal view. There is an intestinal mass on the duodenum (D), with evidence of wall thickening and a loss of layering. The pancreaticoduodenal LN (between callipers) has increased in size, presents hypoechoic parenchyma and is rounded. Cytological analysis of the fine-needle aspiration sample was compatible with a lymphoma.

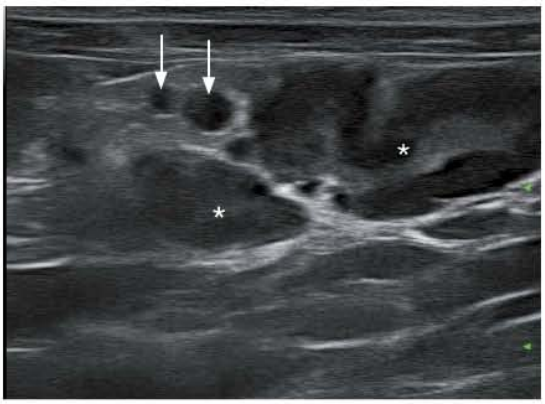

Figure 15. Patient with an intestinal lymphoma, but categorised as having a greater T-lymphocyte population in the biopsy. In this example there is evidence of jejunal lymphadenopathy with irregular contours, a heterogeneous echogenicity and a more hyperechoic central area while the periphery is more hypoechoic (asterisks). There is also a transverse view of the jejunal vessels (artery and vein) (arrows).

Diagnostic parameters for the identification of a malignant lymphadenopathy (Nyman and O'Brien, 2007):

- **short/long axis ratio of the LN > 0.5,**
- **distribution pattern of the vessels in the LN, and**
- **variations in the resistive and pulsatility indices.**

Lymphadenopathy is associated with reactive, inflammatory and neoplastic processes (Fig. 16). The ultrasound characteristics of normal, reactive and malignant (metastatic) LNs overlap each other (Nyman and O'Brien, 2007) (Fig. 17). The observation of very large lymph nodes with heterogeneous areas may be related to benign or malignant infiltration and can be associated with a pyogranulomatous condition (Fig. 18) or a neoplasm (Fig. 19) (D'Anjou, 2008). A fine-needle aspiration needs to be performed on the LNs to obtain cytological confirmation of the diagnosis.

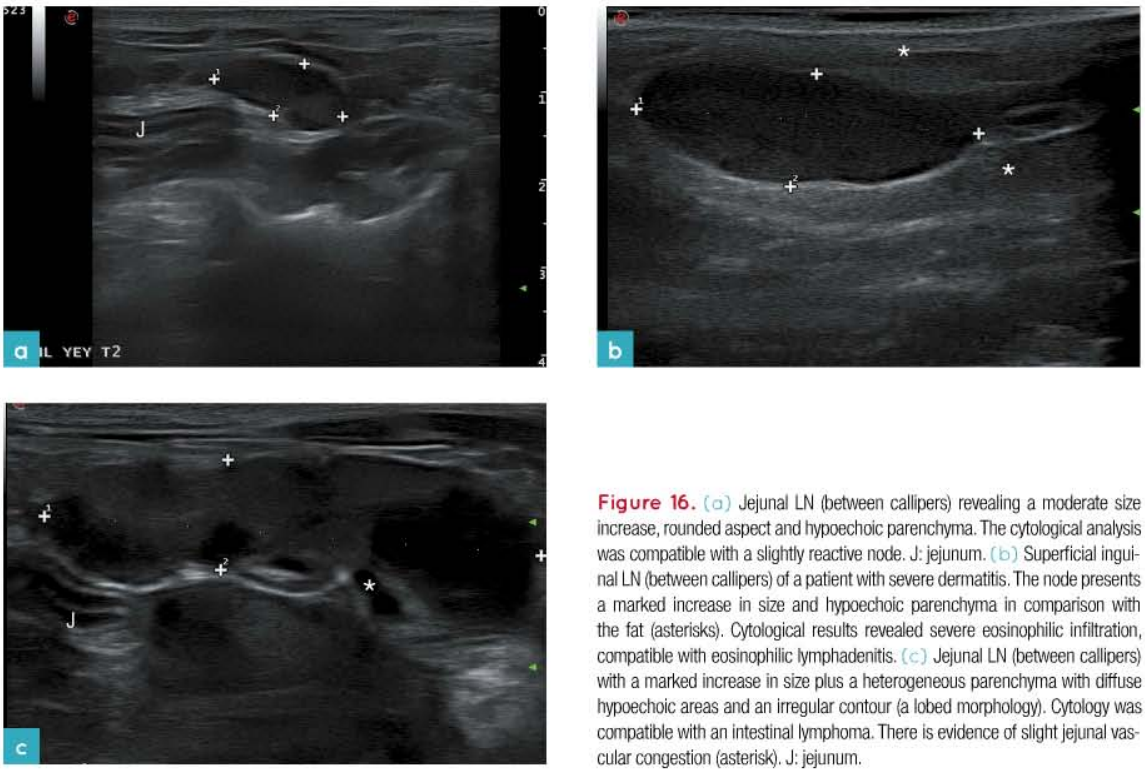

Figure 16. (a) Jejunal LN (between callipers) revealing a moderate size increase, rounded aspect and hypoechoic parenchyma. The cytological analysis was compatible with a slightly reactive node. J: jejunum. (b) Superficial inguinal LN (between callipers) of a patient with severe dermatitis. The node presents a marked increase in size and hypoechoic parenchyma in comparison with the fat (asterisks). Cytological results revealed severe eosinophilic infiltration, compatible with eosinophilic lymphadenitis. (c) Jejunal LN (between callipers) with a marked increase in size plus a heterogeneous parenchyma with diffuse hypoechoic areas and an irregular contour (a lobed morphology). Cytology was compatible with an intestinal lymphoma. There is evidence of slight jejunal vascular congestion (asterisk). J: jejunum.

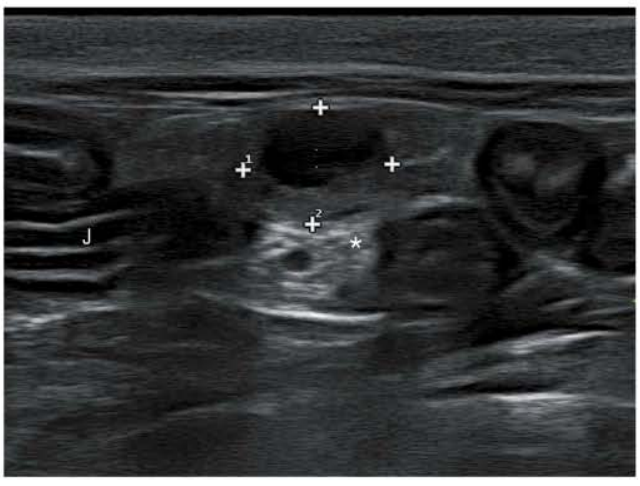

Figure 17. View of the caudal mesenteric LN (between callipers) in a patient with an intestinal mass that was diagnosed as a jejunal haemangiomapericytoma in the biopsy evaluation. The node has a rounded shape, an increased size and an internal area between hypo- and anechoic which produces acoustic enhancement (asterisk). The biopsy revealed signs of dilated lymphatic sinuses (compatible with lymph stasis/lymphangiectasis) without evidence of neoplastic cells. In the present image, it is possible that the volume of lymph (low cellularity fluid) contained in the lymphatic sinuses may be the cause of the notable acoustic enhancement. J: jejunum.

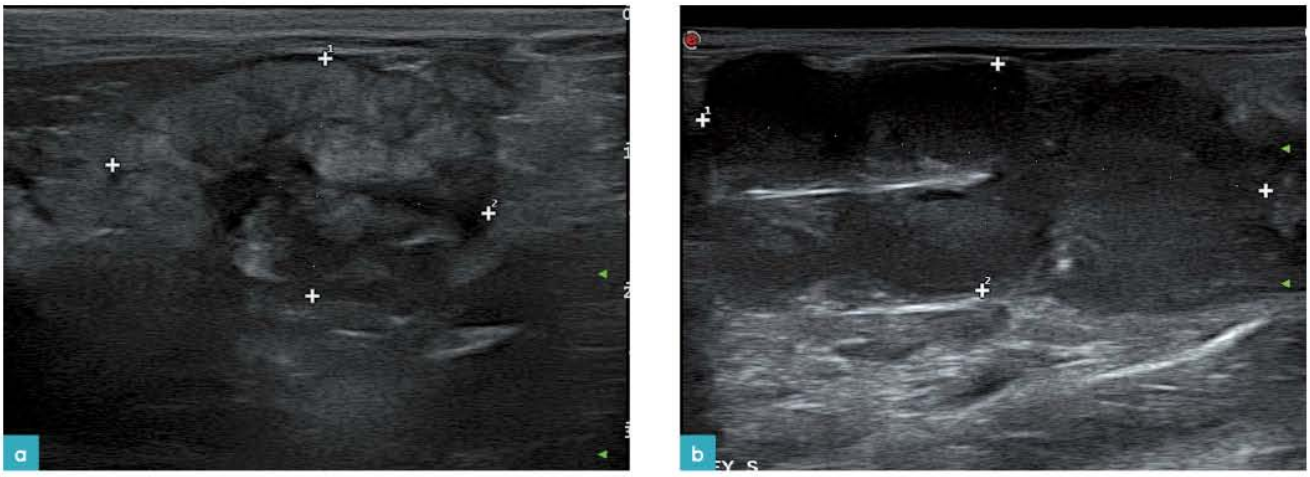

Figure 18. (a) Image of jejunal LN with a large increase in size, irregular contour and heterogeneous parenchyma (between callipers). Hypoechoic areas are visible within the LN, indicative of necrosis. Cytological results were compatible with a pyogranulomatous infiltration typical of FIP. (b) Another patient positive for FIP, but in this case the jejunal LN (between callipers) has a hypoechoic parenchyma, irregular margins (lobed appearance) with a hyperechoic central line and increased considerably in size.

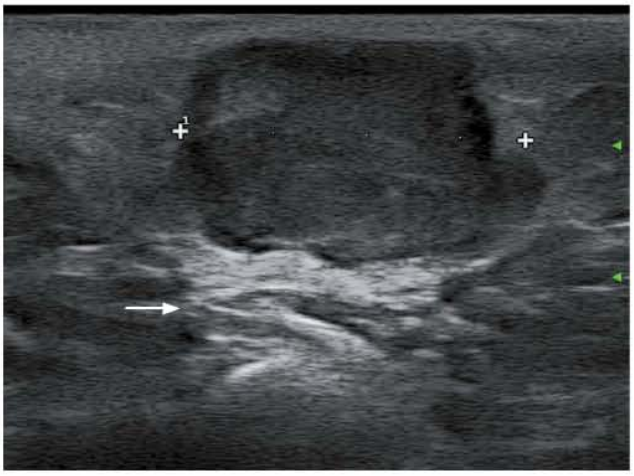

Figure 19. Patient with mammary masses. The superficial inguinal LN (between callipers) presents an increased size, irregular margins and a hypoechoic parenchyma with some echogenic areas. The hyperechogenicity of the surrounding fat (arrow), compatible with inflammation, is apparent. Cytology was compatible with metastasis of a simple tubular mammary carcinoma.

PERITONEAL AND RETROPERITONEAL MASSES

There are different types of intra-abdominal masses in cats that may have no relation with a specific organ: abscesses, granulomas, haematomas, lipomas and mesotheliomas. Fibrosarcomas and haemangiosarcomas have also been reported as mesenteric masses (Culp et al., 2008; Haddad and Goldschmidt, 2010).

Abscesses appear as a mass-like structure with a poorly-defined hyperechoic wall. The internal architecture is complex, although it can be summarised as enclosed pockets of hypoechoic fluid with echogenic remnants and gas (in the form of hyperechoic foci producing reverberation artefacts). In function of the cellularity, acoustic enhancement may be observed. If the abscess contains caseous material, then an acoustic shadow could be observed (D'Anjou, 2008; Widmer et al., 2015).

Watch video online

Video 1. Granulomatous infiltration of the lymph nodes secondary to FIP

Same patient as in Fig. 20. Multiple, diffusely distributed, hyperechoic nodes can be observed throughout the mesentery, medial to the spleen (which is located in the most ventral part of the nodes, close to the near field in the image).

Granulomas and pyogranulomas are uncommon; nevertheless, they appear as intra-abdominal masses with no relation to any abdominal organs and have a homogeneous hyperechoic appearance. Cats with FIP may manifest multiple mesenteric granulomas (Fig. 20, Video 1). Other findings in cats with FIP include a liver with diffuse or focal hyperechogenicity, a hyperechoic medullary band on the kidney, a hypoechoic subcapsular renal band, peritoneal and retroperitoneal effusion, abdominal lymphadenopathy manifesting as hypoechoic masses, a hypoechoic spleen and orchitis (Lewis and O'Brien, 2010).

Granulomas and pyogranulomas may also be associated with retained surgical gauze or mycosis (Black et al., 2001; Mai et al., 2001). The presence of surgical gauze pads can produce a marked acoustic shadow (Fig. 21, Video 2).

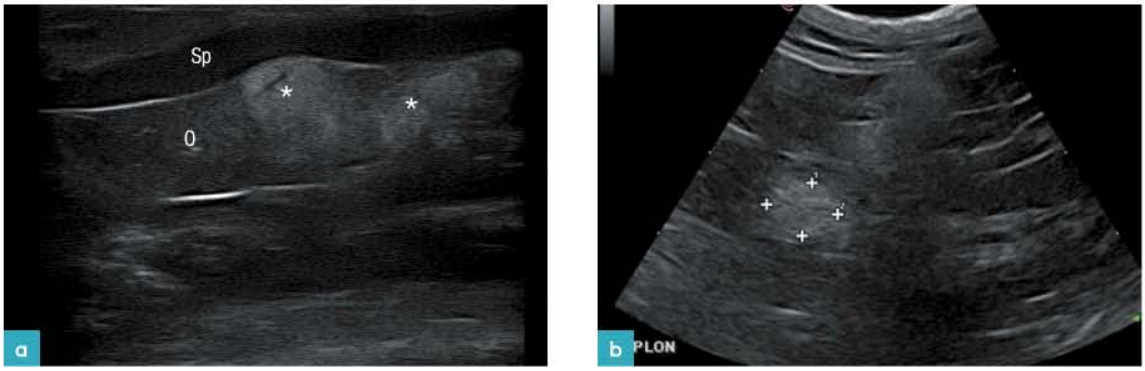

Figure 20. Patient with multiple nodes in the gastrosplenic ligament, cytologically compatible with a granulomatous infiltration secondary to FIP. (a) The gastrosplenic omentum (O) is observed medial to the spleen (Sp), in the presence of hyperechoic nodes and with a poorly-defined contour (asterisks). (b) Image of the same patient showing another node in the mesentery (between callipers).

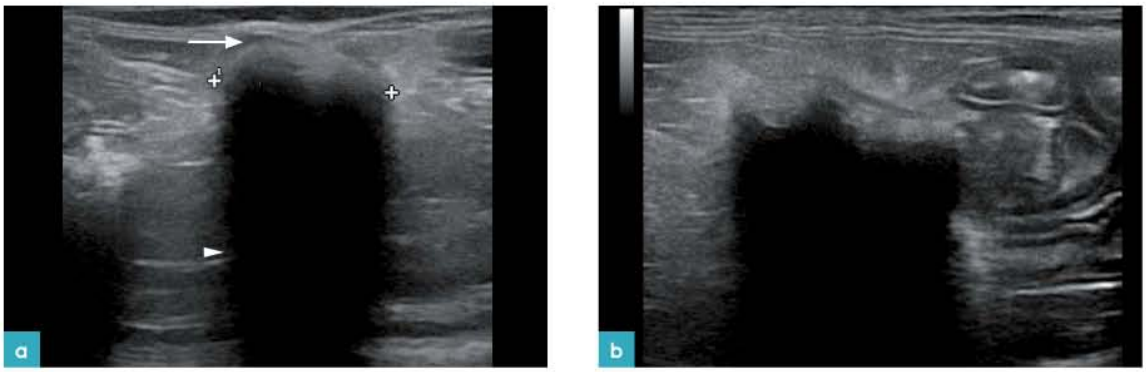

Figure 21. Mesentery of a patient with a gauze pad retained from a previous operation. (a) Note the structure with a hyperechoic surface (between callipers) and its associated marked clean acoustic shadowing (arrowhead). The hyperechoic surface is coated with a fine hypoechoic band of slightly irregular thickness (arrow). (b) Image of the same structure but viewed from a marginally different plane in which it reveals a more irregular surface. The mesentery surrounding the gauze pad is hyperechoic due to associated inflammation. Images courtesy of Yara López.

Watch video online

Video 2. Retained surgical gauze

A hyperechoic structure with marked acoustic shadowing within the mesentery is visible close to the intestinal loops (which appear on the right of the image). There is a thin and slightly irregular hypoechoic band surrounding the hyperechoic surface, while the band is in turn surrounded by mesenteric fat which appears hyperechoic due to associated inflammation. Images courtesy of Yara López.

A case has been reported of granulomas with fungal aggregates producing hyper-reflective foci with echo attenuation that could easily be confused with calcifications (Black et al., 2001). Foreign bodies, such as grass awns or twigs, can also trigger a pyogranulomatous response (D'Anjou, 2008) (Fig. 22).

The ultrasound appearance of haematomas varies with time. They appear as a mass with a heterogeneous echogenicity, or else hypoechoic, and poorly-defined margins in the peritoneum. Other organs may also be affected (Beraud and Carozzo, 2007; Widmer et al., 2015). Haematomas can be secondary to acute traumas, coagulopathies or cystocentesis (Widmer et al., 2015). Haematomas can produce large intra-abdominal masses and it may be difficult to determine the origin of bleeding using ultrasound techniques (Beraud and Carozzo, 2007).

Lipomas and infiltrative lipomas can be found in different parts of the abdomen, including the omentum, the mesentery and the retroperitoneal space (D'Anjou, 2008). On ultrasound they are observed as homogeneous echogenic masses that may be either uniform with a granular internal echotexture or they can manifest a heterogeneous and hypoechoic echogenicity (D'Anjou, 2008; Dennis, 2010; Widmer et al., 2015).

Nodular fat necrosis can result in an abdominal mass that affects the adipose tissue, hence it presents a higher incidence in obese cats. It has been described as a well-defined hyperechoic and hyperattenuating mass (due to the presence of calcified material) with a hypoechoic centre (D'Anjou, 2008; Dennis et al., 2010; Schwarz et al., 2000) (Fig. 23, Video 3).

Peritoneal tumours are uncommon in cats. Carcinomatosis, sarcomatosis and lymphomatosis are defined as a peritoneal extension of a neoplasm which may have originated in the liver, pancreas or intestine. The presence of free fluid improves visualisation of the nodes. Their size, shape and echogenicity vary and they tend to be accompanied by lymphadenopathy (D'Anjou, 2008; Dennis et al., 2010) (Fig. 24).

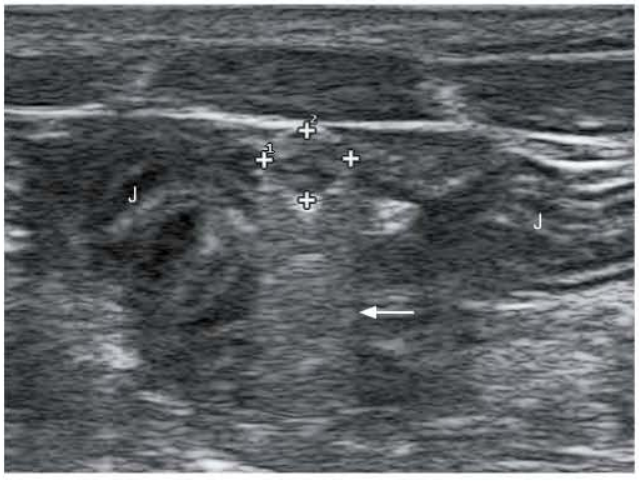

Figure 22. A round foreign body (between callipers) is visible in the abdominal cavity, located in the mesentery between the intestinal loops (J). The structure caused reverberation (arrow) and corresponded to a shotgun pellet. In this case there were no signs of an associated granuloma.

An ultrasound study of 14 cats with lymphomatosis revealed that each of the subjects suffered peritoneal effusion and had masses in the connective tissue. Other findings include primary or metastatic masses in abdominal organs, lymphadenomegaly, pleural effusion, plus masses in the parietal and visceral peritonea (Monteiro and O'Brien, 2004).

Mesenteric neoplasms have been reported in areas where gauze pads (Haddad and Goldschmidt, 2010) or foreign bodies have been retained. Figure 25 presents a haemangiosarcoma originating in the mesentery due to a shotgun pellet which became embedded in the mesentery.

Watch video online

Video 3. Nodular fat necrosis

A node with a thin well-defined hyperechoic wall appears on the left of the image and below that there is a hypoechoic band followed by a hyperechoic surface with associated acoustic shadowing. A second, smaller node, with similar characteristics to the previous one, appears later in the video on the right of the screen.

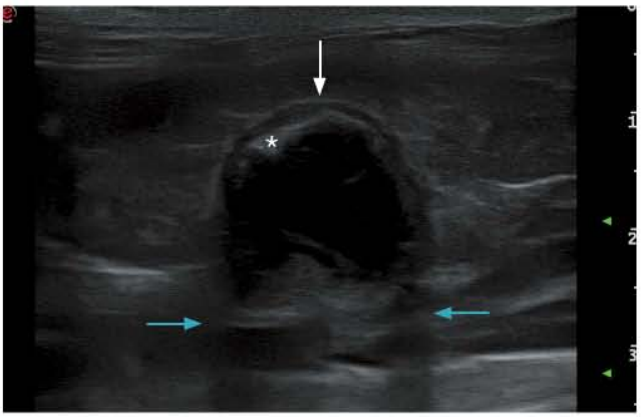

Figure 23. View of a male cat that had previously undergone a splenectomy. A node can be seen on the peritoneum, in the splenic region. The node has a thin well-defined hyperechoic wall (white arrow) and below that there is a hypoechoic band followed by a hyperechoic surface (asterisk) with associated acoustic shadowing (blue arrows) suggesting calcification of the lesion. These findings are compatible with fat necrosis.

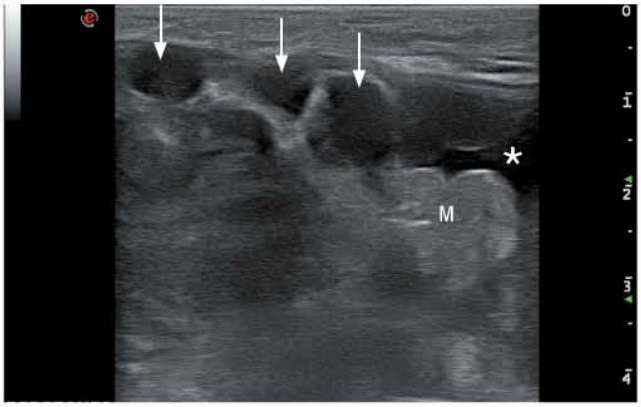

Figure 24. Peritoneum of a nine-year-old female cat with a carcinoid tumour in the mesentery. Multiple hypoechoic nodes (arrows) can be seen diffusely distributed throughout the mesentery (M), corresponding to carcinomatosis. Free fluid can also be noted (asterisk).

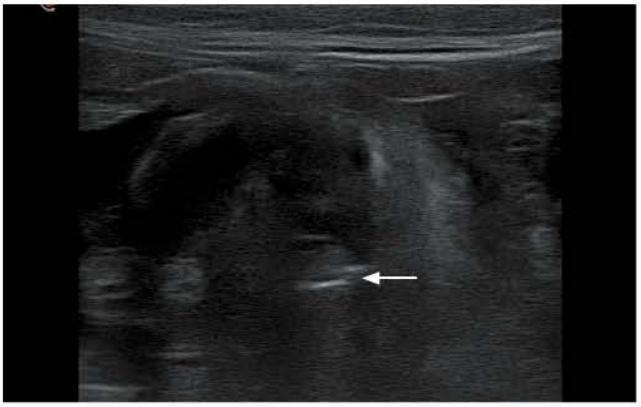

Figure 25. There is a heterogeneous mass that contains a structure with two hyperechoic lines and slight reverberation (arrow) within its interior; this corresponds to a shotgun pellet retained in the mesentery of a patient that was shot in the past. The histopathology of the mass was compatible with a haemangiosarcoma.

DISORDERS OF LARGE VESSELS

Thrombosis is the presence of coagulated blood in the lumen of the aorta, its branches or in the CVC. (Smith and Tobias, 2004). The abdominal vascular alteration most frequently observed in cats is aortic thromboembolism (Fig. 26) (Fuentes, 2012). The ultrasound appearance of a thrombus varies according to its chronicity. Initially there is little echogenicity and the thrombus is difficult to observe. The application of colour Doppler, power Doppler or pulsed-wave Doppler can reveal the presence of a thrombus in the lumen of a vessel (Fig. 27). With time, the thrombus becomes more echogenic and it is apparent how it attaches to the vascular wall, plus the filling defect can be observed with B-mode ultrasound (D'Anjou, 2008; Dennis et al., 2010; Widmer et al., 2015).

Distal aortic and iliac thromboembolism is common in cats with cardiomyopathy and an increased left atrium. Other possible causes of thrombosis are neoplastic invasion, paraneoplastic lesions or foreign bodies; in some cases the origin cannot be determined (Reimer et al., 2006).

One case has been described of a male cat that was shot, in which the pellet entered through the left ventricle and caused embolisation at the abdominal aorta; the cat did not present any cardiovascular signs when it arrived at the clinic. The only clinical sign was paralysis of the posterior limbs (Kettner and Kirberger, 2006).

There are very few reports of thrombosis of the portal vein in cats. The only cases have been observed in cats with portosystemic shunts (see Chapter 4), a hepatic neoplasm, acute cholangitis and in cases of centrilobular hepatic necrosis (Rogers et al., 2008).

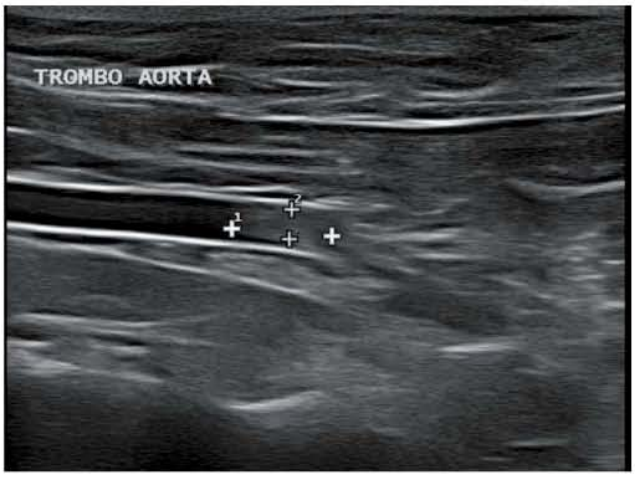

Figure 26. An oval, echogenic structure (between callipers) is located in the lumen of the terminal abdominal aorta and is blocking normal blood flow towards the hinquarters of the animal. Structure compatible with an aortic thrombus.

Figure 27. (a) Thrombus (asterisk) situated in the aorta (arrowhead). (b) Colour Doppler image showing the thrombus (asterisk) and the cup-shaped vascular flow (in blue, going away from the transducer) which delimits its margins.

REFERENCES

Beraud R, Carozzo C. Perirenal expanding haematoma in a cat. *J Small Anim Pract.* 2007, 48(1):43-45.

Black SS, Abemethy TE, Tyler JW et al. Intra-Abdominal Dermatophytic Pseudomycetoma in a Persian Cat. *J Vet Intern Med.* 2001, 15(3):245-248.

Cropper N. Pansteatitis in Cats Fed Fish-based Commercial Foods. *Can Vet J.* 1980, 21(6):192-193.

Culp W, Drobatz K, Glassman M et al. Feline visceral hemangiosarcoma. *J Vet Intern Med.* 2008, 22(1):148-152.

Culp W, Weisse C, Kellogg ME et al. Spontaneous hemoperitoneum in cats: 65 cases (1994-2006). *J Am Vet Med Assoc*. 2010, 236(9):978-982.

D'Anjou MA. Abdominal cavity, Lymph nodes, and Great Vessels. In: Penninck D, D'Anjou MA, eds. *Atlas of Small Animal Ultrasonography*. 1st ed. Ames (IA): Blackwell Publishing. 2008, 445-463.

Dennis R, Kirberger RM, Barr F et al. Other abdominal structures: abdominal wall, peritoneal and retroperitoneal cavities, parenchymal organs. In: Dennis R, Kirberger RM, Barr F et al., eds. *Handbook of Small Animal Radiology and Ultrasound: Techniques and Differential Diagnoses*. 2nd ed. Edinburgh [etc.]: Elsevier. 2010, 229-263.

Evans HE, De Lahunta A. The digestive apparatus and abdomen. In: Evans HE, De Lahunta A, eds. Miller's Anatomy of the Dog. St. Louis, Mo: Elsevier. 2013, 281-337.

Fuentes VL. Arterial Thromboembolism: Risks, realities and a rational first-line approach. *J Feline Med Surg.* 2012, 14(7):459-470.

Haddad JL, Goldschmidt MH. Fibrosarcoma arising at the site of a retained surgical sponge in a cat. *Vet Clin Pathol.* 2010, 39(2):241-246.

Kettner F, Kirberger RM. Aortic foreign body (airgun pellet) embolism in a cat. *J Small Anim Pract.* 2006, 47(4):221-225.

Kinns J, Mai W. Association Between Malignancy and Sonographic Heterogeneity in Canine and Feline Abdominal Lymph Nodes. *Vet Radiol Ultrasound.* 2007, 48(6):565-569.

Kinns J. Abdomen. In: Barr F, Gaschen L, eds. *BSAVA Manual of Canine and Feline Ultrasonography*,1st ed. Quedgeley: British Small Animal Veterinary Association. 2011, 72-84.

Lewis KM, O'brien RT. Abdominal ultrasonographic findings associated with feline infectious peritonitis: A retrospective review of 16 cases. *J Anim Hosp Assoc.* 2010, 46:152-160.

Mai W, Ledieu D, Venturini L et al. Ultrasonographic appearance of intra-abdominal granuloma secondary to retained surgical sponge. *Vet Radiol Ultrasound.* 2001, 42(2):157-160.

Mattoon JS, Berry CR, Nyland TG. Abdominal Ultrasound Scanning Techniques. In: Mattoon JS, Nyland TG, eds. Small Animal Diagnostic Ultrasound. 3rd ed. St. Louis, Missouri: Elsevier. 2015, 94-127.

Monteiro CB, O'brien RT. A retrospective study on the sonographic findings of abdominal carcinomatosis in 14 cats. *Vet Radiol Ultrasound.* 2004, 45(6):559-564.

Nomina Anatomica Veterinaria (NAV). Fifth Edit. (International committee veterinary gross anatomical nomenclature, ed.). Oslo: ICVGAN, 2012. http://www.wava-amav.org/Downloads/nav_2012.pdf.

Nyman HT, O'Brien RT. The Sonographic Evaluation of Lymph Nodes. *Clin Tech Small Anim Pract.* 2007, 22(3):128-137.

Reimer SB, Kittleson MD, Kyles AE. Use of Rheolytic Thrombectomy in the Treatment of Feline Distal Aortic Thromboembolism. *J Vet Intern Med.* 2006, 20(2):290-296.

Rogers CL, O'toole TE, Keating JH et al. Portal vein thrombosis in cats: 6 cases (2001-2006). *J Vet Intern Med.* 2008;22(2):282-287.

Saar Li, Getty R. Sistema linfático de los carnívoros. In: Getty R, ed. S.Sisson - J.D.Grossman. *Anatomía de Los Animales Domésticos*. 5th ed. Barcelona [etc.]: Masson; 1982, 1811-1831.

Schreurs E, Vermote K, Barberet V et al. Ultrasonographic anatomy of abdominal lymph nodes in the normal cat. *Vet Radiol Ultrasound.* 2008, 49(1):68-72.

Schwarz T, Morandi F, Gnudi G, et al. Nodular fat necrosis in the feline and canine abdomen. *Vet Radiol Ultrasound.* 2000, 41(4):335-339.

Smith A, Tobias H. Feline arterial thromboembolism: an update. *Vet Clin Small Anim.* 2004, 34(5):1245-1271.

Spaulding KA. Ultrasound corner sonographic evaluation of peritoneal effusion in small animals. *Vet Radiol Ultrasound.* 1993, 34(6):427-431.

Watson AD. More on feline pansteatitis. *Can Vet J.* 1980;21(11):321.

Widmer WR, Mattoon JS, Nyland TG. Peritoneal Fluid, Lymph Nodes, Masses, Peritoneal Cavity, Great Vessels Thrombosis and Focused Examinations. In: Mattoon JS, Nyland TG, eds. Small Animal Diagnostic Ultrasound. 3rd edition. St. Louis, Missouri: Elsevier Saunders; 2015, 501-516.

Zini E, Hauser B, Ossent P et al. Pansteatitis and severe hypocalcaemia in a cat. *J Feline Med Surg.* 2007, 9(2):168-171.

11. REFERENCES

Agthe, P., Caine, A. R., Posch, B., & Herrtage, M. E. (2009). Ultrasonographic Appearance of Jejunal Lymph Nodes in Dogs Without Clinical Signs of Gastrointestinal Disease. *Veterinary Radiology & Ultrasound*, *50*(2), 195–200.

Beukers, M., Vilaplana Grosso, F., & Voorhout, G. (2013). Computed Tomographic Characteristics of Presumed Normal Canine Abdominal Lymph Nodes. *Veterinary Radiology & Ultrasound*, *54*(6), 610–617.

Bezuidenhout, A. J. (2013). The lymphatic system. In H. E. Evans & A. De Lahunta (Eds.), *Miller's anatomy of the dog* (Forth edit., pp. 535 – 562). St. Louis, Mo: Elsevier.

Bushberg, J. T., Seibert, J. a, Leidholdt, E. M., & Boone, J. M. (2002a). Computed tomography. In *The essential physics of medical imaging* (Second edit., pp. 321–372). Philadelphia: Lippincott Williams & Wilkins.

Bushberg, J. T., Seibert, J. A., Leidholdt, E. M., & Boone, J. M. (2002b). Ultrasound. In *The essential physics of medical imaging* (Second edit., pp. 469 – 553). Philadelphia, NJ: Lippincott Williams & Wilkins.

D'Anjou, M.-A. (2008). Abdominal cavity, Lymph nodes, and Great Vessels. In D. Penninck & M.-A. D'Anjou (Eds.), *Atlas of small animal ultrasonography* (First edit., pp. 445 – 463). Ames, I: Blackwell Publishing Ltd.

D'Anjou, M.-A. (2013). Principles of computed tomography and magnetic resonance imaging. In D. E. Thrall (Ed.), *Textbook of veterinary diagnostic radiology* (Sixth edit., pp. 50 – 73). St. Louis, Mo: Elsevier.

Drost, W. T. (2013). Physics of the ultrasound imaging. In D. E. Thrall (Ed.), *Textbook of veterinary diagnostic radiology* (Sixth edit., pp. 38 – 49). St. Louis, Mo: Elsevier.

Dyce, K. M., Sack, W. O., & Wensing, C. J. G. (2002). Textbook of veterinary anatomy. Philadelphia, NJ: Saunders.

Gendler, A., Lewis, J. R., Reetz, J. A., & Schwarz, T. (2008). Computed tomographic features of oral squamous cell carcinoma in cats: 18 cases (2002–2008). Journal of the American Veterinary Medical Association 319–325.

Henninger, W. (2003). Use of computed tomography in the diseased feline thorax. *Journal of Small Animal Practice*, *44*(2), 56–64.

Karnik, K., Reichle, J. K., Fischetti, A. J., & Goggin, J. M. (2009). Computed Tomographic Findings of Fungal Rhinitis and Sinusitis in Cats. *Veterinary Radiology & Ultrasound*, *50*(1), 65–68.

Kealy, J. K., McAllister, H., & Graham, J. P. (2011a). Soft Tissues. In J. K. Kealy, H. McAllister, & J. P. Graham (Eds.), *Diagnostic radiology and ultrasonography of the dog and cat* (Fifth edit., pp. 543 – 562). St. Louis, Mo: Elsevier Saunders.

Kealy, J. K., McAllister, H., & Graham, J. P. (2011b). The radiograph. In J. K. Kealy, H. McAllister, & J. P. Graham (Eds.), *Diagnostic radiology and ultrasonography of the dog and cat* (Fifth edit., pp. 10–22). St. Louis, Mo: Elsevier Saunders.

Khanna, R., Sharma, A. D., Khanna, S., Kumar, M., & Shukla, R. C. (2011). Usefulness of ultrasonography for the evaluation of cervical lymphadenopathy. *World Journal of Surgical Oncology*, *9*(1), 29.

Kinns, J., & Mai, W. (2007). Association between malignancy and sonographic heterogeneity in canine and feline abdominal lymph nodes. *Veterinary Radiology & Ultrasound*, *48*(6), 565–569.

Lee, N., Won, S., Choi, M. M., Kim, J., Yi, K., Chang, D., Yoon, J. (2012). CT thoracic duct

lymphography in cats by popliteal lymph node iohexol injection. *Veterinary Radiology & Ultrasound*, *53*(2), 174–180.

Leinonen, M. R., Raekallio, M. R., Vainio, O. M., Ruohoniemi, M. O., Biller, D. S., & O´Brien, R. T. (2010). Quantitative contrast-enhanced ultrasonographic analysis of perfusion in the kidneys, liver, pancreas, small intestine, and mesenteric lymph nodes in healthy cats. *American Journal of Veterinary Research*, *71*(11), 1305–1311.

Llabres-Diaz, F. J. (2004). Ultrasonography of the medial iliac lymph nodes in the dog. *Veterinary Radiology & Ultrasound*, *45*(2), 156–165.

Mattoon, J. S., Berry, C. R., & Nyland, T. G. (2015). Abdominal Ultrasound Scanning Techniques. In J. S. Mattoon & T. G. Nyland (Eds.), *Small Animal Diagnostic Ultrasound* (Third edit., pp. 94 – 127). St. Louis, Mo: Elsevier.

Mattoon, J. S., & Nyland, T. G. (2015). Fundamentals of diagnostic ultrasound. In J. S. Mattoon & T. G. Nyland (Eds.), *Small Animal Diagnostic Ultrasound* (Third edit., pp. 1–49). St. Louis, Mo: Elsevier.

Mohseni, S., Shojaiefard, A., Khorgami, Z., Alinejad, S., Ghorbani, A., & Ghafouri, A. (2014). Peripheral lymphadenopathy: Approach and diagnostic tools. *Iranian Journal of Medical Sciences*, *39*(2 SUPPL.), 158–170.

Nakamura, K., Takagi, S., Sasaki, N., Bandula Kumara, W. R., Murakami, M., Ohta, H., … Takiguchi, M. (2010). Contrast-enhanced ultrasonography for characterization of canine focal liver lesions. *Veterinary Radiology and Ultrasound*, *51*(1), 79–85.

NAV. (2012). *Nomina anatomica veterinaria*. (veterinary gross anatomical nomenclature International committee, Ed.) (Fifth Edit.). Oslo: ICVGAN.

Nemanic, S., & Nelson, N. C. (2012). Ultrasonography and noncontrast computed tomography of medial retropharyngeal lymph nodes in healthy cats. *American Journal of Veterinary Research*, *73*(9), 1377–1385.

Nyman, H. T., Kristensen, A. T., Flagstad, A., & Mcevoy, F. J. (2004). A review of the sonographic assessment of tumor metastases in liver and superficial lymph nodes. *Veterinary Radiology & Ultrasound*, *45*(5), 438–448.

Nyman, H. T., Kristensen, A. T., Skovgaard, I. M., & McEvoy, F. J. (2005). Characterization of normal and abnormal canine superficial lymph nodes using gray-scale B-mode, color flow mapping, power, and spectral doppler ultrasonography: A multivariate study. *Veterinary Radiology and Ultrasound*, *46*(5), 404–410.

Nyman, H. T., & O'Brien, R. T. (2007). The Sonographic Evaluation of Lymph Nodes. *Clin Tech Small Anim Pract*, *22*(3), 128–137.

Ohlerth, S., & Scharf, G. (2007). Computed tomography in small animals - Basic principles and state of the art applications. *Veterinary Journal*, *173*(2), 254–271.

Oliveira, C. R., O'Brien, R. T., Matheson, J. S., & Carrera, I. (2012). Computed tomographic features of feline nasopharyngeal polyps. *Veterinary Radiology & Ultrasound, 53*(4), 406–11.

Patsikas, M. N., Papadopoulou, P. L., Charitanti, A., Kazakos, G. M., Soultani, C. B., Tziris, N. E., … Stamoulas, K. G. (2010). Computed Tomography and Radiographic Indirect Lymphography for Visualization of Mammary Lymphatic Vessels and the Sentinel Lymph Node in Normal Cats. *Veterinary Radiology & Ultrasound*, *51*(3), 299–304.

Rossi, F., Leone, V. F., Vignoli, M., Laddaga, E., & Terragni, R. (2008). Use of contrast-enhanced ultrasound for characterization of focal splenic lesions. *Veterinary Radiology and Ultrasound*, *49*(2), 154–164.

Rossi, F., Patsikas, M. N., & Wisner, E. R. (2011). Abdominal lymph nodes and lymphatic collecting system. In T. Schwarz & J. H. Saunders (Eds.), *veterinary computed tomography* (pp. 371 – 379). Ames : Iowa: Wiley-Blackwell.

Saar, L. I., & Getty, R. (1982). Sistema linfático de los carnívoros. In R. Getty (Ed.), *S.Sisson - J.D.Grossman. Anatomía de los animales domesticos* (Fifth edit., pp. 1811–1831). Barcelona : Spain : Masson.

Salwei, R. M., O'Brien, R. T., & Matheson, J. S. (2005). Characterization of lymphomatous lymph nodes in dogs using contrast harmonic and power doppler ultrasound. *Veterinary Radiology and Ultrasound*, *46*(5), 411–416.

Saunders, J. H., & Ohlerth, S. (2011). CT physics and instrumentation - mechanical desing. In T. Schwarz & J. H. Saunders (Eds.), *veterinary computed tomography* (pp. 1 – 8). Ames : Iowa: Wiley-Blackwell.

Schreurs, E., Vermote, K., Barberet, V., Daminet, S., Rudorf, H., & Saunders, J. H. (2008). Ultrasonographic Anatomy of Abdominal Lymph Nodes in the Normal Cat. *Veterinary Radiology & Ultrasound*, *49*(1), 68–72.

Schwarz, T., & O'Brien, R. T. (2011). CT Acquisition principles. In T. Schwarz & J. H. Saunders (Eds.), *veterinary computed tomography* (First edit., pp. 9 – 27). Ames, I: Wiley-Blackwell.

Schwarz, T., & Saunders, J. (2011). *Veterinary computed tomography*. Ames, I: Wiley-Blackwell.

Steinkamp, H. J., Cornehl, M., Hosten, N., Pegios, W., Vogl, T., & Felix, R. (1995). Cervical lymphadenopathy: Ratio of long- to short-axis diameter as a predictor of malignancy. *British Journal of Radiology*, *68*(807), 266–270.

Steinkamp, H. J., Hosten, N., Richter, C., Schedel, H., & Felix, R. (1994). Enlarged cervical lymph nodes at helical CT. *Radiology*, *191*, 795–798.

Sugimura, M., Kudo, N., & Takahata, K. (1955). Studies on the lympnodi of cats: I. Macroscopical observations on the lymphonodi of heads and necks. *Japanese Journal of Veterinary Research*, *3*(2), 90 – 104.

Sugimura, M., Kudo, N., & Takahata, K. (1956). Studies of lymphonodi of cats: II. Macroscopical observations on the lymphonodi of the body surfaces, thoracic and pelvic limbs. *Japanese Journal of Veterinary Research*, *4*(3), 101 – 112.

Sugimura, M., Kudo, N., & Takahata, K. (1958). Studies on the lymphonodi of cats: III. Macroscopical observations on the lymphonodi in the abdominal and pelvic cavities. *Japanese Journal of Veterinary Research*, *6*(2), 69 – 88.

Sugimura, M., Kudo, N., & Takahata, K. (1959). Studies on the lymphonodi of cats: IV. Macroscopical observations on the lymphonodi in the thoracic cavity and supplemental observations on those in the head and neck. *Japanese Journal of Veterinary Research*, *7*(1-4), 27 – 51.

Tobón Restrepo, M. (2015). Ultrasound of the abdominal cavity, lymph nodes and large vessels. In R. Novellas Torroja, E. Dominguez Miño, Y. Espada Gerlach, Y. Martínez Pereira, & M. Tobón Restrepo (Eds.), *Diagnostic ultrasound in cats* (First edit., pp. 211 – 229). Zaragoza, S: Servet editorial - Grupo Asís Biomedia S.L.

Tohnosu, N., Onoda, S., & Isono, K. (1989). Ultrasonographic evaluation of cervical lymph node metastases in esophageal cancer with special reference to the relationship between the short to long axis ratio (S/L) and the cancer content. *JCU J Clin Ultrasound*, *17*(2), 101–106.

Tompkins, M. B. (1993). Lymphoid system. In *Atlas of feline anatomy for veterinarians* (pp. 113 – 126). Philadelphia [etc.] : W.B. Saunders Company.

Vassallo, P., Wernecke, K., Roos, N., & Peters, P. (1992). Differentiation of benign from malignant superficial lymphadenopathy: the rol of high-resolution US. *Radiology*, (183), 215–220.

Widmer, W. R., Mattoon, J. S., & Nyland, T. G. (2015). Peritoneal Fluid, Lymph Nodes, Masses, Peritoneal Cavity, Great Vessels Thrombosis and Focused Examinations. In J. S. Mattoon & T. G. Nyland (Eds.), *Small Animal Diagnostic Ultrasound* (Third edit., pp. 501 – 516). St. Louis, Mo: Elsevier Saunders.

Wunderbaldinger, P. (2006). Problems and prospects of modern lymph node imaging. *Modern Lymphnode Imaging*, *58*(3), 325–337.